UNIWERSYTET MEDYCZNY
IM. PIASTÓW ŚLĄSKICH WE WROCŁAWIU

Małgorzata Anna Strzelecka

Synteza i ocena potencjału przeciwnowotworowego nowych 1,3,4-oksadiazolowych oraz 1,2,4-triazolowych pochodnych 4,6-dimetylo-2-sulfanylopirydyno-3-karboksyamidu

Synthesis and evaluation of the anticancer potential of new 1,3,4-oxadiazole and 1,2,4-triazole derivatives of 4,6-dimethyl-2-sulfanylpyridine-3-carboxsamide

Rozprawa doktorska

w oparciu o monotematyczny cykl publikacji
w dziedzinie nauk medycznych i nauk o zdrowiu
w dyscyplinie nauki farmaceutyczne

Promotor:

dr hab. Piotr Świątek, prof. uczelni

Katedra i Zakład Chemii Leków
Wydział Farmaceutyczny

Wrocław 2024

Dziękuję promotorowi mojej rozprawy doktorskiej,

dr. hab. Piotrowi Świątkowi, prof. uczelni

za wszelką pomoc merytoryczną, zaangażowanie oraz życzliwość

okazane podczas realizacji niniejszej pracy

Dziękuję również całemu zespołowi Katedry i Zakładu Chemii Leków

za wspaniałe towarzystwo, serdeczność i wsparcie

w pracy naukowej i dydaktycznej

oraz Współautorom publikacji

za owocną współpracę

Niniejszą pracę doktorską dedykuję

ukochanemu Mężowi, cudownym Synom oraz najdroższym Rodzicom

SPIS TREŚCI

WYKAZ PUBLIKACJI STANOWIĄCYCH PODSTAWĘ ROZPRAWY DOKTORSKIEJ 4
WYKAZ STOSOWANYCH SKRÓTÓW 5
STRESZCZENIE W JĘZYKU POLSKIM 7
SUMMARY 9
1. WPROWADZENIE 11
2. CEL PRACY 15
3. MATERIAŁY I METODY 17
3.1 Synteza oraz potwierdzenie struktur nowych pochodnych 4,6-dimetylo-2-sulfanylo-pirydyno-3-karboksyamidu 17
3.2 Ocena aktywności biologicznej *in vitro* oraz badania *in silico* tytułowych związków 18
4. WYNIKI 19
4.1 Synteza nowych pochodnych 4,6-dimetylo-2-sulfanylopirydyno-3-karboksyamidu 19
4.1.1 1,3,4-Oksadiazolowe pochodne zawierające ugrupowanie *N*-acylohydrazonowe (seria **I**) 20
4.1.2 1,3,4-Oksadiazolowe pochodne o budowie *N*-zasad Mannicha (seria **II**) 21
4.1.3 1,2,4-Triazolowe pochodne o budowie zasad Schiffa (seria **III**) 22
4.2 Ocena aktywności przeciwnowotworowej w badaniach *in vitro* oraz badania *in silico* związków serii **I**, **II** i **III** 23
4.2.1 Badania *in vitro* oraz *in silico* związków serii **I** 23
4.2.2 Badania *in vitro* oraz *in silico* związków serii **II** 26
4.2.3 Badania *in vitro* oraz *in silico* związków serii **III** 29
5. PODSUMOWANIE I WNIOSKI 34
BIBLIOGRAFIA 37
CAŁKOWITY DOROBEK NAUKOWY 43
PUBLIKACJE WCHODZĄCE W SKŁAD ROZPRAWY DOKTORSKIEJ 48
PUBLIKACJA **P1** WRAZ Z MATERIAŁAMI UZUPEŁNIAJĄCYMI 49
PUBLIKACJA **P2** WRAZ Z MATERIAŁAMI UZUPEŁNIAJĄCYMI 80
PUBLIKACJA **P3** WRAZ Z MATERIAŁAMI UZUPEŁNIAJĄCYMI 116
OŚWIADCZENIA WSPÓŁAUTORÓW PUBLIKACJI **P1**, **P2** I **P3** 159

WYKAZ PUBLIKACJI STANOWIĄCYCH PODSTAWĘ ROZPRAWY DOKTORSKIEJ

PUBLIKACJA P1

Piotr Świątek*, Teresa Glomb*, Agnieszka Dobosz, Tomasz Gębarowski, Kamil Wojtkowiak, Aneta Jezierska, Jarosław J. Panek, Małgorzata Świątek, Małgorzata Strzelecka: Biological evaluation and molecular docking studies of novel 1,3,4-oxadiazole derivatives of 4,6-dimethyl-2-sulfanylpyridine-3-carboxamide. International Journal of Molecular Sciences, 2022, 23, art. 549. DOI: https://doi.org/10.3390/ijms23010549

IF_{2022}: **6,208** Punkty MEiN: **140**

PUBLIKACJA P2

Małgorzata Strzelecka, Teresa Glomb*, Małgorzata Drąg-Zalesińska, Julita Kulbacka, Anna Szewczyk, Jolanta Saczko, Paulina Kasperkiewicz-Wasilewska, Nina Rembiałkowska, Kamil Wojtkowiak, Aneta Jezierska, Piotr Świątek*: Synthesis, anticancer activity and molecular docking studies of novel *N*-Mannich bases of 1,3,4-oxadiazole based on 4,6-dimethylpyridine scaffold. International Journal of Molecular Sciences, 2022, 23, art. 11173. DOI: https://doi.org/10.3390/ijms231911173

IF_{2022}: **6,208** Punkty MEiN: **140**

PUBLIKACJA P3

Małgorzata Strzelecka*, Benita Wiatrak, Paulina Jawień, Żaneta Czyżnikowska, Piotr Świątek: New Schiff bases derived from dimethylpyridine-1,2,4-triazole hybrid as cytotoxic agents targeting gastrointestinal cancers: Design, synthesis, biological evaluation and molecular docking studies. Bioorganic Chemistry, 2023, 139, art. 106758. DOI: https://doi.org/10.1016/j.bioorg.2023.106758

IF_{2023}: **5,1** Punkty MEiN: **140**

**Autor korespondencyjny*

Sumaryczna wartość współczynnika IF: 17.516

Sumaryczna wartość punktacji MEiN: 420

WYKAZ STOSOWANYCH SKRÓTÓW

A375	*melanoma cel line*; linia komórkowa czerniaka
A549	*lung adenocarcinoma cell line*; linia komórkowa gruczolakoraka płuc
BCL-2	*B-Cell Leukemia/Lymphoma-2*; białko białaczki/chłoniaka z komórek B
C32	*amelanotic melanoma cel line*; linia komórkowa czerniaka amelanotycznego
Caco-2	*colorectal adenocarcinoma cel line*; linia komórkowa gruczolakoraka jelita grubego
CCD841CoN	*normal colon epithelial cell line*; prawidłowa linia komórkowa nabłonka jelita grubego
c-MET	*c-mesenchymal-epithelial transition factor*; receptor dla czynnika wzrostu komórek wątrobowych
COX	*cyclooxygenase*; cyklooksygenaza
DCF	*2′,7′-dichlorofluorescein*; 2′,7′-dichlorofluoresceina wykazująca fluorescencję
DCFH	*2′,7′-dichlorodihydrofluorescein*; 2′,7′-dichlorodihydrofluoresceina pozbawiona fluorescencji
DFT	*Density Functional Theory*; teoria funkcjonałów gęstości
EGFR	*epidermal growth factor receptor*; receptor naskórkowego czynnika wzrostu
ELISA	*Enzyme-Linked Immunosorbent Assay*; test immunoenzymatyczny
EPG	*gastric adenocarcinoma cell lines*; linia komórkowa gruczolakoraka żołądka
FTIR	*Fourier-transform infrared spectroscopy*; spektroskopia w podczerwieni z transformacją Fouriera
HaCaT	*human epidermal keratinocytes*; linia komórkowa keratynocytów człowieka
HBA	*Hydrogen Bond Acceptor*; akceptor wiązań wodorowych
HBD	*Hydrogen Bond Donor*; donor wiązań wodorowych
HER-2	*epidermal growth factor receptor 2*; receptor naskórkowego czynnika wzrostu 2
HRMS	*High-resolution mass spectrometry*; wysokorozdzielcza spektrometria mas
HT-29	*primary colorectal adenocarcinoma cell line*; linia komórkowa pierwotnego gruczolakoraka jelita grubego
hTrkA	*tropomyosin-receptor kinase A*; receptor neurotroficznego czynnika wzrostu nerwów
IARC	*International Agency for Research on Cancer*; Międzynarodowa Agencja Badań nad Rakiem
IC_{50}	*the half maximal inhibitory concentration*; połowa wartości maksymalnego stężenia hamującego
IL-6	*interleukin 6*; interleukina 6
LC-MS	*Liquid Chromatography-Mass Spectrometry*; chromatografia cieczowa połączona ze spektrometrią mas

LoVo	*colorectal adenocarcinoma cell line*; linia komórkowa gruczolakoraka jelita grubego
LoVo/Dx	*doxorubicin-resistant colorectal adenocarcinoma cell line*; linia komórkowa gruczolakoraka jelita grubego oporna na doksorubicynę
NHDF	*normal human dermal fibroblasts cell line*; linia komórkowa zdrowych ludzkich fibroblastów skórnych
NLPZ	niesteroidowe leki przeciwzapalne
NMR	*nuclear magnetic resonance*; jądrowy rezonans magnetyczny
MCF-7	*breast cancer cell line*; linia komórkowa raka piersi
MDM2	*murine double minute 2*; białko transformujące o aktywności inhibitora p53
MDR	*multidrug resistant*; oporność wielolekowa
MS	*Mass Spectrometry*; spektrometria mas
MTT	*3-(4,5-dimethylthiazol-2-yl)-2,5-diphenyltetrazolium bromide*; bromek 3-(4,5-dimetylotiazol-2-ylo)-2,5-difenylotetrazoliowy
MW	*Molecular Weight*; masa molekularna związku
OTM	*Olive Tail Moment*; „moment ogonowy" - parametr oceny uszkodzenia DNA
P-gp	*P-glycoprotein*; glikoproteina P
Ppm	*parts per milion*; liczba części na milion
Rh-123	*Rhodamine-123*; Rodamina 123
SAR	*Structure-Activity Relationship*; zależność struktura-aktywność
SNB-19	*glioma cell line*; linia komórkowa glejaka
TLC	*Thin-Layer Chromatography*; chromatografia cienkowarstwowa
V79	*Chinese hamster lung fibroblast*; fibroblasty płuc chomika Chińskiego
VEGFR	*vascular endothelial growth factor receptor*; receptor czynnika wzrostu śródbłonka naczyniowego
VERO	*African green monkey kidney epithelial cells*; komórki nabłonkowe nerki zielonej małpy afrykańskiej

STRESZCZENIE W JĘZYKU POLSKIM

Choroby nowotworowe są jedną z głównych przyczyn zgonów na świecie. Pomimo znacznego postępu, jaki dokonał się w diagnostyce oraz leczeniu onkologicznym, szacuje się, że w 2022 roku z powodu nowotworów zmarło prawie 10 milionów osób [1]. Trudne i długotrwałe leczenie, liczne skutki uboczne terapii onkologicznej oraz rosnąca oporność komórek nowotworowych na stosowane chemioterapeutyki wymuszają konieczność poszukiwania nowych, bardziej skutecznych i bezpiecznych leków przeciwnowotworowych.

Celem niniejszej rozprawy doktorskiej była synteza 1,3,4-oksadiazolowych i 1,2,4-triazolowych pochodnych 4,6-dimetylo-2-sulfanylopirydyno-3-karboksyamidu o potencjale przeciwnowotworowym oraz ocena ich aktywności biologicznej. W świetle najnowszych danych literaturowych, związki zawierające pierścienie oksadiazolu bądź triazolu wykazują znaczące właściwości cytostatyczne [2,3]. Aby wzmocnić aktywność biologiczną nowych połączeń, wbudowano do ich struktury dodatkowo różne ugrupowania farmakoforowe (grupy *N*-acylohydrazonową, aminometylową czy azometinową), korzystne ze względu na aktywność przeciwnowotworową [4–6]. Zaproponowana koncepcja budowy nowych połączeń jest spójna z ideą hybrydyzacji molekularnej – powszechnej strategii stosowanej w chemii medycznej, mającej na celu uzyskanie nowych substancji o zwiększonej aktywności biologicznej.

Zaprojektowane połączenia zostały otrzymane na drodze kilkuetapowej syntezy prowadzonej metodami klasycznymi. W jej wyniku uzyskano szereg półproduktów oraz 33 nowe, nieopisane dotąd w literaturze związki finalne, w tym 19 1,3,4-oksadiazolowych pochodnych stanowiących serie **I** i **II** oraz 14 pochodnych 1,2,4-triazolu stanowiących serię **III**. Po potwierdzeniu tożsamości otrzymanych połączeń metodami spektralnymi, przeprowadzono w warunkach *in vitro* ocenę ich aktywności przeciwnowotworowej. Wykonano także badania *in silico* wybranych związków celem określenia niektórych parametrów fizykochemicznych oraz wskazania ich prawdopodobnego mechanizmu działania przeciwnowotworowego.

Wyniki przeprowadzonych badań *in vitro* udowodniły wysoki potencjał przeciwnowotworowy niektórych połączeń a także pozwoliły na wyciągnięcie ogólnych wniosków dotyczących zależności między strukturą a aktywnością cytotoksyczną pochodnych 4,6-dimetylo-2-sulfanylopirydyno-3-karboksyamidu. Spośród wszystkich serii, 1,3,4-oksadiazolowe pochodne o budowie *N*-zasad Mannicha (seria **III**) były najmniej

aktywne przeciwnowotworowo. Związkami, które najsilniej hamowały żywotność komórek nowotworowych, szczególnie linii niedrobnokomórkowego raka płuc (A549) oraz gruczolakoraka okrężnicy (LoVo) były *N*-acylohydrazonowe pochodne serii **II**. Najbardziej obiecujący związek **13**, posiadający ugrupowanie 2-bromobenzylidenowe, dodatkowo silnie hamował aktywność COX-1 i COX-2 oraz wykazywał działanie antyoksydacyjne. Dobrą bądź umiarkowaną aktywnością cytotoksyczną wobec linii komórkowych raka żołądka (EPG) oraz jelita grubego (HT-29) charakteryzowały się wybrane związki serii **III** o budowie zasad Schiffa. Ponadto określono, że prawdopodobny mechanizm ich działania związany jest z aktywnością proapoptotyczną. Należy zaznaczyć, że cechą wspólną związków serii **I** jak i **III** jest obecność w łańcuchu bocznym wiązania azometinowego (–N=CH-), co może wskazywać na jego kluczową rolę w wystąpieniu aktywności cytotoksycznej w tej grupie związków. Warto podkreślić, że wszystkie badane połączenia charakteryzowały się niższą cytotoksycznością w stosunku do komórek prawidłowych w porównaniu z tą, wyznaczoną dla komórek zmienionych nowotworowo.

Biorąc pod uwagę wyniki dotychczas przeprowadzonych badań należy stwierdzić, że poszukiwanie leków przeciwnowotworowych w grupie pochodnych 4,6-dimetylo-2-sulfanylopirydyno-3-karboksyamidu jest wysoce zasadne. Uchwycone w analizie SAR (*structure-activity relationship*) zależności stanowią podstawę do dalszych modyfikacji strukturalnych pochodnych opartych na szkielecie 4,6-dimetylo-2-sulfanylopirydyno-3-karboksyamidu, mających na celu otrzymanie nowych, jeszcze bardziej aktywnych połączeń.

SUMMARY

Cancer is one of the leading causes of death worldwide. Despite the significant development in oncological diagnosis and treatment during the past decades, it was estimated that almost 10.0 million cancer-related deaths were reported in 2022 [1]. Difficult and long-term treatment, numerous adverse effects of cancer therapies and the growing resistance of neoplastic cells to the chemotherapeutics used necessitate the search for new, more effective and selective anticancer agents.

The aim of the present doctoral dissertation was the synthesis of 1,3,4-oxadiazole and 1,2,4-triazole derivatives of 4,6-dimethyl-2-sulfanylpyridine-3-carboxamide with anticancer potential and evaluation of their biological properties. In light of the latest literature data, compounds containing oxadiazole or triazole rings exhibit significant cytostatic properties [2,3]. To enhance the biological activity of the new molecules, various pharmacophore groups (*N*-acyl hydrazone, aminomethyl or azomethine groups), which are beneficial due to their anticancer activity, were additionally introduced [4–6]. The proposed concept of structural design of new compounds is consistent with the idea of molecular hybridization - a common strategy used in medicinal chemistry, aimed at obtaining new substances with increased biological activity.

The designed compounds were obtained in a multi-step synthesis using classical methods. As a result, several intermediates and 33 new final compounds, previously undescribed in the literature, were obtained, including 19 of 1,3,4-oxadiazole derivatives constituting series **I** and **II**, and 14 of 1,2,4-triazole derivatives constituting series **III**. After confirming the structures of the obtained compounds using spectral methods, their *in vitro* anticancer activity was assessed. *In silico* tests of selected compounds were also performed to determine some of the physicochemical parameters and to indicate their probable mode of anticancer activity.

The results of *in vitro* assays proved the high anticancer potential of some compounds. Also, based on the obtained results, it can be possible to allow for drawing general conclusions from the structure-activity relationship analysis of the tested molecules. Among all series, 1,3,4-oxadiazole derivatives with the *N*-Mannich base structure (series **III**) were the least anticancer active. The compounds that most strongly inhibited the viability of cancer cells, especially the lines of non-small cell lung cancer (A549) and colon adenocarcinoma (LoVo), were *N*-acyl hydrazone derivatives of series **II**. The most promising compound **13**, having

a 2-bromobenzylidene moiety, additionally strongly inhibited the activity of COX-1 and COX-2, and exhibited antioxidant properties. Good to moderate cytotoxic activity against gastric (EPG) and colon cancer (HT-29) cell lines was displayed by selected compounds of series **III** with the structure of Schiff bases. Moreover, it was determined that the probable mode of their action is related to pro-apoptotic activity. It should be noted that a common feature of compounds of series **I** and **III** is the presence of an azomethine bond (–N=CH-) in the side chain, which may indicate its key role in the cytotoxic activity in this group of compounds. It is worth mentioning, that all tested derivatives were characterized by lower cytotoxicity towards normal cells compared to those determined for cancer cells.

Taking into account the results of the studies, it should be concluded that the search for anticancer drugs in the group of 4,6-dimethyl-2-sulfanylpyridine-3-carboxamide derivatives is highly justified. The relationships captured in the SAR (*structure-activity relationship*) analysis constitute the basis for further structural modifications of derivatives based on the 4,6-dimethyl-2-sulfanylpyridine-3-carboxamide skeleton, aimed at obtaining new, more active compounds.

1. WPROWADZENIE

Choroby cywilizacyjne są zespołem dolegliwości o zasięgu globalnym, któremu wyraźnie sprzyja gwałtowny wzrost populacji oraz postępująca industrializacja. Występują one zarówno w krajach wysoko rozwiniętych, jak i rozwijających się. Choć nie są chorobami zakaźnymi, w zastraszającym tempie rozprzestrzeniają się, doprowadzając do przedwczesnych zgonów. Nowotwory obok schorzeń sercowo-naczyniowych są jedną z najbardziej rozpowszechnionych chorób cywilizacyjnych na świecie. Według najnowszych danych opublikowanych przez Międzynarodową Agencję Badań nad Rakiem (IARC), w 2022 roku choroby nowotworowe w skali światowej spowodowały śmierć blisko 10 milionów osób, z czego aż 2 miliony zgonów dotyczyło populacji Europy [1]. Nowotwory złośliwe stanowią istotny problem nie tylko wśród ludzi starszych, ale są też główną przyczyną przedwczesnej umieralności w młodszych grupach wiekowych. Na tym tle Polska negatywnie wyróżnia się wśród krajów europejskich. Szczególnie niepokoi to, że od kilku lat choroby onkologiczne są najczęstszą przyczyną śmierci kobiet w Polsce przed 65 rokiem życia – stanowią około 28% zgonów w grupie młodych kobiet i około 41% zgonów wśród kobiet w średnim wieku [7]. Mało optymistyczną prognozą jest przewidywany wzrost zachorowań na nowotwory oraz zgonów z nimi związanych w ciągu najbliższych dekad, wynikający zarówno ze starzenia się społeczeństwa, jak i z częstego narażenia populacji na czynniki rakotwórcze, przede wszystkim związane z zanieczyszczeniem środowiska oraz prowadzonym stylem życia.

Pomimo znaczącego postępu, jaki dokonał się w poznaniu zjawisk leżących u podstaw transformacji nowotworowej oraz opracowaniu nowych metod farmakoterapii, leczenie chorób onkologicznych wciąż pozostaje wyzwaniem. Jest to niewątpliwie spowodowane tym, że nowotwór jako szczególny rodzaj utworzonej *de novo* tkanki ukształtowanego już organizmu, skutecznie wyłamuje się spod kontroli rozmaitych mechanizmów regulujących jego funkcje. Niekontrolowana proliferacja i wykładniczy wzrost ilości komórek nowotworowych spowodowane są przede wszystkim unikaniem przez zmienione komórki programowanej śmierci – apoptozy. Poznanie procesów leżących u podstaw tego zjawiska może zatem stanowić drogę do jego modulacji i eliminacji, a stosowanie substancji indukujących apoptozę pozwoli na skuteczną walkę z komórkami nowotworowymi [8].

Obecnie w terapii onkologicznej wykorzystuje się głównie leczenie miejscowe obejmujące chirurgię i radioterapię, oraz leczenie systemowe wykorzystujące chemioterapię (w tym terapię celowaną), immunoterapię i hormonoterapię. Istotnym problemem

związanym z ogólnoustrojowym podaniem leków, szczególnie chemioterapeutyków o aktywności cytostatycznej, pozostaje ich wysoka toksyczność względem prawidłowych, szybko dzielących się komórek, co objawia się poważnymi skutkami ubocznymi [9]. Ze względu na małą selektywność klasycznej chemioterapii, coraz popularniejszą strategią walki z chorobami nowotworowymi staje się terapia wykorzystująca leki ukierunkowane na konkretny cel i szlaki metaboliczne nieprawidłowych komórek [10,11]. U wybranych pacjentów terapia celowana w porównaniu z klasyczną, niewątpliwie poprawia wyniki leczenia i kontroli choroby onkologicznej, a ze względu na mniejszą toksyczność pozytywnie wpływa także na jakość życia chorych leczonych w ten sposób. Początek XXI wieku to również przełomowe dokonania stale rozwijającej się dziedziny, jaką jest genetyka. Dzięki jej osiągnięciom poznano nową formę leczenia - terapię genową. Jest ona obiektem licznych badań klinicznych mających na celu ocenić jej skuteczność oraz bezpieczeństwo. Dużym ograniczeniem dla upowszechnienia tej strategii leczenia pozostaje jej wysoka cena [12].

Niekwestionowanym problemem w walce z nowotworami jest oporność komórek rakowych na zastosowane leczenie. Rozwija się ona zarówno w trakcie leczenia klasycznego jak i terapii ukierunkowanej molekularnie [13]. Stanowi ona główną przyczynę niepowodzeń systemowego leczenia onkologicznego.

Ze względu na zmienną efektywność konwencjonalnych metod leczenia, naukowcy starają się znaleźć alternatywę dla klasycznej chemioterapii. Jedną z nich jest chemoprewencja, czyli zastosowanie substancji naturalnych lub syntetycznych w celu zapobiegania, opóźnienia lub odwracania zmian zainicjowanych kancerogenezą [14]. W przeciwieństwie do chemioterapii, chemoprewencja może ingerować we wczesne etapy procesu nowotworzenia, przede wszystkim hamować inicjację i promocję nowotworu (tzw. chemoprewencja wczesna).

W wielu badaniach wykazano związek pomiędzy nowotworzeniem i przewlekłym stanem zapalnym. Tę tezę potwierdza fakt, że niesteroidowe leki przeciwzapalne (NLPZ) wykazują zdolność hamowania wczesnych etapów kancerogenezy [15,16]. Ich potencjalny mechanizm chemoprewencyjnego działania tłumaczony jest inhibicją aktywności cyklooksygenazy (COX), której nadekspresję zaobserwowano w wielu typach nowotworów. Sugeruje się, że zwiększonej aktywności COX-2 i zwiększonemu wytwarzaniu prostaglandyn towarzyszą: zahamowanie apoptozy i zwiększona proliferacja komórek, pobudzenie angiogenezy w obrębie guza oraz zwiększony potencjał do tworzenia przerzutów.

Wśród poszukiwanych nowych, skutecznych a zarazem bezpiecznych substancji przeciwnowotworowych znaczącą rolę odgrywają związki zawierające w swojej strukturze pięcioczłonowe pierścienie heterocykliczne bogate w azot. W świetle najnowszych danych literaturowych, przedmiotem rosnącego zainteresowania wśród naukowców są pochodne 1,3,4-oksadiazolu oraz 1,2,4-triazolu, wykazujące szeroki zakres aktywności biologicznych, między innymi działanie przeciwbakteryjne [17–19], przeciwgrzybicze [20,21], przeciwpadaczkowe [22,23], przeciwbólowe i przeciwzapalne [24,25]. Na podstawie analizy bazy danych *Web of Science* można wywnioskować, iż badania nad pochodnymi 1,2,4-oksadiazolu oraz 1,2,4-triazolu o aktywności przeciwnowotworowej intensywnie się rozwijają (Rysunek 1) [26].

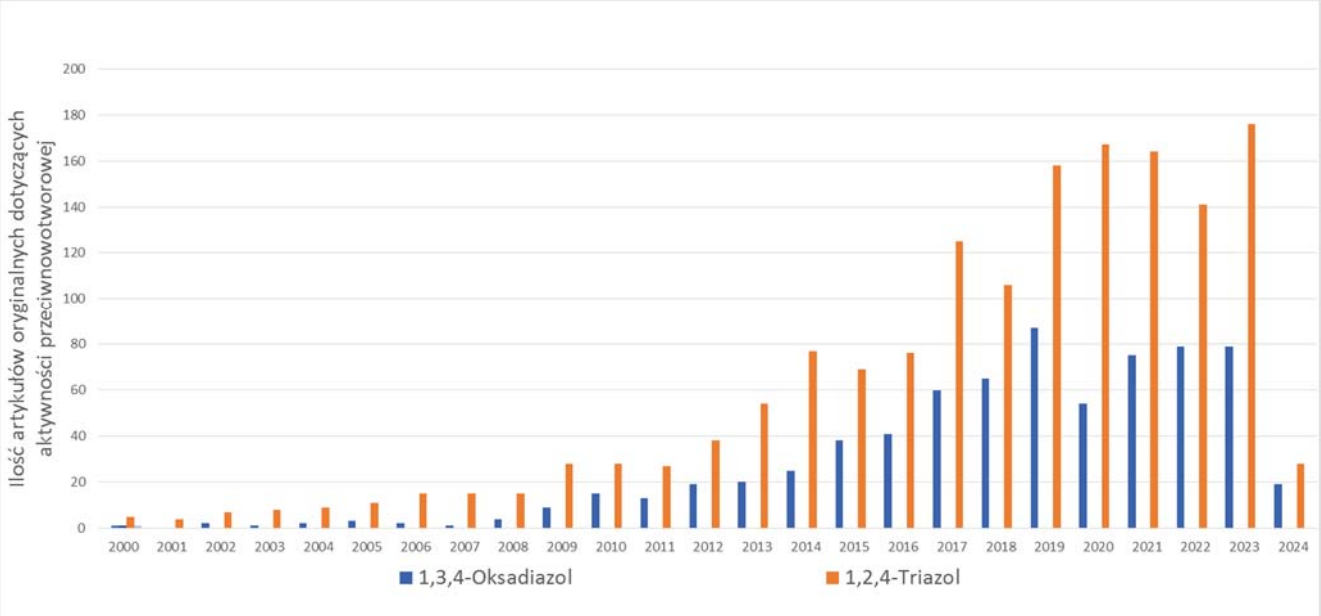

Rysunek 1. Liczba artykułów oryginalnych zawierających słowa kluczowe: „1,3,4-oxadiazole, anticancer" (niebieski) oraz „1,2,4-triazole, anticancer" (pomarańczowy) w latach 2000-2024.

Wyniki badań aktywności przeciwnowotworowej związków zawierających w swojej strukturze pierścienie 1,3,4-oksadiazolu bądź 1,2,4-triazolu, wskazują, że prawdopodobny mechanizm działania tych połączeń oparty jest między innymi o hamowanie anhydrazy IX [27,28], zaburzenie procesu polimeryzacji tubuliny [29,30], indukcję procesu apoptozy poprzez zaburzanie różnych szlaków przekazywania sygnału (m.in. inhibicję białek BCL-2) [31,32] oraz hamowanie czynników wzrostu stymulujących komórki nowotworowe (inhibicja EGFR czy VEGFR) [33,34]. Obecnie na rynku farmaceutycznym dostępnych jest kilka substancji stosowanych w chemioterapii, których struktura chemiczna zawiera pierścienie 1,3,4-oksadiazolu bądź 1,2,4-triazolu (Rysunek 2).

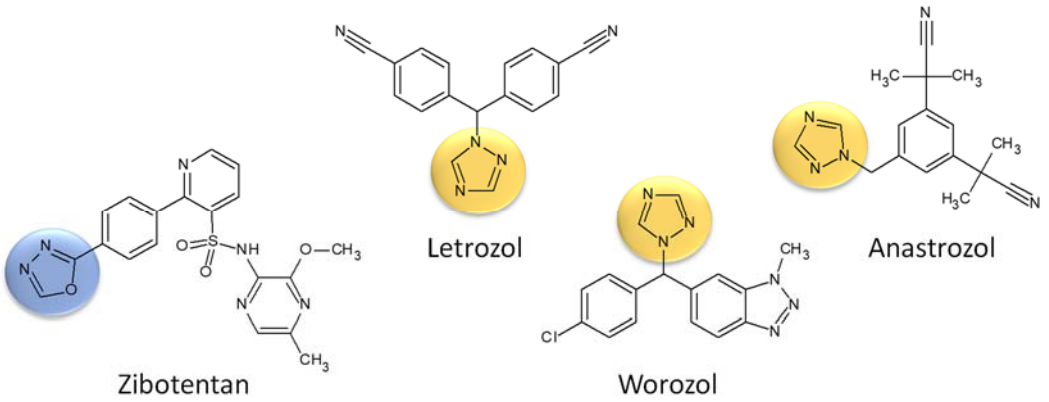

Rysunek 2. Stosowane w medycynie leki przeciwnowotworowe zawierające w swojej strukturze pierścienie 1,3,4-oksazolu oraz 1,2,4-triazolu.

W Katedrze i Zakładzie Chemii Leków prowadzone są od lat badania nad aktywnością biologiczną związków opartych na szkielecie 4,6-dimetyloizotiazolo[5,4-*b*]pirydyny, a od niedawna również jej jednopierścieniowej pochodnej - 4,6-dimetylo-2-sulfanylopirydyno-3-karboksyamidem. Wybrane *N*-acylohydrazonowe pochodne tej struktury, przedstawione wzorem ogólnym na Rysunku 3, w badaniach *in vitro* wykazywały istotne hamowanie aktywności cyklooksygenazy, szczególnie izoformy COX-1 oraz charakteryzowały się aktywnością antyoksydacyjną oraz cytotoksyczną wobec różnych linii komórek nowotworowych, przy zachowaniu relatywnie niskiej toksyczności w stosunku do komórek prawidłowych [35].

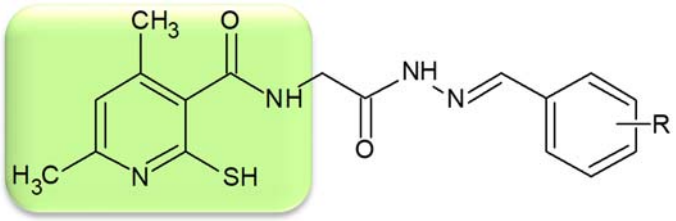

Rysunek 3. Wzór ogólny hydrazonowych pochodnych 4,6-dimetylo-2-sulfanylopirydyno-3-karboksyamidu.

Z dokonanego przeglądu piśmiennictwa wynika, że związki o budowie *N*-acylohydrazonów, lub też jak podaje anglojęzyczna literatura hydrazydo-hydrazonów, ze względu na swoje interesujące właściwości biologiczne oraz proste metody syntezy, stanowią przedmiot zainteresowania wielu zespołów badawczych [36–38]. Niektórzy autorzy sugerują, że ugrupowanie –C(=O)NHN=CH- może pełnić rolę farmakoforu, odpowiedzialnego za aktywność przeciwnowotworową związków.

2. CEL PRACY

Biorąc pod uwagę udokumentowaną aktywność przeciwnowotworową substancji, w których występują pięcioczłonowe pierścienie heterocykliczne oraz kontynuując prace nad pochodnymi 4,6-dimetylo-2-sulfanylopirydyno-3-karboksyamidu, za główny cel niniejszej rozprawy doktorskiej obrano otrzymanie kilku serii nowych związków hybrydowych o aktywności przeciwnowotworowej. Analizując trendy obowiązujące we współczesnej chemii medycznej, można zauważyć, że łączenie małocząsteczkowych fragmentów o udowodnionej aktywności biologicznej w jedną cząsteczkę, zwaną hybrydą molekularną, jest powszechną strategią otrzymywania nowych substancji aktywnych, w tym związków o aktywności przeciwnowotworowej [39,40]. Koncepcja budowy zaplanowanych połączeń, zawierających w swojej strukturze pierścienie 1,3,4-oksadiazolu oraz 1,2,4-triazolu, została przedstawiona na Rysunku 4. Wprowadzenie dodatkowo różnych ugrupowań farmakoforowych (grupy *N*-acylohydrazonowej, aminometylowej czy azometinowej) miało na celu otrzymanie związków o zwiększonej efektywności cytotoksycznej i jest spójne z ideą hybrydyzacji molekularnej.

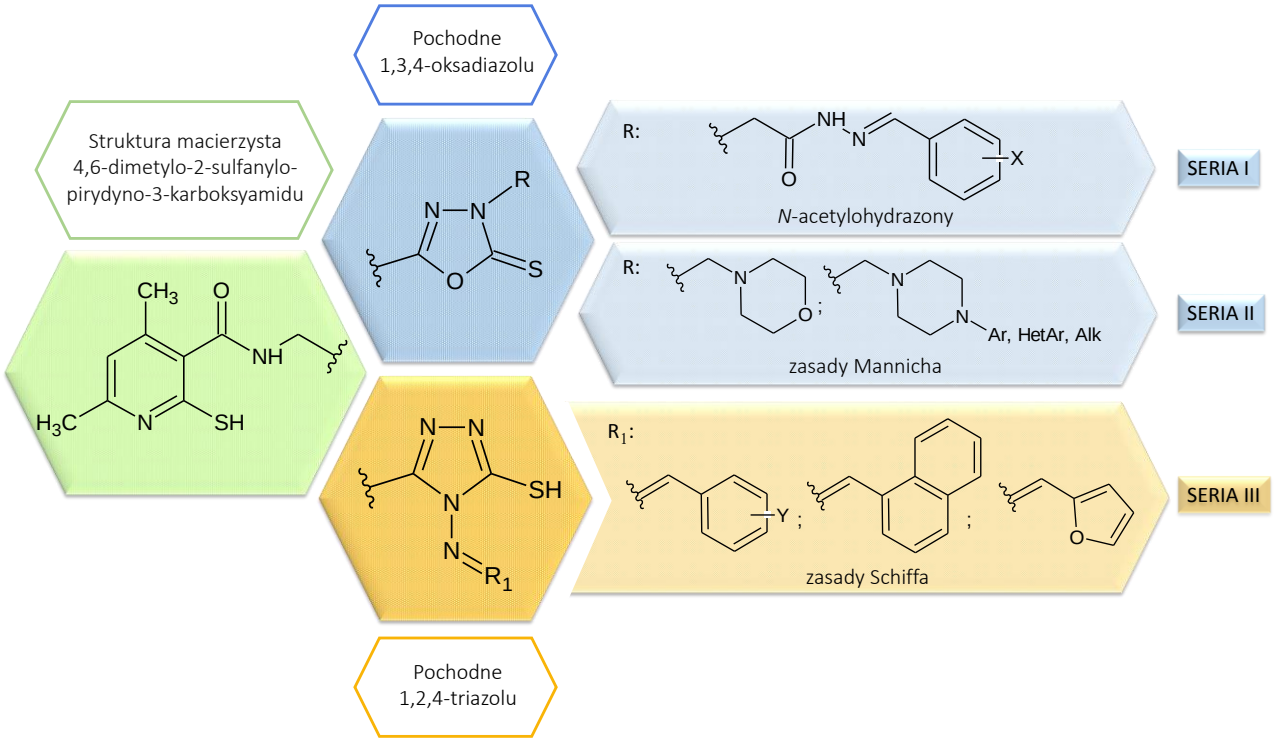

Rysunek 4. Koncepcja budowy nowych pochodnych 4,6-dimetylo-2-sulfanylopirydyno-3-karboksyamidu serii **I**, **II** i **III**.

Na cel główny zrealizowanych badań składały się następujące cele cząstkowe:

- Synteza 1,3,4-oksadiazolowych (seria **I** i **II**) oraz 1,2,4-triazolowych (seria **III**) pochodnych 4,6-dimetylo-2-sulfanylopirydyno-3-karboksyamidu;
- Potwierdzenie tożsamości otrzymanych związków poprzez analizę danych spektroskopowych (FTIR, ^{1}H oraz ^{13}C NMR, MS, a dla wybranych związków również HRMS);
- Ocena aktywności cytotoksycznej wszystkich otrzymanych związków metodą MTT wobec wybranych linii komórek nowotworowych oraz komórek prawidłowych;
- Ocena zdolności hamowania oraz powinowactwa pochodnych 1,3,4-oksadiazolowych serii **I** do obu izoform cyklooksygenazy (COX-1 i COX-2) z użyciem testów enzymatycznych oraz technik dokowania molekularnego celem określenia ich potencjalnej aktywności chemoprewencyjnej;
- Wytypowanie najaktywniejszych pochodnych oraz wykonanie dodatkowych badań biologicznych w modelu *in vitro* oraz badań *in silico* w celu wyjaśnienia ich prawdopodobnego mechanizmu działania;
- Próba opisania zależności struktura-aktywność w grupie nowych pochodnych 4,6-dimetylo-2-sulfanylopirydyno-3-karboksyamidu w oparciu o uzyskane wyniki aktywności biologicznej.

3. MATERIAŁY I METODY

3.1 Synteza oraz potwierdzenie struktur nowych pochodnych 4,6-dimetylo-2-sulfanylopirydyno-3-karboksyamidu

Synteza zaplanowanych półproduktów oraz związków końcowych została przeprowadzona przy użyciu rozpuszczalników i odczynników chemicznych zakupionych od komercyjnych dostawców (Alchem, Wrocław, Polska; Chemat, Gdańsk, Polska; Archem, Łany, Polska). Bezwodny etanol otrzymany został według standardowej procedury. Postęp reakcji był monitorowany dzięki użyciu techniki chromatografii cienkowarstwowej (*Thin-Layer Chromatography*, TLC) z wykorzystaniem płytek aluminiowych pokrytych żelem krzemionkowym (Silica Gel 60 ze wskaźnikiem fluorescencyjnym 254 nm, Sigma-Aldrich, Niemcy). Były one rozwijane w komorze szklanej z zastosowaniem odpowiednio dobranych eluentów (octan etylu oraz jego mieszaniny z metanolem w różnych stosunkach objętościowych). Płytki analizowano w świetle UV przy długości fali 254 nm. Otrzymane związki zostały oczyszczone metodą krystalizacji z etanolu bądź wodnego roztworu etanolu (95%, v/v). Dla wszystkich pochodnych oznaczono wartość temperatury topnienia techniką kapilarną przy użyciu aparatu Electro-Thermal Mel-Temp 1101D (Cole-Parmer, Vernon Hills, IL, USA).

W celu potwierdzenia budowy nowo otrzymanych związków wykonano odpowiednie pomiary spektralne - spektroskopię magnetycznego rezonansu jądrowego (NMR), spektroskopię w podczerwieni (IR), spektrometrię mas (MS, a dla wybranych związków również metodę wysokorozdzielczą HRMS), wykorzystując aparaturę znajdującą się w Pracowni Analizy Elementarnej i Badań Strukturalnych Wydziału Farmaceutycznego Uniwersytetu Medycznego we Wrocławiu.

Widma magnetycznego rezonansu jądrowego - protonowe (^{1}H NMR, 300 MHz) oraz węglowe (^{13}C NMR, 75 MHz) zostały zarejestrowane na spektrometrze NMR Bruker 300 MHz (Bruker Analytische Messtechnik GmbH, Rheinstetten, Niemcy), stosując tetrametylosilan (TMS) jako substancję wzorcową. Badane próbki były rozpuszczane w komercyjnie dostępnym rozpuszczalniku deuterowanym – dimetylosulfotlenku (DMSO-d_6). Przesunięcia chemiczne (δ) wyrażono w bezwymiarowych jednostkach (ppm), stałe sprzężenia *J* w hercach (Hz) a multipletowość sygnałów opisana była jako pojedynczy (*singlet*, s), podwójny (*dublet*, d), potrójny (*triplet*, t), poczwórny (*quartet*, q) oraz wielokrotny (*multiplet*, m) dla

nieokreślonych pasm. Otrzymane widma opracowano w programie TopSpin 4.1.4 (Bruker BioSpin GmbH).

Widma w podczerwieni (FTIR) zostały wykonane z użyciem spektrofotometru podczerwieni Nicolet iS50 z transformacją Fouriera (Thermo Fisher Scientific Inc., Waltham, Massachusetts, USA) z przystawką osłabionego całkowitego odbicia podczerwieni (*Attenuated Total Reflectance*, ATR). Pomiaru dokonano na próbkach w formie stałej a położenie pasm w widmie, określane liczba falową ($\bar{\upsilon}$), wyrażono w odwrotności centymetra (cm^{-1}). Otrzymane widma opracowano w programie OMNIC Specta (Thermo Fisher Scientific Inc.).

Widma masowe (MS) zostały zarejestrowane w jonizacji dodatniej z wykorzystaniem techniki elektrorozpylania (*electrospray ionization*, ESI-MS) na aparacie Bruker Daltonics Compact ESI-Mass Spectrometer 21 (Bruker Daltonik, GmbH, Brema, Niemcy). Próbki były przygotowywane w odpowiednio dobranych rozpuszczalnikach o czystości LC-MS (metanol, woda, chloroform, izopropanol oraz ich mieszanin). Otrzymane widma masowe opracowano w programie Bruker Compass DataAnalysis wersja 4.2 (Bruker Daltonik GmbH), w którym również obliczono teoretyczną masę monoizotopową wykrytych jonów.

3.2 Ocena aktywności biologicznej *in vitro* oraz badania *in silico* tytułowych związków

Spis materiałów oraz szczegółowe opisy wszystkich eksperymentów przeprowadzonych w ramach badań biologicznych nowych związków, metodyka przeprowadzonego dokowania molekularnego i innych użytych technik *in silico*, a także opisy wykorzystanych metod statystycznych zostały zamieszczone w częściach eksperymentalnych publikacji bądź materiałach dodatkowych wchodzących w skład cyklu (**P1**-**P3**).

4. WYNIKI

4.1 Synteza nowych pochodnych 4,6-dimetylo-2-sulfanylopirydyno-3-karboksyamidu

Zgodnie z koncepcją zaprezentowaną na Rysunku 4 zrealizowano syntezę trzech serii nowych pochodnych 4,6-dimetylo-2-sulfanylopirydyno-3-karboksyamidu, zawierających w swojej strukturze pierścienie 1,3,4-oksadiazolu bądź 1,2,4-triazolu. Ścieżkę syntezy docelowych pochodnych przedstawiono na Schemacie 1.

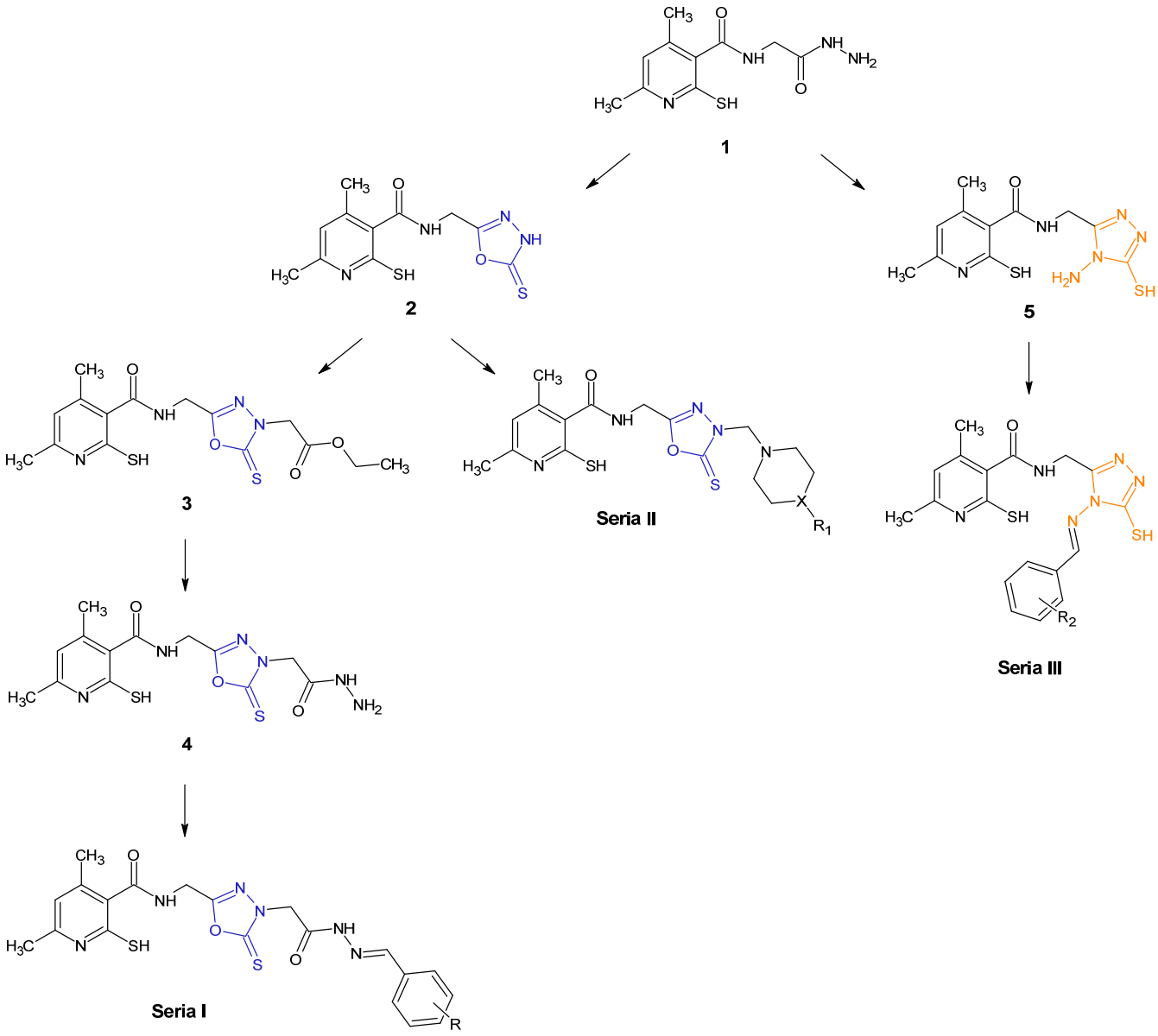

Schemat 1. Ogólny schemat syntezy nowych pochodnych 4,6-dimetylo-2-sulfanylopirydyno-3-karboksyamidu serii **I**, **II** i **III**.

Kluczowym substratem do otrzymania zarówno oksadiazolowych (seria **I** i **II**), jak i triazolowych pochodnych (seria **III**) był opisany wcześniej przez zespół prof. Świątka *N*-(2-hydrazynylo-2-oksoetylo)-4,6-dimetylo-2-sulfanylopirydyno-3-karboksyamid **1** [41].

4.1.1 1,3,4-Oksadiazolowe pochodne zawierające ugrupowanie *N*-acylohydrazonowe (seria I)

W celu otrzymania pochodnych zawierających w swojej strukturze pierścień 1,3,4-oksadiazolu w pierwszym etapie zaplanowanej syntezy hydrazyd **1** ogrzewano we wrzeniu z dwusiarczkiem węgla (CS_2) w etanolowym roztworze wodorotlenku potasu (KOH). Następnie mieszaninę reakcyjną zakwaszono rozcieńczonym kwasem solnym (15% HCl) otrzymując 4,6-dimetylo-*N*-[(5-sulfanylideno-4,5-dihydro-1,3,4-oksadiazol-2-ylo)metylo]-2-sulfanylo-pirydyno-3-karboksyamid **2** (Schemat 1), będący substratem zarówno dla serii **I**, jak i **II**.

Dalsza synteza związków serii **I** przebiegała trójetapowo. Pierwszy etap polegał na alkilowaniu atomu azotu *N*-4 pierścienia 1,3,4-oksadiazolu związku **2** bromooctanem etylu w etanolowo-wodnym roztworze KOH. W kolejnym kroku, otrzymaną pochodną estrową **3** poddano reakcji hydrazynolizy przy użyciu 10-krotnego nadmiaru wodzianu hydrazyny w środowisku wrzącego metanolu. Otrzymany hydrazyd **4** poddano reakcji kondensacji z różnie podstawionymi aldehydami aromatycznymi. Reakcję prowadzono w metanolu z dodatkiem katalitycznej ilości kwasu octowego w temperaturze wrzenia mieszaniny reakcyjnej. W efekcie uzyskano w sumie 12 nowych, nieopisanych dotąd w literaturze związków, w tym 9 finalnych pochodnych o budowie *N*-acylohydrazonów, stanowiących pierwszą serię (seria **I**) 1,3,4-oksadiazolowych pochodnych 4,6-dimetylo-2-sulfanylo-pirydyno-3-karboksyamidu.

Z analizy widm ^{1}H NMR wynika, że w obrębie finalnych *N*-acylowych pochodnych hydrazonów, podobnie jak w innych związkach o wzorze ogólnym R_1–C(=O)–NH–N=C–R_2, stwierdzono występowanie zjawiska tautomerii (Rysunek 5). Obecność wiązania podwójnego -C=N- powoduje, iż związki mogą występować w formie izomerów geometrycznych *Z*/*E*, z kolei ograniczenie rotacji wokół wiązania amidowego mającego charakter wiązania podwójnego decyduje o występowaniu dwóch struktur konformacyjnych *cis*/*trans*. Różne praktyczne i obliczeniowe doświadczenia opisane w literaturze wykazały istnienie *N*-acylohydrazonów w geometrii *E* z mniejszą zawadą przestrzenną izomeru, a podwojenie sygnałów rezonansowych w widmach NMR przypisano obecności konformerów *cis* i *trans* [42,43]. W widmach ^{1}H NMR dla pochodnych serii **I** w wyniku izomerii konformacyjnej

zaobserwowano zduplikowane sygnały dla atomów wodoru ugrupowań -CH_2-C(O)-, –C(O)NH– oraz –N=CH–, co korelowało z wynikami raportowanymi w literaturze.

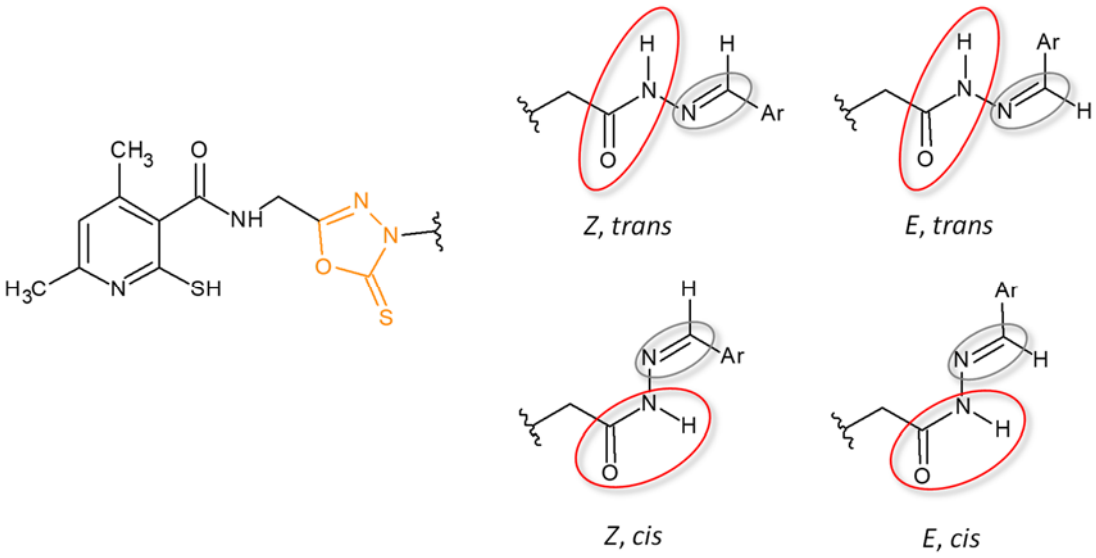

Rysunek 5. Cztery teoretycznie możliwe izomery związków serii **I**.

Szczegóły dotyczące zrealizowanych prac syntetycznych przedstawiono na Schemacie 1 oraz opisano w Rozdziale 3.1 publikacji **P1**. Struktura każdego otrzymanego związku została potwierdzona dzięki wykorzystaniu technik spektralnych a dane analityczne oraz właściwości fizykochemiczne zostały zebrane i opisane w części eksperymentalnej publikacji **P1**.

4.1.2 1,3,4-Oksadiazolowe pochodne o budowie *N*-zasad Mannicha (seria II)

Kontynuując badania nad syntezą pochodnych 1,3,4-oksadiazolu, zdecydowano się otrzymać struktury o budowie *N*-zasad Mannicha (seria **II**, Schemat 1). Na drodze jednoetapowej reakcji 1,3,4-oksadiazolowej pochodnej **2** z formaliną oraz wybraną aminą drugorzędową (morfoliną lub różnie podstawionymi pochodnymi piperazyny), prowadzonej w środowisku etanolu w temperaturze pokojowej, otrzymano 10 nowych, nieopisanych wcześniej w literaturze pochodnych o budowie *N*-zasad Mannicha, stanowiących drugą serię (seria **II**) 1,3,4-oksadiazolowych pochodnych 4,6-dimetylo-2-sulfanylopirydyno-3-karboksyamidu.

Cechą wspólną związków serii **II** była obecność w widmach ^{1}H NMR sygnałów rezonansowych przy ok. 5.00 ppm odpowiadających protonom łącznika metylenowego ugrupowania aminometylenowego oraz sygnałów protonów H-2,6 oraz H-3,5 pochodzących

z pierścieni piperazyny oraz morfoliny, obserwowanych w postaci dwóch multipletów o intensywności czterech protonów każdy, w zakresach 2.34-2.87 ppm oraz 2.67-3.73 ppm.

Koncepcja budowy oraz synteza 1,3,4-oksadiazolowych pochodnych serii **II** zostały szczegółowo przedstawione na Rysunku 1, Schemacie 1 oraz w Rozdziałach 1 i 2.1 publikacji **P2**. Wszystkie nowe związki scharakteryzowano w oparciu o analizę spektroskopową. Dane analityczne oraz właściwości fizykochemiczne zostały zebrane i opisane w części eksperymentalnej publikacji **P2** oraz w suplemencie.

4.1.3 1,2,4-Triazolowe pochodne o budowie zasad Schiffa (seria III)

Kluczowym etapem w syntezie związków serii **III** było otrzymanie 4,6-dimetylo-*N*-[(4-amino-5-sulfanylo-4*H*-1,2,4-triazol-2-ylo)metylo]-2-sulfanylo-pirydyno-3-karboksyamidu **5** (Schemat 1). W tym celu przeprowadzono reakcję hydrazydu **1** z dwusiarczkiem węgla w etanolowym roztworze KOH w temperaturze pokojowej. Utworzoną sól ditiokarbazynianu potasu odsączano i poddano reakcji z wodzianem hydrazyny we wrzącym etanolu. Zakwaszenie mieszaniny skutkowało utworzeniem odpowiedniej 4-amino-1,2,4-triazolo-5-sulfanylowej pochodnej **5**. Synteza finalnych związków o charakterze zasad Schiffa została przeprowadzona w reakcji kondensacji pierwszorzędowej grupy aminowej w pozycji *N*-4 pierścienia 1,2,4-triazolu związku **5** z aromatycznymi i heteroaromatycznymi aldehydami w środowisku wrzącego etanolu, w obecności katalitycznej ilości kwasu octowego. W efekcie uzyskano w sumie 16 nowych, nieopisanych dotąd w literaturze związków, w tym 14 pochodnych o budowie zasad Schiffa, stanowiących trzecią serię (seria **III**) pochodnych 4,6-dimetylo-2-sulfanylopirydyno-3-karboksyamidu.

Znamiennym dla związków o budowie zasad Schiffa była obecność w widmach ^{1}H NMR sygnałów rezonansowych przy ok. 10 ppm pochodzących od protonu grupy azometinowej –CH=N-, oraz sygnałów protonów aromatycznych obserwowanych w zakresie 6.75-8.32 ppm.

Koncepcja budowy oraz synteza finalnych pochodnych zostały szczegółowo przedstawione na Schemacie 1 oraz w Rozdziałach 1 i 2.1 publikacji **P3**. Ponadto, w części chemicznej oraz eksperymentalnej tej pracy oraz w suplemencie znajdują się wyczerpujące informacje dotyczące właściwości fizykochemicznych oraz dane z analizy spektralnej wszystkich nowych struktur.

4.2 Ocena aktywności przeciwnowotworowej w badaniach *in vitro* oraz badania *in silico* związków serii I, II i III

4.2.1 Badania *in vitro* oraz *in silico* związków serii I

Wstępna ocena aktywności biologicznej 1,3,4-oksadiazolowych pochodnych 4,6-dimetylo-2-sulfanylopirydyno-3-karboksyamidu serii **I** została przeprowadzona we współpracy z Panem dr Tomaszem Gębarowskim z Katedry Biostruktury i Fizjologii Zwierząt Uniwersytetu Przyrodniczego we Wrocławiu oraz z Panią dr Agnieszką Dobosz z Katedry i Zakładu Podstaw Nauk Medycznych Uniwersytetu Medycznego we Wrocławiu. Dokowanie molekularne oraz obliczenia statyczne metodami chemii kwantowej (DFT) zostały wykonane przez zespół Pani dr hab. Anety Jezierskiej, profesor uczelni z Zespołu Struktury i Dynamiki Makroukładów Uniwersytetu Wrocławskiego.

W pierwszym etapie badań biologicznych została oceniona zdolność *N*-acylowych pochodnych hydrazonów serii **I** do hamowania cyklooksygenazy oraz ustalony sposób ich wiązania się z centrum aktywnym enzymu. Szlak przemian kwasu arachidonowego związany z syntezą prostanoidów oraz jego rola w promocji i progresji nowotworów u człowieka od lat jest przedmiotem wielu analiz [44–47]. Wykazano w nich, że cyklooksygenaza, której nadekspresja często występuje w wielu typach nowotworów, odgrywa istotną rolę w regulacji procesów związanych z proliferacją, angiogenezą, opornością na apoptozę czy zdolnością przerzutowania. Hamowanie przez związki serii **I** aktywności dwóch izoform cyklooksygenazy (COX-1 i COX-2) zbadano wykorzystując dostępny komercyjnie enzymatyczny test płytkowy Cayman's COX Colorimetric Inhibitor Screening Assay. Największą zdolność hamującą obie izoformy enzymu COX-1 i COX-2 wykazywał związek **13** (numeracja pochodzi z publikacji **P1**), z ugrupowaniem 2-bromobenzylidenowym (Rysunek 6). Co warto podkreślić, charakteryzował się on wyższą aktywnością hamującą COX niż leki referencyjne użyte w teście – piroksykam i meloksykam. Związki oznaczone symbolami **5**, **11** i **12** (Rysunek 6) działały preferencyjnie względem izoformy COX-1, a ich wyznaczone stężenia hamujące IC_{50} (wartość stężenia związku badanego stanowiącego połowę wartości maksymalnego stężenia hamującego) były niższe niż dla leków odniesienia.

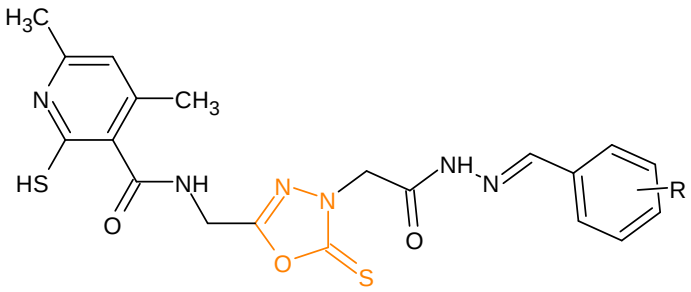

R:
5 -H
6 4-F
7 4-CH_3
8 4-SCH_3
9 4-CN
10 4-Cl
11 4-CF_3
12 3-Cl
13 **2-Br**

Rysunek 6. Wzór ogólny związków serii **I.**

Badanie *in silico* przeprowadzone z wykorzystaniem metody chemii kwantowej bazującej na teorii funkcjonału gęstości (DFT) ujawniło występowanie dwóch rodzajów konformacji dla związków serii **I** – konformacji rozciągniętej oraz konformacji upakowanej, tzw. „kanapkowej" (Rysunek 7). Dla każdego związku, w każdej konformacji, przeprowadzono badania dokowania molekularnego w celu określenia sposobu ich wiązania z miejscem aktywnym owczej oraz ludzkiej COX-1, a także mysiej oraz ludzkiej COX-2 w odniesieniu do meloksykamu oraz rofekoksybu, jako leków działających odpowiednio, preferencyjnie hamująco względem COX-2 oraz selektywnie hamująco względem COX-2.

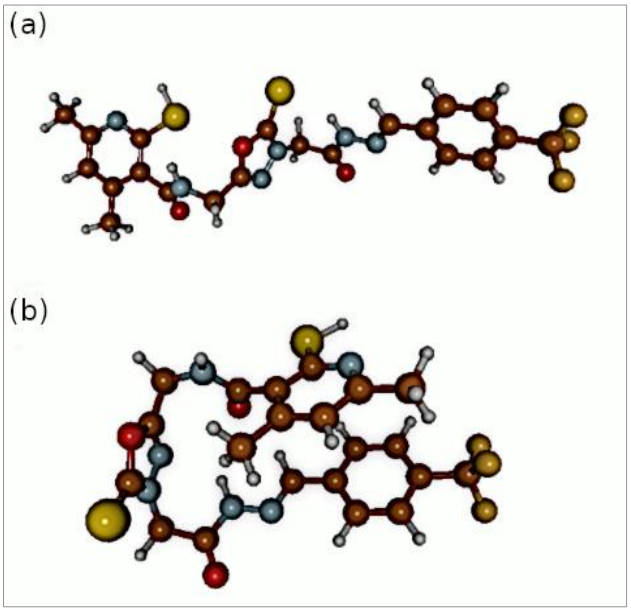

Rysunek 7. Optymalizacja strukturalna związków serii **I** na przykładzie związku **11**;
(a) konformacja rozciągnięta, (b) konformacja upakowana.

Uzyskane wyniki sugerują, że związek **11**, z ugrupowaniem 4-trifluorometylobenzylidenowym wykazuje największe powinowactwo do kieszeni wiążącej COX-1 i COX-2 z energiami swobodnymi wiązania niższymi niż leki referencyjne, a grupa trifluorometylowa odpowiada za wiązania halogenowe stabilizujące ligand w kieszeni.

Co więcej, wyraźnie widać, że pochodna hydrazydowa **4** wykazuje najmniejsze powinowactwo do kieszeni wiążącej cyklooksygenazy, prawdopodobnie ze względu na brak stabilizujących oddziaływań niekowalencyjnych jakie zapewnia wprowadzenie pierścienia aromatycznego obecnego w związkach finalnych.

Kolejny etap zaplanowanych badań *in vitro* zakładał ocenę aktywności cytotoksycznej badanej serii związków z wykorzystaniem testu MTT, a wyniki zaprezentowano jako wartości IC_{50} (stężenie związku badanego, które zredukowało odsetek żywych komórek o 50% w odniesieniu do kontroli). Kolorymetryczny test MTT oparty jest na pomiarze aktywności enzymu mitochondrialnego – dehydrogenazy bursztynianowej, obecnej w żywych komórkach i jego zdolności do przekształcania rozpuszczalnej soli tetrazolowej (MTT), w formę zredukowaną, czyli nierozpuszczalny formazan. W komórkach uszkodzonych metabolicznie lub martwych nie powstają kryształki formazanu, co ma odzwierciedlenie w pomiarach absorbancji roztworu. Badanie cytotoksyczności związków serii **I** zostało przeprowadzone wobec czterech linii komórek nowotworowych: niedrobnokomórkowego raka płuc (A549), raka piersi (MCF-7), raka jelita grubego (LoVo) i jego lekoopornej sublinii (LoVo/Dx), oraz trzech linii komórek prawidłowych: ludzkich fibroblastów (NHDF) oraz fibroblastów pochodzenia zwierzęcego (VERO, V79). Spośród wymienionych nowotworów, najwyższą wrażliwość na związki serii **I** wykazywały linie komórkowe LoVo oraz A549, których wzrost badane pochodne hamowały w zakresie stężeń $IC_{50} = 2.89 \pm 0.08 – 4.34 \pm 0.56$ μM. Należy podkreślić fakt, że efekt cytotoksyczny wobec komórek nienowotworowych był znacznie słabszy, a indeks terapeutyczny wyliczony względem komórek prawidłowych (NHDF/LoVo oraz NHDF/A549) mieścił się w zakresie 13-20.

W ostatnim etapie badań dokonano oceny potencjału antyoksydacyjnego związków serii **I**. Powszechnie wiadomo, że zaburzenia równowagi między wytwarzaniem reaktywnych form tlenu a wydajnością systemów antyoksydacyjnych prowadzi do stresu oksydacyjnego w komórkach, a co za tym idzie do uszkodzenia ważnych makrocząsteczek, tj. DNA, białek i lipidów [48]. Jako, że integralność i stabilność genomu są warunkiem prawidłowego funkcjonowania komórek, oksydacyjne uszkodzenia DNA mogą stanowić element zapoczątkowujący m.in. proces nowotworowy [49]. W celu zbadania potencjału antyoksydacyjnego *N*-acylowych pochodnych hydrazonów wykonano test polegający na pomiarze fluorescencji 2',7'-dichlorofluoresceiny (DCF), produktu powstałego w obecności wolnych rodników w wyniku reakcji utlenienia niefluorescencyjnego barwnika – 2',7'-dichlorodihydrofluoresceiny (DCFH). Badanie przeprowadzono w warunkach hodowli komórkowych na linii prawidłowej V79 oraz linii nowotworowej LoVo. Pochodna

hydrazydowa oznaczona symbolem **4** oraz związek **13** wykazywały najwyższe działanie przeciwutleniajace z badanej serii, było ono jednak niższe od zastosowanych znanych antyoksydantów – kwasu askorbinowego i troloksu.

4.2.2 Badania *in vitro* oraz *in silico* związków serii II

Obiecujące wyniki badań cytotoksyczności związków serii **I** zachęciły do otrzymania kolejnych pochodnych 1,3,4-oksadiazolu, tym razem o budowie *N*-zasad Mannicha oraz sprawdzenia ich potencjału przeciwnowotworowego.

Wstępna ocena aktywności biologicznej 1,3,4-oksadiazolowych pochodnych 4,6-dimetylo-2-sulfanylopirydyno-3-karboksyamidu serii **II** została przeprowadzona we współpracy z zespołem Pani śp. prof. Jolanty Saczko z Katedry i Zakładu Biologii Molekularnej i Komórkowej oraz z dr hab. Małgorzatą Drąg-Zalesińską z Zakładu Histologii i Embriologii Uniwersytetu Medycznego we Wrocławiu, natomiast dokowanie molekularne wykonał zespół Pani dr hab. Anety Jezierskiej, profesor uczelni z Zespołu Struktury i Dynamiki Makroukładów Uniwersytetu Wrocławskiego.

W celu zbadania potencjału cytotoksycznego nowych związków wykonano test MTT wobec pięciu linii ludzkich komórek nowotworowych: melanotycznego (A375) i amelanotycznego (C32) czerniaka, glejaka (SNB-19), oraz wrażliwego (MCF-7/WT) i lekoopornego (MCF-7/Dx) raka piersi, używając cisplatyny jako leku referencyjnego. W warunkach testu zaobserwowano znaczne obniżenie żywotności komórek raka skóry (A375 oraz C32) w wyniku działania dwóch związków **5** i **6** (numeracja pochodzi z publikacji **P2**), zawierających odpowiednio, ugrupowanie 3,4-dichloro- oraz 4-trifluorometylofenylo-piperazynowe (Rysunek 8). Związki te zostały wybrane do dalszych badań.

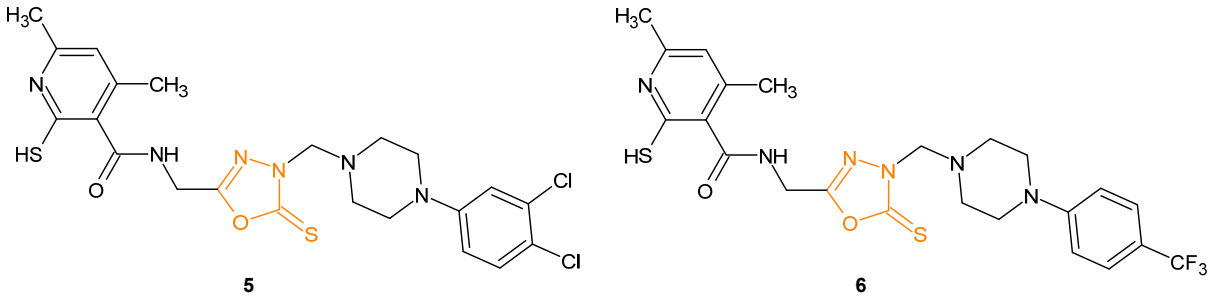

Rysunek 8. Wzory strukturalne najaktywniejszych w teście MTT związków serii **II**.

Aby sprawdzić, czy zasady Mannicha **5** i **6** są selektywnie cytotoksyczne wobec linii komórek czerniaka, do badań włączono prawidłową linię komórkową — ludzkie keratynocyty (HaCaT). W przeprowadzonym teście związek oznaczony symbolem **6** charakteryzował się niższą cytotoksycznością wobec komórek prawidłowych niż związek **5**,

przy czym komórki czerniaka amelanotycznego (C32) okazały się być najmniej wrażliwe ze wszystkich użytych w badaniu linii komórkowych. Co należy podkreślić, obie zasady Mannicha hamowały żywotność keratynocytów w stężeniach 2- do 4-krotnie wyższych niż cisplatyna.

W celu dalszej oceny wpływu związków **5** i **6** na przeżywalność komórek nowotworowych w warunkach *in vitro* wykonano test klonogenny, oceniający zdolność do tworzenia kolonii przez komórki czerniaka poddanych działaniu wybranych związków (Rysunek 9), oraz test podwojenia populacji. Wyniki były spójne z danymi uzyskanymi z testu MTT – związek **5** zmniejszał wyraźnie żywotność komórek nowotworowych w niższych stężeniach niż jego fluorowa pochodna. Z kolei związek **6** w dawkach 100 μM wykazywał selektywną cytotoksyczność w stosunku do badanych komórek nowotworowych czerniaka, nie wpływając istotnie na żywotność keratynocytów.

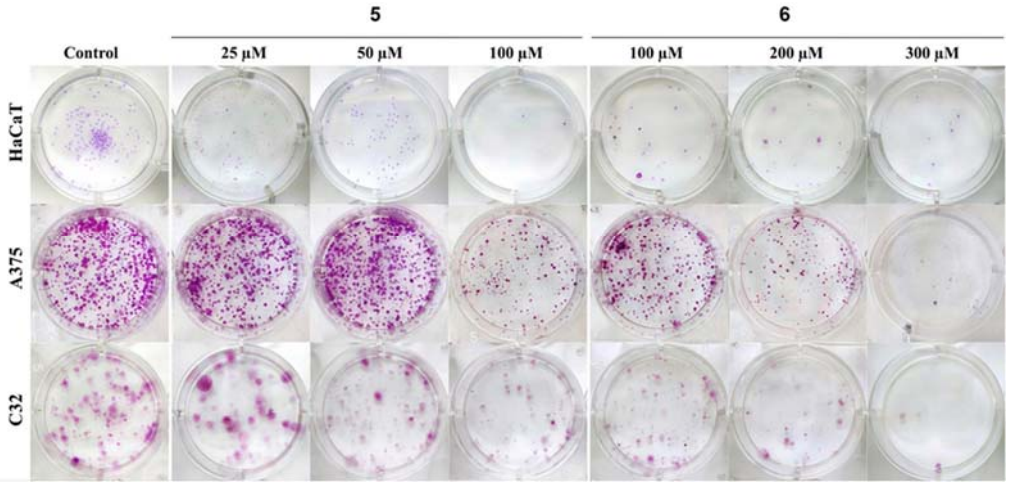

Rysunek 9. Ocena potencjału klonogennego komórek czerniaków (C32 i A375) oraz komórek prawidłaowych (HaCaT) po inkubacji z badanymi związkami **5** i **6**.

Kolejny etap badań polegał na określeniu stopnia uszkodzenia DNA komórek nowotworowych czerniaka w wyniku działania wybranych związków przy użyciu testu kometowego (*Comet assay*). Analizując uzyskane wyniki zauważono, że dla związku **6** w stężeniu 100 μM ilość komórek nowotworowych ulegających apoptozie jest najwyższa. Dane te korelowały z wielkością uszkodzenia DNA mierzoną tzw. „momentem ogonowym" (*Olive Tail Moment*, OTM) będącym iloczynem odległości pomiędzy środkiem głowy komety oraz środkiem głowy ogona komety oraz procentowej ilości DNA zawartej w ogonie komety. Analizowane parametry testu kometowego potwierdziły genotoksyczny charakter obu badanych związków.

W ostatnim etapie badań *in vitro* oceniono wpływ związków **5** i **6** na cytoszkielet aktynowy keratynocytów oraz dwóch linii czerniaków (C32 i A375). Sieć włókien aktynowych

wypełniająca komórkę ma ogromne znaczenie dla jej funkcjonowania. Pełni ona istotną rolę również w stanach patologicznych, decydując m.in. o zdolności nowotworów do migracji i tworzenia przerzutów [50,51]. W przeprowadzonym badaniu struktura cytoszkieletu aktynowego komórek prawidłowych grupy kontrolnej była uporządkowana i dobrze widoczna. W przypadku komórek nowotworowych, włókna F-aktyny miały strukturę bardziej chaotyczną, zlokalizowaną głównie na obrzeżach komórek, co jest odzwierciedleniem odmiennej morfologii i fizjologii komórek nowotworowych i prawidłowych. Po 24-godzinnej inkubacji komórek z badanymi związkami obserwowano zaburzenia struktury ich cytoszkieletu (Rysunek 10). Związek **5** w stężeniu 100 μM powodował uszkodzenie włókien aktynowych wszystkich badanych komórek. Z kolei związek **6** w stężeniu 100 μM wykazywał negatywny wpływ na organizację cytoszkieletu komórek nowotworowych obu linii, jednocześnie nie naruszając struktury szkieletu komórkowego keratynocytów.

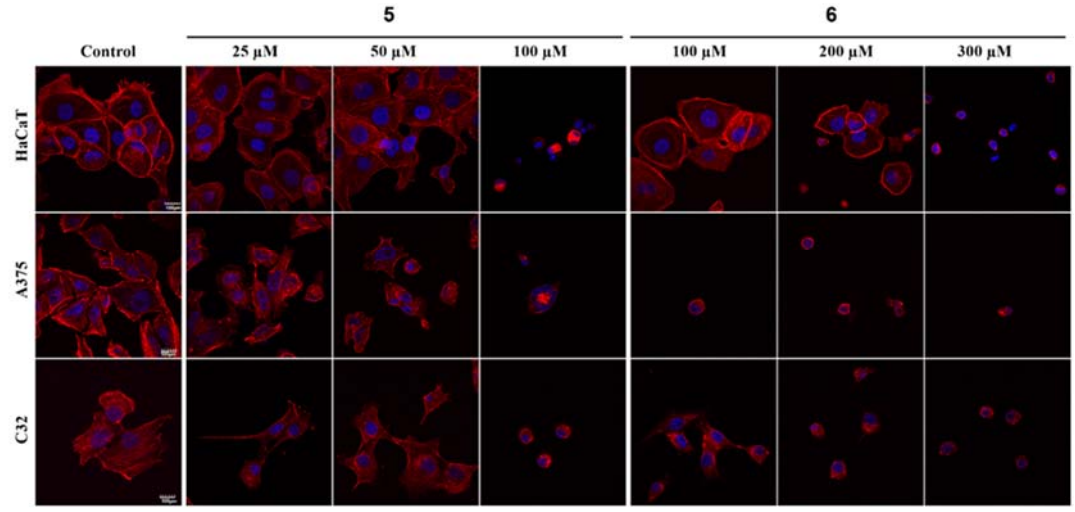

Rysunek 10. Wizualizacja organizacji cytoszkieletu aktynowego komórek HaCaT, A375 oraz C32 w 60-krotnym powiększeniu po 24-godzinnej inkubacji ze związkami **5** i **6** w różnych stężeniach; DAPI (4',6-diamidyno-2-fenyloindol) został użyty do wybarwienia jąder komórkowych (niebieski), znakowana fluorescencyjnie falloidyna została użyta do wizualizacji cytoszkieletu aktynowego (czerwony).

W badaniach *in silico* wszystkie nowo otrzymane *N*-zasady Mannicha zadokowano do czterech wybranych receptorów wykazujących aktywność kinazy tyrozynowej: receptora dla czynnika wzrostu komórek wątrobowych (c-MET), receptorów naskórkowego czynnika wzrostu (EGFR, HER-2) oraz receptora dla neurotroficznego czynnika wzrostu nerwów (hTrkA). Aktywność związków porównano względem znanych inhibitorów tych białek, a mianowicie erlotynibu, neratynibu i tepotynibu. Dobór celów molekularnych podyktowany był znaczeniem wymienionych białek w procesie nowotworzenia [52–54]. Uzyskane wyniki sugerują, że pochodne z ugrupowaniem 4-nitrofenylopiperazynowym (związek **7**) oraz benzdioksolan-5-ylometylopiperazynowym (związek **11**) wykazywały największe

powinowactwo do kieszeni wiążącej badanych receptorów (Rysunek 11), przy czym związek **11** wykazywał najniższą energię swobodną wiązania do receptora hTrkA, niższą niż użyte leki referencyjne. Najmniejsze powinowactwo do wybranych receptorów wykazywała zasada Mannicha z ugrupowaniem morfolinowym.

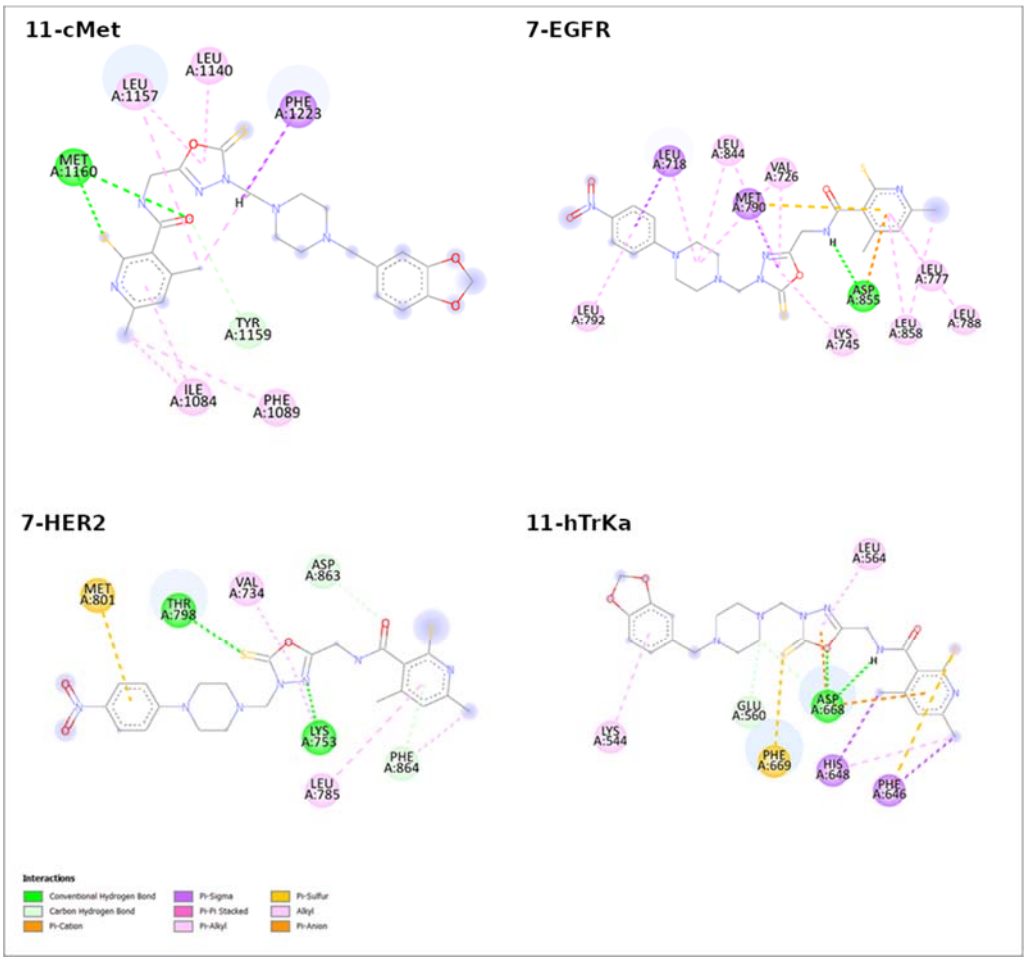

Rysunek 11. Oddziaływania związków **7** oraz **11**, charakteryzujących się najniższymi energiami wiązania z miejscami aktywnymi białek cMET, EGFR, HER2 oraz hTrkA.

4.2.3 Badania *in vitro* oraz *in silico* związków serii III

Wstępna ocena aktywności cytotoksycznej została wykonana we współpracy z zespołem Pani dr hab. Benity Wiatrak z Katedry i Zakładu Farmakologii Uniwersytetu Medycznego we Wrocławiu, natomiast dokowanie molekularne wykonała Pani dr hab. Żaneta Czyżnikowska z Katedry i Zakładu Podstaw Nauk Chemicznych Uniwersytetu Medycznego we Wrocławiu.

Badania cytotoksyczności hydrazydu **1** oraz pochodnych o budowie Zasad Schiffa wykonane zostały metodą MTT na różnych liniach komórek nowotworowych związanych z przewodem pokarmowym (linia komórkowa raka żołądka EPG, linie komórkowe raka jelita

grubego HT29, Caco-2, LoVo oraz LoVo/Dx) oraz na linii komórek prawidłowych jelita grubego (CCD 841 CoN). 5-Fluorouracyl oraz cisplatyna zostały użyte jako leki odniesienia. Spośród badanych związków 4-metoksybenzylidenowa pochodna **4h** (Rysunek 12, numeracja pochodzi z publikacji **P3**) wykazywała znaczące działanie przeciwko komórkom raka żołądka (IC_{50} = 12.10±3.10 μM). Z kolei najlepszą aktywność względem komórek nowotworowych jelita grubego wykazywały fluoropochodne (**4d** i **4e**) oraz związek z ugrupowaniem 4-dietyloaminobenzylidenowym (**4l**) (Rysunek 12), a wyznaczone dla nich wartości IC_{50} mieściły się w zakresie 52.80±4.20 – 84.60±4.00 μM. Wart podkreślenia jest fakt, że wszystkie badane związki wykazywały korzystniejszy profil bezpieczeństwa w porównaniu z lekami odniesienia.

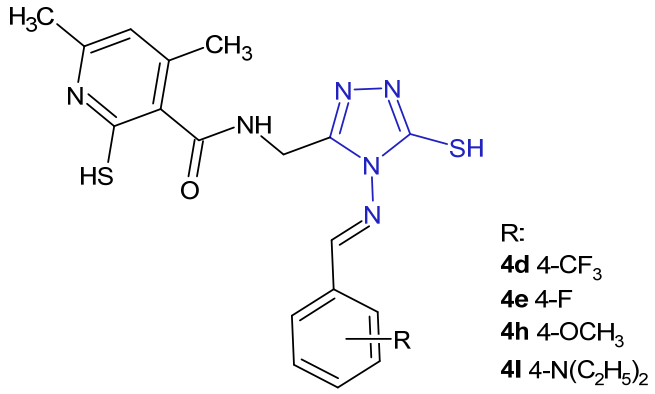

Rysunek 12. Struktury wybranych związków serii **III**.

W kolejnym badaniu - teście akumulacji rodaminy 123 (Rh-123), oceniono wpływ trzech wybranych zasad Schiffa **4d**, **4e** i **4l** na czynność transportową glikoproteiny P (P-gp) w komórkach raka jelita grubego linii HT-29, LoVo i LoVo/Dx. Wysoką ekspresją tego białka charakteryzują się nowotwory tkanek, w których w warunkach fizjologicznych również występuje wysoki poziom P-gp. Są to m.in. nowotwory jelita grubego oraz żołądka, charakteryzujące się dużą opornością na leczenie [55,56]. Wyniki najnowszych badań wskazują, że udział P-gp w oporności wielolekowej (*multidrug resistant*, MDR) nie ogranicza się tylko do zmniejszania stężenia cytostatyków wewnątrz komórek nowotworowych, ale także polega na hamowaniu procesu apoptozy [57,58]. Przeprowadzone eksperymenty wykazały, że związki **4d**, **4e** i **4l** zwiększały akumulację Rh-123, co było związane z hamowaniem czynności transportującej białka P-gp. Najsilniejszy efekt hamujący obserwowany był w lekoopornych komórkach nowotworowych LoVo/Dx, gdzie ekspresja białka P-gp jest dużo większa niż w pozostałych badanych liniach. Związek oznaczony symbolem **4l** okazał się najsilniejszym inhibitorem P-gp z badanej serii. Werapamil

zastosowany jako lek referencyjny wykazywał silniejsze działanie hamujące P-gp w obrębie komórek LoVo/Dx, a niższe dla linii HT-29 i LoVo w porównaniu ze związkami badanymi.

W celu zbadania właściwości proapoptotycznych pochodnych **4d**, **4e** oraz **4l** oceniono morfologię komórek nowotworowych jelita grubego HT-29 po inkubacji z badanymi związkami metodą barwienia aneksyną V i jodkiem propidyny. Wszystkie badane zasady Schiffa prowadziły do wzrostu odsetka komórek z cechami apoptozy w porównaniu z kontrolą (Rysunek 13). Najsilniejsze właściwości proapoptotyczne wykazywała pochodna oznaczona symbolem **4l** powodując 7.5-krotny wzrost odsetka komórek apoptotycznych. Jednocześnie obserwowano wzrost ilości komórek nekrotycznych do wartości maksymalnie 11.70%. Komórki traktowane doksorubicyną, jako lekiem referencyjnym, wykazywały większy odsetek komórek apoptotycznych i nekrotycznych w porównaniu z badanymi związkami.

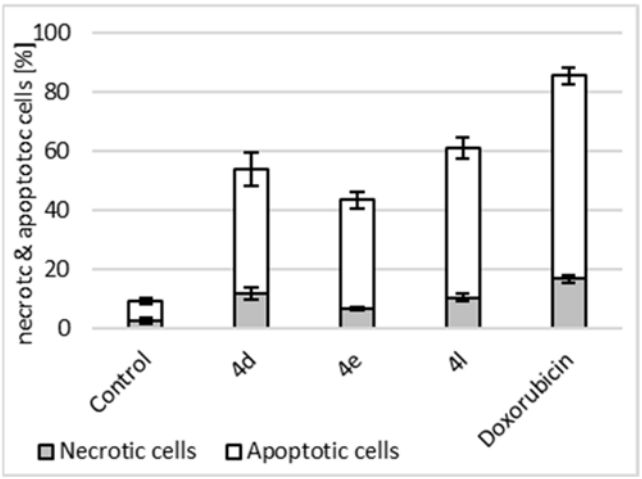

Rysunek 13. Wpływ związków **4d**, **4e** oraz **4l** na odsetek komórek apoptotycznych i nekrotycznych linii HT-29. Doksorubicyna została użyta jako lek referencyjny.

Najbardziej aktywną pochodną **4l** zbadano następnie w kierunku jej wpływu na poziom markerów apoptotycznych - proteiny p53 oraz kaspazy-3. Wiadomo, że kaspaza-3 jest główną kaspazą wykonawczą większości szlaków apoptozy, a wzrost jej stężenia uznano za znacznik postępu śmierci apoptotycznej [59]. Związek **4l** wyraźnie zwiększał stężenie kaspazy-3 w komórkach nowotworowych HT-29, jednak efekt ten był słabszy w porównaniu z doksorubicyną. Badany związek wpływał też na zwiększenie w komórkach linii HT-29 poziomu białka p53, będącego jednym z najważniejszych supresorów transformacji nowotworowej [60]. Biorąc pod uwagę powyższe wyniki, można założyć, że zasada Schiffa **4l** może działać cytotoksycznie poprzez kierowanie komórek nowotworowych na drogę śmierci apoptotycznej, będącej wynikiem wzrostu stężenia kaspazy-3 oraz białka p53.

Badania biologiczne związku **4l** poszerzono o pomiar stężenia interleukiny 6 (IL-6) w supernatantach hodowli komórkowej linii HT-29 za pomocą immunoenzymatycznego testu ELISA. IL-6 jest cytokiną o właściwościach prozapalnych, mającą istotne znaczenie w nowotworzeniu [61]. Jej podwyższony poziom został zauważony i powiązany ze złymi prognozami u pacjentów chorujących na raka jelita grubego [62]. Uzyskane wyniki pokazują, że badana zasada Schiffa tylko nieznacznie wpływa na obniżenie poziomu IL-6.

Badanie z zakresu dokowania molekularnego dla związku **4l** do centrum aktywnego białka MDM2, będącego negatywnym regulatorem białka p53 ujawniło, że związek dobrze wpasowuje się w kieszeń wiążącą MDM2, przy czym ugrupowania sulfanylowe pirydyny oraz triazolu brały udział w stabilizacji liganda w kieszeni (Rysunek 14). Związek **4l** został też przebadany pod kątem jego zdolności do oddziaływania z kaspazą-3. Badania dokowania potwierdzają możliwość oddziaływania zasady Schiffa z centrum aktywnym białka (Rysunek 15).

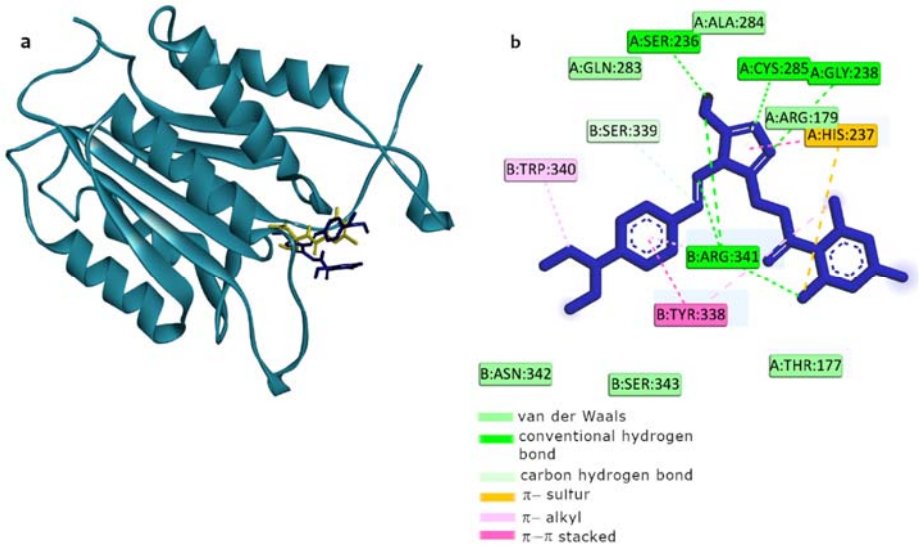

Rysunek 14. a) Położenie związku **4l** (granatowy) oraz znanego inhibitora (żółty) w kieszeni wiążącej kaspazy-3; b) oddziaływania związku **4l** z aminokwasami miejsca aktywnego kaspazy-3.

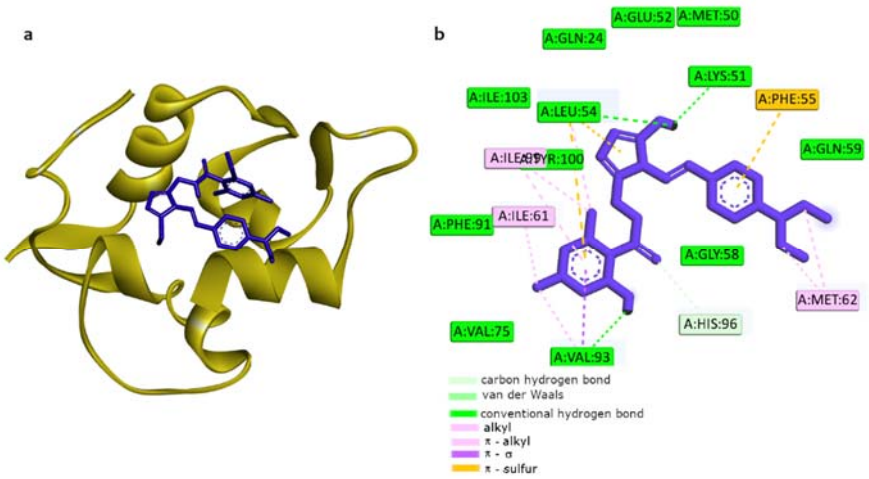

Rysunek 15. a) Położenie związku **4l** w kieszeni wiążącej MDM2; b) oddziaływania związku **4l** z aminokwasami miejsca aktywnego białka MDM2.

Powszechnie wiadomo, że aktywność biologiczna związków chemicznych jest wypadkową ich właściwości fizykochemicznych. Biorąc to pod uwagę, dla najaktywniejszych w badaniach *in vitro* związków wyznaczono teoretycznie m.in. wartości współczynnika podziału oktanol/woda (logP), a także obliczono liczbę miejsc o donorowym (*Hydrogen Bond Donor*, HBD) bądź akceptorowym (*Hydrogen Bond Acceptor*, HBA) charakterze dla wiązań wodorowych. Na podstawie tych danych oraz masy cząsteczkowej badanych związków (*Molecular Weight*, MW) korzystając z „reguły pięciu" opracowanej przez Lipińskiego można stwierdzić, że finalne zasady Schiffa spełniają określone kryteria lekopodobieństwa. Dalsza ocena dostępności biologicznej *in silico* wybranych związków sugeruje, że głównym izoenzymem zaangażowanym w metabolizm związków prawdopodobnie jest CYP2C19 oraz CYP2C9. Z przeprowadzonej analizy wynika również, że związki charakteryzują się słabym wchłanianiem jelitowym oraz nie przechodzą przez barierę krew-mózg. Wyniki analizy *in silico* wpływu hamującego na glikoproteinę P korelowały z tymi, uzyskanymi w badaniach *in vitro*.

5. PODSUMOWANIE I WNIOSKI

W ramach zrealizowanych prac badawczych, będących podstawą niniejszej rozprawy doktorskiej, zsyntetyzowano oraz przebadano w kierunku aktywności przeciwnowotworowej łącznie 35 nowych, nieopisanych dotąd pochodnych 4,6-dimetylo-2-sulfanylopirydyno-3-karboksyamidu.

Zaprojektowane związki otrzymano na drodze kilkuetapowej syntezy prowadzonej metodami klasycznymi. Jako substrat zastosowano związek **1** z resztą hydrazydową (Schemat 1), która w obecności odpowiednich reagentów ulegała cyklizacji do pochodnej 1,3,4-oksadiazolu. Stanowiła ona związek wyjściowy do otrzymania dwóch serii – *N*-acylowych pochodnych hydrazonów (seria **I**) oraz połączeń o budowie *N*-zasad Mannicha (seria **II**), opisanych w pracach, odpowiednio **P1** i **P2**. Z kolei produkt cyklizacji hydrazydu **1** zawierający pierścień 1,2,4-triazolu był podstawą do otrzymania pochodnych o budowie zasad Schiffa (seria **III**), opisanych w publikacji **P3**. Tożsamość nowych produktów finalnych oraz związków pośrednich potwierdzono za pomocą analizy spektralnej.

Przeprowadzone badania *in vitro* potwierdziły wysoki potencjał przeciwnowotworowy niektórych otrzymanych połączeń. Na podstawie wyników testu MTT stwierdzono, iż grupą związków charakteryzującą się najwyższą aktywnością cytotoksyczną były pochodne serii **I** o budowie *N*-acylohydrazonów, działające w stężeniach kilku mikromoli wobec linii niedrobnokomórkowego raka płuc (A549) oraz gruczolakoraka okrężnicy (LoVo), przy zachowaniu relatywnie niskiej toksyczności w stosunku do komórek prawidłowych (NHDF). Najbardziej obiecujący związek oznaczony symbolem **13**, posiadający ugrupowanie 2-bromobenzylidenowe, dodatkowo silnie hamował aktywność COX-1 i COX-2 oraz wykazywał działanie antyoksydacyjne, także w warunkach stresu oksydacyjnego. Może to sugerować jego znaczny potencjał chemoprewencyjny w terapii nowotworów. Dobrą bądź umiarkowaną aktywnością cytotoksyczną wobec linii komórkowych raka żołądka (EPG) oraz jelita grubego (HT-29) charakteryzowały się wybrane związki serii **III** o budowie zasad Schiffa. Należy zaznaczyć, że cechą wspólną związków serii **I** jak i **III** jest obecność w łańcuchu bocznym wiązania azometinowego (-CH=N-), będącego ugrupowaniem farmakoforowym obecnym w wielu związkach o właściwościach przeciwnowotworowych. Co warto podkreślić, najaktywniejsze pochodne tej serii okazały się być nietoksyczne (związek **4h**) lub ponad trzy razy mniej toksyczne (związki **4d**, **4e** i **4l**) względem komórek prawidłowych jelita grubego (CCD 841 CoN). Celem wyjaśnienia mechanizmu działania wybranych zasad Schiffa

przeprowadzono w warunkach hodowli komórkowych ocenę ich wpływu na aktywność transportową glikoproteiny P oraz badanie właściwości proapoptotycznych. Na jej podstawie można wyciągnąć wniosek, że działanie cytotoksyczne prawdopodobnie zachodzi na drodze apoptozy indukowanej hamowaniem P-gp oraz zwiększonym stężeniem kaspazy-3 oraz białka p53 w zmienionych nowotworowo komórkach. Analizując wyniki testu MTT *N*-zasad Mannicha serii **II** okazało się, że wprowadzanie ugrupowania aminometylowego do pochodnych 1,3,4-oksadiazolu zamiast reszty *N*-acylohydrazonowej niekorzystnie wpłynęło na aktywność cytotoksyczną. Najbardziej aktywnymi związkami tej serii były pochodne **5** i **6**, zawierające w swojej strukturze ugrupowanie 3,4-dichloro- oraz 4-trifluorometylofenylopiperazynowe. W poszerzonych badaniach biologicznych na liniach komórkowych czerniaka (C32 oraz A375) działały proapoptotycznie, a także zaburzały strukturę cytoszkieletu aktynowego badanych komórek.

Uzyskane wyniki aktywności przeciwnowotworowej związków serii **I** - **III** pozwoliły wyciągnąć ogólne wnioski na temat zależności między strukturą a aktywnością cytotoksyczną w grupie pochodnych 4,6-dimetylo-2-sulfanylopirydyno-3-karboksyamidu (Rysunek 16).

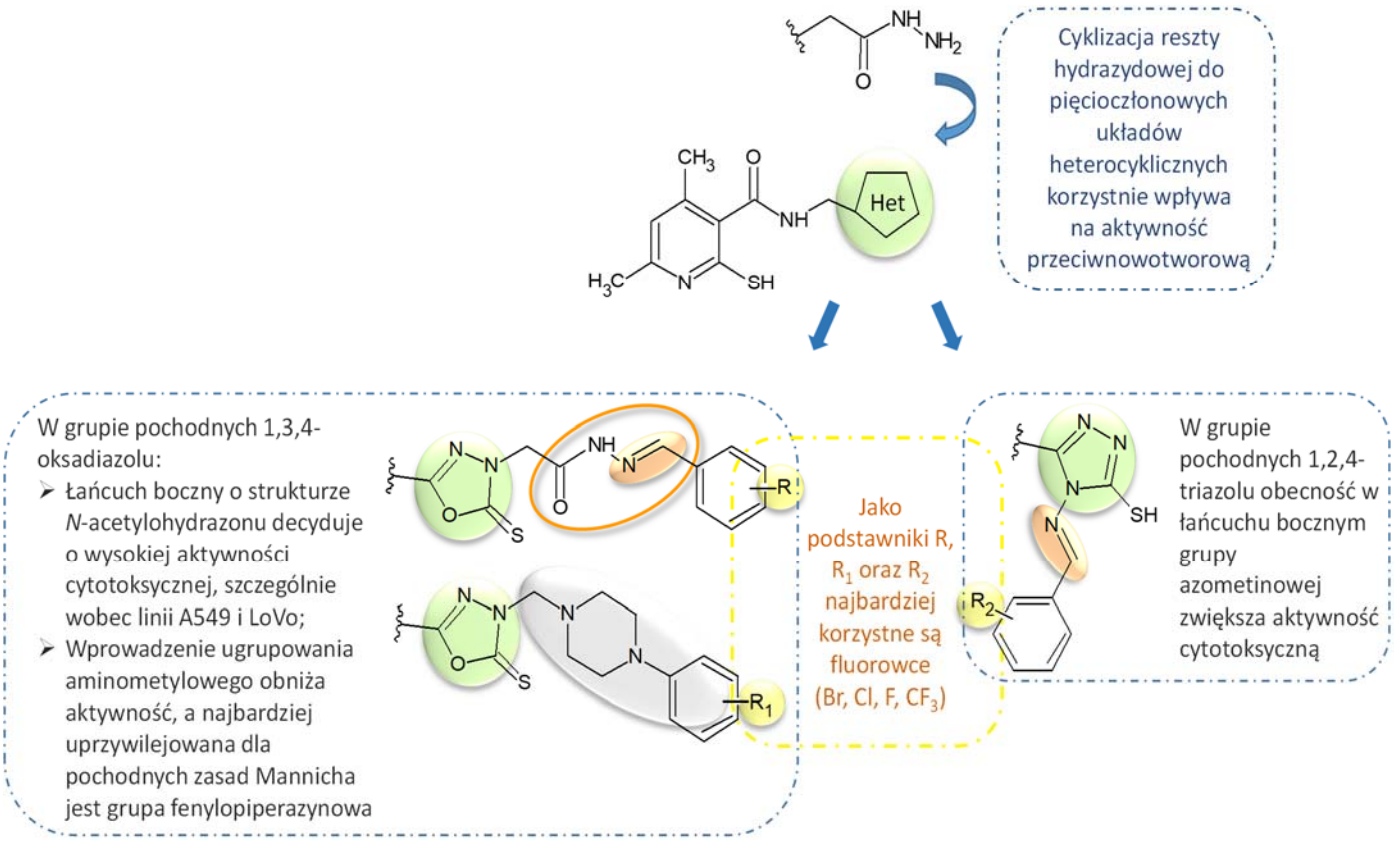

Rysunek 16. Ogólne zależności struktury i aktywności cytotoksycznej w grupie pochodnych 4,6-dimetylo-2-sulfanylopirydyno-3-karboksyamidu.

Z analizy SAR wynika, iż cyklizacja reszty hydrazydowej związku wyjściowego **1** (Schemat 1) do pięcioczłonowych pierścieni heterocyklicznych jest korzystna dla aktywności cytotoksycznej wobec komórek zmienionych nowotworowo. Dalsza modyfikacja polegająca na wprowadzaniu do pierścieni różnych ugrupowań zawierających elementy farmakoforowe (grupy azometinowa, *N*-acetylohydrazonowa, aminometylowa) w zmienny sposób wpływa na aktywność. Biorąc pod uwagę właściwości cytotoksyczne związków serii **I** i **III**, można założyć, że zarówno połączenia 1,3,4-oksadiazolu jak i 1,2,4-triazolu posiadające wiązanie azometinowe stanowią najbardziej interesujący kierunek dalszych badań w odniesieniu do aktywności przeciwnowotworowej w tej grupie pochodnych. Uwzględniając z kolei wpływ podstawienia pierścieni fenylowych obecnych w związkach serii **I – III** na aktywność widać, że najbardziej preferowane jest podstawienie grupami o charakterze elektonoakceptorowym, w szczególności fluorowcami (Br, Cl, F, CF_3).

Podsumowując należy stwierdzić iż, wyniki przeprowadzonych badań poszerzyły stan wiedzy w zakresie poszukiwania leków przeciwnowotworowych w grupie pochodnych 4,6-dimetylo-2-sulfanylopirydyno-3-karboksyamidu. Uzyskane informacje dotyczące cech strukturalnych najbardziej aktywnych związków stanowią podstawę do dalszych prac nad racjonalnym projektowaniem nowych cząsteczek o potencjalnej aktywności przeciwnowotworowej. Ponadto, obiecujące właściwości związków serii **I** stanowią zachętę do dalszych badań w kierunku określenia mechanizmu działania cytotoksycznego tych połączeń.

BIBLIOGRAFIA

[1] International Agency for Research on Cancer, https://gco.iarc.fr/today/en [*dostęp z dnia 5.02.2024*]

[2] Kapoor, G.; Bhutani, R.; Pathak, D. P.; Chauhan, G.; Kant, R.; Grover, P.; Nagarajan, K.; Siddiqui, S. A. Current Advancement in the Oxadiazole-Based Scaffolds as Anticancer Agents. *Polycyclic Aromatic Compounds* 2022, *42* (7), 4183–4215. https://doi.org/10.1080/10406638.2021.1886123.

[3] Gupta, O.; Pradhan, T.; Chawla, G. An Updated Review on Diverse Range of Biological Activities of 1,2,4-Triazole Derivatives: Insight into Structure Activity Relationship. *Journal of Molecular Structure* 2023, 1274, 134487. https://doi.org/10.1016/j.molstruc.2022.134487.

[4] Kassab, A. E. Anticancer Agents Incorporating the N-Acylhydrazone Scaffold: Progress from 2017 to Present. *Archiv der Pharmazie* 2023, 356, 2200548. https://doi.org/10.1002/ardp.202200548.

[5] Roman, G. Anticancer Activity of Mannich Bases: A Review of Recent Literature. *ChemMedChem*. 2022, 17, 202200258. https://doi.org/10.1002/cmdc.202200258.

[6] Sztanke, K.; Maziarka, A.; Osinka, A.; Sztanke, M. An Insight into Synthetic Schiff Bases Revealing Antiproliferative Activities in Vitro. *Bioorganic and Medicinal Chemistry* 2013, *21* (13), 3648–3666. https://doi.org/10.1016/J.BMC.2013.04.037.

[7] Wojciechowska, U.; Barańska, K.; Michałek, I.; Olasek, P.; Miklewska, M.; Didkowska, Cancer incidence and mortality in Poland in 2020. Nowotwory. *Journal of Oncology* 2023, 73 (3), 129-145. DOI: https://doi.org/10.5603/NJO.2023.0026

[8] Carneiro, B. A.; El-Deiry, W. S. Targeting Apoptosis in Cancer Therapy. *Nature Reviews Clinical Oncology* 2020, 395–417. https://doi.org/10.1038/s41571-020-0341-y.

[9] Manfredi, S. The "Old" Cytotoxic Drugs, the Basis of Anti-Cancer Treatments. *Therapies* 2022, *77* (2), 251–255. https://doi.org/10.1016/J.THERAP.2021.11.006.

[10] Dailah, H. G.; Hommdi, A. A.; Koriri, M. D.; Algathlan, E. M.; Mohan, S. Potential Role of Immunotherapy and Targeted Therapy in the Treatment of Cancer: A Contemporary Nursing Practice. *Heliyon* 2024, *10* (2), 24559. https://doi.org/10.1016/J.HELIYON.2024.E24559.

[11] Jalil, A. T.; Jehad, M. T.; Al-Ameer, L. R.; Khallawi, A. Q.; Essa, I. M.; Merza, M. S.; Zabibah, R. S.; Al-Hili, F. Revolutionizing Treatment for Triple-Negative Breast Cancer: Harnessing the Power of Exosomal MiRNAs for Targeted Therapy. *Pathology - Research and Practice* 2023, *250*, 154825. https://doi.org/10.1016/J.PRP.2023.154825.

[12] Belete, T. M. The Current Status of Gene Therapy for the Treatment of Cancer. *Biologics: Targets and Therapy* 2021, *15*, 67–77. https://doi.org/10.2147/BTT.S302095.

[13] Bukowski, K.; Kciuk, M.; Kontek, R. Mechanisms of Multidrug Resistance in Cancer Chemotherapy. *International Journal of Molecular Sciences* 2020, 21 (9), 3233. https://doi.org/10.3390/ijms21093233.

[14] Mohan Shankar, G.; Swetha, M.; Keerthana, C. K.; Rayginia, T. P.; Anto, R. J. Cancer Chemoprevention: A Strategic Approach Using Phytochemicals. *Frontiers in Pharmacology* 2022, 12, 809308. https://doi.org/10.3389/fphar.2021.809308.

[15] Maniewska, J.; Jeżewska, D. Non-steroidal Anti-inflammatory Drugs in Colorectal Cancer Chemoprevention. *Cancers* 2021, 13, 594. https://doi.org/10.3390/cancers13040594.

[16] Katona, B. W.; Weiss, J. M. Chemoprevention of Colorectal Cancer. *Gastroenterology* 2020, *158* (2), 368–388. https://doi.org/10.1053/J.GASTRO.2019.06.047.

[17] Chen, Y.; Luo, X.; Wang, Y.; Xing, Z.; Chen, J. Design and Synthesis Novel Amide Derivatives Containing an 1,3,4-Oxadiazole Moiety as Potential Antibacterial Agents. *Journal of Heterocyclic Chemistry* 2022, *59* (7), 1160–1168. https://doi.org/10.1002/jhet.4455.

[18] Glomb, T.; Świątek, P. Antimicrobial Activity of 1,3,4-Oxadiazole Derivatives. *International Journal of Molecular Sciences* 2021, 22, 6979. https://doi.org/10.3390/ijms22136979.

[19] Strzelecka, M.; Świątek, P. 1,2,4-Triazoles as Important Antibacterial Agents. *Pharmaceuticals* 2021, 14, 224. https://doi.org/10.3390/ph14030224.

[20] Wang, X.; Chai, J.; Kong, X.; Jin, F.; Chen, M.; Yang, C.; Xue, W. Expedient Discovery for Novel Antifungal Leads: 1,3,4-Oxadiazole Derivatives Bearing a Quinazolin-4(3*H*)-One Fragment. *Bioorganic and Medicinal Chemistry* 2021, *45*, 116330. https://doi.org/10.1016/J.BMC.2021.116330.

[21] Kazeminejad, Z.; Marzi, M.; Shiroudi, A.; Kouhpayeh, S. A.; Farjam, M.; Zarenezhad, E. Novel 1, 2, 4-Triazoles as Antifungal Agents. *BioMed Research International* 2022, 4584846. https://doi.org/10.1155/2022/4584846.

[22] Kaproń, B.; Czarnomysy, R.; Wysokiński, M.; Andrys, R.; Musilek, K.; Angeli, A.; Supuran, C. T.; Plech, T. 1,2,4-Triazole-Based Anticonvulsant Agents with Additional ROS Scavenging Activity Are Effective in a Model of Pharmacoresistant Epilepsy. *Journal of Enzyme Inhibition and Medicinal Chemistry* 2020, *35* (1), 993–1002. https://doi.org/10.1080/14756366.2020.1748026.

[23] Chauhan, B.; Kumar, R.; Salahuddin; Singh, H.; Afzal, O.; Altamimi, A. S. A.; Abdullah, M. M.; Yar, M. S.; Ahsan, M. J.; Kumar, N.; Yadav, S. K. Design, Synthesis, *In Vivo*, and *In Silico* Evaluation of Benzothiazoles Bearing a 1,3,4-Oxadiazole Moiety as New Antiepileptic Agents. *ACS Omega* 2022, 8, 2, 2520–2530. https://doi.org/10.1021/acsomega.2c06967.

[24] Hamoud, M. M. S.; Osman, N. A.; Rezq, S.; A. A. Abd El-wahab, H.; E. A. Hassan, A.; Abdel-Fattah, H. A.; Romero, D. G.; Ghanim, A. M. Design and Synthesis of Novel 1,3,4-Oxadiazole and 1,2,4-Triazole Derivatives as Cyclooxygenase-2 Inhibitors with Anti-Inflammatory and Antioxidant Activity in LPS-Stimulated RAW264.7 Macrophages. *Bioorganic Chemistry* 2022, *124*, 105808. https://doi.org/10.1016/J.BIOORG.2022.105808.

[25] Azim, T.; Wasim, M.; Akhtar, M. S.; Akram, I. An *in Vivo* Evaluation of Anti-Inflammatory, Analgesic and Anti-Pyretic Activities of Newly Synthesized 1,2,4-Triazole Derivatives. *BMC Complementary Medicine and Therapies* 2021, 21 (1). https://doi.org/10.1186/s12906-021-03485-x.

[26] Web of Science, https://www.webofscience.com/wos/woscc/basic-search [*dostęp 8.01.2024*]

[27] Elsawi, A. E.; Elbadawi, M. M.; Nocentini, A.; Almahli, H.; Giovannuzzi, S.; Shaldam, M.; Salem, R.; Ibrahim, T. M.; Abdel-Aziz, H. A.; Supuran, C. T.; Eldehna, W. M. 1,5-Diaryl-1,2,4-Triazole Ureas as New SLC-0111 Analogues Endowed with Dual Carbonic Anhydrase and VEGFR-2 Inhibitory Activities. *Journal of Medicinal Chemistry* 2023, *66* (15), 10558–10578. https://doi.org/10.1021/acs.jmedchem.3c00721.

[28] Thacker, P. S.; Angeli, A.; Argulwar, O. S.; Tiwari, P. L.; Arifuddin, M.; Supuran, C. T. Design, Synthesis and Biological Evaluation of Coumarin Linked 1,2,4-Oxadiazoles as Selective Carbonic Anhydrase IX and XII Inhibitors. *Bioorganic Chemistry* 2020, *98*, 103739. https://doi.org/10.1016/J.BIOORG.2020.103739.

[29] Naaz, F.; Ahmad, F.; Lone, B. A.; Pokharel, Y. R.; Fuloria, N. K.; Fuloria, S.; Ravichandran, M.; Pattabhiraman, L.; Shafi, S.; Shahar Yar, M. Design and Synthesis of Newer 1,3,4-Oxadiazole and 1,2,4-Triazole Based Topsentin Analogues as Anti-Proliferative Agent Targeting Tubulin. *Bioorganic Chemistry* 2020, *95*, 103519. https://doi.org/10.1016/J.BIOORG.2019.103519.

[30] Yousef, T. A.; Alhamzani, A. G.; Abou-Krisha, M. M.; Kanthimathi, G.; Raghu, M. S.; Kumar, K. Y.; Prashanth, M. K.; Jeon, B. H. Synthesis, Molecular Docking Study and Anticancer Activity of Novel 1,3,4-Oxadiazole Derivatives as Potential Tubulin Inhibitors. *Heliyon* 2023, *9* (2). https://doi.org/10.1016/j.heliyon.2023.e13460.

[31] Ono, Y.; Ninomiya, M.; Kaneko, D.; Sonawane, A. D.; Udagawa, T.; Tanaka, K.; Nishina, A.; Koketsu, M. Design and Synthesis of Quinoxaline-1,3,4-Oxadiazole Hybrid Derivatives as Potent Inhibitors of the Anti-Apoptotic Bcl-2 Protein. *Bioorganic Chemistry* 2020, *104*, 104245. https://doi.org/10.1016/J.BIOORG.2020.104245.

[32] Han, M. İ.; Tunç, C. Ü.; Atalay, P.; Erdoğan, Ö.; Ünal, G.; Bozkurt, M.; Aydın, Ö.; Çevik, Ö.; Küçükgüzel, G. Design, Synthesis, and *in Vitro* and *in Vivo* Anticancer Activity Studies of New (*S*)-Naproxen Thiosemicarbazide/1,2,4-Triazole Derivatives. *New Journal of Chemistry* 2022, *46* (13), 6046–6059. https://doi.org/10.1039/d1nj05899a.

[33] Shirzad, M. M.; Kulabaş, N.; Erdoğan, Ö.; Çevik, Ö.; Dere, D.; Yelekçi, K.; Danış, Ö.; Küçükgüzel, İ. Novel Azole-Urea Hybrids as VEGFR-2 Inhibitors: Synthesis, *in Vitro* Antiproliferative Evaluation and *in Silico* Studies. *Journal of Molecular Structure* 2023, *1294*, 136448. https://doi.org/10.1016/J.MOLSTRUC.2023.136448.

[34] Osmaniye, D.; Görgülü, Ş.; Sağlık, B. N.; Levent, S.; Özkay, Y.; Kaplancıklı, Z. A. Synthesis and Biological Evaluation of Novel 1,3,4-Oxadiazole Derivatives as Anticancer Agents and Potential EGFR Inhibitors. *Journal of Heterocyclic Chemistry* 2022, *59* (3), 518–532. https://doi.org/10.1002/jhet.4398.

[35] Świątek, P.; Gębczak, K.; Gębarowski, T.; Urniaz, R. Biological Evaluation and Molecular Docking Studies of Dimethylpyridine Derivatives. *Molecules* 2019, *24* (6). https://doi.org/10.3390/molecules24061093.

[36] Akdağ, K.; Tok, F.; Karakuş, S.; Erdoğan, Ö.; Çevik, Ö.; Koçyiğit-Kaymakçıoğlu, B. Synthesis and Biological Evaluation of Some Hydrazide-Hydrazone Derivatives as Anticancer Agents. *Acta Chimica Slovenica* 2022, *69* (4), 863–875. https://doi.org/10.17344/acsi.2022.7614.

[37] Popiołek, Ł.; Patrejko, P.; Gawrońska-Grzywacz, M.; Biernasiuk, A.; Berecka-Rycerz, A.; Natorska-Chomicka, D.; Piątkowska-Chmiel, I.; Gumieniczek, A.; Dudka, J.; Wujec, M. Synthesis and *in Vitro* Bioactivity Study of New Hydrazide-Hydrazones of 5-Bromo-2-Iodobenzoic Acid. *Biomedicine & Pharmacotherapy* 2020, *130*, 110526. https://doi.org/10.1016/J.BIOPHA.2020.110526.

[38] Han, M. İ.; Atalay, P.; Tunç, C. Ü.; Ünal, G.; Dayan, S.; Aydın, Ö.; Küçükgüzel, G. Design and Synthesis of Novel (*S*)-Naproxen Hydrazide-Hydrazones as Potent VEGFR-2 Inhibitors and Their Evaluation *in Vitro*/*in Vivo* Breast Cancer Models. *Bioorganic and Medicinal Chemistry* 2021, *37*, 116097. https://doi.org/10.1016/J.BMC.2021.116097.

[39] Nepali, K.; Sharma, S.; Sharma, M.; Bedi, P. M. S.; Dhar, K. L. Rational Approaches, Design Strategies, Structure Activity Relationship and Mechanistic Insights for Anticancer Hybrids. *European Journal of Medicinal Chemistry* 2014, *77*, 422–487. https://doi.org/10.1016/J.EJMECH.2014.03.018.

[40] Singh, A. K.; Kumar, A.; Singh, H.; Sonawane, P.; Paliwal, H.; Thareja, S.; Pathak, P.; Grishina, M.; Jaremko, M.; Emwas, A. H.; Yadav, J. P.; Verma, A.; Khalilullah, H.; Kumar, P. Concept of Hybrid Drugs and Recent Advancements in Anticancer Hybrids. *Pharmaceuticals*. 2022, 15 (9), 1071. https://doi.org/10.3390/ph15091071.

[41] Świątek, P.; Saczko, J.; Rembiałkowska, N.; Kulbacka, J. Synthesis of New Hydrazone Derivatives and Evaluation of Their Efficacy as Proliferation Inhibitors in Human Cancer Cells. *Medicinal Chemistry (Los. Angeles).* 2019, *15* (8), 903–910. https://doi.org/10.2174/1573406415666190128100524.

[42] Kumar, P.; Kadyan, K.; Duhan, M.; Sindhu, J.; Singh, V.; Saharan, B. S. Design, Synthesis, Conformational and Molecular Docking Study of Some Novel Acyl Hydrazone Based Molecular Hybrids as Antimalarial and Antimicrobial Agents. *Chemistry Central Journal* 2017, *11* (1), 115. https://doi.org/10.1186/s13065-017-0344-7.

[43] Munir, R.; Javid, N.; Zia-Ur-rehman, M.; Zaheer, M.; Huma, R.; Roohi, A.; Athar, M. M. Synthesis of Novel N-Acylhydrazones and Their c-n/n-n Bond Conformational Characterization by Nmr Spectroscopy. *Molecules* 2021, *26* (16). https://doi.org/10.3390/molecules26164908.

[44] Williams, C. S.; Mann, M.; Dubois, R. N.; The role of cyclooxygenases in inflammation, cancer, and development. *Oncogene* 1999, 18 (55), 7908-7916. doi:10.1038/sj.onc.1203286

[45] Dempke, W.; Rie, C.; Grothey, A.; Schmoll, H.-J. Cyclooxygenase-2: a novel target for cancer chemotherapy?. *Journal of Cancer Research and Clinical Oncology* 2001, 127(7), 411-417. doi:10.1007/s004320000225

[46] Howe, L. R. Inflammation and Breast Cancer. Cyclooxygenase/Prostaglandin Signaling and Breast Cancer. *Breast Cancer Research* 2007, 9 (4), 210. https://doi.org/10.1186/bcr1678.

[47] Negi, R. R.; Rana, S. V.; Gupta, V.; Gupta, R.; Chadha, V. D.; Prasad, K. K.; Dhawan, D. K. Over-Expression of Cyclooxygenase-2 in Colorectal Cancer Patients. *Asian Pacific Journal of Cancer Prevention* 2019, *20* (6), 1675–1681. https://doi.org/10.31557/APJCP.2019.20.6.1675.

[48] Bonekamp, N. A.; Völkl, A.; Fahimi, H. D.; Schrader, M. Reactive Oxygen Species and Peroxisomes: Struggling for Balance. *BioFactors* 2009, 35, 346–355. https://doi.org/10.1002/biof.48.

[49] Prasad, S.; Gupta, S. C.; Tyagi, A. K. Reactive Oxygen Species (ROS) and Cancer: Role of Antioxidative Nutraceuticals. *Cancer Letters* 2017, *387*, 95–105. https://doi.org/10.1016/J.CANLET.2016.03.042.

[50] Yamaguchi, H.; Condeelis, J. Regulation of the Actin Cytoskeleton in Cancer Cell Migration and Invasion. *Biochimica et Biophysica Acta (BBA) - Molecular Cell Reaserch* 2007, *1773* (5), 642–652. https://doi.org/10.1016/J.BBAMCR.2006.07.001.

[51] Nersesian, S.; Williams, R.; Newsted, D.; Shah, K.; Young, S.; Evans, P. A.; Allingham, J. S.; Craig, A. W. Effects of Modulating Actin Dynamics on HER2 Cancer Cell Motility and Metastasis. *Scientific Reports* 2018, *8* (1). https://doi.org/10.1038/s41598-018-35284-9.

[52] Arteaga, C. Targeting HER1/EGFR: A Molecular Approach to Cancer Therapy. *Seminars in Oncology* 2003, *30* (3H), 3–14. https://doi.org/10.1016/s0093-7754(03)00185-4.

[53] Sierra, J. R.; Tsao, M. S. C-MET as a Potential Therapeutic Target and Biomarker in Cancer. *Therapeutic Advances in Medical Oncology* 2011, S21–S35. https://doi.org/10.1177/1758834011422557.

[54] Vaishnavi, A.; Le, A. T.; Doebele, R. C. TRKing down an Old Oncogene in a New Era of Targeted Therapy. *Cancer Discovery* 2015, 25–34. https://doi.org/10.1158/2159-8290.CD-14-0765.

[55] Hinoshita, E.; Uchiumi, T.; Taguchi, K.-I.; Kinukawa, N.; Tsuneyoshi, M.; Maehara, Y.; Sugimachi, K.; Kuwano, M. Increased Expression of an ATP-Binding Cassette Superfamily Transporter, Multidrug Resistance Protein 2, in Human Colorectal Carcinomas 1. *Clinical Cancer Research* 2000, 6 (6), 2401-2407.

[56] Xu, H.-W.; Xu, L.; Hao, J.-H.; Liu, H. Expression of P-Glycoprotein and Multidrug Resistance-Associated Protein Is Associated with Multidrug Resistance in Gastric Cancer. *Journal of International Medical Research* 2010, 38 (1), 34-42. doi:10.1177/147323001003800104 2010; Vol. 38.

[57] Zu, Y.; Yang, Z.; Tang, S.; Han, Y.; Ma, J. Effects of P-Glycoprotein and Its Inhibitors on Apoptosis in K562 Cells. *Molecules* 2014, *19* (9), 13061–13075. https://doi.org/10.3390/molecules190913061.

[58] Souza, P. S.; Madigan, J. P.; Gillet, J. P.; Kapoor, K.; Ambudkar, S. V.; Maia, R. C.; Gottesman, M. M.; Leung Fung, K. Expression of the Multidrug Transporter P-Glycoprotein Is Inversely Related to That of Apoptosis-Associated Endogenous TRAIL.

Experimental Cell Research 2015, *336* (2), 318–328. https://doi.org/10.1016/j.yexcr.2015.06.005.

[59] Asadi, M.; Taghizadeh, S.; Kaviani, E.; Vakili, O.; Taheri-Anganeh, M.; Tahamtan, M.; Savardashtaki, A. Caspase-3: Structure, Function, and Biotechnological Aspects. *Biotechnology and Applied Biochemistry* 2022, 1633–1645. https://doi.org/10.1002/bab.2233.

[60] Kulesza, M.; Agnieszka, D. M.; Pieńkowska-Grela, B. Repair or Perish - The Role of P53 Protein in a Cell's Life. *Nowotwory*. Via Medica 2019, pp 168–178. https://doi.org/10.5603/NJO.2019.0031.

[61] Bromberg, J.; Wang, T. C. Inflammation and Cancer: IL-6 and STAT3 Complete the Link. *Cancer Cell* 2009, 79–80. https://doi.org/10.1016/j.ccr.2009.01.009.

[62] Waldner, M. J.; Foersch, S.; Neurath, M. F. Interleukin-6 - A Key Regulator of Colorectal Cancer Development. *International Journal of Biological Sciences*. 2012, 1248–1253. https://doi.org/10.7150/ijbs.4614.

CAŁKOWITY DOROBEK NAUKOWY

Małgorzata Anna Strzelecka

Wykaz publikacji

1. Publikacje w czasopismach naukowych

1.1 Publikacje w czasopiśmie z IF

Lp	Opis bibliograficzny	IF	Punkty ministerialne
1	Malinka Wiesław, Świątek Piotr, **Śliwińska Małgorzata**, Szponar Bogumiła, Gamian Andrzej, Karczmarzyk Zbigniew, Fruziński Andrzej: Synthesis of novel isothiazolopyridines and their in vitro evaluation against Mycobacterium and Propionibacterium acnes, Bioorganic & Medicinal Chemistry, 2013, vol. 21, nr 17, s. 5282-5291, DOI:10.1016/j.bmc.2013.06.027	2,951	30
2	Krzyżak Edward, **Śliwińska Małgorzata**, Malinka Wiesław: Synthesis and fluorescence properties of new ester derivatives of isothiazolo [4,5-b] pyridine, Journal of Fluorescence, 2015, vol. 25, nr 2, s. 277-282, DOI:10.1007/s10895-015-1504-6	1,601	25
3	Świątek Piotr, **Strzelecka Małgorzata**, Urniaz Rafał, Gębczak Katarzyna, Gębarowski Tomasz, Gąsiorowski Kazimierz, Malinka Wiesław: Synthesis, COX-1/2 inhibition activities and molecular docking study of isothiazolopyridine derivatives, Bioorganic & Medicinal Chemistry, 2017, vol. 25, nr 1, s. 316-326, DOI:10.1016/j.bmc.2016.10.036	2,881	30
4	Świątek Piotr, **Strzelecka Małgorzata**: Isothiazolopyridine Mannich bases and their antibacterial effect, Advances in Clinical and Experimental Medicine, 2019, vol. 28, nr 7, s. 967-972, DOI:10.17219/acem/99310	1,514	70
5	Nowak Maciej Roman, Zdunek Rafał, Pliński Edward, Świątek Piotr, **Strzelecka Małgorzata**, Malinka Wiesław, Plińska Stanisława: Recognition of pharmacological bi-heterocyclic compounds by using terahertz time domain spectroscopy and chemometrics, Sensors, 2019, vol. 19, nr 15, art.3349 [18 s.], DOI:10.3390/s19153349	3,275	100
6	**Strzelecka Małgorzata**, Świątek Piotr: 1,2,4-triazoles as important antibacterial agents, Pharmaceuticals, 2021, vol. 14, nr 3, art.224 [28 s.], DOI:10.3390/ph14030224	5,215	100
7	Świątek Piotr, Glomb Teresa, Dobosz Agnieszka, Gębarowski Tomasz, Wojtkowiak Kamil, Jezierska Aneta, Panek Jarosław J., Świątek Małgorzata, **Strzelecka Małgorzata**: Biological evaluation and molecular docking studies of novel 1,3,4-oxadiazole derivatives of 4,6-dimethyl-2-sulfanylpyridine-3-carboxamide, International Journal of Molecular Sciences, 2022, vol. 23, nr 2, art.549 [25 s.], DOI:10.3390/ijms23010549	5,6	140
8	**Strzelecka Małgorzata**, Glomb Teresa, Drąg-Zalesińska Małgorzata, Kulbacka Julita, Szewczyk Anna, Saczko Jolanta, Kasperkiewicz-Wasilewska Paulina, Rembiałkowska Nina, Wojtkowiak Kamil, Jezierska Aneta, Świątek Piotr: Synthesis, anticancer activity and molecular docking studies of novel n-mannich bases of 1,3,4-oxadiazole based on 4,6-dimethylpyridine scaffold, International Journal of Molecular Sciences, 2022, vol. 23, nr 19, art.11173 [24 s.], DOI:10.3390/ijms231911173	5,6	140
9	**Strzelecka Małgorzata**, Wiatrak Benita, Jawień Paulina, Czyżnikowska Żaneta, Świątek Piotr: New Schiff bases derived from dimethylpyridine-1,2,4-triazole hybrid as cytotoxic agents targeting gastrointestinal cancers: Design, synthesis, biological evaluation and molecular docking studies, Bioorganic Chemistry, 2023, vol. 139, art.106758 [14 s.], DOI:10.1016/j.bioorg.2023.106758	5,1*	140
SUMA:		**33,737**	**775**

*IF za 2022 rok

2. Monografie naukowe

2.3 Rozdziały

Lp	Opis bibliograficzny	Punkty ministerialne
1	Nowak Kacper, Grzelczak Michał, Szlachetko Bogusław, Sterczewski Łukasz A., Pliński Edward F., Świątek Piotr, **Strzelecka Małgorzata**, Plińska Stanisława: Terahertz investigations on some bi-heterocyclic compounds, W: 21st International Conference on Microwave, Radar and Wireless Communications (MIKON 2016). Kraków, Poland, 9-11 May, 2016 [USB-Drive], [Piscataway, NJ] 2016, IEEE, [3], ISBN 978-1-5090-2214-4, [Publikacja uwzględniona w Web of Science], DOI:10.1109/MIKON.2016.7492097	15
2	Nowak K., Grzelczak M.P., Szlachetko B., Sterczewski L.A., Pliński E.F., Świątek Piotr, **Strzelecka Małgorzata**, Plińska Stanisława, Malinka Wiesław: Chemometrics of bi-heterocyclic kind of drug specimens in the THz domain, W: 41st International Conference on Infrared, Millimeter, and Terahertz Waves (IRMMW-THz). Copenhagen, Denmark, September 25-30, 2016, [Piscataway, NJ] 2016, IEEE, [2], ISBN 978-1-4673-8485-8, [Publikacja uwzględniona w Web of Science], DOI:10.1109/IRMMW-THz.2016.7758792	15
3	Nowak M.R., Nowak K., Grzelczak M., Szlachetko B., Sterczewski L., Pliński E.F., Świątek Piotr, **Strzelecka Małgorzata**, Plińska Stanisława, Malinka Wiesław: Machine learning applied to bi-heterocyclic drugs recognition, W: 42nd International Conference on Infrared, Millimeter, and Terahertz Waves (IRMMW-THz). Cancun, Mexico, August 27 - September 01, 2017 [USB Drive], [Piscataway, NJ] 2017, IEEE, poz.TD.38, ISBN 978-1-5090-6049-8, [Publikacja w wydawnictwie z listy MNiSW], DOI:10.1109/IRMMW-THz.2017.8067180	20
SUMA:		**50**

4. Abstrakty

Lp	Opis bibliograficzny
1	Świątek Piotr, Malinka Wiesław, **Śliwińska Małgorzata**, Gamian Andrzej: New isothiazolopyridines and their in vitro antibacterial activity, W: The Eighth Multidisciplinary Conference on Drug Research - MKNOL 2012. Ossa k. Rawy Mazowieckiej, 30 May - 1 June 2012. Book of abstracts, Warszawa 2012, Pielaszek Research, 66-67 poz.99, ISBN 83-89585-34-0
2	Redzicka Aleksandra, Malinka Wiesław, **Śliwińska Małgorzata**, Szczęśniak-Sięga Berenika: Synthesis and antibacterial activity of pyrrolo[3,4-c]pyrrole derivatives, W: Vth Conversatory on Medicinal Chemistry. Lublin, 13-15.09.2012 2012, poz.P-60
3	**Śliwińska Małgorzata**, Redzicka Aleksandra, Świątek Piotr, Malinka Wiesław: Synteza nowych, amidowych pochodnych izotiazolo-[5,4-b]pirydyny o potencjalnej aktywności analgetycznej, W: Szkoła Chemii Medycznej. Wrocław, 17-18 października 2013 2013, [47] poz.PP-25
4	**Śliwińska Małgorzata**, Krzyżak Edward, Malinka Wiesław, Redzicka Aleksandra: Synthesis and fluorescence properties of new ester derivatives of isothiazolo[5,4- b]pyridine, W: VI Konwersatorium Chemii Medycznej. Lublin, 18-20 września 2014 2014, 176 poz.P97
5	**Śliwińska Małgorzata**, Redzicka Aleksandra, Świątek Piotr, Malinka Wiesław: Aktywność przeciwbakteryjna nowych, arylopiperazynowych pochodnych izotiazolo[5,4-b]pirydyny, W: II Sympozjum "Szkoła Chemii Medycznej". Wrocław, 17-19 czerwca 2015 2015, [78] poz.PP-34
6	Świątek Piotr, **Śliwińska Małgorzata**, Redzicka Aleksandra, Malinka Wiesław: Synthesis and potent antibacterial activity of new 4,6-dimethylpyridine derivatives, W: VII Konwersatorium Chemii Medycznej & VIII Sympozjum PTBI. Lublin, 17-19 września 2015 2015, 178 poz.P101, ISBN 978-83-63657-38-3
7	Redzicka Aleksandra, Świątek Piotr, **Śliwińska Małgorzata**, Malinka Wiesław, Secewicz Anna, Junka Adam: Synthesis and antimicrobial activity of pyrrole N-arylhydrazone derivatives, W: VIII Konwersatorium Chemii Medycznej. Lublin, 15-17.09.2016 2016, poz.P12

Lp	Opis bibliograficzny
8	Świątek Piotr, Glomb Teresa, Redzicka Aleksandra, **Strzelecka Małgorzata**: Isothiazolopyridine Mannich bases and their antibacterial effect, W: XI Multidyscyplinarna Konferencja Nauki o Leku "Nauka dla przemysłu, przemysł dla nauki". Warszawa, 14-16 listopada 2018. Książka abstraktów 2018, 119 poz.P39
9	**Strzelecka Małgorzata**, Przychodna Martyna, Glomb Teresa, Świątek Piotr: Synthesis of novel 1,2,4-triazole-3-thione-derived N-Mannich bases with potential pharmacological activity, W: X Konwersatorium Chemii Medycznej. Lublin, 3-5 września 2021. Book of abstracts, Lublin 2021, [116] poz.P67
10	**Strzelecka Małgorzata**, Wiatrak Benita, Jawień Paulina, Czyżnikowska Żaneta, Świątek Piotr: Design, synthesis and cytotoxic evaluation of new 1,2,4-triazole-Schiff bases, W: XI Konwersatorium Chemii Medycznej. [Lublin], 14-16 września 2023. Książka abstraktów [online] 2023, poz.P58

Impact factor: 33,737

Punkty ministerialne: 825

Signed by / Podpisano przez:

Dominika Sidorska

Date / Data: 2024-02-09 11:09

OSOBA SPORZĄDZAJĄCA: AGNIESZKA BARAN

FILIA NR 1 BG UMW

Wykaz projektów badawczych

1. Projekt w ramach subwencji Uniwersytetu Medycznego we Wrocławiu 2024 pt. „Synteza oraz badania właściwości antyangiogennych i przeciwnowotworowych nowych, hydrazonowych pochodnych izotiazolopirydyny.” [*numer w trakcie nadawania*], **Kierownik projektu**
2. Projekt dla Młodych Naukowców realizowany w latach 2014-2017 pt. „Synteza nowych pochodnych izotiazolo[5,4-b]pirydyny oraz pirolo-3,4-dikarboksyimidu o potencjalnej aktywności analgetycznej.”, Pbmn183, **Kierownik projektu**

Wykaz nagród

1. Nagroda JM Rektora Zespołowa I stopnia za osiągnięcia naukowe w 2022 r. za artykuł naukowy
2. Nagroda JM Rektora Zespołowa I stopnia za osiągnięcia naukowe w 2022 r. za artykuł naukowy
3. Nagroda JM Rektora (za osiągnięcia 2021) Zespołowa I stopnia za publikację
4. Nagroda JM Rektora (za osiągnięcia 2019) Zespołowa I stopnia za publikację
5. Nagroda JM Rektora (za osiągnięcia 2017) Zespołowa II stopnia za publikację
6. Zespołowa Nagroda JM Rektora (za osiągnięcia 2015) za cykl prac nt. syntezy, właściwości fizykochemicznych i farmakologicznych pochodnych układów heterocyklicznych

PUBLIKACJE WCHODZĄCE W SKŁAD ROZPRAWY DOKTORSKIEJ

PUBLIKACJA P1

WRAZ Z MATERIAŁAMI UZUPEŁNIAJĄCYMI

International Journal of
Molecular Sciences

IMPACT FACTOR 5.6
Indexed in: PubMed
CITESCORE 7.8

Article

Biological Evaluation and Molecular Docking Studies of Novel 1,3,4-Oxadiazole Derivatives of 4,6-Dimethyl-2-sulfanylpyridine-3-carboxamide

Piotr Świątek, Teresa Glomb, Agnieszka Dobosz, Tomasz Gębarowski, Kamil Wojtkowiak, Aneta Jezierska, Jarosław J. Panek, Małgorzata Świątek and Małgorzata Strzelecka

Special Issue
Bioactive Oxadiazoles 2.0

Edited by
Dr. Antonio Palumbo Piccionello

MDPI

https://doi.org/10.3390/ijms23010549

International Journal of
Molecular Sciences

MDPI

Article

Biological Evaluation and Molecular Docking Studies of Novel 1,3,4-Oxadiazole Derivatives of 4,6-Dimethyl-2-sulfanylpyridine-3-carboxamide

Piotr Świątek [1,*], Teresa Glomb [1,*], Agnieszka Dobosz [2], Tomasz Gębarowski [3], Kamil Wojtkowiak [4], Aneta Jezierska [4], Jarosław J. Panek [4], Małgorzata Świątek [5] and Małgorzata Strzelecka [1]

1 Department of Medicinal Chemistry, Faculty of Pharmacy, Wroclaw Medical University, Borowska 211, 50-556 Wroclaw, Poland; malgorzata.strzelecka@umw.edu.pl
2 Department of Medical Science Foundation, Faculty of Pharmacy, Wroclaw Medical University, Borowska 211, 50-556 Wroclaw, Poland; agnieszka.dobosz@umw.edu.pl
3 Department of Biostructure and Animal Physiology, Wroclaw University of Environmental and Life Sciences, Kożuchowska 1/3, 51-631 Wroclaw, Poland; tomasz.gebarowski@upwr.edu.pl
4 Faculty of Chemistry, University of Wroclaw, F. Joliot-Curie 14, 50-383 Wrocław, Poland; kamil.wojtkowiak@chem.uni.wroc.pl (K.W.); aneta.jezierska@chem.uni.wroc.pl (A.J.); jaroslaw.panek@chem.uni.wroc.pl (J.J.P.)
5 Hospital Pharmacy, University Clinical Hospital, Borowska 213, 50-556 Wrocław, Poland; mswiatek@usk.wroc.pl
* Correspondence: piotr.swiatek@umw.edu.pl (P.Ś.); teresa.glomb@umw.edu.pl (T.G.); Tel.: +48-717840391 (P.Ś. & T.G.)

check for updates

Citation: Świątek, P.; Glomb, T.; Dobosz, A.; Gębarowski, T.; Wojtkowiak, K.; Jezierska, A.; Panek, J.J.; Świątek, M.; Strzelecka, M. Biological Evaluation and Molecular Docking Studies of Novel 1,3,4-Oxadiazole Derivatives of 4,6-Dimethyl-2-sulfanylpyridine-3-carboxamide. *Int. J. Mol. Sci.* **2022**, *23*, 549. https://doi.org/10.3390/ijms23010549

Academic Editor: Antonio Palumbo Piccionello

Received: 1 December 2021
Accepted: 31 December 2021
Published: 4 January 2022

Publisher's Note: MDPI stays neutral with regard to jurisdictional claims in published maps and institutional affiliations.

Copyright: © 2022 by the authors. Licensee MDPI, Basel, Switzerland. This article is an open access article distributed under the terms and conditions of the Creative Commons Attribution (CC BY) license (https://creativecommons.org/licenses/by/4.0/).

Abstract: To date, chronic inflammation is involved in most main human pathologies such as cancer, and autoimmune, cardiovascular or neurodegenerative disorders. Studies suggest that different prostanoids, especially prostaglandin E_2, and their own synthase (cyclooxygenase enzyme-COX) can promote tumor growth by activating signaling pathways which control cell proliferation, migration, apoptosis, and angiogenesis. Non-steroidal anti-inflammatory drugs (NSAIDs) are used, alongside corticosteroids, to treat inflammatory symptoms particularly in all chronic diseases. However, their toxicity from COX inhibition and the suppression of physiologically important prostaglandins limits their use. Therefore, in continuation of our efforts in the development of potent, safe, non-toxic chemopreventive compounds, we report herein the design, synthesis, biological evaluation of new series of Schiff base-type hybrid compounds containing differently substituted *N*-acyl hydrazone moieties, 1,3,4-oxadiazole ring, and 4,6-dimethylpyridine core. The anti-COX-1/COX-2, antioxidant and anticancer activities were studied. Schiff base **13**, containing 2-bromobenzylidene residue inhibited the activity of both isoenzymes, COX-1 and COX-2 at a lower concentration than standard drugs, and its COX-2/COX-1 selectivity ratio was similar to meloxicam. Furthermore, the results of cytotoxicity assay indicated that all of the tested compounds exhibited potent anti-cancer activity against A549, MCF-7, LoVo, and LoVo/Dx cell lines, compared with piroxicam and meloxicam. Moreover, our experimental study was supported by density functional theory (DFT) and molecular docking to describe the binding mode of new structures to cyclooxygenase.

Keywords: dimethylpyridine; 1,3,4-oxadiazole; cyclooxygenase; cytotoxicity; molecular docking

1. Introduction

In recent years, the hybridization strategy has gained a noticeable attention in developing new medications. Hybrid molecules are designed through fusing at least two active pharmacophores in a single-hybrid molecule to improve the biological efficacy and minimize the possible toxicity relative to the parent drug. Hybridization strategy has been widely used to develop new anti-inflammatory drugs [1–3].

Inflammation is defined as a complex dynamic defensive process, in which the body responds to injury, infection via microbes, trauma, or toxins in the vascularized tissues. The influx of various cells of the host immune system (e.g., leukocytes, macrophages, mast cells), and release of numerous substances called inflammatory mediators (such as cytokines, free radicals, and eicosanoids, mainly prostaglandins) to the site of damage lead to pronounced vascular changes, including vasodilation, increased permeability and the formation of local edema, and the pain reaction associated with irritation of the pain receptors. This sequential cascade of events, both vascular and cellular, is responsible for the processes of repair, healing and reconstituting of damaged tissue. In pathological conditions the impairment of the effectiveness of repair mechanisms may be a major factor in the progression of various chronic diseases and disorders, including asthma, diabetes, cancer, cardiovascular diseases, arthritis, and inflammatory bowel disease [4–6].

Non-steroidal anti-inflammatory drugs (NSAIDs) are a diverse class of medicines commonly used for the treatment of acute and chronic inflammatory conditions, pain, and fever. Both their benefits and side effects arise due to inhibition of cyclooxygenase enzyme (COX) that catalyzes the conversion of arachidonic acid into prostaglandin H_2 (PGH_2), a precursor for the synthesis of biologically active prostanoids (prostaglandins PGD_2, PGE_2, PGF_{2a}, prostacyclin PGI_2, and thromboxane TxA_2). Currently, it is documented that there are, at least two COX isoforms, COX-1 and COX-2. The role of COX-1 (constitutively expressed in most tissue types) and COX-2 (generally considered as inducible) is complex and depends on many factors, mainly the organ in which it acts. It is well-known that therapy with non-selective COX inhibitors is associated with a number of side effects including gastrointestinal erosions, renal failure, the exacerbation of hypertension, sodium and water retention. That toxicity is attributed to the inhibition of the COX-1-mediated generation of the cytoprotective prostanoids, such as PGE_2 and PGI_2. The dissimilarity in the structure of COX-1 and COX-2 isoenzyme resulted in the development of selective COX-2 inhibitors referred to as coxibs. COX-2 expression is greatly increased at inflammatory sites in response to cytokines such as interferon, TNFα, IL1, hormones, growth factors and hypoxia. The introduction of COXIBs offered an efficacious alternative to non-selective NSAIDs with improved gastrointestinal tolerability. However, long-term placebo-controlled studies revealed cardiovascular side effects that led to the withdrawal of some COXIBs from the American and European markets [7–9]. Due to the complexity of inflammation, blocking the synthesis of prostanoids is not able to completely limit this process, therefore new compounds are also tested for multidirectional effects on other components, including the generation of reactive oxygen and nitrogen species, modulation and neutralization of inflammatory cytokines and biogenic amines released by stimulated inflammatory cells [5,10]. This pleiotropic approach could be the key to more effective inhibition of inflammation.

Over the past decades, it has been suggested that NSAIDs may have possible anticancer activity. This effect is attributed to the inhibition of COX enzymes, especially COX-2 activity, the overexpression of which in various neoplastic tissues promotes proliferation and inhibits apoptotic death of cancer cells, stimulates angiogenesis, and increases the ability to invade the tumor. These observations have led the researchers to study specific COX-2 inhibitors as chemopreventive and potential chemotherapeutic agents [4,11–13].

Compounds with a hydrazide-hydrazone pharmacophore moiety, otherwise known as *N*-acyl hydrazones, constitute a class of organic compounds that have great potential in medicinal chemistry in the design of new drugs. They contain an azomethine group (–NH–N=CH–) bound to the carbonyl group that is responsible for their multidirectional biological applications. In addition, this group can play a significant role as an organic intermediate for the synthesis of new, more complex compounds, e.g., heterocyclic. The versatility of *N*-acyl hydrazones in medical chemistry is based on the ease of their synthesis, as they are usually formed in a condensation reaction between aldehydes or ketones with hydrazides [14–16]. Literature studies show that the *N*-acyl hydrazone moiety is characterized by various activities, e.g., anticancer [17–20], antimicrobial [21–24], anticonvulsant [25]. The analgesic

and anti-inflammatory effect seems to be particularly important [26,27], and researchers have shown that many of the derivatives exhibit a mechanism of action related to the inhibition of cyclooxygenase [28,29]. This may result, firstly, from the relative acidity of the amide hydrogen of *N*-acyl hydrazone group, and secondly, from the ability of this group to stabilize free radicals. In addition, *N*-acyl hydrazone moiety has a structural similarity to *bis*-allylic moiety of unsaturated fatty acids, e.g., arachidonic acid [30–32].

The 1,3,4-oxadiazole ring, due to its properties, is an important element in the development of new drugs [33]. It is a bioisostere for carbonyl-containing derivatives, and is also a valid pharmacophore component, increasing the ability of oxadiazole-containing molecules to bind to a various ligands (e.g., muscarinic receptors, benzodiazepine receptors, dopamine, serotonin and norepinephrine transporters) [34–41]. According to the literature, compounds containing 1,3,4-oxadiazole moiety have confirmed various biological effects, including anticancer [42,43], antimicrobial [44–47], antidepressant [48] and anticonvulsant [49]. Particularly noteworthy is their analgesic and anti-inflammatory activity [50,51], in many cases associated with the inhibition of cyclooxygenase [52–54].

In our previous paper, we have reported the synthesis of twelve different Schiff base derivatives of *N*-(2-hydrazinyl-2-oxoethyl)-4,6-dimethyl-2-sulfanylpyridine-3-carboxamide (Figure 1) [55]. The compounds were tested for anti-COX, antioxidant and anticancer activity. The derivatives showed promising properties, therefore we decided to obtain analogous structures additionally containing the pharmacophoric ring of 1,3,4-oxadiazole. The heterocyclic moiety may enhance the pharmacological action of the entire molecule.

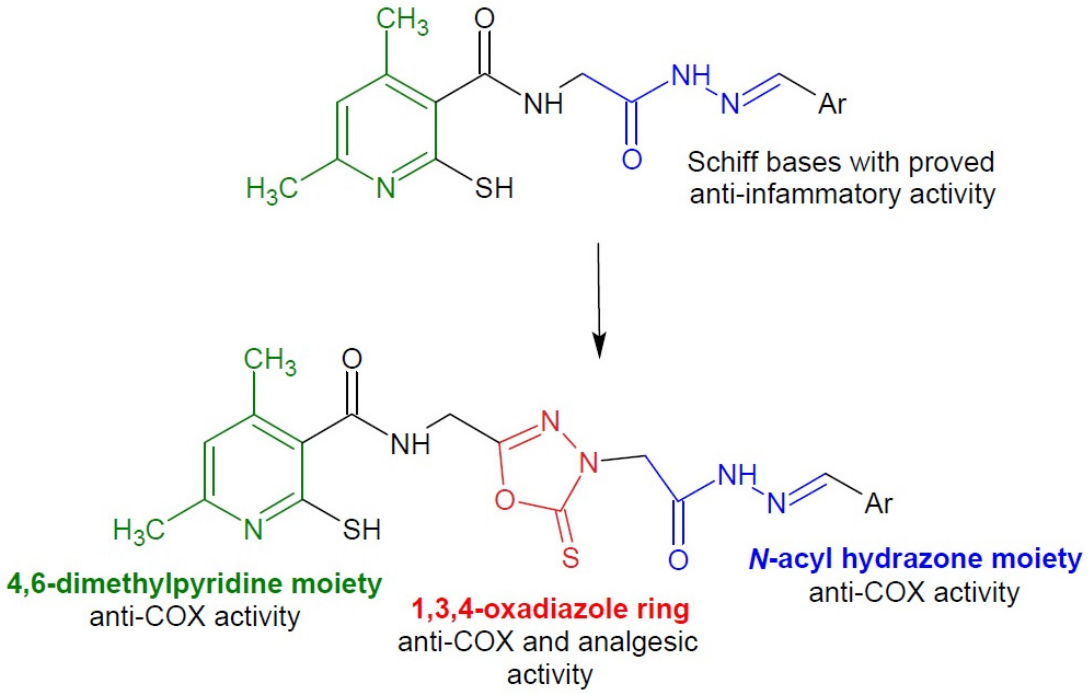

Figure 1. Scheme of the hybridization concept with the activity of individual structures.

Based on the above information, it can be concluded that our newly synthesized derivatives, which are hybrid compounds connecting the structure of 4,6-dimethylpyridine, 1,3,4-oxadiazole ring and *N*-acyl hydrazone moiety, may exhibit significant anti-inflammatory and chemopreventive effects, and their mechanism of action may be associated with anti-COX, antioxidant and anticancer activities (Figure 1). Considering that the binding pocket of COX-2 isoenzyme is bigger than that of COX-1, we expect that the extensive structure of new molecules will enhance the COX-2 selectivity compared to the previous Schiff bases, which inhibited COX-1 at lower concentrations than COX-2 [56].

The new compounds were examined as prospective COX-1/COX-2 inhibitors. Moreover, antioxidant and cytotoxic properties against A549 (pulmonary basial cell alveolar adenocarcinoma), MCF-7 (breast adenocarcinoma), LoVo (colon adenocarcinoma), and its drug resistant subline LoVo/Dx cell lines were studied to check the chemopreventive potential of the compounds. In addition, the structure study was performed on the basis of density functional theory (DFT) to investigate the energetic properties of the studied compounds depending on their conformation. Finally, molecular docking was carried out in order to suggest the binding mode and correlate it with biological activity.

2. Results and Discussion

2.1. Chemistry

The synthesis of *N*-(2-hydrazinyl-2-oxoethyl)-4,6-dimethyl-2-sulfanylpyridine-3-carboxamide **1** was performed according to the protocols published previously [19]. Scheme 1 presents the synthesis of compounds which have not been described in the literature yet. Analytical and spectroscopic properties of all newly obtained derivatives were in good agreement with their predicted structures and are summarized in the experimental section. Initially, compound **1** was heated at reflux in the presence of carbon disulfide in basic conditions in ethanol. Subsequently, the reaction mixture was poured onto crushed ice and acidified with hydrochloric acid. As a result, hydrazide **1** was subjected to intramolecular cyclization and formation of a five-membered 1,3,4-oxadiazol-2-thione ring. In the next step, compound **2** was reacted with ethyl bromoacetate in a water-ethanolic potassium hydroxide solution. Thus, the ester derivative **3** was obtained. Subsequently, compound **3** was converted into hydrazide **4** by reaction with hydrazine hydrate. The synthesis of nine different Schiff base derivatives of compound **4** was carried out by the reaction of compound **4** with several aromatic aldehydes in methanol in the presence of a catalytic amount of acetic acid with good yields. The purity of the synthesized compounds was checked by elemental analyses. The structures of the various synthesized compounds were determined based on spectral data analysis, such as FT-IR and ^{1}H NMR and ^{13}C NMR.

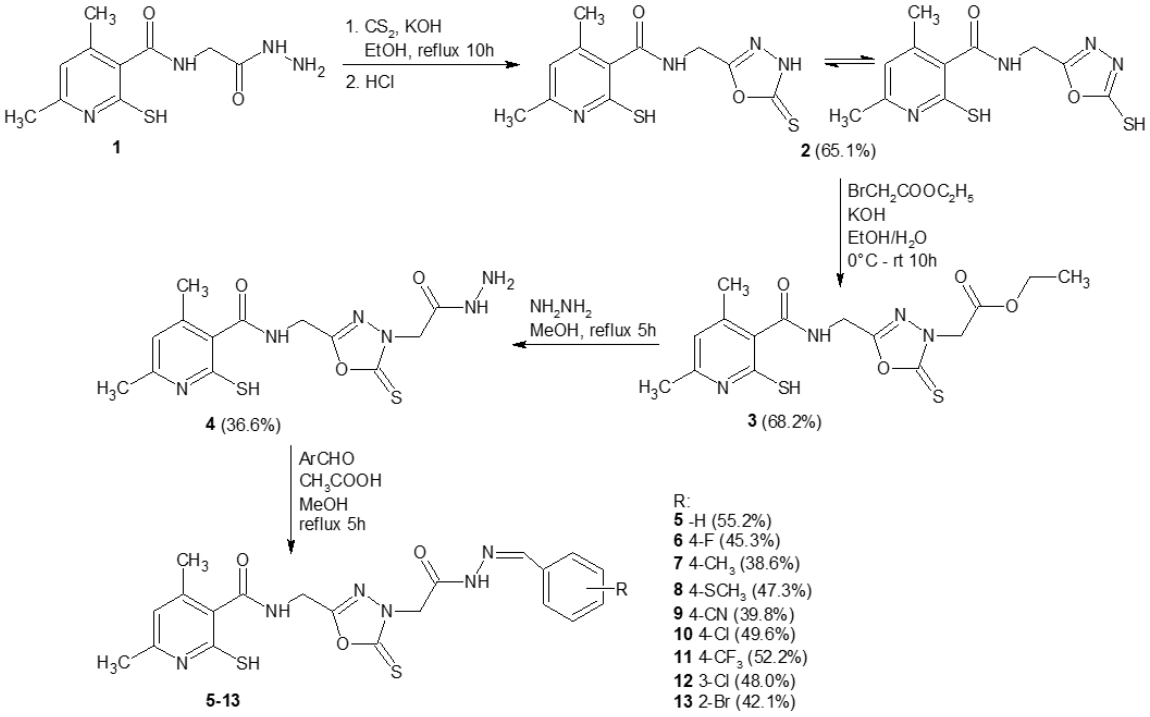

Scheme 1. Scheme of the synthesis of new compounds **5**–**13** with the yields in brackets.

The FT-IR spectrum of hydrazide **4** showed peaks at 1648 and 1623 cm^{-1} due to two carbonyl functions derived from the amide and hydrazide structure. Additionally, the IR spectra of compounds **4** and **5–13** exhibited in the 3294–3035 cm^{-1} range, the NH_2 and NH weak band of the $NHNH_2$, CONH and CONH-N= functions.

The ^{1}H NMR spectrum of hydrazide **4** displayed no signals belonging to the OCH_2CH_3 group; instead, new signals derived from the hydrazide structure appeared at 6.07 ($NHN\mathbf{H_2}$) and 9.29 ($N\mathbf{H}NH_2$) ppm integrating for two protons and one proton, respectively. The ^{1}H NMR spectra of compounds **5–13** displayed additional signals due to the azomethine group and the aromatic ring derived from the aldehyde moiety at the aromatic region, while the signal belonging to NH_2 group of the hydrazide structure did not appear.

It should be noted that the ^{1}H NMR spectra of compounds **5–13** show double signals corresponding to two amidic NH protons, azometine moiety protons and methylene protons. According to the literature, compounds having an arylidene-hydrazide structure may exist as *E*/*Z* geometrical isomers around the C=N double bond and as *cis*/*trans* amide conformers. It has been reported that when compounds containing an imine bond are dissolved in dimethyl-d_6 sulfoxide, they are present in the form of a geometrical *E* isomer. The *Z* isomer can be stabilized in less polar solvents by an intramolecular hydrogen bond [57–60]. In this study, the spectral data were obtained in dimethyl-d_6 sulfoxide solution and no signal belonging to *Z* isomer was observed. On the other hand, the *cis-trans* conformers of *E* isomer were present in the dimethyl-d_6 sulfoxide solution of compounds **5–13**. In the ^{1}H NMR spectra of **5–13**, in particular, two sets of signals each belonging to the CH_2 group, N=CH group and CONH group of *cis* and *trans* conformers were observed between 3.96 and 4.44, 7.96 and 8.54, 11.56 and 11.99 ppm respectively. The upfield lines of protons of the listed groups were assigned to the *cis*-conformer of the amide structure, while the downfield lines of the protons of the same groups were assigned to the *trans*-conformer of the amide structure [59].

2.2. Biological Tests

2.2.1. Cyclooxygenase Inhibition Assay

The compounds were studied for their potencies to inhibit COX-1 and COX-2 enzymes by the colorimetric inhibitor screening assay. The IC_{50} values (i.e., the concentration of tested compounds (μM) that can exert 50% inhibition of the enzyme activity) and the COX-2/COX-1 selectivity ratios were calculated after 2 min of incubation for each investigated and reference compound (piroxicam and meloxicam).

As can be seen from the data presented in Table 1, hydrazide **4** and its 4-methylsulfanylbenzylidene derivative **8** showed only COX-1 inhibitory activity, while the compound with 4-chlorobenzylidene moiety **10** selectively inhibited the activity of COX-2 isoenzyme. Four of the Schiff bases **5**, **11**, **12** and **13** with unsubstituted benzylidene moiety or containing 4-trifluoro, 3-chloro, 2-bromo groups, respectively exhibited higher anti-COX-1 activity compared with piroxicam and meloxicam. What is more, compound **13** inhibited the activity of COX-2 at a lower concentration than standards, and its COX-2/COX-1 selectivity ratio was similar to meloxicam.

2.2.2. MTT Assay

The MTT (3-[4,5-dimethylthiazol-2-yl]-2,5-diphenyl tetrazolium bromide) assay was used to determine the cytotoxicity of tested compounds towards different cell lines: normal human dermal fibroblasts (NHDF), kidney epithelial cells (VERO), fibroblasts from Chinese hamster lung (V79) and four human cancer cells: A549 (pulmonary basal cell alveolar adenocarcinoma), MCF-7 (breast adenocarcinoma), LoVo (colon adenocarcinoma), and its drug resistant subline LoVo/Dx. The cell lines used in this study express COX-1 and COX-2. The LoVo line expressed COX-1, the LoVo/Dx subline express both COX-1 and COX-2 [61]. The A549 and MCF-7 lines shows expression of both enzymes [62,63].

Table 1. IC_{50} values and mean SD for COX-1 and COX-2 activities after 2 min of incubation with tested compounds, $n = 5$.

Compound	IC_{50} [μM] ± SD		COX-2/COX-1 Selectivity Ratio
	COX-1	COX-2	
4	135.20 ± 5.99	NA	-
5	73.91 ± 3.03	186.95 ± 15.25	2.53
6	144.79 ± 20.88	173.93 ± 5.84	1.20
7	147.55 ± 19.81	184.43 ± 18.84	1.25
8	156.65 ± 12.12	NA	-
9	153.89 ± 6.29	102.58 ± 10.61	0.67
10	NA	127.54 ± 1.87	-
11	86.19 ± 2.60	169.75 ± 19.14	1.97
12	66.84 ± 5.19	90.71 ± 19.61	1.36
13	84.37 ± 5.89	73.23 ± 5.66	0.80
Piroxicam	87.44 ± 4.17	80.11 ± 1.26	0.92
Meloxicam	128.76 ± 4.72	76.38 ± 6.46	0.59

Note: Data are shown as a mean ± standard deviation, NA stands for "not applicable".

This assay is suitable for the measurement of drug sensitivity in cultured cells, specified as the concentration of the compound required to achieve 50% growth inhibition, compared to the growth of the control cultured without any drug (50% inhibitory concentration, IC_{50}) [64]. The results of the experiment were made for screening purpose, and are presented in Table 2.

Table 2. MTT results—NHDF, VERO, V79, A459, MCF-7, LoVo and LoVo/Dx IC_{50} (μM) values and mean SD for the studied compounds.

Compound	IC_{50} [μM] ± SD						
	NHDF	VERO	V79	A549	MCF-7	LoVo	LoVo/Dx
4	57.46 ± 1.22	77.44 ± 5.84	71.70 ± 5.80	3.84 ± 0.30	9.63 ± 1.66	3.01 ± 0.20	5.73 ± 3.84
5	58.97 ± 1.49	100.1 ± 13.49	84.30 ± 3.40	3.62 ± 0.43	6.37 ± 1.09	3.13 ± 0.17	5.69 ± 1.03
6	58.21 ± 0.92	59.62 ± 5.42	80.70 ± 5.60	4.05 ± 0.26	6.37 ± 0.19	3.20 ± 0.26	7.07 ± 2.48
7	58.23 ± 2.00	68.31 ± 3.24	47.70 ± 1.73	3.72 ± 0.54	6.33 ± 0.56	3.46 ± 0.39	7.89 ± 1.78
8	58.69 ± 1.94	50.38 ± 2.45	71.10 ± 2.40	4.34 ± 0.56	9.41 ± 4.80	3.60 ± 0.55	21.00 ± 5.92
9	59.44 ± 1.90	89.76 ± 8.43	77.70 ± 4.41	3.36 ± 0.20	8.22 ± 5.98	3.24 ± 0.10	6.87 ± 1.45
10	59.90 ± 2.04	129.8 ± 9.50	56.10 ± 5.42	3.52 ± 0.19	6.19 ± 0.19	3.12 ± 0.23	22.31 ± 2.10
11	58.99 ± 3.62	104.5 ± 4.98	55.20 ± 2.75	3.72 ± 0.24	8.29 ± 4.45	3.12 ± 0.31	17.50 ± 8.73
12	58.73 ± 2.21	79.2 ± 14.44	52.80 ± 7.20	3.88 ± 0.50	9.04 ± 2.84	3.07 ± 0.21	22.56 ± 8.19
13	59.26 ± 3.43	55.66 ± 1.84	65.40 ± 4.04	3.16 ± 0.21	7.23 ± 0.49	2.89 ± 0.08	9.40 ± 5.97
Piroxicam	162.23 ± 22.85	NA	213.10 ± 23.25	110.12 ± 28.23	NA	122.16 ± 10.20	125.50 ± 11.23
Meloxicam	195.66 ± 35.22	NA	200.80 ± 17.80	148.30 ± 27.58	NA	129.56 ± 8.80	142.30 ± 9.46

Note: Data are shown as a mean ± standard deviation, NA stands for "not applicable".

Firstly, the effect of the new compounds on healthy cells (NHDF, V79 and VERO) were performed. With regards to NHDF cells, both, hydrazide **4** and all of the Schiff bases exhibited similar toxicity (IC_{50} in the range of 57.47–59.9 μM). The VERO line exhibited more differences in cells sensitivity: there was no toxicity caused to VERO cells by standard compounds (piroxicam and meloxicam) and IC_{50} for tested compounds was in the range 50.38 μM for compound **8** to 129.8 μM for compound 10. The results for V79 cell line were more similar to NHDF cells: IC_{50} was in the range 47.70 μM (for compound **7**) to 84.30 μM (for compound **5**).

The anti-cancer activity of the tested compounds was established towards A549 cell line. A549 cells are adenocarcinomic human alveolar basal epithelial cells, used as a model of lung adenocarcinoma [65]. Inhibitory concentrations caused 50% of growth inhibition for these cells were similar for all tested compounds (3.16–4.34 μM), and was 25 to 35 times lower than that of piroxicam and meloxicam. The next tested cell line was MCF-7 from human breast adenocarcinoma. In this case, the standard compounds possessed no antitumor activity in the range of used concentrations, while the inhibitory

concentrations of tested compounds were in the range of 6.33–9.63 μM. Antitumor activity towards LoVo cells (from human colon) was similar as for A549 cells, and the inhibitory concentrations were 34- to 45-fold lower than that of piroxicam and meloxicam. The drug resistant subline LoVo/Dx exhibited more different sensitivity to the tested compounds. Hydrazide **4** and five Schiff bases **5**, **6**, **7**, **9** and **13** with unsubstituted benzylidene moiety or containing 4-fluoro, 4-methyl, 4-cyano and 2-bromo groups, respectively inhibited the growth of LoVo/Dx cells in the concentrations 13- to 22-fold lower than the standards.

The performed investigation revealed that all tested compounds had more significant anticancer activity than piroxicam and meloxicam. Moreover, the therapeutic index, i.e., the ratio of the concentrations that inhibit 50% of healthy and cancerous cells (A549, MCF-7 and LoVo cell lines) was high for all investigated compound, and the IC_{50} values for tumor cells were 1.3- and even 27-fold lower than for normal cells (Table 3).

Table 3. Therapeutic index calculated by ratio of concentrations that inhibit 50% of healthy and cancerous cells.

Compound	Therapeutic Index			
	NHDF/A549	**NHDF/MCF-7**	**NHDF/LoVo**	**NHDF/LoVo/Dx**
4	14.40 ± 0.70 [a]	6.16 ± 0.98 [a]	18.26 ± 1.20 [a]	8.97 ± 3.21
5	15.82 ± 1.78 [a]	9.29 ± 1.29 [a]	16.93 ± 1.34 [a]	7.60 ± 1.50 [a]
6	13.64 ± 1.32 [a]	9.21 ± 0.03 [a]	16.51 ± 2.01 [a]	2.94 ± 0.77 [a]
7	17.71 ± 0.49 [a]	9.42 ± 0.54 [a]	18.35 ± 0.02 [a]	8.88 ± 1.63 [a]
8	17.03 ± 0.34 [a]	7.76 ± 4.27	19.24 ± 0.77 [a]	2.70 ± 0.16 [a]
9	15.86 ± 0.05 [a]	12.10 ± 5.01	18.96 ± 0.73 [a]	4.02 ± 2.04
10	15.26 ± 1.41 [a]	9.49 ± 0.07 [a]	19.16 ± 0.59 [a]	2.84 ± 1.00
11	18.76 ± 0.16 [a]	8.87 ± 5.03	20.49 ± 0.62 [a]	8.89 ± 3.50
12	1.50 ± 0.18 [a]	18.67 ± 3.51 [a]	1.32 ± 0.07 [a]	1.29 ± 0.07 [a]
13	1.32 ± 0.01 [a]	26.92 ± 3.05 [a]	1.50 ± 0.17 [a]	1.37 ± 0.16
Piroxicam	15.01 ± 0.86 [a]	-	19.13 ± 0.87 [a]	15.31 ± 6.67
Meloxicam	16.41 ± 1.55 [a]	-	18.86 ± 0.55 [a]	10.57 ± 1.68 [a]

Note: Data are shown as a mean ± standard deviation. [a] Represents the significance level at $p < 0.05$.

2.2.3. Evaluation of Reactive Oxygen Species (ROS) Level Inside the Cells

ROS participates in various redox-regulatory mechanisms of cells to maintain homeostasis. When the system's ability to neutralize and eliminate free radicals and active intermediates fails, the intracellular redox potential shifts towards oxidative stress leading to DNA mutations, which can further promote neoplastic transformation. A chronic inflammation is the main system capable of inducing an oxidative stress. Prostaglandins induce the expression of certain inflammatory cytokines, which can, in turn, enhance the production of ROS. The inhibition of these paths at an early stage of neoplasia may be a critical moment in the process of chemoprevention. [66]. Taking this into account, the next part of the investigations was the ROS scavenging activity of studied compounds examined under or without the influence of oxidative stress, generated by the presence of H_2O_2 inside the cell cultures. As in the previous tests, two oxicams (meloxicam and piroxicam) were taken as the reference drugs (Tables 4 and 5) due to their proven ability to scavenging ROS [67–69].

Two cell lines were chosen for investigations: V79 (Chinese hamster lung fibroblasts) and LoVo. V79 normal cells are widely used as the cell line tested in the studies of the oxidative stress [70–72]. These cells are a living system model to explain the mechanism of ROS effects caused by varied compounds [73].

The tests established on V79 cell line revealed that among ten tested compounds, two of them (hydrazide **4** and Schiff base **13** containing 2-bromobenzylidene group) showed significant ROS scavenging activity under normal conditions almost two times higher than the standard drugs. The same compounds exhibited the best values during oxidative stress, induced by H_2O_2 (Table 4).

Table 4. ROS scavenging activity of tested compounds on V79 cell line. The results were expressed as E/E_0 ratios, where E_0 are the control samples without tested compounds, $n = 5$.

Compound	without H_2O_2	with H_2O_2
	Mean $E/E_0 \pm$ SD	
4	0.53 ± 0.22 [a]	0.42 ± 0.08 [a]
5	0.82 ± 0.13	0.59 ± 0.21 [a]
6	0.82 ± 0.17	0.97 ± 0.11
7	1.03 ± 0.39	0.81 ± 0.23
8	0.85 ± 0.29	0.72 ± 0.11 [a]
9	0.78 ± 0.31	0.71 ± 0.12 [a]
10	0.73 ± 0.27	0.82 ± 0.37
11	0.67 ± 0.24	1.12 ± 0.20
12	0.68 ± 0.27	0.62 ± 0.25
13	0.59 ± 0.08 [a]	0.50 ± 0.15 [a]
Piroxicam	0.98 ± 0.17	0.67 ± 0.17 [a]
Meloxicam	1.15 ± 0.19	0.85 ± 0.18
Ascorbic acid	0.83 ± 0.13	0.22 ± 0.12 [a]
Trolox	0.71 ± 0.05 [a]	0.15 ± 0.08 [a]

Note: Data are shown as a mean ± standard deviation. [a] Represents the significance level at $p < 0.05$.

Table 5. ROS scavenging activity of tested compounds on LoVo cell line. The results were expressed as E/E_0 ratios, where E_0 are the control samples without tested compounds, $n = 5$.

Compound	without H_2O_2	with H_2O_2
	Mean $E/E_0 \pm$ SD	
4	0.69 ± 0.33	0.83 ± 0.08 [a]
5	0.72 ± 0.21	0.87 ± 0.21
6	0.74 ± 0.22	0.88 ± 0.04 [a]
7	1.07 ± 0.38	0.95 ± 0.27
8	0.65 ± 0.20 [a]	0.80 ± 0.22
9	0.76 ± 0.22	0.91 ± 0.19
10	0.85 ± 0.27	0.91 ± 0.14
11	1.24 ± 0.65	0.84 ± 0.17
12	0.91 ± 0.43	0.79 ± 0.16
13	0.70 ± 0.30	0.69 ± 0.10[a]
Piroxicam	0.72 ± 0.19	0.81 ± 0.19
Meloxicam	1.06 ± 0.32	0.89 ± 0.16
Ascorbic acid	0.89 ± 0.11	0.32 ± 0.09 [a]
Trolox	0.85 ± 0.13	0.29 ± 0.15 [a]

Note: Data are shown as a mean ± standard deviation. [a] Represents the significance level at $p < 0.05$.

Considering the test on LoVo line 4-methylsulphanylbenzylidene derivative (**8**) showed high ROS scavenging activity under normal conditions. On the other hand the best activity during oxidative stress characterized compounds **4** and **13** as in the case of the first cell line V79 (Table 5, Figure 2).

Comparing the antioxidant activity of our ten tested compounds to standard ROS scavengers: trolox and ascorbic acid, we can see that the activity of all compounds tested on V79 line, is lower than trolox and ascorbic acid (Table 4). Trolox and ascorbic acid antioxidant activities were previously tested by Szczęśniak-Sięga et al. on V79 cell line in the similar conditions, and the values of their mean E/E_0 were similar to our results [74]. The same situation is observed for LoVo line, where the antioxidant activity of tested compounds were also lower than for standard scavengers, but very similar for all tested compounds (Table 5).

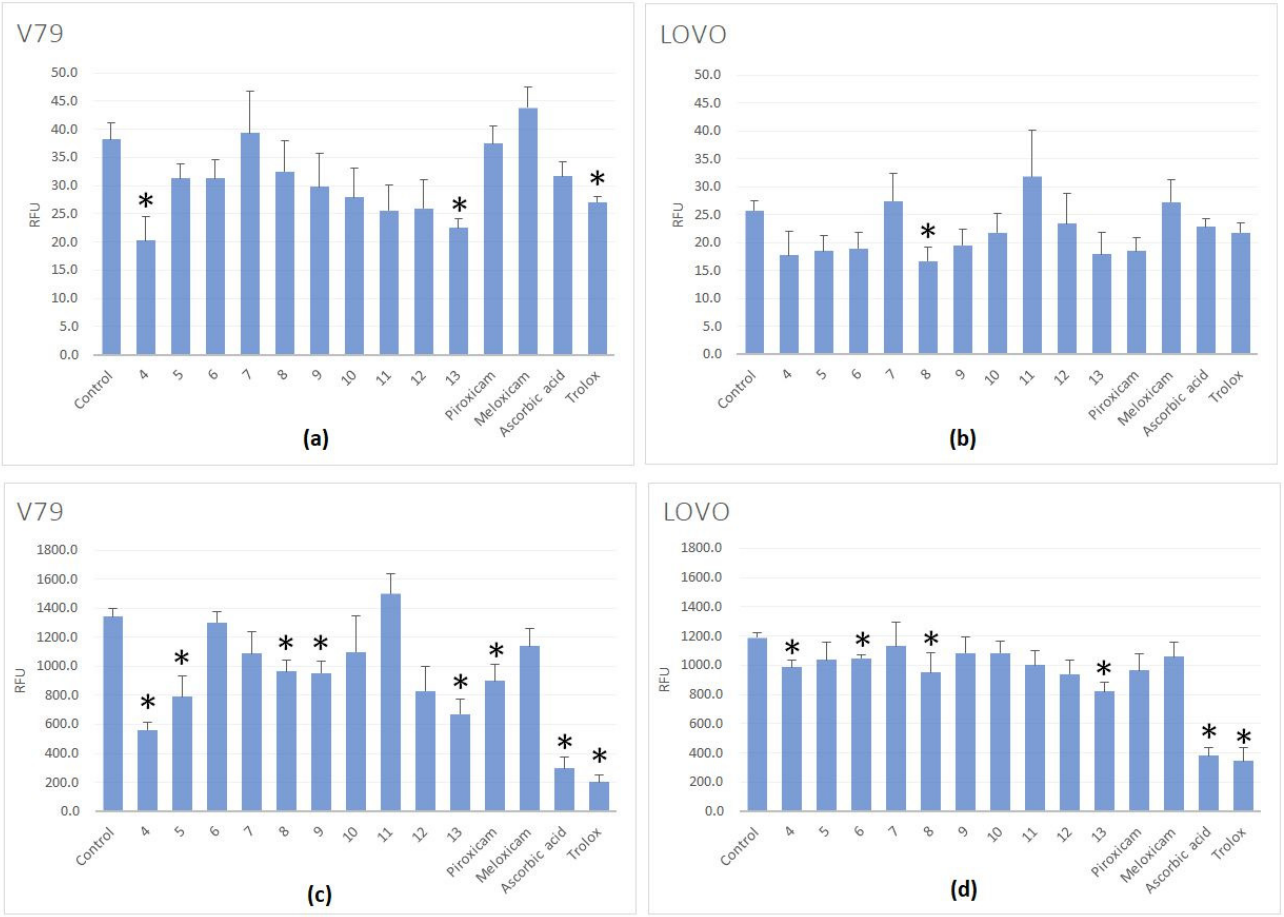

Figure 2. ROS levels in V79 and LOVO cells incubated in the presence of tested compounds (in concentration of 100 μM): untreated with H_2O_2 (**a**,**b**) and treated with H_2O_2 (100 μM, 30 min) (**c**,**d**). Results are presented as RFU (relative fluorescent units) of fluorescence levels. The statistical significance of the differences between the results for the tested compounds, compared to the control, was calculated using Tukey's post hoc test (* $p < 0.05$).

According to the results, it can be seen that our tested compounds can protect healthy cells against oxidative stress to a greater extent than cancer cells.

2.3. Static Density Functional Theory (DFT) Models and Molecular Docking Study

Molecular modeling techniques are useful in development of the interaction models between ligands and receptors. Within this study we applied diverse methods to characterize the receptors (sequence similarity evaluation), the ligands themselves (density functional theory, DFT) and their interactions with protein receptors (docking studies). We will start with the discussion of the protein models. For human COX-1 (PDB-Protein Data Bank code: 6Y3C [75]), the sequence similarity to ovine protein model (PDB code: 4O1Z [76]) was equal to 91% and for the human COX-2 (PDB code: 5KIR [77]) the resemblance to the murine model (PDB code: 4M11 [76]) reached 88%—the sequence alignments are presented in Figure S1 of Supplementary Material. Sequence homology between human receptors was close to 66%, hence the different mode of binding, as well as affinity energies, were anticipated. Significant homology in the binding places between COX-1 orthologes was seen—the binding site of the protein structure with 6Y3C code (apo form, with no ligand molecule) was inferred from knowledge of the 4O1Z binding pocket-molecular docking has shown that our assumption was correct and even if affinity energies for human COX-1 were slightly lower, the docking procedure itself was successful. Residues such as Leu352,

PhE-518, Ser530, Trp387 and Val349 were involved in the direct interactions with ligands in all the studied receptors.

Two types of conformations of the studied set of compounds were found in the DFT structural optimizations: one that assumed more packed, sandwich-like structure—denoted by additional "S" in brackets after the compound number—and the second one which was more extended (with "E" in brackets after the compound number). The details are shown in the Figure 3 and in the Supplementary Materials (Table S1).

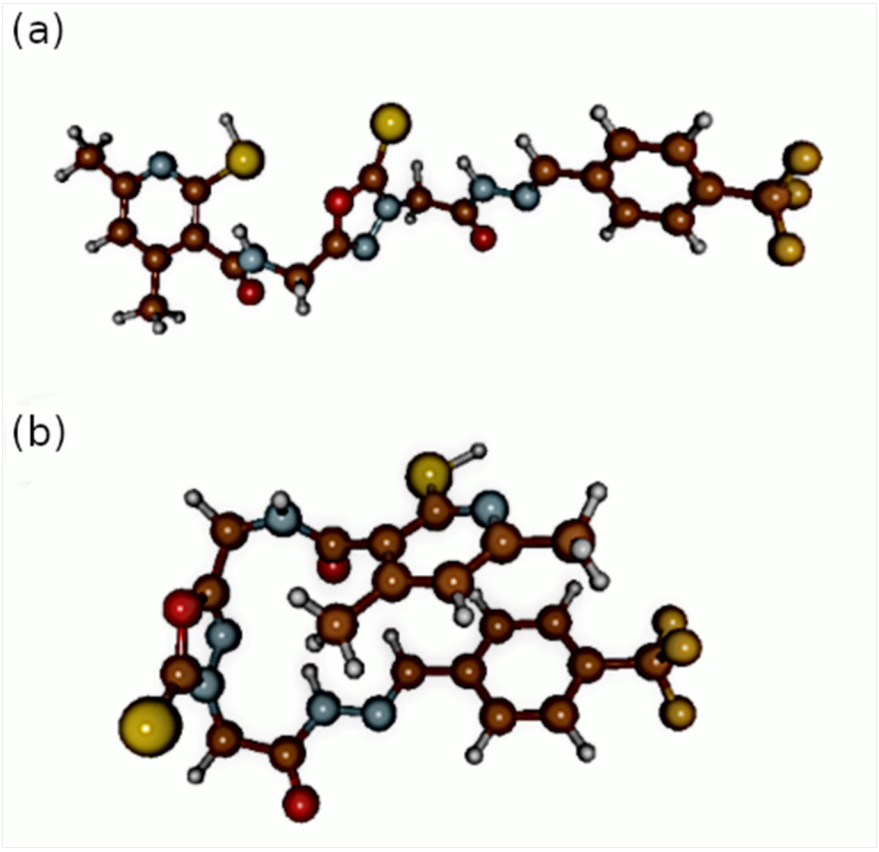

Figure 3. Optimized structures of the compound denoted by number **11**. The atoms coloring scheme is as follows: brown-carbon, blue-nitrogen, red-oxygen, yellow-sulphur, orange-fluorine and white-hydrogen; (**a**) extended conformation of **11** (**b**) sandwich-like conformation of **11**.

The structures exhibited diverse features, including intramolecular N-H . . . O hydrogen bonds and non-covalent stacking-like interactions between the phenyl and pyridine rings, which affected the located conformations and their stability. The set of compounds shares the common part and differs generally only by the phenyl ring substitution. The applied energetic criterion—relative energy between the conformers of a given compound—shows that the sandwich-like structures are in general ca. 8–10 kcal/mol lower in energy. This energy separation between conformers was found in the gas phase DFT study based on different initial arrangement of the central 1,3,4-oxadiazole ring. Both types of conformations were then examined via the docking approach.

In the next step, the protein-ligand complex was analyzed using the flexible docking method. The idea of the flexible docking is that both the ligand and the selected receptor residues are treated as conformationally flexible. The initial conformation of the ligand is modified to adapt to the binding site and the selected residues of the binding site are also allowed to reorient. Initial docking validation was performed, and it consisted of re-docking of the ligands that were previously co-crystallized with the corresponding receptors. It was meloxicam (MXM) for both ovine COX-1 (4O1Z) and murine COX-2 (4M11), and rofecoxib (RCX) for COX-2 (5KIR) from *Homo sapiens*. For human COX-1 (6Y3C) validation was

not possible because of lack of the co-crystallized ligand alongside the protein in the PDB repository. The validation set of the docked structures was very similar to the crystallized cases (see Figure 4): the RMSD (root-mean-square deviation) factor for the ligand position was equal to 1.418 Å for rofecoxib in 5KIR, 0.930 Å for meloxicam in 4M11 and 1.037 Å for meloxicam in 4O1Z. The RMSD was calculated based on the structures with the highest conformational similarity to the co-crystallized ligands. For every structure of the MXM and RCX, the lowest RMSD value was obtained for conformations with the second lowest affinity energy.

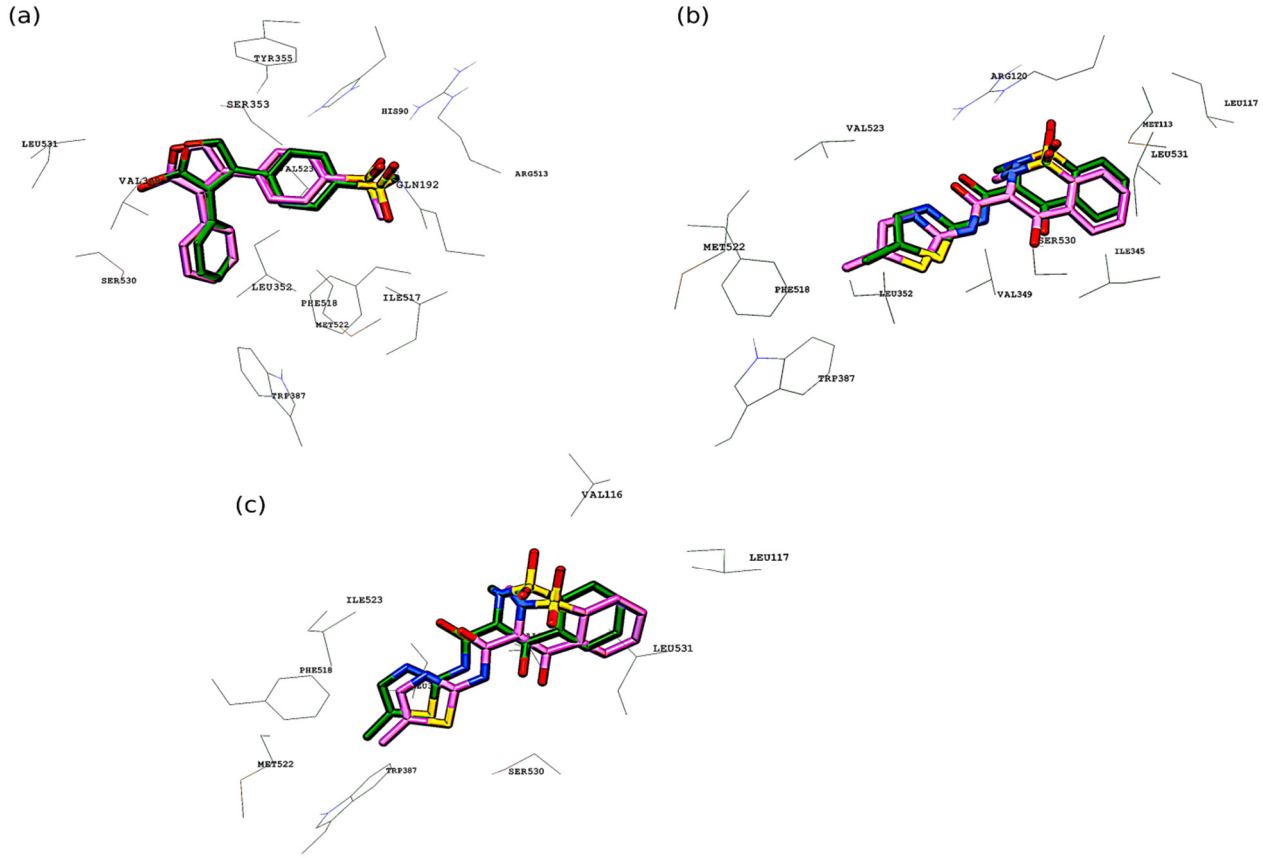

Figure 4. Validation of the docking protocol. Alignment of co-crystallized (pink carbon atoms) and docked structures (green carbon atoms) of: (**a**) RCX to COX-2 (5KIR), (**b**) MXM to COX-2 (4M11), (**c**) MXM to COX-1 (4O1Z).

After successful validation of the docking protocol, the further characterization of the binding pocket interactions with the set of the studied molecules was performed. The complicated network of interactions, difficult to present in a 3D representation is provided in the 2D form in Figure S2 of the Supplementary Material. The most favorable structures with regards to the binding affinity energy (presented in Figures 5 and 6) were chosen for detailed analysis. The most active extended-conformation compound towards the human COX-1 was **11(E)**. The stability of the binding of this compound by the human COX-1 can be explained by formation of hydrogen bonds between the Arg120, Ser530 and Asn375 residues and the ligand (depicted in Figure S2). Stabilizing non-covalent interaction (halogen bonding) was detected by the Discovery Studio Visualizer 2021 [78] between one of the fluorine substituents of the phenyl ring and the Phe-529 residue (also see Figure S2). Other non-covalent interactions present in the binding pocket are graphically presented in Figure S2. The structure represented by **11(S)** compound was also the most stabilized among the others of sandwich-like conformations. In this case, the most important modes of the binding contained also the hydrogen bonds between the ligand and the Arg120,

Asn375 residues. Numerous other non-covalent interactions were detected, and they are presented in Figure S2.

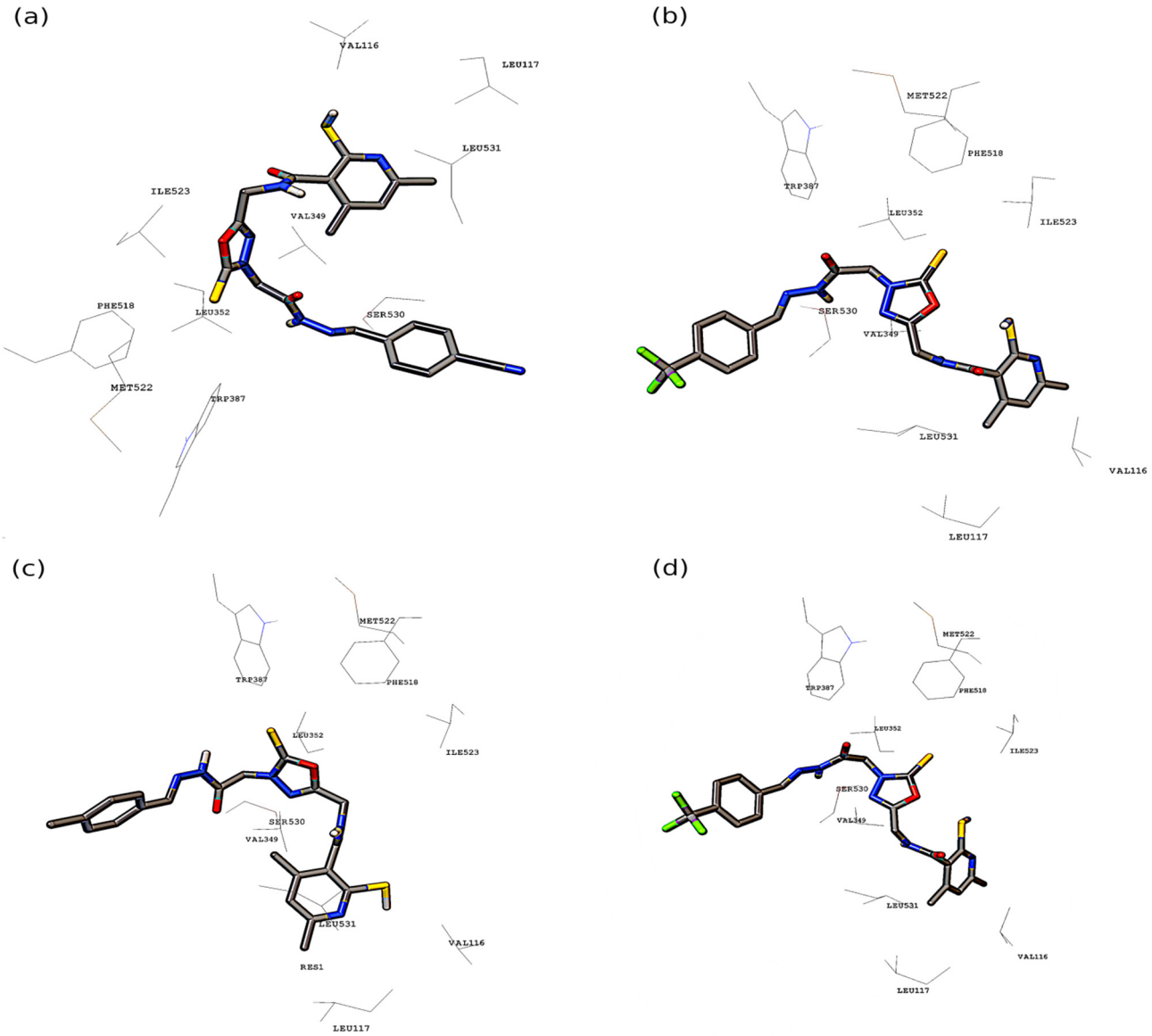

Figure 5. The most energetically favorable conformations of examined compounds in the active site of COX-1: (**a**) **9(S)** docked to ovine COX-1, (**b**) **11(E)** docked to human COX-1, (**c**) **7(E)** docked to ovine COX-1, (**d**) **11(S)** docked to human COX-1.

It is worth noting that the docking to the apo structure of the human COX-1 was successful because of the use of the flexible docking protocol and previous characterization of the similarity of the binding sites with the use of bioinformatics tools (see Figure S1). For the ovine COX-1, the affinity energies were generally larger by ca. 2 kcal/mol for each compound comparing with the previous receptor (Tables 6 and 7). The most selective extended structure was **7(E)** and the best among the sandwich-like structures was **9(S)**. For the **7(E)** compound a large number of π-π stacked, amide-π stacked, π-sulphur and π-σ interactions were present (see Figure S2). In the case of **9(S)** the π-alkyl, π-σ, alkyl and also π-sulphur interactions were the most significant. The binding energy for both **7(E)** and **9(S)** compounds exceeded -10.0 kcal/mol. The extended **11(E)** compound was found as the most active for the *Mus musculus* COX-2 (Table 8). The halogen bonds formation between fluorine substituents of ligand phenyl ring and Met522 residue was observed. The Arg120 residue

and the nitrogen from the ligand pyridine ring were involved in the hydrogen bonding; non-covalent interactions are depicted in Figure S2. Its affinity towards *Mus musculus* COX-2 was even higher than that of the co-crystallized ligand-MXM. Among sandwich-like structures the most promising seems to be the **9(S)** molecule. In this case, the hydrogen bonds between the ligand and the residues Ser530 and Arg120 are present. Plethora of Van der Waals interactions between alkyl and aromatic parts of ligand and valine and leucine residues were also present (see Figure S2). The human COX-2 was bounded more efficiently by extended conformation of the examined compounds (Table 9). The differences were most significant for **11(E)** where the affinity energy between two investigated structures varied by more than 2 kcal/mol. The **11(E)** molecule in the binding pocket was stabilized by the network of intermolecular hydrogen bonds between the ligand and the Thr94, His90, Ser353, Tyr355 and Arg120 residues. Numerous non-covalent interactions were detected, and they are graphically presented in Figure S2. The **13(S)** molecule had the highest affinity towards the receptor among the sandwich-like structures. The major role was played by the amide-π stacked and π-σ as well as other non-covalent interactions present in the binding pocket (for details see Figure S2).

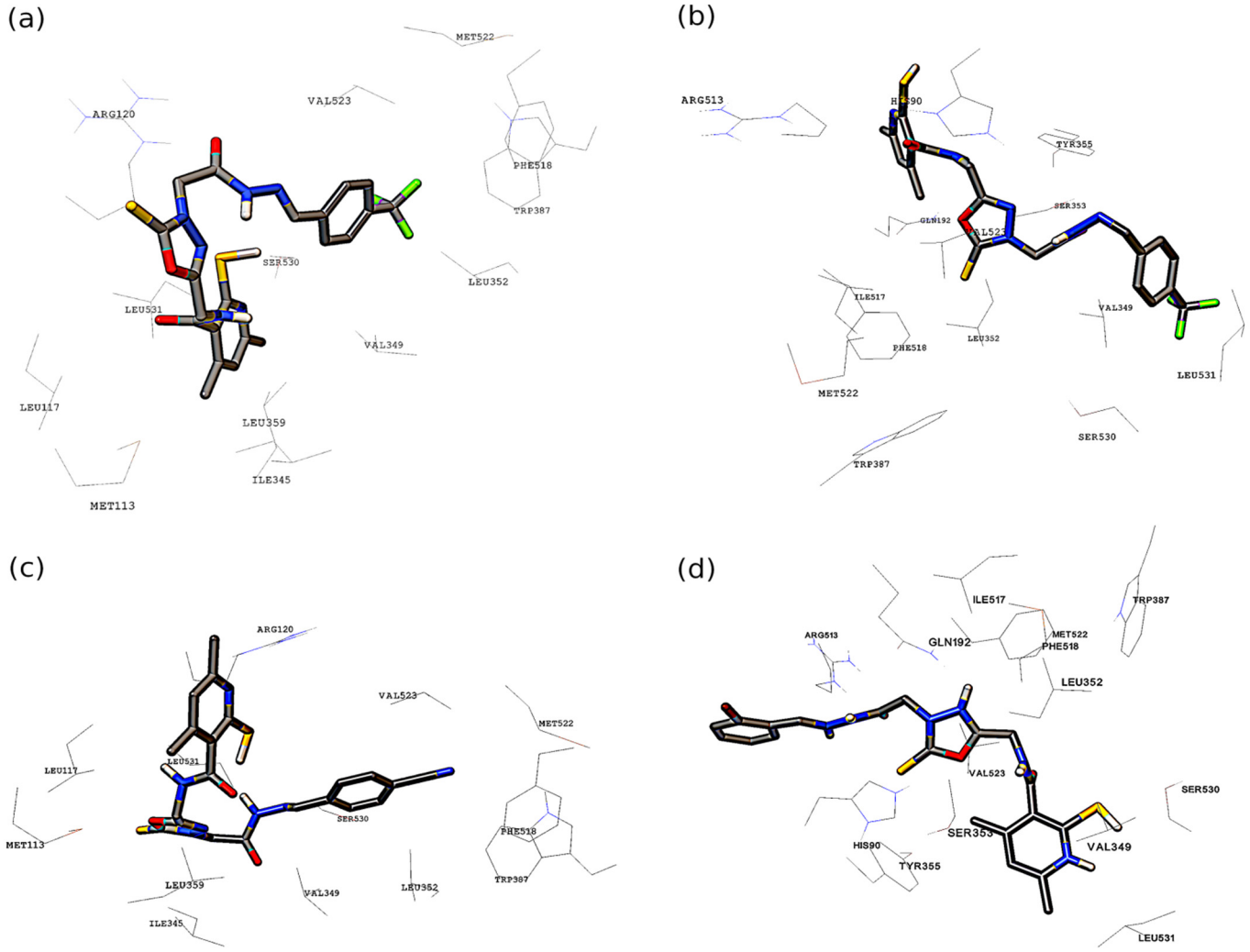

Figure 6. The most energetically favorable conformations of examined compounds in the active site of COX-2: (**a**) **11(S)** docked to murine COX-2, (**b**) **11(E)** docked to human COX-2, (**c**) **9(E)** docked to murine COX-2, (**d**) **13(S)** docked to human COX-2.

Table 6. The binding affinity energy obtained for the studied compounds interacting with the COX-1 (PDB code 6Y3C) receptor.

COX-1 [75]			
Compound	**Affinity Energy [kcal/mol]**	**Compound**	**Affinity Energy [kcal/mol]**
4(E)	−6.7	**4(S)**	−6.0
5(E)	−7.5	**5(S)**	−8.2
6(E)	−7.0	**6(S)**	−8.0
7(E)	−7.0	**7(S)**	−8.2
8(E)	−7.6	**8(S)**	−7.8
9(E)	−6.8	**9(S)**	−8.3
10(E)	−7.8	**10(S)**	−7.9
11(E)	−8.7	**11(S)**	−8.5
12(E)	−7.0	**12(S)**	−8.2
13(E)	−8.3	**13(S)**	−8.3
RCX/MXM	−8.1/−6.4	Piroxicam	−7.5

Table 7. The binding affinity energy obtained for the studied compounds interacting with the COX-1 (PDB code 4O1Z) receptor.

COX-1 [76]			
Compound	**Affinity Energy [kcal/mol]**	**Compound**	**Affinity Energy [kcal/mol]**
4(E)	−8.4	**4(S)**	−8.0
5(E)	−10.1	**5(S)**	−10.2
6(E)	−10.2	**6(S)**	−10.4
7(E)	−10.7	**7(S)**	−10.6
8(E)	−9.8	**8(S)**	−9.5
9(E)	−10.4	**9(S)**	−10.7
10(E)	−8.6	**10(S)**	−9.5
11(E)	−9.8	**11(S)**	−10.3
12(E)	−7.9	**12(S)**	−8.3
13(E)	−8.7	**13(S)**	−8.3
RCX/MXM	−9.5/−9.1	Piroxicam	−9.7

Concluding the docking study, we have found the substituent effect to change the affinity energy by 2–3 kcal/mol, which is a moderate but visible effect (ca. 20%). It was also found that the sandwich-like structures varied less in the affinity energies than the extended conformations. This is especially for the human COX-1, where only molecule conformations for structure **4** possessed lower affinity comparing to other compounds. The affinity energy differences between the most and the least favorable conformations of each of the ligands were ca. 3–4 kcal/mol. The affinities for the most stable structures varied even less. Generally speaking, the lower affinity energies were obtained when the docking procedure was applied to human and murine COX-2 receptors. The compound **4** was the least selective for the examined receptors, probably due to the lack of stabilizing non-covalent interactions provided by the phenyl ring and its substituents. It was most pronounced for receptors with 6Y3C, 4M11 and 5KIR PDB codes. The **11(S)** compound could be considered as potentially the most promising structure and it seems that the CF_3 substituent of the phenyl ring plays an important role in stabilizing that ligand in the binding pocket (due to the intermolecular halogen bonds formation).

Table 8. The binding affinity energy obtained for the studied compounds interacting with the COX-2 (PDB code 4M11) receptor.

COX-2 [76]			
Compound	**Affinity Energy [kcal/mol]**	**Compound**	**Affinity Energy [kcal/mol]**
4(E)	−8.8	**4(S)**	−9.0
5(E)	−10.0	**5(S)**	−10.1
6(E)	−10.6	**6(S)**	−10.4
7(E)	−10.7	**7(S)**	−10.6
8(E)	−10.1	**8(S)**	−10.1
9(E)	−10.6	**9(S)**	−10.9
10(E)	−10.3	**10(S)**	−10.8
11(E)	−11.5	**11(S)**	−10.8
12(E)	−10.2	**12(S)**	−10.6
13(E)	−10.4	**13(S)**	−10.6
RCX/MXM	−10.3/−10.0	Piroxicam	−10.4

Table 9. The binding affinity energy obtained for the studied compounds interacting with the COX-2 (PDB code 5KIR) receptor.

COX-2 [77]			
Compound	**Affinity Energy [kcal/mol]**	**Compound**	**Affinity Energy [kcal/mol]**
4(E)	−9.3	**4(S)**	−9.4
5(E)	−10.8	**5(S)**	−9.4
6(E)	−9.8	**6(S)**	−10.2
7(E)	−10.0	**7(S)**	−9.5
8(E)	−9.6	**8(S)**	−9.1
9(E)	−10.1	**9(S)**	−9.6
10(E)	−10.0	**10(S)**	−9.4
11(E)	−11.4	**11(S)**	−10.2
12(E)	−10.2	**12(S)**	−9.7
13(E)	−10.8	**13(S)**	−10.9
RCX/MXM	−10.9/−9.9	Piroxicam	−9.8

3. Materials and Methods

3.1. Chemistry

3.1.1. Instruments and Chemicals

All solvents, reagents and chemicals used during experiments described in this paper were delivered by commercial suppliers (Alchem, Wrocław, Poland; Chemat, Gdańsk, Poland; Archem, Łany, Poland) and were used without further purification. Any dry solvents were received due to standard procedures. Reaction progress was monitored by the thin-layer chromatography (TLC) technique, on TLC plates made of 60-254 silica gel, and was visualised by UV light at 254/366 nm. Melting points of final compounds were determined on Electrothermal Mel-Temp 1101D apparatus (Cole-Parmer, Vernon Hills, IL, USA) using open capillary method, no correction needed. ^{1}H NMR (300 MHz) and ^{13}C NMR (75 MHz) spectra were recorded using Bruker 300 MHz NMR spectrometer (Bruker Analytische Messtechnik GmbH, Rheinstetten, Germany) in DMSO-d_6, with tetramethylsilane (TMS) as an internal reference. Chemical shifts (δ) were reported in ppm. In order to record and read spectra, TopSpin 3.6.2. (Bruker Daltonik, GmbH, Bremen, Germany) program was used. Elemental analyses for carbon, nitrogen and hydrogen were carried out on a Carlo Erba NA 1500 analyzer and were within ±0.4% of the theoretical value. FT-IR spectra were measured on Nicolet iS50 FT-IR Spectrometer (Thermo Fisher Scientific, Waltham, MA, USA). Frequencies were reported in cm^{-1}. All samples were solid, and spectra were read by OMNIC Spectra 2.0 (Thermo Fisher Scientific, Waltham, MA, USA).

3.1.2. Preparation and Experimental Properties of Compounds **2**–**13**

The synthesis protocols and experimental data for compound **1** have already been reported [19].

Synthesis of 4,6-dimethyl-*N*-[(5-sulfanylidene-4,5-dihydro-1,3,4-oxadiazol-2-yl)methyl)-2-sulfanylpyridine-3-carboxamide **2**.

The hydrazide 1 (1.27 g, 0.005 mol) and KOH (0.56 g, 0.01 mol) were dissolved in ethanol (50 mL) in a round bottom flask. To this stirring mixture carbon disulphide (3 mL, 0.05 mol) was added and the whole was refluxed for 10 h till evolution of hydrogen sulfide was ceased. Then, the reaction mixture was cooled and slowly acidified with diluted hydrochloric acid. Formed precipitate was filtered off, washed with cold water, dried and recrystallized from ethanol giving white solid of compound **2**.

Yield: 65.1%, m.p.: 270–274 °C

FT-IR (selected lines, γ_{max}, cm^{-1}): 3155, 3028 (NH), 2888 (C-H aliph.), 1623 (C=O)

^{1}H NMR (300 MHz, DMSO-d_6): δ = 2.06 (s, 3H, CH_3), 2.27 (s, 3H, CH_3), 4.41–4.43 (d, 2H, CH_2, J = 6 Hz), 6.49 (s, 1H, H-$_{pyridine}$), 8.81 (t, 1H, NH, J = 6 Hz), 13.28 (s, 1H, SH), 14.40 (s, 1H, NH);

Synthesis of ethyl 2-(5-((2-sulfanyl-4,6-dimethylpyridine-3-carboxamido)methyl)-2-sulfanylidene-2,3-dihydro-1,3,4-oxadiazol-3-yl)acetate **3**.

A 100 mL round bottom flask containing 1.2 g (0.02 mol) of potassium hydroxide, 60 mL of ethanol, 6 mL of water was placed on a magnetic stirrer. Then, after dissolving the KOH, 2.96 g (0.01 mol) of compound **2** was added. The reaction was carried out at 0–5 °C. Then 1.1 mL (0.01 mol) of ethyl bromoacetate was added and left for 10 h on a magnetic stirrer. The resulting precipitate was filtered off and allowed to dry. The product **3** was then crystallized from ethanol.

Yield: 68.2%, m.p.: 155–160 °C.

FT-IR (selected lines, γ_{max}, cm^{-1}): 3185 (NH), 2984, 2930 (C-H aliph.), 1736 (C=O), 1640 (C=O).

^{1}H NMR (300 MHz, DMSO-d_6): δ = 1.15–1.21 (m, 3H, CH_3), 2.05 (s, 3H, CH_3), 2.26 (s, 3H, CH_3), 4.11–4.13 (m, 2H, CH_2), 4.18 (s, 2H, CH_2), 4.54–4.56 (d, 2H, CH_2, J = 6 Hz), 6.48 (s, 1H, H-$_{pyridine}$), 8.82 (t, 1H, NH, J = 6 Hz), 13.28 (s, 1H, SH);

Synthesis of *N*-{[4-(2-hydrazinyl-2-oxoethyl)-5-sulfanylidene-4,5-dihydro-1,3,4-oxadiazol-2-yl] methyl}-4,6-dimethyl-2-sulfanylpyridine-3-carboxamide **4**.

In a 100 mL round bottom flask, 3.68 g (0.01 mol) of compound **3** and 30 mL of methanol were placed. The resulting mixture was refluxed with stirring. After the compound 3 had dissolved, 5.1 mL of hydrazine hydrate was added, and the mixture was heated for 5 h. The obtained precipitate was filtered off and allowed to dry. The compound **4** was then recrystallized in methanol.

Yield: 36.6%, m.p.: 201–205 °C.

FT-IR (selected lines, γ_{max}, cm^{-1}): 3294 (NH_2), 3169, 3035 (NH), 1648 (C=O), 1623 (C=O)

^{1}H NMR (300 MHz, DMSO-d_6): δ = 2.06 (s, 3H, CH_3), 2.27 (s, 3H, CH_3), 3.80 (s, 2H, CH_2), 4.53–4.55 (d, 2H, CH_2, J = 6 Hz), 6.07 (s, 2H, NH_2) 6.52 (s, 1H, H-$_{pyridine}$), 8.70 (t, 1H, NH, J = 6 Hz), 9.29 (s, 1H, NH), 13.32 (s, 1H, SH);

General Procedure for Preparation of Compounds **5**–**13**.

An amount of 0.18 g (5×10^{-4} mol) of compound **4** and 25 mL of methanol were placed in a 100 mL round bottom flask. The obtained mixture was heated under reflux until the compound 4 has dissolved completely. Then 2 mL of acetic acid and 7.5×10^{-4} mol of appropriate benzaldehyde were added to the mixture. The mixture was heated for 5 h. The resulting precipitate was filtered off and allowed to dry, then crystallized from ethanol.

4,6-Dimethyl-*N*-{[4-(2-(2-benzylidenehydrazinyl)-2-oxoethyl)-5-sulfanylidene-4,5-dihydro-1,3,4-oxadiazol-2-yl]methyl}-2-sulfanylpyridine-3-carboxamide **5**.

Yield: 55.2%, m.p.: 236–239 °C.

FT-IR (selected lines, γ_{max}, cm^{-1}): 3245, 3043 (NH), 2928 (C-H aliph.), 1644 (C=O), 1626 (C=O).

^{1}H NMR (300 MHz, DMSO-d_6): δ = 2.06 (s, 3H, CH_3), 2.27 (s, 3H, CH_3), 4.00, 4.42 (2s, 2H, CH_2), 4.53–4.55 (d, 2H, CH_2, *J* = 6 Hz), 6.52 (s, 1H, H-$_{pyridine}$), 7.41–7.43 (m, 3H, ArH), 7.67–7.68 (m, 2H, ArH), 8.01, 8.18 (2s, 1H, CH), 8.69 (t, 1H, NH, *J* = 6 Hz), 11.62, 11.71 (2s, 1H, NH), 13.36 (s, 1H, SH);

^{13}C NMR (75 MHz, DMSO-d_6): δ = 18.78, 19.76, 33.17, 33.87, 115.86, 127.57, 129.52, 130.74, 134.64, 137.08, 144.15, 146.84, 148.79, 152.45, 154.15, 164.15, 167.08, 169.52, 173.67, 188.55.

4,6-Dimethyl-*N*-{[4-(2-(2-(4-fluorobenzylidene)hydrazinyl)-2-oxoethyl)-5-sulfanylidene-4,5-dihydro-1,3,4-oxadiazole-2-yl]methyl}-2-sulfanylpyridine-3-carboxamide **6**.

Yield: 45.3%, m.p.: 295–298 °C.

FT-IR (selected lines, γ_{max}, cm^{-1}): 3206, 3056 (NH), 2932 (C-H aliph.), 1657 (C=O), 1627 (C=O).

^{1}H NMR (300 MHz, DMSO-d_6): δ = 2.06 (s, 3H, CH_3), 2.27 (s, 3H, CH_3), 3.99, 4.41 (2s, 2H, CH_2), 4.53–4.55 (d, 2H, CH_2, *J* = 6 Hz), 6.52 (s, 1H, H-$_{pyridine}$), 7.24–7.30 (m, 2H, ArH), 7.72–7.76 (m, 2H, ArH), 8.00, 8.18 (2 s, 1H, CH), 8.69 (t, 1H, NH, *J* = 6 Hz), 11.63, 11.72 (2 s, 1H, NH), 13.36 (s, 1H, SH);

^{13}C NMR (75 MHz, DMSO-d_6): δ = 18.76, 19.73, 33.27, 33.92, 115.76, 127.53, 129.56, 130.77, 134.54, 137.11, 144.18, 146.83, 148.81, 152.35, 154.17, 164.15, 167.02, 169.55, 173.67, 188.52.

4,6-Dimethyl-*N*-{[4-(2-(2-(4-methylbenzylidene)hydrazinyl)-2-oxoethyl)-5-sulfanylidene-4,5-dihydro-1,3,4-oxadiazole-2-yl]methyl}-2-sulfanylpyridine-3-carboxamide **7**.

Yield: 38.6%, m.p.: 215–220 °C.

FT-IR (selected lines, γ_{max}, cm^{-1}): 3210, 3064 (NH), 2929 (C-H aliph.), 1646 (C=O), 1621 (C=O).

^{1}H NMR (300 MHz, DMSO-d_6): δ = 2.06 (s, 3H, CH_3), 2.27 (s, 3H, CH_3), 2.32 (s, 3H, CH_3), 3.98, 4.40 (2 s, 2H, CH_2), 4.53–4.55 (d, 2H, CH_2, *J* = 6 Hz), 6.47 (s, 1H, H-$_{pyridine}$), 7.55–7.57 (m, 2H, ArH), 7.74–7.76 (m, 2H, ArH), 7.98, 8.14 (2 s, 1H, CH), 8.69 (t, 1H, NH, *J* = 6 Hz), 11.56, 11.67 (2 s, 1H, NH), 13.36 (s, 1H, SH);

^{13}C NMR (75 MHz, DMSO-d_6): δ = 18.78, 19.76, 21.46, 33.27, 33.92, 115.61, 127.57, 129.03, 130.25, 134.51, 137.09, 141.96, 146.83, 148.81, 152.35, 154.17, 161.96, 165.86, 169.52, 173.62, 188.50.

4,6-Dimethyl-*N*-{[4-(2-(2-(4-methysulfanylbenzylidene)hydrazinyl)-2-oxoethyl)-5-sulfanylidene-4,5-dihydro-1,3,4-oxadiazole-2-yl]methyl}-2-sulfanylpyridine-3-carboxamide **8**.

Yield: 47.3%, m.p.: 235–238 °C.

FT-IR (selected lines, γ_{max}, cm^{-1}): 3197 (NH), 2916 (C-H aliph.), 1642 (C=O), 1620 (C=O).

^{1}H NMR (300 MHz, DMSO-d_6): δ = 2.06 (s, 3H, CH_3), 2.27 (s, 3H, CH_3), 2.52 (s, 3H, CH_3), 3.98, 4.40 (2 s, 2H, CH_2), 4.53–4.55 (d, 2H, CH_2, *J* = 6 Hz), 6.52 (s, 1H, H-$_{pyridine}$), 7.59–7.62 (m, 2H, ArH), 7.74–7.77 (m, 2H, ArH), 7.96, 8.13 (2 s, 1H, CH), 8.69 (t, 1H, NH, *J* = 6 Hz), 11.58, 11.67 (2 s, 1H, NH), 13.59 (s, 1H, SH);

^{13}C NMR (75 MHz, DMSO-d_6): δ = 14.63, 18.78, 19.76, 33.31, 33.87, 126.10, 127.81, 129.27, 130.74, 134.51, 137.09, 143.18, 147.03, 148.72, 152.35, 154.34, 161.23, 165.86, 169.52, 173.62, 187.23.

4,6-Dimethyl-*N*-{[4-(2-(2-(4-cyanobenzylidene)hydrazinyl)-2-oxoethyl)-5-sulfanylidene-4,5-dihydro-1,3,4-oxadiazole-2-yl]methyl}-2-sulfanylpyridine-3-carboxamide **9**.

Yield: 39.8%, m.p.: 298–300 °C.

FT-IR (selected lines, γ_{max}, cm^{-1}): 3202 (NH), 2918 (C-H aliph.), 2224 (CN) 1667 (C=O), 1620 (C=O).

^{1}H NMR (300 MHz, DMSO-d_6): δ = 2.06 (s, 3H, CH_3), 2.27 (s, 3H, CH_3), 4.02, 4.35 (2 s, 2H, CH_2), 4.53–4.55 (d, 2H, CH_2, *J* = 6 Hz), 6.52 (s, 1H, H-$_{pyridine}$), 7.87 (s, 4H, ArH), 8.05, 8.24 (2 s, 1H, CH), 8.69 (t, 1H, NH, *J* = 6 Hz), 11.85, 11.96 (2 s, 1H, NH), 13.36 (s, 1H, SH);

^{13}C NMR (75 MHz, DMSO-d_6): δ = 18.69, 19.54, 33.20, 33.49, 97.18, 112.56, 116.22, 125.93, 128.43, 129.27, 133.22, 137.09, 143.18, 147.03, 148.72, 152.35, 154.34, 161.23, 167.50, 169.52, 187.52.

4,6-Dimethyl-*N*-{[4-(2-(2-(4-chlorobenzylidene)hydrazinyl)-2-oxoethyl)-5-sulfanylidene-4,5-dihydro-1,3,4-oxadiazole-2-yl]methyl}-2-sulfanylpyridine-3-carboxamide **10**.

Yield: 49.6%, m.p.: 278–280 °C.

FT-IR (selected lines, γ_{max}, cm^{-1}): 3333, 3210 (NH), 2932 (C-H aliph.), 1647 (C=O), 1624 (C=O).

^{1}H NMR (300 MHz, DMSO-d_6): δ = 2.06 (s, 3H, CH_3), 2.27 (s, 3H, CH_3), 3.99, 4.41 (2 s, 2H, CH_2), 4.53–4.55 (d, 2H, CH_2, J = 6 Hz), 6.52 (s, 1H, H-$_{pyridine}$), 7.47–7.50 (m, 2H, ArH), 7.69–7.72 (m, 2H, ArH), 7.99, 8.17 (2 s, 1H, CH), 8.69 (t, 1H, NH, J = 6 Hz), 11.68, 11.78 (2 s, 1H, NH), 13.36 (s, 1H, SH);

^{13}C NMR (75 MHz, DMSO-d_6): δ = 18.63, 18.74, 33.33, 33.84, 125.90, 127.67, 129.02, 131.14, 134.31, 136.95, 143.23, 146.93, 148.67, 152.28, 154.42, 161.27, 165.93, 169.62, 173.48, 188.23.

4,6-Dimethyl-*N*-{[4-(2-(2-(4-trifluoromethylbenzylidene)hydrazinyl)-2-oxoethyl)-5-sulfanylidene-4,5-dihydro-1,3,4-oxadiazole-2-yl]methyl}-2-sulfanylpyridine-3-carboxamide **11**.

Yield: 52.2%, m.p.: 253–255 °C.

FT-IR (selected lines, γ_{max}, cm^{-1}): 3292, 3179 (NH), 2942 (C-H aliph.), 1680 (C=O), 1647 (C=O).

^{1}H NMR (300 MHz, DMSO-d_6): δ = 2.06 (s, 3H, CH_3), 2.27 (s, 3H, CH_3), 4.02, 4.44 (2 s, 2H, CH_2), 4.53–4.55 (d, 2H, CH_2, J = 6 Hz), 6.52 (s, 1H, H-$_{pyridine}$), 7.77–7.80 (m, 2H, ArH), 7.88–7.91 (m, 2H, ArH), 8.08, 8.26 (2 s, 1H, CH), 8.71 (t, 1H, NH, J = 6 Hz), 11.81, 11.92 (2 s, 1H, NH), 13.38 (s, 1H, SH);

^{13}C NMR (75 MHz, DMSO-d_6): δ = 18.54, 18.69, 19.62, 33.45, 33.78, 126.10, 127.72, 128.82, 131.36, 134.45, 136.75, 143.48, 146.76, 148.22, 152.43, 154.65, 161.46, 165.23, 169.42, 173.33, 187.95.

4,6-Dimethyl-*N*-{[4-(2-(2-(3-chlorobenzylidene)hydrazinyl)-2-oxoethyl)-5-sulfanylidene-4,5-dihydro-1,3,4-oxadiazole-2-yl]methyl}-2-sulfanylpyridine-3-carboxamide **12**

Yield: 48.0%, m.p.: 273–275 °C.

FT-IR (selected lines, γ_{max}, cm^{-1}): 3200 (NH), 2931 (C-H aliph.), 1651 (C=O), 1626 (C=O)

^{1}H NMR (300 MHz, DMSO-d_6): δ = 2.06 (s, 3H, CH_3), 2.27 (s, 3H, CH_3), 4.00, 4.42 (2 s, 2H, CH_2), 4.53–4.55 (d, 2H, CH_2, J = 6 Hz), 6.52 (s, 1H, H-$_{pyridine}$), 7.44–7.46 (m, 2H, ArH), 7.64–7.66 (m, 1H, ArH), 7.74–7.76 (m, 1H, ArH), 7.99, 8.17 (2 s, 1H, CH), 8.70 (t, 1H, NH, J = 6 Hz), 11.72, 11.85 (2 s, 1H, NH), 13.36 (s, 1H, SH);

^{13}C NMR (75 MHz, DMSO-d_6): δ = 18.52, 18.65, 32.13, 33.56, 126.01, 127.23, 128.83, 130.74, 134.62, 137.72, 143.55, 147.12, 148.28, 152.68, 154.89, 161.65, 166.33, 170.42, 172.18, 188.12.

4,6-Dimethyl-*N*-{[4-(2-(2-(2-bromobenzylidene)hydrazinyl)-2-oxoethyl)-5-sulfanylidene-4,5-dihydro-1,3,4-oxadiazole-2-yl]methyl}-2-sulfanylpyridine-3-carboxamide **13**.

Yield: 42.1%, m.p.: 285–288 °C.

FT-IR (selected lines, γ_{max}, cm^{-1}): 3349, 3205 (NH), 2934 (C-H aliph.), 1664 (C=O), 1648 (C=O).

^{1}H NMR (300 MHz, DMSO-d_6): δ = 2.06 (s, 3H, CH_3), 2.27 (s, 3H, CH_3), 4.00, 4.43 (2 s, 2H, CH_2), 4.53–4.55 (d, 2H, CH_2, J = 6 Hz), 6.52 (s, 1H, H-$_{pyridine}$), 7.32–7.34 (m, 1H, ArH), 7.44–7.46 (m, 1H, ArH), 7.66–7.68 (m, 1H, ArH), 7.90–7.92 (m, 1H, ArH), 8.36, 8.54 (2 s, 1H, CH), 8.69 (t, 1H, NH, J = 6 Hz), 11.82, 11.99 (2 s, 1H, NH), 13.36 (s, 1H, SH);

^{13}C NMR (75 MHz, DMSO-d_6): δ = 18.73, 18.84, 32.59, 34.26, 124.96, 126.58, 129.03, 131.24, 133.67, 137.12, 143.55, 147.65, 147.83, 153.43, 155.68, 161.23, 165.84, 169.62, 171.67, 188.16.

3.2. Biological Section

3.2.1. Cell Lines

Six cell lines were used in the investigations. Three of them were normal: NHDF (normal human dermal fibroblasts), purchased from Lonza (Verviers, Belgium), V79 (fibroblasts from Chinese hamster lung) and VERO (kidney epithelial cells) obtained from ECACC (European Collection of Authenticated Cell Cultures). The rest of cells were human cancer cell lines: LoVo (colon adenocarcinoma), their drug resistant subline LoVo/Dx and A549 (pulmonary basial cell alveolar adenocarcinoma) cell line. Cancer lines were also obtained from ECACC.

3.2.2. Cell Culture Conditions

Each cell line was grown in the culture media recommended by supplier. Before the test they were detached with trypsin/EDTA solution, then to neutralize the effect of Trypsin/EDTA solution, FBS containing medium was used. After centrifugation the cells were stained with 0.4% solution of trypan blue, counted and inspected for viability using microscope. In the end, cells were inserted into 96-well culture plates and incubated in CO_2 incubator (37 °C, 24 h). The number of cells was 2×10^3 cells per well. The tested compounds with different concentrations (5, 10, 20, 50, 100 μM) were dissolved in DMSO and then added to the cells (the final DMSO concentration was 0.1%). The cultures were incubated for another 48 h. After that time the cells were collected to be used in tests.

3.2.3. Cyclooxygenase Inhibitory Activity

A COX Colorimetric Inhibitor Screening Assay Kit, produced by Cayman Chemical Company, Ann Arbor, MI, USA, was used. It used the colorimetric monitoring of oxidized form of TMPD (*N*,*N*,*N*′,*N*′-tetramethyl-*p*-phenylenediamine) which was produced during reduction of prostaglandin G_2 (PGG_2) to PGH_2. The change of colour was observed and measured spectrofotometrically at 590 nm. Reagents used it this assay were: COX-1 and COX-2 enzymes, Tris-HCl buffer, solutions of heme in DMSO and TMPD, arachidonic acid, KOH. To be sure that 100% enzymatic activity was achieved each sample was measured 3 times. The probes were measured after two minutes of incubation with tested compounds in the comparison to the initial activity of enzyme. It allowed to determine IC_{50} value, where 50% inhibition of the enzyme activity was observed.

3.2.4. MTT Assay

MTT assay was used to find out how tested compounds influence the metabolic activity of investigated cell lines. The cells were incubated with tested compounds. After removing of supernatant, 1 mg/mL of MTT solution in MEM was added to the plate (to each well) and then the plates were incubated at 37 °C for 2 h. The medium was removed again, and formazan crystals were dissolved in isopropanol. A Varioscan LUX microplate reader (Thermo Fisher Scientific, Waltham, MA, USA) was used to measure absorbance at 570 nm.

3.2.5. Estimation of Intracellular ROS Level

First, the tested compounds (in concentration of 100 μM) were added to the cell cultures and cells were incubated for 4 h. Then cells were washed and incubated with DCFH-DA (non-fluorescent probe) in dark at 37 °C for 2 h at CO_2 [79]. Non-fluorescent, non-polar DCFH-DA (2′7′-dichlorodihydrofluorescein diacetate) at concentration of 25 μM was used as a marker of oxidative stress to determine the intracellular ROS levels. Then the cells were washed with PBS two times and 100 μL of H_2O_2 were added for 30 min, which is proper time to decompose all H_2O_2 [80]. In this time, DCFH-DA which penetrated into the cells, was hydrolyzed by esterases to polar, non-fluorescent DCFH (2′7′-dichlorodihydrofluorescein) and then oxidized in the presence of ROS (reactive oxygen species) to fluorescent DCF (2′7′-dichlorofluorescein). DCF was measured using Varioscan LUX microplate reader (Thermo Fisher Scientific, Waltham, MA, USA) at λ_{ex} = 485 nm and λ_{em} = 535 nm. Then results were presented as E/E_0 where E is test sample value and E_0—control value.

3.2.6. Statistics

All results in Tables are presented as mean ± SEM (standard error of the mean) relative to the control (E/E_0). E is the culture with the tested compound and E_0 is the negative control without the compound. The routine statistical methods: two-way analysis of variance ANOVA as well as Tukey's post-hoc test were used. It allowed us to determine the statistical significance of results, where $p < 0.05$ was set as significant. The statistical indicators were estimated using Statistica 13.3 software.

3.3. Molecular Modeling—Computational Methodology

Initial models of the investigated compounds (see Figure 1) were constructed in the Molden 6.6 program [81] with the aim of quantum-chemical structural optimization before the main docking runs. The structure of each compound was optimized in accordance with default procedures in the Gaussian 16 suite of programs [82]. Energy minimization was carried out with the ωB97XD functional [83] derived within the framework of density functional theory (DFT) [84,85], with the correlation-consistent Dunning basis set denoted as cc-pVDZ [86]. In order to confirm that the optimized geometries correspond to the energy minima on the potential energy surface (PES), harmonic frequencies calculations were also conducted (yielding no imaginary frequencies). Resulting energy values were used to estimate the conformational preferences. Further, docking runs were carried out for the studied series of compounds. The structures of the receptors were taken from the Protein Data Bank (PDB) [87]. The compounds were docked into COX-1 (PDB code 4O1Z) [76] from *Ovis aries* and COX-2 (PDB code 4M11) [76] from *Mus musculus* models, which were loaded with the ligand (meloxicam, MXM). Additionally, COX-1 (PDB code 6Y3C) [75] and COX-2 (PDB code 5KIR) [77], cyclooxygenases counterparts from *Homo sapiens*, were also taken into consideration as receptors—of these, only the human COX-2 was loaded with rofecoxib (RCX) ligand, while the human COX-1 was in the apo form. Sequence alignments and similarity were generated with the ClustalW software [88]. Water molecules and co-factors that were in proximity to the binding site of receptors were removed. The Gasteiger charges and polar hydrogen atoms were added to the examined receptors and ligands. The flexible parts of the receptors were inferred from the knowledge of the center of co-crystallized ligands and the grid was set to the dimensions of 20 × 20 × 20 Å. The flexible part of the receptor was defined as residues located within 3.5 Å for COX-1 and within 4.0 Å for COX-2 from the centers of the binding pockets. The docking calculations were performed with exhaustiveness of 32 and energy range equal to 10 kcal/mol. The validation of the procedure was carried out with usage of the MXM and RCX ligands from the PDB database and, solely for the purpose to check the validation of the used computational setup, the polar hydrogens were not added. Editing of the protein structure (water and ligand removal) was carried out with the assistance of the VMD 1.9.3 program [89]. The preparation of the ligand and receptor, molecular docking and the visualization of the results were performed with the AutoDockTools 1.5.7 [90], AutoDock Vina 1.1.2 [91] and the open-source PyMOL 2.3.0 [92] packages. The 2D diagrams were prepared in the Discovery Studio Visualizer 2019 [78] with the use of the most energetically favorable geometries of the examined compounds, and the script vina_split of the AutoDock Vina 1.1.2 program [91] was used to split merged conformations from one PDBQT file into separate entries.

4. Conclusions

In the current study, we have presented experimental and theoretical results obtained for new Schiff base-type compounds. The reaction pathways and synthetic procedures have been presented. The physico-chemical properties of the compounds were characterized by NMR and IR spectroscopy. The biological activity was investigated based on diverse biological assays. It was found that Schiff base **13** inhibited the activity of both isoenzymes, COX-1 and COX-2 at a lower concentration than standard drugs, and its COX-2/COX-1 selectivity ratio was detected to be similar to meloxicam. The results of cytotoxicity assay showed that all of the tested compounds exhibited potent anti-cancer activity against A549, MCF-7, LoVo, and LoVo/Dx cell lines.

Finally, the quantum-chemical based DFT method simulations were performed. Two main possible conformations were investigated, and it was found that lower relative energy corresponded to the sandwich-like structure. As the last step of the study, the flexible docking method was applied and it was found that in comparison to known inhibitors of cyclooxygenases and affinity energies of docking meloxicam, piroxicam and rofecoxib to the receptors were similar to most of the energies obtained for the investigated structures.

These results indicate that the examined ligands could exhibit a significant activity towards human COX-1 and COX-2 receptors.

Considering the results obtained, we wish to underline that the combination of 1,3,4-oxadiazole and hydrazide-hydrazone pharmacophore moieties has yielded promising results, and additional studies on these compounds are necessary. The research into their effects on apoptosis, the cell cycle and inflammation is planned to improve our understanding of their mechanisms of action.

Supplementary Materials: The following are available online at https://www.mdpi.com/article/10.3390/ijms23010549/s1.

Author Contributions: Conceptualization, P.Ś., M.S., T.G. (Teresa Glomb); methodology, P.Ś., T.G. (Tomasz Gębarowski), K.W.; software, K.W., A.J., J.J.P.; validation, K.W., A.J., J.J.P.; formal analysis, P.Ś., M.S., T.G. (Teresa Glomb), A.D., K.W., A.J., J.J.P., M.Ś.; investigation, P.Ś., M.S., T.G. (Teresa Glomb), T.G. (Tomasz Gębarowski), K.W.; writing—original draft preparation, P.Ś., M.S., T.G. (Teresa Glomb), A.D., K.W., M.Ś.; writing—review and editing, P.Ś., M.S., T.G. (Teresa Glomb), T.G. (Tomasz Gębarowski), A.J., J.J.P.; visualization, P.Ś., M.S., T.G. (Teresa Glomb), K.W.; supervision, P.Ś., A.J., J.J.P.; project administration, P.Ś.; funding acquisition, P.Ś. All authors have read and agreed to the published version of the manuscript.

Funding: This research was funded by the Ministry of Health subvention according to the number SUB.D070.21.094 from the IT Simple system of Wroclaw Medical University.

Acknowledgments: Kamil Wojtkowiak, Aneta Jezierska and Jarosław J. Panek gratefully acknowledge the use of computational resources generously granted by Academic Computer Centre Cyfronet AGH in Kraków (Prometheus, part of the PL-Grid infrastructure), Wrocław Centre for Networking and Supercomputing (WCSS Wrocław), Centre of Informatics Tricity Academic Supercomputer and Network (CI TASK Gdańsk) and Poznan Supercomputing and Networking Center (PSNC).

Conflicts of Interest: The authors declare no conflict of interest.

References

1. Meshram, M.A.; Bhise, U.O.; Makhal, P.N.; Kaki, V.R. Synthetically-Tailored and Nature-Derived Dual COX-2/5-LOX Inhibitors: Structural Aspects and SAR. *Eur. J. Med. Chem.* **2021**, *225*, 113804. [CrossRef]
2. Szczukowski, Ł.; Krzyżak, E.; Wiatrak, B.; Jawień, P.; Marciniak, A.; Kotynia, A.; Świątek, P. New N-Substituted-1,2,4-Triazole Derivatives of Pyrrolo[3,4-d]Pyridazinone with Significant Anti-Inflammatory Activity—Design, Synthesis and Complementary In Vitro, Computational and Spectroscopic Studies. *Int. J. Mol. Sci.* **2021**, *22*, 11235. [CrossRef]
3. Glomb, T.; Wiatrak, B.; Gębczak, K.; Gębarowski, T.; Bodetko, D.; Czyżnikowska, Ż.; Świątek, P. New 1,3,4-Oxadiazole Derivatives of Pyridothiazine-1,1-Dioxide with Anti-Inflammatory Activity. *Int. J. Mol. Sci.* **2020**, *21*, 9122. [CrossRef]
4. Leuti, A.; Fazio, D.; Fava, M.; Piccoli, A.; Oddi, S.; Maccarrone, M. Bioactive Lipids, Inflammation and Chronic Diseases. *Adv. Drug Deliv. Rev.* **2020**, *159*, 133–169. [CrossRef]
5. Arulselvan, P.; Fard, M.T.; Tan, W.S.; Gothai, S.; Fakurazi, S.; Norhaizan, M.E.; Kumar, S.S. Role of Antioxidants and Natural Products in Inflammation. *Oxidative Med. Cell. Longev.* **2016**, *2016*, 5276130. [CrossRef]
6. Coussens, L.M.; Werb, Z. Inflammation and Cancer. *Nature* **2002**, *420*, 860–867. [CrossRef]
7. Khan, S.; Andrews, K.L.; Chin-Dusting, J.P.F. Cyclo-Oxygenase (COX) Inhibitors and Cardiovascular Risk: Are Non-Steroidal Anti-Inflammatory Drugs Really Anti-Inflammatory? *Int. J. Mol. Sci.* **2019**, *20*, 4262. [CrossRef]
8. Süleyman, H.; Demircan, B.; Karagöz, Y. Anti-Inflammatory and Side Effects of Cyclooxygenase Inhibitors. *Pharmacol. Rep.* **2007**, *59*, 247–258.
9. Bindu, S.; Mazumder, S.; Bandyopadhyay, U. Non-Steroidal Anti-Inflammatory Drugs (NSAIDs) and Organ Damage: A Current Perspective. *Biochem. Pharmacol.* **2020**, *180*, 114147. [CrossRef]
10. Campos, D.C.O.; Costa, A.S.; Luz, P.B.; Soares, P.M.G.; Alencar, N.M.N.; Oliveira, H.D. Morinda Citrifolia Lipid Transfer Protein 1 Exhibits Anti-Inflammatory Activity by Modulation of pro- and Anti-Inflammatory Cytokines. *Int. J. Biol. Macromol.* **2017**, *103*, 1121–1129. [CrossRef]
11. Wang, M.T.; Honn, K.V.; Nie, D. Cyclooxygenases, Prostanoids, and Tumor Progression. *Cancer Metastasis Rev.* **2007**, *26*, 525–534. [CrossRef]
12. Setia, S.; Vaish, V.; Sanyal, S.N. Chemopreventive Effects of NSAIDs as Inhibitors of Cyclooxygenase-2 and Inducers of Apoptosis in Experimental Lung Carcinogenesis. *Mol. Cell. Biochem.* **2012**, *366*, 89–99. [CrossRef]
13. Umezawa, S.; Higurashi, T.; Komiya, Y.; Arimoto, J.; Horita, N.; Kaneko, T.; Iwasaki, M.; Nakagama, H.; Nakajima, A. Chemoprevention of Colorectal Cancer: Past, Present, and Future. *Cancer Sci.* **2019**, *110*, 3018–3026. [CrossRef]

14. Kajal, A.; Bala, S.; Sharma, N.; Kamboj, S.; Saini, V. Therapeutic Potential of Hydrazones as Anti-Inflammatory Agents. *Int. J. Med. Chem.* **2014**, *2014*. [CrossRef]
15. Thota, S.; Rodrigues, D.A.; de Sena Murteira Pinheiro, P.; Lima, L.M.; Fraga, C.A.M.; Barreiro, E.J. N-Acylhydrazones as Drugs. *Bioorg. Med. Chem. Lett.* **2018**, *28*, 2797–2806. [CrossRef]
16. Popiołek, Ł. Hydrazide-Hydrazones as Potential Antimicrobial Agents: Overview of the Literature since 2010. *Med. Chem. Res.* **2017**, *26*, 287–301. [CrossRef]
17. Nasr, T.; Bondock, S.; Rashed, H.M.; Fayad, W.; Youns, M.; Sakr, T.M. Novel Hydrazide-Hydrazone and Amide Substituted Coumarin Derivatives: Synthesis, Cytotoxicity Screening, Microarray, Radiolabeling and in Vivo Pharmacokinetic Studies. *Eur. J. Med. Chem.* **2018**, *151*, 723–739. [CrossRef]
18. Das Mukherjee, D.; Kumar, N.M.; Tantak, M.P.; Datta, S.; Ghosh Dastidar, D.; Kumar, D.; Chakrabarti, G. NMK-BH2, a Novel Microtubule-Depolymerising Bis (Indolyl)-Hydrazide-Hydrazone, Induces Apoptotic and Autophagic Cell Death in Cervical Cancer Cells by Binding to Tubulin at Colchicine—Site. *Biochim. Biophys. Acta-Mol. Cell Res.* **2020**, *1867*, 118762. [CrossRef]
19. Świątek, P.; Saczko, J.; Rembiałkowska, N.; Kulbacka, J. Synthesis of New Hydrazone Derivatives and Evaluation of Their Efficacy as Proliferation Inhibitors in Human Cancer Cells. *Med. Chem.* **2019**, *15*, 903–910. [CrossRef]
20. Horchani, M.; Della Sala, G.; Caso, A.; D'Aria, F.; Esposito, G.; Laurenzana, I.; Giancola, C.; Costantino, V.; Jannet, H.B.; Romdhane, A. Molecular Docking and Biophysical Studies for Antiproliferative Assessment of Synthetic Pyrazolo-Pyrimidinones Tethered with Hydrazide-Hydrazones. *Int. J. Mol. Sci.* **2021**, *22*, 2742. [CrossRef]
21. Beteck, R.M.; Seldon, R.; Jordaan, A.; Warner, D.F.; Hoppe, H.C.; Laming, D.; Legoabe, L.J.; Khanye, S.D. Quinolone-Isoniazid Hybrids: Synthesis and Preliminary: In Vitro Cytotoxicity and Anti-Tuberculosis Evaluation. *Medchemcomm* **2019**, *10*, 326–331. [CrossRef]
22. Bekhit, A.A.; Saudi, M.N.; Hassan, A.M.M.; Fahmy, S.M.; Ibrahim, T.M.; Ghareeb, D.; El-Seidy, A.M.; Nasralla, S.N.; Bekhit, A.E.D.A. Synthesis, in Silico Experiments and Biological Evaluation of 1,3,4-Trisubstituted Pyrazole Derivatives as Antimalarial Agents. *Eur. J. Med. Chem.* **2019**, *163*, 353–366. [CrossRef]
23. Popiołek, Ł. Updated Information on Antimicrobial Activity of Hydrazide–Hydrazones. *Int. J. Mol. Sci.* **2021**, *22*, 9389. [CrossRef]
24. Senkardes, S.; Kaushik-Basu, N.; Durmaz, I.; Manvar, D.; Basu, A.; Atalay, R.; Guniz Kucukguzel, S. Synthesis of Novel Diflunisal Hydrazide-Hydrazones as Anti-Hepatitis C Virus Agents and Hepatocellular Carcinoma Inhibitors. In *European Journal of Medicinal Chemistry*; Elsevier Masson SAS: Issy-les-Moulineaux, France, 2016; Volume 108, pp. 301–308. [CrossRef]
25. Angelova, V.; Karabeliov, V.; Andreeva-Gateva, P.A.; Tchekalarova, J. Recent Developments of Hydrazide/Hydrazone Derivatives and Their Analogs as Anticonvulsant Agents in Animal Models. *Drug Dev. Res.* **2016**, *77*, 379–392. [CrossRef]
26. Zeeshan, S.; Naveed, M.; Khan, A.; Atiq, A.; Arif, M.; Ahmed, M.N.; Kim, Y.S.; Khan, S. N-Pyrazoloyl and N-Thiopheneacetyl Hydrazone of Isatin Exhibited Potent Anti-Inflammatory and Anti-Nociceptive Properties through Suppression of NF-KB, MAPK and Oxidative Stress Signaling in Animal Models of Inflammation. *Inflamm. Res.* **2019**, *68*, 613–632. [CrossRef]
27. Meira, C.S.; dos Santos Filho, J.M.; Sousa, C.C.; Anjos, P.S.; Cerqueira, J.V.; Dias Neto, H.A.; da Silveira, R.G.; Russo, H.M.; Wolfender, J.L.; Queiroz, E.F.; et al. Structural Design, Synthesis and Substituent Effect of Hydrazone-N-Acylhydrazones Reveal Potent Immunomodulatory Agents. *Bioorg. Med. Chem.* **2018**, *26*, 1971–1985. [CrossRef]
28. Osmaniye, D.; Sağlık, B.N.; Levent, S.; Özkay, Y.; Kaplancıklı, Z.A. Design, Synthesis and Biological Evaluation of New N-Acyl Hydrazones with a Methyl Sulfonyl Moiety as Selective COX-2 Inhibitors. *Chem. Biodivers.* **2021**, *18*, e2100521. [CrossRef]
29. De Oliveira Moraes, A.D.T.; de Miranda, M.D.S.; Jacob, Í.T.T.; da Cruz Amorim, C.A.; de Moura, R.O.; da Silva, S.Â.S.; Soares, M.B.P.; de Almeida, S.M.V.; de Lima Souza, T.R.C.; de Oliveira, J.F.; et al. Synthesis, in Vitro and in Vivo Biological Evaluation, COX-1/2 Inhibition and Molecular Docking Study of Indole-N-Acylhydrazone Derivatives. *Bioorg. Med. Chem.* **2018**, *26*, 5388–5396. [CrossRef]
30. Moussa, Z.; Al-Mamary, M.; Al-Juhani, S.; Ahmed, S.A. Preparation and Biological Assessment of Some Aromatic Hydrazones Derived from Hydrazides of Phenolic Acids and Aromatic Aldehydes. *Heliyon* **2020**, *6*, e05019. [CrossRef]
31. De Melo, T.R.F.; Chelucci, R.C.; Pires, M.E.L.; Dutra, L.A.; Barbieri, K.P.; Bosquesi, P.L.; Trossini, G.H.G.; Chung, M.C.; dos Santos, J.L. Pharmacological Evaluation and Preparation of Nonsteroidal Anti-Inflammatory Drugs Containing an N-Acyl Hydrazone Subunit. *Int. J. Mol. Sci.* **2014**, *15*, 5821–5837. [CrossRef]
32. Mahy, J.P.; Gaspard, S.; Mansuy, D. Phenylhydrazones as New Good Substrates for the Dioxygenase and Peroxidase Reactions of Prostaglandin Synthase: Formation of Iron(III)-Sigma-Phenyl Complexes. *Biochemistry* **1993**, *32*, 4014–4021. [CrossRef]
33. Rana, K.; Salahuddin; Sahu, J.K. Significance of 1,3,4-Oxadiazole Containing Compounds in New Drug Development. *Curr. Drug Res. Rev.* **2021**, *13*, 90–100. [CrossRef]
34. Boström, J.; Hogner, A.; Llinàs, A.; Wellner, E.; Plowright, A.T. Oxadiazoles in Medicinal Chemistry. *J. Med. Chem.* **2012**, *55*, 1817–1830. [CrossRef]
35. Boyd, S.A.; Fung, A.K.L.; Baker, W.R.; Mantei, R.A.; Stein, H.H.; Cohen, J.; Barlow, J.L.; Klinghofer, V.; Wessale, J.L.; Verburg, K.M.; et al. Nonpeptide Renin Inhibitors with Good Intraduodenal Bioavailability and Efficacy in Dog. *J. Med. Chem.* **1994**, *37*, 2991–3007. [CrossRef]
36. Carroll, F.I.; Gray, J.L.; Abraham, P.; Kuzemko, M.A.; Lewin, A.H.; Boja, J.W.; Kuhar, M.J. 3-Aryl-2-(3′-Substituted-1′,2′,4′-Oxadiazol-5′-Yl)Tropane Analogues of Cocaine: Affinities at the Cocaine Binding Site at the Dopamine, Serotonin, and Norepinephrine Transporters. *J. Med. Chem.* **1993**, *36*, 2886–2890. [CrossRef]

37. Street, L.J.; Baker, R.; Castro, J.L.; Chambers, M.S.; Guiblin, A.R.; Hobbs, S.C.; Matassa, V.G.; Reeve, A.J.; Beer, M.S.; Middlemiss, D.N.; et al. Synthesis and Serotonergic Activity of 5-(Oxadiazolyl)Tryptamines: Potent Agonists for 5-HT1D Receptors. *J. Med. Chem.* **1993**, *36*, 1529–1538. [CrossRef]
38. Dunbar, P.G.; Durant, G.J.; Fang, Z.; Abuh, Y.F.; El-Assadi, A.A.; Ngur, D.O.; Periyasamy, S.; Hoss, W.P.; Messer, W.S. Design, Synthesis, and Neurochemical Evaluation of 5-(3-Alkyl-1,2,4-Oxadiazol-5-Yl)-1,4,5,6-Tetrahydropyrimidines as M1 Muscarinic Receptor Agonists. *J. Med. Chem.* **1993**, *36*, 842–847. [CrossRef]
39. Adelstein, G.W.; Yen, C.H.; Dajani, E.Z.; Bianchi, R.G. 3,3-Diphenyl-3-(2-Alkyl-1,3,4-Oxadiazol-5-Yl)Propylcycloalkylamines, a Novel Series of Antidiarrheal Agents. *J. Med. Chem.* **1976**, *19*, 1221–1225. [CrossRef]
40. Tully, W.R.; Gardner, C.R.; Gillespie, R.J.; Westwood, R. 2-(Oxadiazolyl)- and 2-(Thiazolyl)Imidazo[1,2-a]Pyrimidines as Agonists and Inverse Agonists at Benzodiazepine Receptors. *J. Med. Chem.* **1991**, *34*, 2060–2067. [CrossRef]
41. Orlek, B.S.; Blaney, F.E.; Brown, F.; Clark, M.S.G.; Hadley, M.S.; Hatcher, J.; Riley, G.J.; Rosenberg, H.E.; Wadsworth, H.J.; Wyman, P. Comparison of Azabicyclic Esters and Oxadiazoles as Ligands for the Muscarinic Receptor. *J. Med. Chem.* **1991**, *34*, 2726–2735. [CrossRef]
42. EL Mansouri, A.E.; Oubella, A.; Mehdi, A.; AitItto, M.Y.; Zahouily, M.; Morjani, H.; Lazrek, H.B. Design, Synthesis, Biological Evaluation and Molecular Docking of New 1,3,4-Oxadiazole Homonucleosides and Their Double-Headed Analogs as Antitumor Agents. *Bioorg. Chem.* **2021**, *108*, 104558. [CrossRef]
43. Ananth, A.H.; Manikandan, N.; Rajan, R.K.; Elancheran, R.; Lakshmithendral, K.; Ramanathan, M.; Bhattacharjee, A.; Kabilan, S. Design, Synthesis, and Biological Evaluation of 2-(2-Bromo-3-nitrophenyl)-5-phenyl-1,3,4-oxadiazole Derivatives as Possible Anti-Breast Cancer Agents. *Chem. Biodivers.* **2020**, *17*, e1900659. [CrossRef]
44. Al-Wahaibi, L.H.; Mohamed, A.A.B.; Tawfik, S.S.; Hassan, H.M.; El-Emam, A.A. 1,3,4-Oxadiazole N-Mannich Bases: Synthesis, Antimicrobial, and Anti-Proliferative Activities. *Molecules* **2021**, *26*, 2110. [CrossRef]
45. Bordei Telehoiu, A.T.; Nuță, D.C.; Căproiu, M.T.; Dumitrascu, F.; Zarafu, I.; Ioniță, P.; Bădiceanu, C.D.; Avram, S.; Chifiriuc, M.C.; Bleotu, C.; et al. Design, Synthesis and In Vitro Characterization of Novel Antimicrobial Agents Based on 6-Chloro-9H-Carbazol Derivatives and 1,3,4-Oxadiazole Scaffolds. *Molecules* **2020**, *25*, 266. [CrossRef]
46. Song, Z.L.; Zhu, Y.; Liu, J.R.; Guo, S.K.; Gu, Y.C.; Han, X.; Dong, H.Q.; Sun, Q.; Zhang, W.H.; Zhang, M.Z. Diversity-Oriented Synthesis and Antifungal Activities of Novel Pimprinine Derivative Bearing a 1,3,4-Oxadiazole-5-Thioether Moiety. *Mol. Divers.* **2020**, *25*, 205–221. [CrossRef]
47. Glomb, T.; Świątek, P. Antimicrobial Activity of 1,3,4-Oxadiazole Derivatives. *Int. J. Mol. Sci.* **2021**, *22*, 6979. [CrossRef]
48. Tantray, M.A.; Khan, I.; Hamid, H.; Alam, M.S.; Dhulap, A.; Kalam, A. Synthesis of Benzimidazole-Linked-1,3,4-Oxadiazole Carboxamides as GSK-3β Inhibitors with in Vivo Antidepressant Activity. *Bioorg. Chem.* **2018**, *77*, 393–401. [CrossRef]
49. Khokra, S.L.; Kaur, S.; Banwala, S.; Wadhwa, K.; Husain, A. Synthesis, Molecular Docking, and Biological Evaluation of Some Novel 2-(5-Substituted 1,3,4-Oxadiazole-2-Yl)-1,3-Benzothiazole Derivatives as Anticonvulsant Agents. *Cent. Nerv. Syst. Agents Med. Chem.* **2021**, *21*, 130–141. [CrossRef]
50. Kaur, J.; Soto-Velasquez, M.; Ding, Z.; Ghanbarpour, A.; Lill, M.A.; van Rijn, R.M.; Watts, V.J.; Flaherty, D.P. Optimization of a 1,3,4-Oxadiazole Series for Inhibition of Ca^{2+}/Calmodulin-Stimulated Activity of Adenylyl Cyclases 1 and 8 for the Treatment of Chronic Pain. *Eur. J. Med. Chem.* **2019**, *162*, 568–585. [CrossRef]
51. Dewangan, D.; Nakhate, K.T.; Verma, V.S.; Nagori, K.; Badwaik, H.; Nair, N.; Tripathi, D.K.; Mishra, A. Synthesis and Molecular Docking Study of Novel Hybrids of 1,3,4-Oxadiazoles and Quinoxaline as a Potential Analgesic and Anti-Inflammatory Agents. *J. Heterocycl. Chem.* **2018**, *55*, 2901–2910. [CrossRef]
52. Gulnaz, A.R.; Mohammed, Y.H.E.; Khanum, S.A. Design, Synthesis and Molecular Docking of Benzophenone Conjugated with Oxadiazole Sulphur Bridge Pyrazole Pharmacophores as Anti Inflammatory and Analgesic Agents. *Bioorg. Chem.* **2019**, *92*, 103220. [CrossRef]
53. Puttaswamy, N.; Malojiao, V.H.; Mohammed, Y.H.E.; Sherapura, A.; Prabhakar, B.T.; Khanum, S.A. Synthesis and Amelioration of Inflammatory Paw Edema by Novel Benzophenone Appended Oxadiazole Derivatives by Exhibiting Cyclooxygenase-2 Antagonist Activity. *Biomed. Pharmacother.* **2018**, *103*, 1446–1455. [CrossRef]
54. Kashid, B.B.; Salunkhe, P.H.; Dongare, B.B.; More, K.R.; Khedkar, V.M.; Ghanwat, A.A. Synthesis of Novel of 2,5-Disubstituted 1, 3, 4- Oxadiazole Derivatives and Their in Vitro Anti-Inflammatory, Anti-Oxidant Evaluation, and Molecular Docking Study. *Bioorg. Med. Chem. Lett.* **2020**, *30*, 127136. [CrossRef]
55. Świątek, P.; Gębczak, K.; Gębarowski, T.; Urniaz, R. Biological Evaluation and Molecular Docking Studies of Dimethylpyridine Derivatives. *Molecules* **2019**, *24*, 1093. [CrossRef]
56. Świątek, P.; Strzelecka, M.; Urniaz, R.; Gębczak, K.; Gębarowski, T.; Gąsiorowski, K.; Malinka, W. Synthesis, COX-1/2 Inhibition Activities and Molecular Docking Study of Isothiazolopyridine Derivatives. *Bioorg. Med. Chem.* **2017**, *25*, 316–326. [CrossRef]
57. Vicini, P.; Incerti, M.; Doytchinova, I.A.; La Colla, P.; Busonera, B.; Loddo, R. Synthesis and Antiproliferative Activity of Benzo[d]Isothiazole Hydrazones. *Eur. J. Med. Chem.* **2006**, *41*, 624–632. [CrossRef]
58. Palla, G.; Predieri, G.; Domiano, P.; Vignali, C.; Turner, W. Conformational Behaviour and E/Z Isomerization of N-Acyl and N-Aroylhydrazones. *Tetrahedron* **1986**, *42*, 3649–3654. [CrossRef]
59. Wyrzykiewicz, E.; Prukała, D. New Isomeric *N* -Substituted Hydrazones of 2-, 3-and 4-Pyridinecarboxaldehydes. *J. Heterocycl. Chem.* **1998**, *35*, 381–387. [CrossRef]

60. Galić, N.; Perić, B.; Kojić-Prodić, B.; Cimerman, Z. Structural and Spectroscopic Characteristics of Aroylhydrazones Derived from Nicotinic Acid Hydrazide. *J. Mol. Struct.* **2001**, *559*, 187–194. [CrossRef]
61. Tesei, A.; Ulivi, P.; Fabbri, F.; Rosetti, M.; Leonetti, C.; Scarsella, M.; Zupi, G.; Amadori, D.; Bolla, M.; Zoli, W. In Vitro and In Vivo Evaluation of NCX 4040 Cytotoxic Activity in Human Colon Cancer Cell Lines. *J. Transl. Med.* **2005**, *3*, 7. [CrossRef]
62. Zheng, C.Y.; Xiao, W.; Zhu, M.X.; Pan, X.J.; Yang, Z.H.; Zhou, S.Y. Inhibition of Cyclooxygenase-2 by Tetramethylpyrazine and Its Effects on A549 Cell Invasion and Metastasis. *Int. J. Oncol.* **2012**, *40*, 2029–2037. [CrossRef]
63. Hu, L.X.; Du, Y.Y.; Zhang, Y.; Pan, Y.Y. Synergistic Effects of Exemestane and Aspirin on MCF-7 Human Breast Cancer Cells. *Asian Pac. J. Cancer Prev.* **2012**, *13*, 5903–5908. [CrossRef]
64. van Meerloo, J.; Kaspers, G.J.L.; Cloos, J. Cell Sensitivity Assays: The MTT Assay. In *Cancer Cell Culture. Methods in Molecular Biology (Methods and Protocols)*; Cree, I.A., Ed.; Humana Press: Clifton, NJ, USA, 2011; Volume 731, pp. 237–245. [CrossRef]
65. A549 Cell Line: Cell Culture and Transfection Protocol. Available online: https://www.a549.com/ (accessed on 25 November 2021).
66. Federico, A.; Morgillo, F.; Tuccillo, C.; Ciardiello, F.; Loguercio, C. Chronic Inflammation and Oxidative Stress in Human Carcinogenesis. *Int. J. Cancer* **2007**, *121*, 2381–2386. [CrossRef]
67. Ferrari, G.V.; Natera, J.; Paulina Montaña, M.; Muñoz, V.; Gutiérrez, E.L.; Massad, W.; Miskoski, S.; García, N.A. Scavenging of Photogenerated ROS by Oxicams. Possible Biological and Environmental Implications. *J. Photochem. Photobiol. B Biol.* **2015**, *153*, 233–239. [CrossRef]
68. Van Antwerpen, P.; Nève, J. In Vitro Comparative Assessment of the Scavenging Activity against Three Reactive Oxygen Species of Non-Steroidal Anti-Inflammatory Drugs from the Oxicam and Sulfoanilide Families. *Eur. J. Pharmacol.* **2004**, *496*, 55–61. [CrossRef]
69. García, N.A.; Bregliani, M.; Pajares, A. Interaction of Non-Steroidal Anti-Inflammatory Drugs (NSAIDs) with Reactive Oxygen Species (ROS): Possible Biomedical Implications. In *Pain Relief—From Analgesics to Alternative Therapies*; Maldonado, C., Ed.; InTechOpen: London, UK, 2017. [CrossRef]
70. Hong, J.H.; Lee, I.S. Cytoprotective Effect of Artemisia Capillaris Fractions on Oxidative Stress-Induced Apoptosis in V79 Cells. *BioFactors* **2009**, *35*, 380–388. [CrossRef]
71. Chubatsu, L.S.; Gennari, M.; Meneghini, R. Glutathione Is the Antioxidant Responsible for Resistance to Oxidative Stress in V79 Chinese Hamster Fibroblasts Rendered Resistant to Cadmium. *Chem. Biol. Interact.* **1992**, *82*, 99–110. [CrossRef]
72. Boojar, M.M.A.; Shockravi, A. On the Cytotoxicity and Status of Oxidative Stress of Two Novel Synthesized Tri-Aza Macrocyclic Diamides as Studied in the V79 Cell Lines. *Bioorg. Med. Chem.* **2007**, *15*, 3437–3444. [CrossRef]
73. Speit, G.; Haupter, S.; Schütz, P.; Kreis, P. Comparative Evaluation of the Genotoxic Properties of Potassium Bromate and Potassium Superoxide in V79 Chinese Hamster Cells. *Mutat. Res.-Genet. Toxicol. Environ. Mutagen.* **1999**, *439*, 213–221. [CrossRef]
74. Szczęśniak-Siega, B.; Gębczak, K.; Gębarowski, T.; Maniewska, J. Synthesis, COX-1/2 Inhibition and Antioxidant Activities of New Oxicam Analogues Designed as Potential Chemopreventive Agents. *Acta Biochim. Pol.* **2018**, *65*, 199–207. [CrossRef]
75. Miciaccia, M.; Belviso, B.D.; Iaselli, M.; Cingolani, G.; Ferorelli, S.; Cappellari, M.; Loguercio Polosa, P.; Perrone, M.G.; Caliandro, R.; Scilimati, A. Three-Dimensional Structure of Human Cyclooxygenase (HCOX)-1. *Sci. Rep.* **2021**, *11*, 1–18. [CrossRef]
76. Xu, S.; Hermanson, D.J.; Banerjee, S.; Ghebreselasie, K.; Clayton, G.M.; Garavito, R.M.; Marnett, L.J. Oxicams Bind in a Novel Mode to the Cyclooxygenase Active Site via a Two-Water-Mediated h-Bonding Network. *J. Biol. Chem.* **2014**, *289*, 6799–6808. [CrossRef]
77. Orlando, B.J.; Malkowski, M.G. Crystal Structure of Rofecoxib Bound to Human Cyclooxygenase-2. *Acta Crystallogr. Sect. Struct. Biol. Commun.* **2016**, *72*, 772–776. [CrossRef]
78. *DSV: Discover Studio Visualiser, V21.1.0.20298*; BIOVIA, Dassault Systèmes: San Diego, SA, USA, 2020.
79. Eruslanov, E.; Kusmartsev, S. Identification of ROS Using Oxidized DCFDA and Flow-Cytometry. *Methods Mol. Biol.* **2010**, *594*, 57–72. [CrossRef]
80. Loo, A.E.K.; Halliwell, B. Effects of Hydrogen Peroxide in a Keratinocyte-Fibroblast Co-Culture Model of Wound Healing. *Biochem. Biophys. Res. Commun.* **2012**, *423*, 253–258. [CrossRef]
81. Schaftenaar, G.; Noordik, J.H. Molden: A Pre- and Post-Processing Program for Molecular and Electronic Structures. *J. Comput. Aided. Mol. Des.* **2000**, *14*, 123–134. [CrossRef]
82. Frisch, M.J.; Trucks, G.W.; Schlegel, H.B.; Scuseria, G.E.; Robb, M.A.; Cheeseman, J.R.; Scalmani, G.; Barone, V.; Mennucci, B.; Petersson, G.A. *Gaussian 16 Revision C.01*; Gaussian, Inc.: Wallingford, CT, USA, 2016.
83. Chai, J.D.; Head-Gordon, M. Long-Range Corrected Hybrid Density Functionals with Damped Atom-Atom Dispersion Corrections. *Phys. Chem. Chem. Phys.* **2008**, *10*, 6615–6620. [CrossRef]
84. Hohenberg, P.; Kohn, W. Inhomogeneous Electron Gas. *Phys. Rev.* **1964**, *136*, B864. [CrossRef]
85. Kohn, W.; Sham, L.J. Quantum Density Oscillations in an Inhomogeneous Electron Gas. *Phys. Rev.* **1965**, *137*, A1697. [CrossRef]
86. Dunning, T.H. Gaussian Basis Sets for Use in Correlated Molecular Calculations. I. The Atoms Boron through Neon and Hydrogen. *J. Chem. Phys.* **1989**, *90*, 1007–1023. [CrossRef]
87. Thompson, J.D.; Higgins, D.G.; Gibson, T.J. CLUSTAL W: Improving the Sensitivity of Progressive Multiple Sequence Alignment through Sequence Weighting, Position-Specific Gap Penalties and Weight Matrix Choice. *Nucleic Acids Res.* **1994**, *22*, 4673–4680. [CrossRef]

88. Larkin, M.A.; Blackshields, G.; Brown, N.P.; Chenna, R.; Mcgettigan, P.A.; McWilliam, H.; Valentin, F.; Wallace, I.M.; Wilm, A.; Lopez, R.; et al. Clustal W and Clustal X Version 2.0. *Bioinformatics* **2007**, *23*, 2947–2948. [CrossRef]
89. Humphrey, W.; Dalke, A.; Schulten, K. VMD: Visual Molecular Dynamics. *J. Mol. Graph.* **1996**, *14*, 33–38. [CrossRef]
90. Forli, S.; Huey, R.; Pique, M.E.; Sanner, M.F.; Goodsell, D.S.; Olson, A.J. Computational protein-ligand docking and virtual drug screening with the AutoDock suite. *Nat. Protoc.* **2016**, *11*, 905–919. [CrossRef]
91. Trott, O.; Olson, A.J. AutoDock Vina: Improving the Speed and Accuracy of Docking with a New Scoring Function, Efficient Optimization, and Multithreading. *J. Comput. Chem.* **2009**, *31*, 455–461. [CrossRef]
92. *PyMOL: The PyMOL Molecular Graphics System, Version 2.3.0*; Schrödinger LLC.: New York, NY, USA, 2020.

Supplementary materials

Biological Evaluation and Molecular Docking Studies of Novel 1,3,4-Oxadiazole Derivatives of 4,6-Dimethyl-2-Sulfanylpyridine-3-Carboxamide

Piotr Świątek [1]*, Teresa Glomb [1]*, Agnieszka Dobosz [2], Tomasz Gębarowski [3], Kamil Wojtkowiak [4], Aneta Jezierska [4], Jarosław J. Panek [4], Małgorzata Świątek [5], Małgorzata Strzelecka [1]

1 Department of Medicinal Chemistry, Faculty of Pharmacy, Wroclaw Medical University, Borowska 211, 50-556 Wroclaw, Poland; malgorzata.strzelecka@umw.edu.pl (M.S.)
2 Department of Medical Science Foundation, Faculty of Pharmacy, Wroclaw Medical University, Borowska 211, 50-556 Wroclaw, Poland; agnieszka.dobosz@umw.edu.pl (A.D.)
3 Department of Biostructure and Animal Physiology, Wroclaw University of Environmental and Life Sciences, Kożuchowska 1/3, 51-631 Wroclaw, Poland; tomasz.gebarowski@upwr.edu.pl (T.G.)
4 University of Wroclaw, Faculty of Chemistry, F. Joliot-Curie 14, 50-383 Wrocław, Poland; jaroslaw.panek@chem.uni.wroc.pl (J.J.P.); aneta.jezierska@chem.uni.wroc.pl (A.J.); kamil.wojtkowiak@chem.uni.wroc.pl (K.W.)
5 Hospital Pharmacy, University Clinical Hospital, Borowska 213, 50-556 Wrocław, Poland; mswiatek@usk.wroc.pl (M.Ś)
* Correspondence: piotr.swiatek@umw.edu.pl (P.Ś.); teresa.glomb@umw.edu.pl (T.G.), Tel.: +48-717840391

(a)

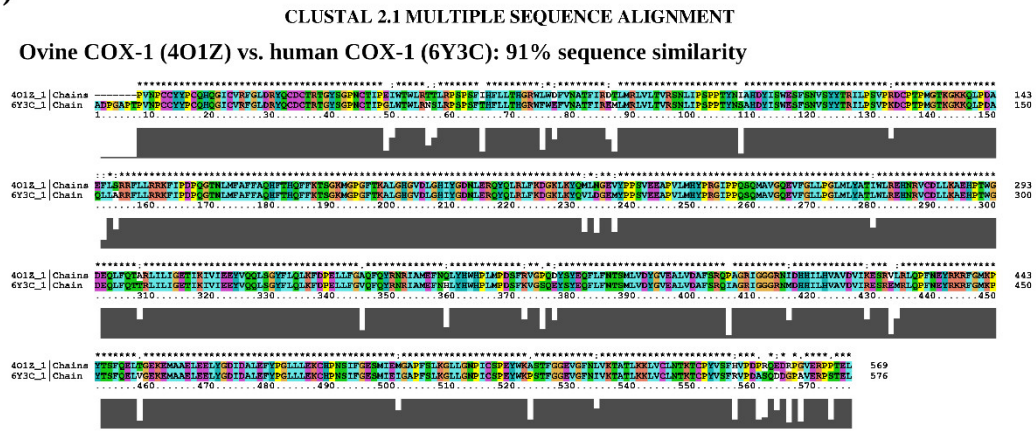

(b)

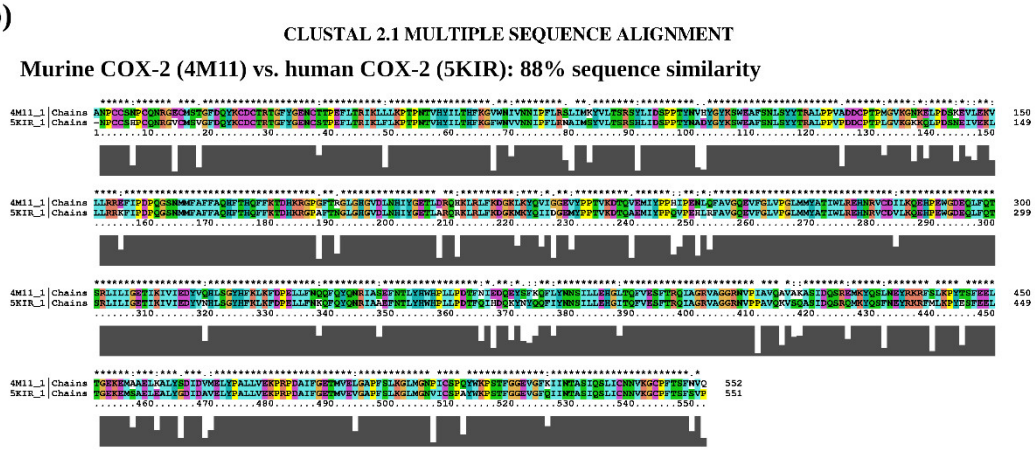

(c)

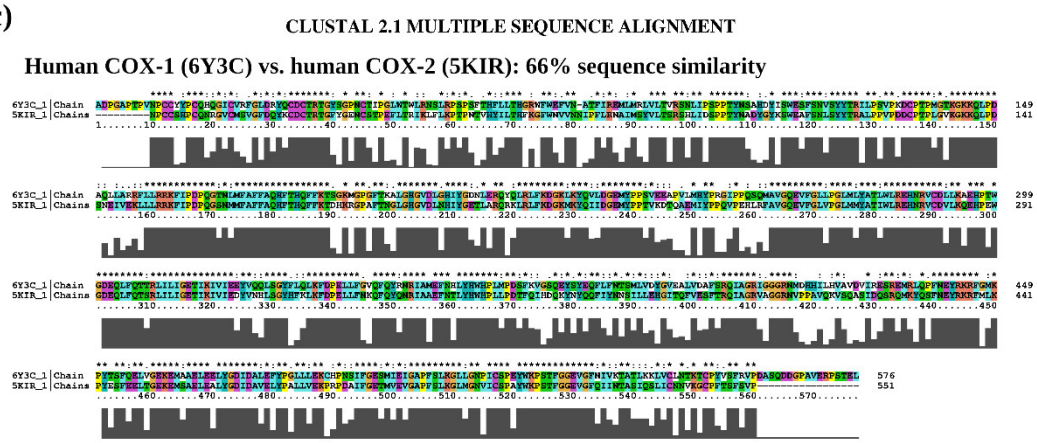

Figure S1. Sequence alignment of the proteins used in the study: (**a**) ovine COX-1 vs. human COX-1, (**b**) murine COX-2 vs. human COX-2, and (**c**) human COX-1 vs. human COX-2.

Table S1. The SCF energies for two series of examined compounds calculated at the ωB97XD/cc-pVDZ level of theory.

Total and relative energy of the structures				
Compound	**SCF energy [kcal/mol]**	**Compound**	**SCF energy [kcal/mol]**	**Relative energy of E vs. S [kcal/mol]**
4(E)	-1164210.45	**4(S)**	-1164209.94	-0.5
5(E)	-1333053.63	**5(S)**	-1333063.04	9.4
6(E)	-1395310.96	**6(S)**	-1395321.67	10.7
7(E)	-1357719.42	**7(S)**	-1357729.16	9.7
8(E)	-1607580.85	**8(S)**	-1607590.47	9.6
9(E)	-1390917.34	**9(S)**	-1390928.55	11.2
10(E)	-1621455.36	**10(S)**	-1621464.66	9.3
11(E)	-1544506.58	**11(S)**	-1544516.83	10.3
12(E)	-1621455.04	**12(S)**	-1621464.31	9.3
13(E)	-2947974.15	**13(S)**	-2947984.65	10.5

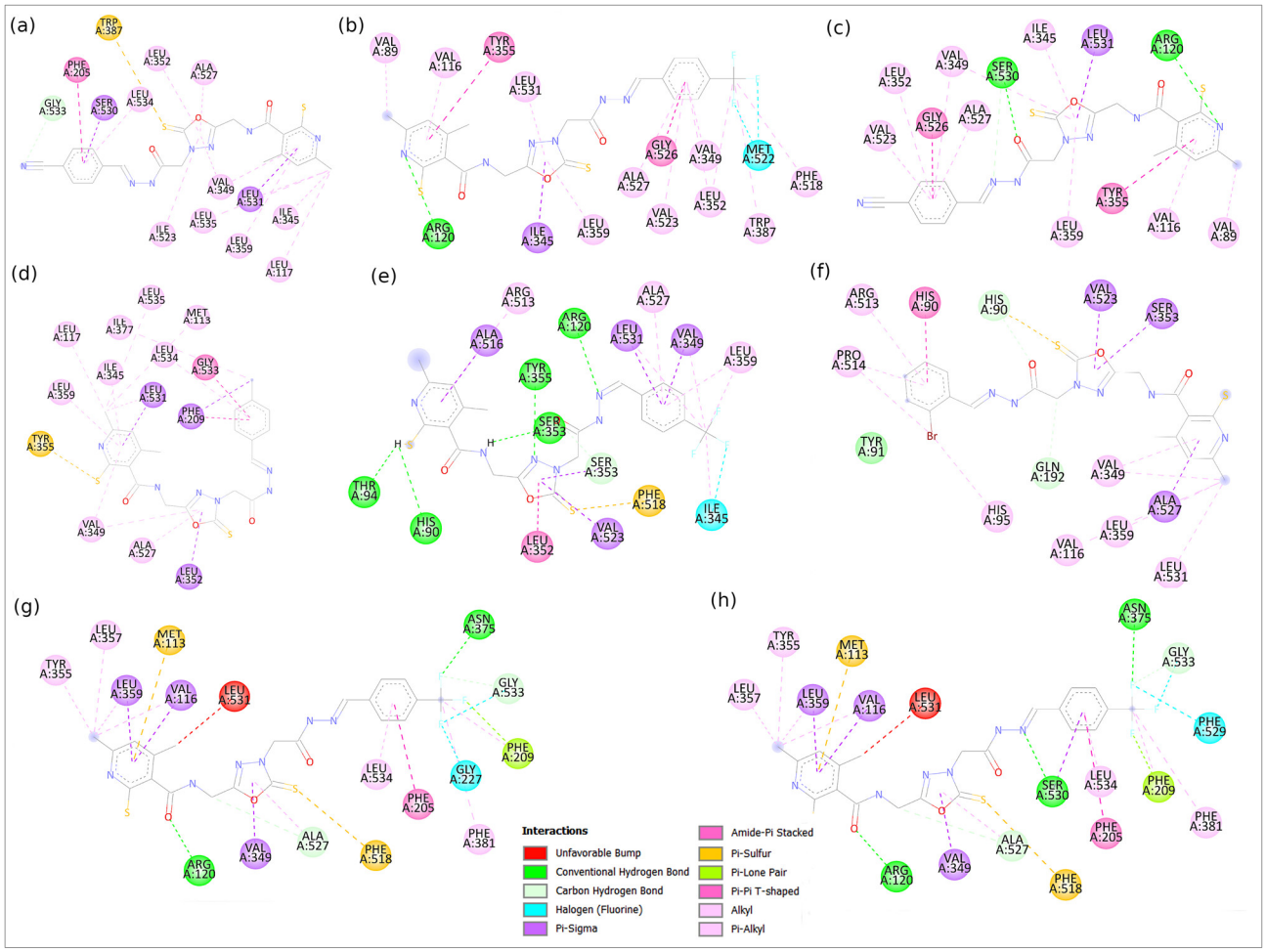

Figure S2. Non-covalent interactions 2D diagram for studied compounds in receptor binding sites: (**a**) **9(S)** in ovine COX1, (**b**) **11(E)** in murine COX2, (**c**) **9(S)** in murine COX2, (**d**) **7(E)** in ovine COX1, (**e**) **11(E)** in human COX2, (**f**) **13(S)** in human COX2, (**g**) **11(S)** in human COX1, (**h**) **11(E)** in human COX1.

PUBLIKACJA P2

WRAZ Z MATERIAŁAMI UZUPEŁNIAJĄCYMI

International Journal of
Molecular Sciences

IMPACT FACTOR 5.6
Indexed in: PubMed
CITESCORE 7.8

Article

Synthesis, Anticancer Activity and Molecular Docking Studies of Novel *N*-Mannich Bases of 1,3,4-Oxadiazole Based on 4,6-Dimethylpyridine Scaffold

Małgorzata Strzelecka, Teresa Glomb, Małgorzata Drąg-Zalesińska, Julita Kulbacka, Anna Szewczyk, Jolanta Saczko, Paulina Kasperkiewicz-Wasilewska, Nina Rembiałkowska, Kamil Wojtkowiak, Aneta Jezierska et al.

Special Issue
Bioactive Oxadiazoles 3.0

Edited by
Dr. Antonio Palumbo Piccionello

MDPI

https://doi.org/10.3390/ijms231911173

International Journal of
Molecular Sciences

MDPI

Article

Synthesis, Anticancer Activity and Molecular Docking Studies of Novel *N*-Mannich Bases of 1,3,4-Oxadiazole Based on 4,6-Dimethylpyridine Scaffold

Małgorzata Strzelecka [1], Teresa Glomb [1,*], Małgorzata Drąg-Zalesińska [2], Julita Kulbacka [3], Anna Szewczyk [3,4], Jolanta Saczko [3], Paulina Kasperkiewicz-Wasilewska [5], Nina Rembiałkowska [3], Kamil Wojtkowiak [6], Aneta Jezierska [6] and Piotr Świątek [1,*]

1 Department of Medicinal Chemistry, Faculty of Pharmacy, Wroclaw Medical University, Borowska 211, 50-556 Wroclaw, Poland
2 Division of Histology and Embryology, Department of Human Morphology and Embryology, Faculty of Medicine, Wroclaw Medical University, Chałubińskiego 6a, 50-368 Wroclaw, Poland
3 Department of Molecular and Cellular Biology, Faculty of Pharmacy, Wroclaw Medical University, Borowska 211, 50-556 Wroclaw, Poland
4 Department of Animal Developmental Biology, Institute of Experimental Biology, University of Wroclaw, Sienkiewicza 21, 50-335 Wroclaw, Poland
5 Department of Bioorganic Chemistry, Faculty of Chemistry, Wroclaw University of Science and Technology, Wybrzeże Wyspiańskiego 27, 50-370 Wroclaw, Poland
6 Faculty of Chemistry, University of Wroclaw, F. Joliot-Curie 14, 50-383 Wroclaw, Poland
* Correspondence: teresa.glomb@umw.edu.pl (T.G.); piotr.swiatek@umw.edu.pl (P.Ś.); Tel.: +48-7-1784-0391 (P.Ś.)

check for updates

Citation: Strzelecka, M.; Glomb, T.; Drąg-Zalesińska, M.; Kulbacka, J.; Szewczyk, A.; Saczko, J.; Kasperkiewicz-Wasilewska, P.; Rembiałkowska, N.; Wojtkowiak, K.; Jezierska, A.; et al. Synthesis, Anticancer Activity and Molecular Docking Studies of Novel *N*-Mannich Bases of 1,3,4-Oxadiazole Based on 4,6-Dimethylpyridine Scaffold. *Int. J. Mol. Sci.* **2022**, *23*, 11173. https://doi.org/10.3390/ijms231911173

Academic Editor: Antonio Palumbo Piccionello

Received: 18 August 2022
Accepted: 20 September 2022
Published: 22 September 2022

Publisher's Note: MDPI stays neutral with regard to jurisdictional claims in published maps and institutional affiliations.

Copyright: © 2022 by the authors. Licensee MDPI, Basel, Switzerland. This article is an open access article distributed under the terms and conditions of the Creative Commons Attribution (CC BY) license (https://creativecommons.org/licenses/by/4.0/).

Abstract: Cancer is one of the greatest challenges in modern medicine today. Difficult and long-term treatment, the many side effects of the drugs used and the growing resistance to treatment of neoplastic cells necessitate new approaches to therapy. A very promising targeted therapy is based on direct impact only on cancer cells. As a continuation of our research on new biologically active molecules, we report herein the design, synthesis and anticancer evaluation of a new series of *N*-Mannich-base-type hybrid compounds containing morfoline or different substituted piperazines moieties, a 1,3,4-oxadiazole ring and a 4,6-dimethylpyridine core. All compounds were tested for their potential cytotoxicity against five human cancer cell lines, A375, C32, SNB-19, MCF-7/WT and MCF-7/DX. Two of the active *N*-Mannich bases (compounds **5** and **6**) were further evaluated for growth inhibition effects in melanoma (A375 and C32), and normal (HaCaT) cell lines using clonogenic assay and a population doubling time test. The apoptosis was determined with the neutral version of comet assay. The confocal microscopy method enabled the visualization of F-actin reorganization. The obtained results demonstrated that compounds **5** and **6** have cytotoxic and proapoptotic effects on melanoma cells and are capable of inducing F-actin depolarization in a dose-dependent manner. Moreover, computational chemistry approaches, molecular docking and electrostatic potential were employed to study non-covalent interactions of the investigated compounds with four receptors. It was found that all the examined molecules exhibit a similar binding affinity with respect to the chosen reference drugs.

Keywords: dimethylpyridine; 1,3,4-oxadiazole; *N*-Mannich base; anticancer activity; cytotoxicity; molecular docking; non-covalent interactions

1. Introduction

Nowadays, the treatment of cancer is an enormous challenge for medicine. In terms of mortality, according to the World Health Organization (WHO), neoplastic disease is the leading cause of death around the world. The most common cancers in 2020 were breast, lung, colon and rectum. High morbidity and mortality result mainly from unhealthy

lifestyle, alcohol and tobacco use or lack of physical activity [1]. Due to the diverse pathogenesis of cancer and the multidirectional nature of mutations in the genetic material, treatment is a very long and complicated process. The ability of neoplastic cells to avoid the apoptosis process, induce angiogenesis, stimulate proliferative factors and be insensitive to growth inhibitory signals leads to uncontrolled cell proliferation in the body [2]. In addition, the side effects of anticancer drugs mainly affecting healthy, rapidly dividing cells, e.g., hair loss, neutropenia, nausea and vomiting, are also a limitation in the treatment process [3]. Unfortunately, more and more cancer cells develop multi-drug resistance (MDR) to chemotherapeutic agents, which makes pharmacotherapy much more challenging. The mechanisms of MDR in cancer cells may be due to increased drug efflux, accelerated drug metabolism or various genetic factors [4,5].

Scientists around the world are working on new methods of fighting cancer, which would allow for increased effectiveness of treatment and minimization of undesirable effects of the therapy. Additionally, an increasingly accurate understanding of the molecular pathogenesis of carcinogenesis allows for the implementation of targeted therapy that focuses only on tumor cells and reduces side effects on healthy tissues [6]. A very popular molecular target of new structures is a group of receptors with tyrosine kinase activity. They include, among others, epidermal growth factor (EGFR, HER2) or mesenchymal–epithelial transition factor (c-MET) receptors. An overexpression of the activity of these receptors in the body results in excessive cell proliferation, their increased survival, and the progression of metastases. Additionally, the overtime activity of these receptors may contribute to the increased cell resistance to the treatment [7–9]. Another target might be tropomyosin receptor kinase A (TrkA)—overexpression of which leads to the tumor progression and invasions [10]. Molecules that directly and selectively inhibit these types of receptors have a great potential for their use in anticancer therapy. Moreover, there are new approaches to cancer treatment, including immunotherapy, stem cell or gene therapy [11,12].

Multi-component reactions (MCRs) constitute a major part in the present-day organic synthesis in the field of drug design. The Mannich reaction, also named as aminomethylation or aminoalkylation reactions, is a three-component condensation between structurally diverse substrates containing at least one active hydrogen atom, an amine reagent (primary or secondary amines), and an aldehyde component [13]. Mannich bases are known to play a vital role in the development of synthetic pharmaceutical chemistry. By the introduction of a polar functional group, aminomethylation increases the hydrophilic properties of drugs and improves their distribution in the human body. The Mannich reaction can also enhance the lipophilic properties of a drug by selection of the appropriate amine reagent [14]. Studies in the literature revealed that Mannich bases derived from various heterocycles exhibit several biological activities, such as antioxidant [15], analgesic and anti-inflammatory [16–18], antimicrobial [19–21] and anticonvulsant [22,23] activities. In addition, there is a growing interest in the anticancer activity of Mannich bases. Several classes of NH-azoles have been aminomethylated with a view to synthesize cytotoxic compounds against human cancers, such as lung, gastric, liver, breast, ovarian, prostate and colon cancers [24–28].

On the other hand, 1,3,4-oxadiazoles are of great importance due to their biological activity as well as synthetic applications in medicinal chemistry [29–33]. It is worth mentioning the excellent anticancer activity of 1,3,4-oxadiazole derivatives demonstrated in several studies, both in in vitro and in vivo models. 1,3,4-Oxadiazoles can exert the antitumor activity through multiple mechanisms, such as targeting epidermal growth factor receptors (EGFR, HER2) [34–37], mesenchymal–epithelial transition factor receptor (c-MET) [38], focal-adhesion kinase (FAK) [28], histone deacetylases (HDAC) [39], telomerase [26,40], thymidylate synthase (TS) [41], tubulin [42] or the DNA structure [27]. 1,3,4-Oxadiazole rings are used as bioisosteres for carbonyl-containing compounds, offering increased water solubility and improved metabolic stability [32,43,44]. Li et al. replaced the amide bond of the scaffold in imatinib, a tyrosine kinase inhibitor used to treat a number of leukemias, to form 1,3,4-oxadiazole analogs of imatinib [45]. This modification

enhanced the inhibitory activity against the human leukemia stem-like cell line (KG1a), and the potencies of compound **I** (Figure 1) being over 30 times more remarkable than that of imatinib.

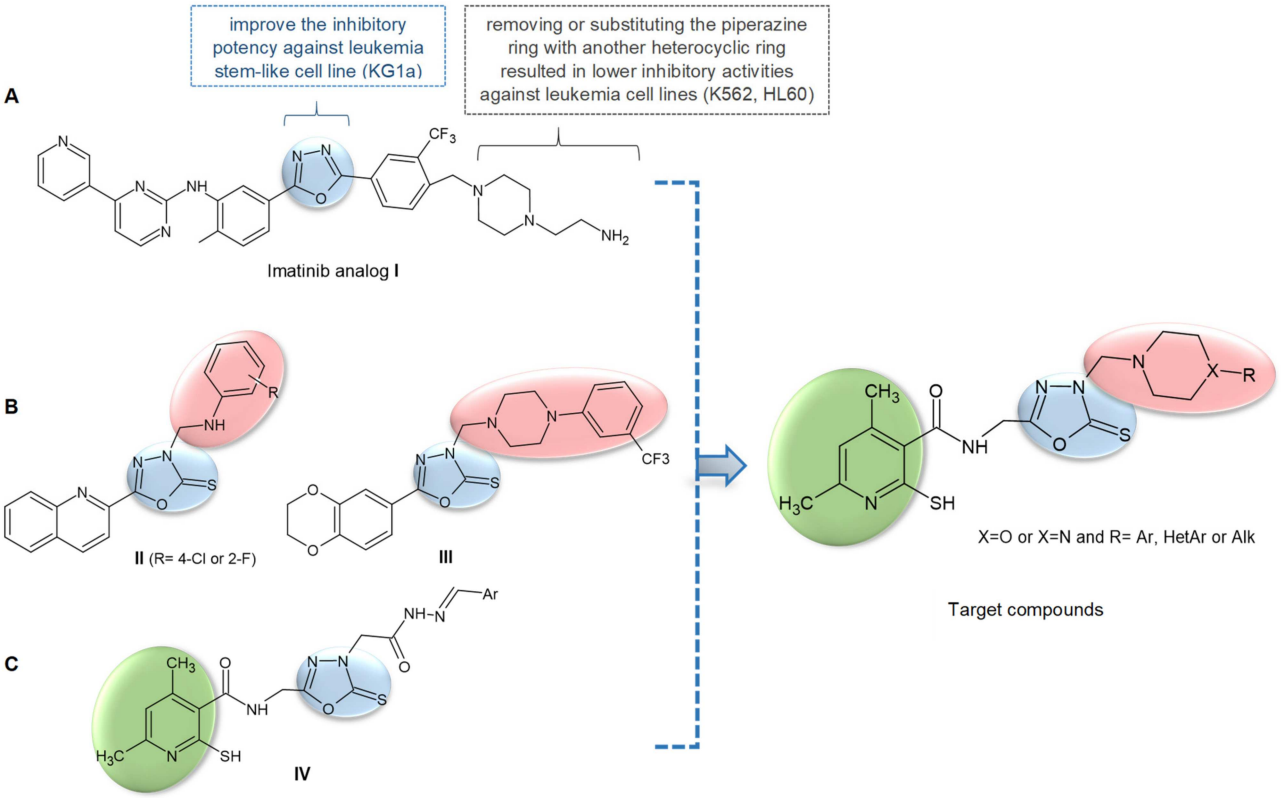

Figure 1. (**A**) The 1,3,4-oxadiazole analog of imatinib with structure–activity relationships; (**B**) 1,3,4-Oxadiazole-derived *N*-Mannich bases with anticancer activity; (**C**) Our previously reported anticancer 1,3,4-oxazdiazole derivatives, and general structure of the target compounds.

The combination of different pharmacophores in the same unit is an attractive approach to discover novel potent drugs, due to the possible synergistic effect. Several reports of Mannich bases of 1,3,4-oxadiazole rings as cytotoxic agents are available in the recent literature. Anticancer screening studies for a series of *N*-Mannich bases of 5-(quinolin-2-yl)-1,3,4-oxadiazole-2(3*H*)-thione showed that compounds **II** (Figure 1) displayed broad-spectrum antitumor activity against a panel consisting of human hepatoma (HepG2), gastric (SGC-7901) and breast (MCF-7) cancer cell lines using the MTT (3-[4,5-dimethylthiazol-2-yl]-2,5-diphenyltetrazolium bromide) method, and were more potent (2.5- or even 27-fold) compared to that of 5-fluorouracil, widely used in the treatment of cancer [26]. Moreover, the tested compounds **II** exhibited a potent telomerase inhibitory potency with IC_{50} ranging from 0.8 to 0.9 μM. Another 1,3,4-oxadiazole-2(3*H*)-thione derivative containing a phenylpiperazine skeleton **III** (Figure 1) exhibited a stronger cytotoxic effect on hepatoma cancer cells (HepG2) with 2.3-fold higher activity than the reference 5-fluorouracil. Additional studies for focal-adhesion kinase inhibition showed remarkable in vitro inhibitory activity of compound **III** (IC_{50} = 0.78 μM) supported by molecular docking of this compound into active site of FAK [28].

In our recently published work, we demonstrated that 1,3,4-oxadiazole derivatives of 4,6-dimethylpyridine **IV** (Figure 1) containing differently substituted *N*-acyl hydrazone moieties exhibited potent anticancer activity against a panel consisting of human lung (A549), breast (MCF-7) and colon (LoVo) and its drug-resistant subline LoVo/Dx cancer cell lines [46]. Encouraged by those promising results, we decided to modify the structure of the above-mentioned derivatives by replacing the Schiff base-type pharmacophore at position 4 of 1,3,4-oxadiazole with secondary amines linked to the heterocycle by a methylene

bridge (Figure 1). The introduction of this aminomethyl function, which resulted in a new series of *N*-Mannich bases, was inspired by the leading research described in the previously cited literature. By such modification, we wanted to determine the impact of the aryl/heteroaryl/alkylpiperazine or morpholine residues on the cytotoxic activity of the compounds and selectivity towards cancer cell lines.

The new compounds were examined for their potential cytotoxicity against selected human cancer cell lines: melanotic (A375) and amelanotic (C32) melanoma, glioblastoma (SNB-19), breast adenocarcinoma (MCF-7/WT) and drug-resistant breast adenocarcinoma (MCF-7/DX); and, additionally, normal cells—human keratinocytes (HaCaT)—were included in the study. Two of the compounds (**5** and **6**) that displayed promising cytotoxic activity in preliminary study were further evaluated for growth inhibition effects in melanoma (A375 and C32) and normal (HaCaT) cell lines using clonogenic assay and a population doubling time test. The apoptosis was determined with the neutral version of comet assay. The confocal microscopy method enabled the visualization of F-actin reorganization. Our experimental findings were supported by computational chemistry approaches: molecular docking and electronic structure study on the basis of electrostatic potential maps (EPMs).

2. Results and Discussion

2.1. Chemistry

The synthesis of *N*-(2-hydrazinyl-2-oxoethyl)-4,6-dimethyl-2-sulfanylpyridine-3-carbo xamide **1** was performed according to the protocols published previously [47]. Scheme 1 presents the synthesis of compounds that have not been described in the literature yet. The spectroscopic properties of all newly obtained derivatives were in good agreement with their predicted structures and are summarized in the experimental section. The formation of final *N*-Mannich bases **3**–**12** was achieved via a convenient and efficient one-step reaction of compound **2** with appropriate secondary amines (piperazine derivatives or morpholine) and formaldehyde in ethanol. The structures of the various synthesized compounds were determined based on spectral data analysis, such as FT-IR, ^{1}H NMR, ^{13}C NMR and MS.

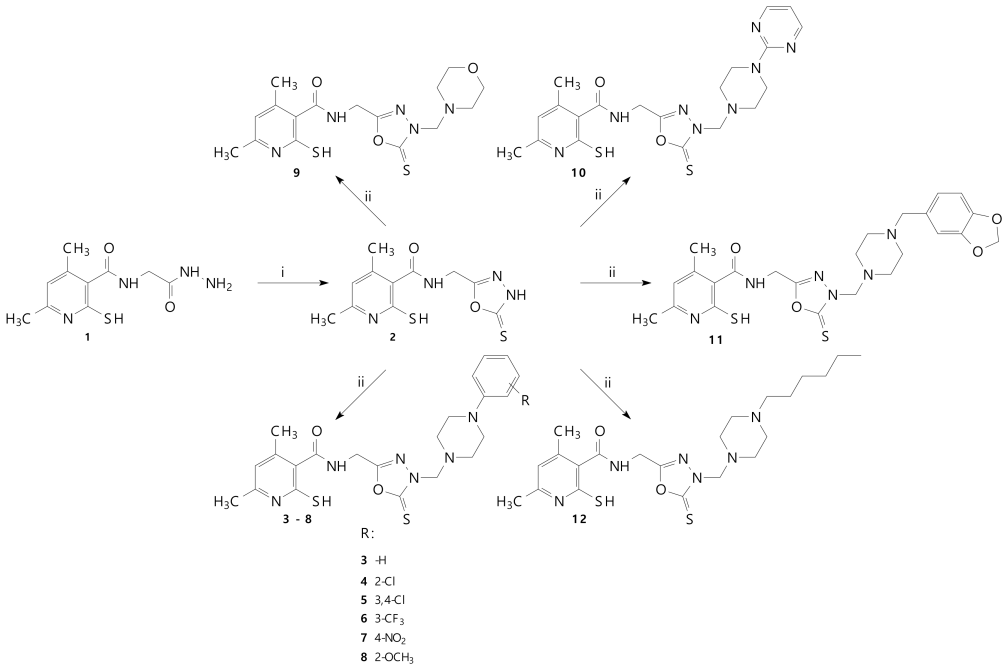

Scheme 1. Scheme of the synthesis of new compounds **3**–**12**. Reagents and conditions: (i) CS_2, KOH, HCl, ethanol, reflux; (ii) formaldehyde, amine, ethanol, RT.

The FT-IR spectra of compounds **3**–**12** showed peaks around 1650–1660 cm^{-1} due to carbonyl function derived from the amide structure. Additionally, the IR spectra exhibited, in the 3285–3155 cm^{-1} range, the NH weak band of the CONH functions.

The distinctive peak in the ^{1}H NMR spectrum near δ 5.00 ppm and the signal at around δ 70.00 ppm in the ^{13}C NMR spectrum clearly indicate the formation of the methylene linker characteristic for Mannich bases. Additionally, in the ^{1}H NMR spectra of the final compounds, the signals of the piperazine or morpholine protons, in the form of two four-proton multiplets in the range of 2.38–3.73 ppm, were recorded. All NMR spectra are presented in Table S1 in Supplementary Materials.

The HRMS (ESI-MS) of **3**–**12** showed the characteristic corresponding peaks to their molecular formula.

2.2. Biological Tests

2.2.1. MTT Cell Viability Assay

The cell viability assay in cytotoxic evaluation is a major step in analyzing the cellular response to toxic compounds and plays a crucial role in determining the cell survival rate and assessment of metabolic activity. The preliminary cytotoxicity study of *N*-Mannich bases **3**–**12** was carried out on five human cancer cell lines: melanotic (A375) and amelanotic (C32) melanoma, glioblastoma (SNB-19), and sensitive (MCF-7/WT) and doxorubicin-resistant (MCF-7/DX) breast adenocarcinoma, using the MTT colorimetric method. The obtained results, shown in Figure 2, demonstrated the highest anticancer potential of compounds **5** and **6**, containing 3,4-dichloro- and 3-trifluorophenylpiperazine moieties, respectively, and these two were selected for the more detailed study. There were selected skin cancer cell lines (A375 and C32), and, additionally, normal cells—human keratinocytes (HaCaT)—were included in the study. The response of cells to incubation with *N*-Mannich bases varied in different cell lines (Figure 3). Both skin cancers and normal cells were highly sensitive to the growth inhibitory activity of compound **5** at a concentration of 100 μM. In the case of compound **6**, melanomas A375 and C32 were more affected at lower concentrations in comparison to keratinocytes. It is worth noting that the A375 cell line was more sensitive to both *N*-Mannich bases than the C32 cell line. The most significant cytotoxic effect was observed for compound **5** against A375 cells (IC_{50} = 80.79 μM) (Table 1). This indicates the cytotoxicity of compounds at low concentrations and short incubation time, which was confirmed by the population doubling time test.

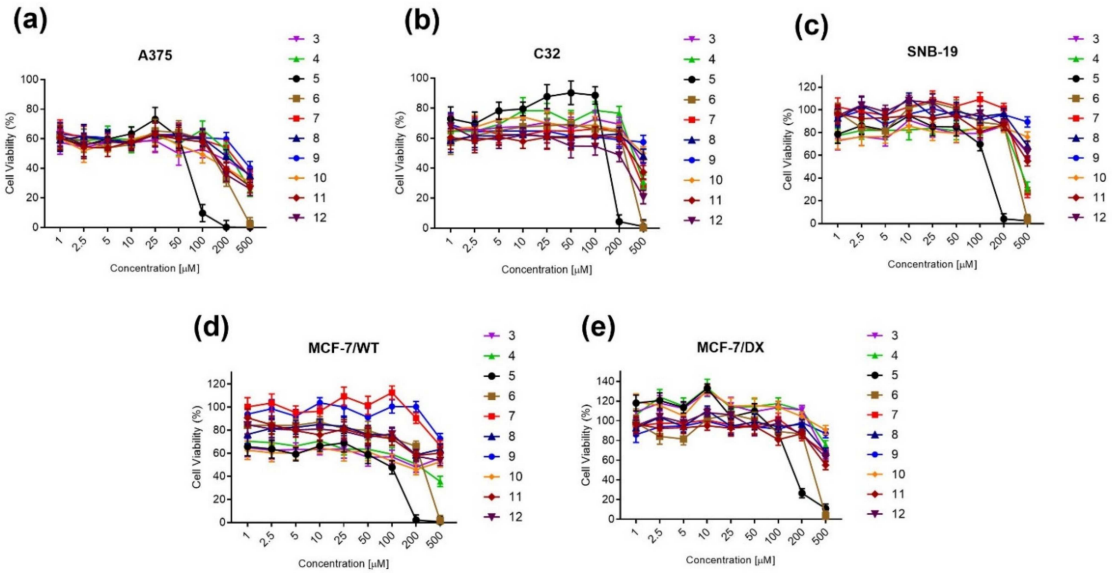

Figure 2. The cell viability after 24 h determined by the MTT colorimetric assay in (**a**) melanotic melanoma A375 cells, (**b**) amelanotic melanoma C32 cells, (**c**) glioblastoma SNB-19 cells, (**d**) breast adenocarcinoma MCF-7/WT cells and (**e**) drug-resistant breast adenocarcinoma MCF-7/DX cells.

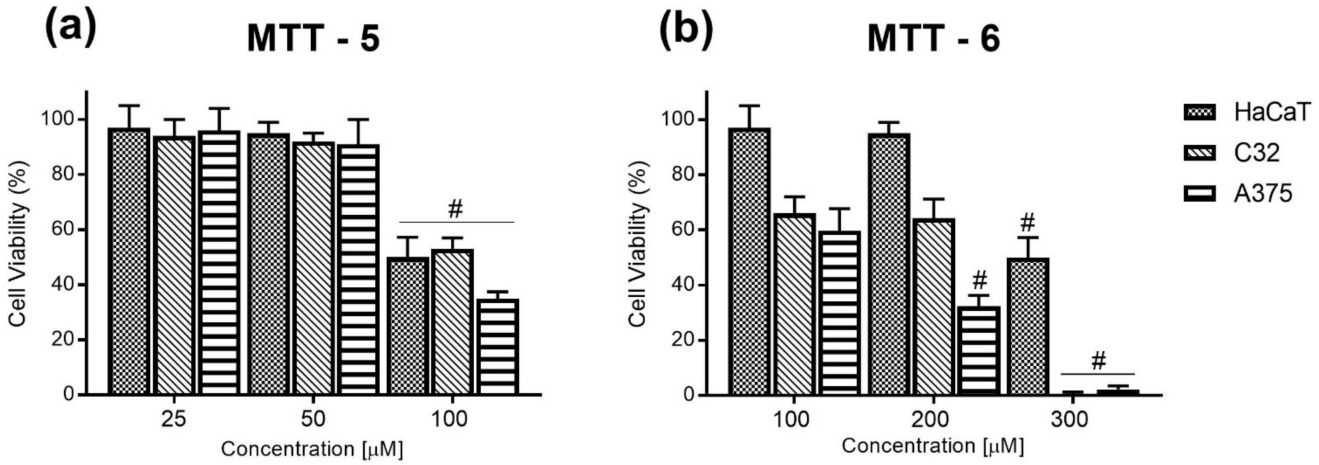

Figure 3. The cell viability after 24 h exposure to (**a**) compound **5** and (**b**) compound **6**, determined by the MTT colorimetric assay in skin cancers: melanotic (A375) and amelanotic (C32) melanoma cells and human keratinocytes (HaCaT). # $p \leq 0.05$.

Table 1. Cytotoxicity index IC_{50} for compounds **5** and **6** for all tested cell lines.

Cell Line	IC_{50} [μM] of Compound 5	IC_{50} [μM] of Compound 6	IC_{50} [μM] of Cisplatin
A375	80.79 ± 4.85	202.47 ± 10.12	15.98 ± 3.31 *
C32	170.28 ± 10.22	304.39 ± 15.21	9.79 ± 1.51 *
SNB-19	126.02 ± 7.56	295.81 ± 14.71	43.47 [48]
MCF-7/WT	119.29 ± 7.16	261.40 ± 13.07	5.75 ± 0.02 [49]
MCF-7/DOX	137.31 ± 8.24	295.81 ± 14.92	47.82 ± 2.45 *
HaCaT	115.12 ± 6.91	270.32 ± 13.25	56.00 ± 7.27 [50]

± values represent SE (standard error); * own data.

2.2.2. Clonogenic Assay

The colony formation assay was used to determine the long-term cytotoxic effect on the growth of cancer cells. In Figure 4a,b are shown the results obtained from the clonogenic assay after exposure of melanoma cells and keratinocytes to compounds **5** and **6**. It was noted that compound **5** significantly inhibited colony formation in A375 cells at two concentrations, 50 and 100 μM. However, the highest cytotoxic effect of compound **5** was observed among human keratinocytes. In the case of the C32 cell line, the results were comparable to the level of control cells. Compound **6** reduced the colony growth of all cell lines in a dose-dependent manner, but at a higher concentration than compound **5**. Figure 4c shows cells plated for clonogenic assay, with characteristic stained colonies.

2.2.3. Population Doubling Time

The results of the doubling time are summarized in Figure 5. Cells were seeded with a plating density of 3000 viable cells. Figure 5 shows growth curves from independent experiments of subcultured cells. The data are presented as population doubling (PD) versus the time. PD was calculated as log2 (number of viable cells/number of plated cells). The growth of the curves was observed for both compounds, with low concentrations showing a logarithmic increase. However, high concentrations showed a loss of cell population all days after seeding, followed by a logarithmic decrease. Untreated cells revealed a logarithmic increase in growth one day after cultivation.

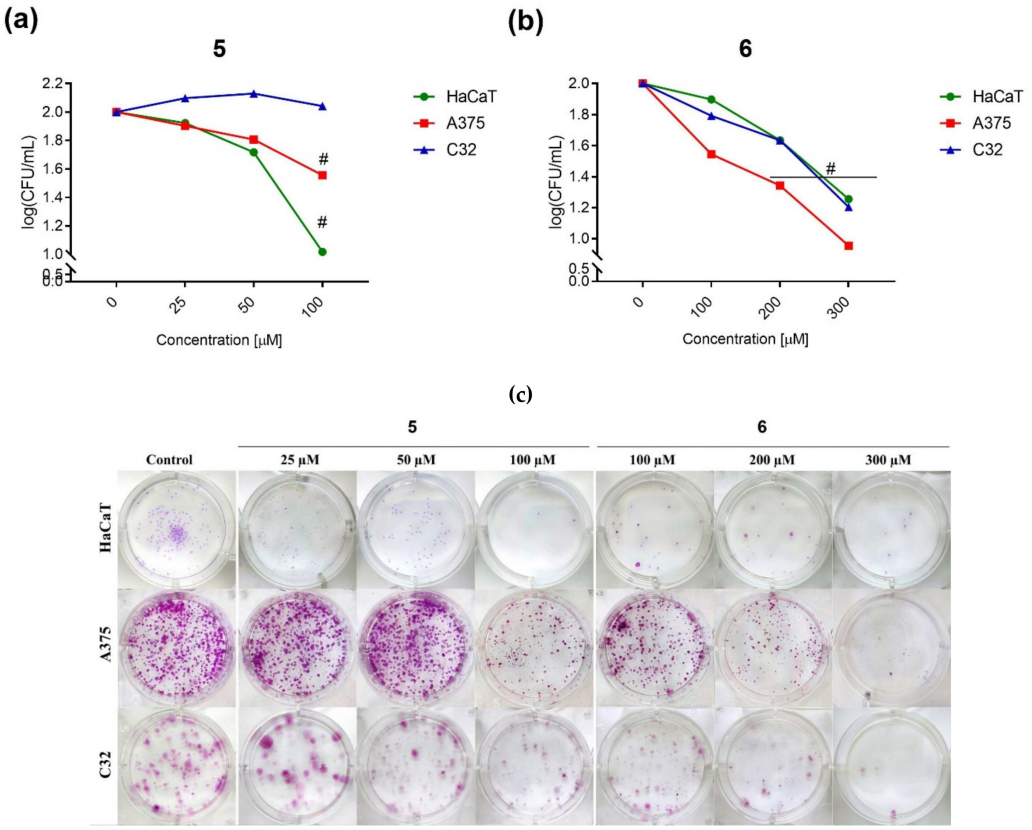

Figure 4. Colony-forming properties of the C32, A375 and HaCaT cells after incubation with (**a**) compound **5** and (**b**) compound **6** (CFU—colony forming units expressed per mL); (**c**) clonogenic assay visualization for **5** and **6** compounds. # $p \leq 0.05$.

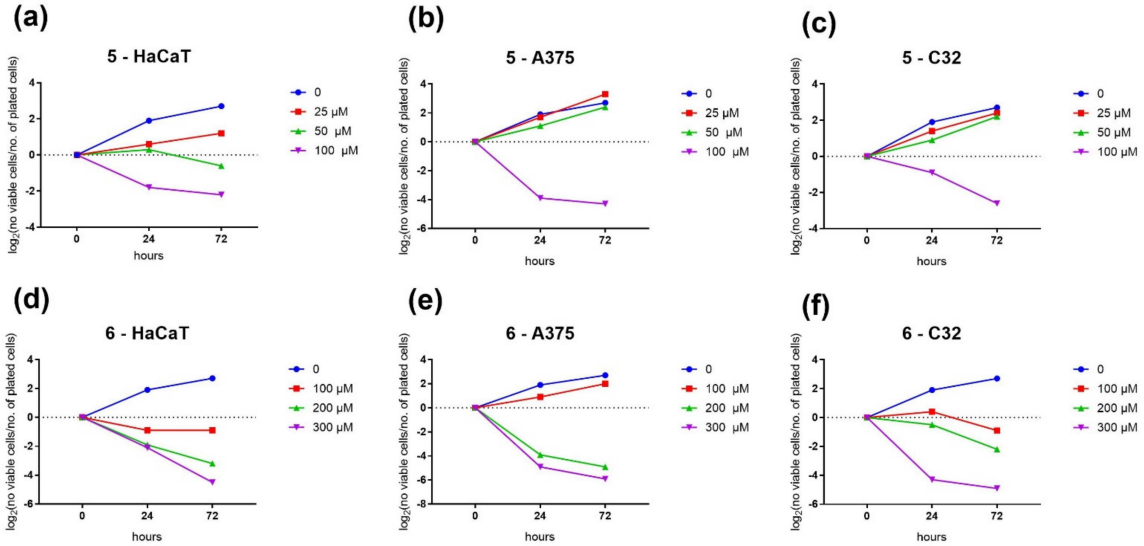

Figure 5. The population doubling time test was performed on human keratinocytes HaCaT (**a**,**d**), a melanotic melanoma cell line (A375) (**b**,**e**) and an amelanotic melanoma cell line (C32) (**c**,**f**) that were incubated at a density of 300 × 10^3/well. Cells were exposed to compounds for 24 h and 72 h at three different concentrations, 25, 50 and 100 μM for compound **5**, and 100, 200 and 300 μM for compound **6**. Control cells were maintained in a growth medium with 10% fetal bovine serum (FBS) without treatment by any compounds. The number of cells was determined by counting using KOVA Slide. The results are presented as a log2 (no. of viable cells/no. of plated cells), performed three times.

2.2.4. Cell Death Detection by Comet Assay

Detection of DNA damage and cell death was investigated by means of the neutral comet assay, where we could distinguish between three types of comets showing late and early apoptosis and not-affected cells. In Figure 6a–c are shown the results obtained from the 24 h exposure to compounds **5** and **6**. We could observe the highest percentage of early apoptotic cells for compound **6** (100 μM) in A375 cells, and late apoptosis was detected for higher concentrations (300 μM). C32 cells were less sensitive, and the percentage of DNA damage was lower than in A375 cells. The obtained results are also confirmed by the olive tail moment (OTM) calculations (Figure 6b), which correspond to the product of the tail length and the fraction of total DNA in the tail. The longest tail was observed in the case of A375 cells exposed to 300 μM of compound **6**. C32 cells revealed the longest tail after the exposure to 100 μM of compound **5** and to 200 μM of compound **6**. Both cell lines were less sensitive to compound **5**, but 100 μM concentration stimulated cells to the early apoptotic state.

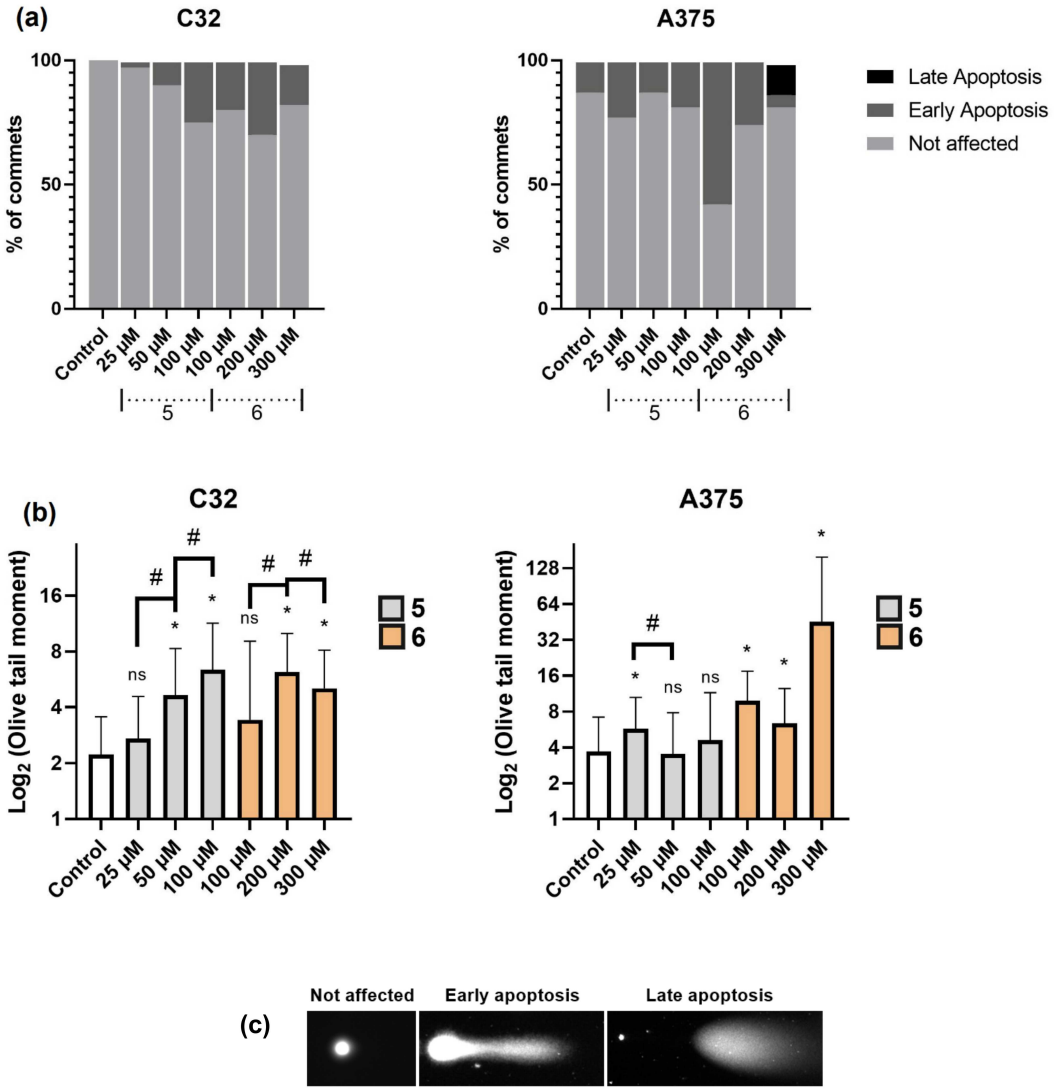

Figure 6. Cell death evaluation by the neutral comet assay results for human melanoma cells: (**a**) A cell death evaluation by the following scoring: not affected; early apoptosis; late apoptosis, the scoring method based on Cortes-Gutierrez [51]; (**b**) Olive tail moment (OTM), which corresponds to the product of the tail length and the fraction of total DNA in the tail; (**c**) An exemplary representation of comets used for scoring. ns—not significant, # $p < 0.05$ significant in comparison to adjacent data, * $p < 0.05$ significant in comparison to control.

2.2.5. Fluorescent Staining of Actin Filaments

The visualization of the F-actin organization in normal and cancer cells is presented in Figure 7. The 24 h exposure to the tested compounds demonstrated the most significant changes in the cytoskeleton organization in all cell lines, after the treatment with compound **5** at 100 µM concentration and with compound **6** at 200 and 300 µM concentration. The compound **6** in 100 µM concentration did not affected normal keratinocytes but significantly damaged melanoma cells, causing cells' shrinkage and reduced cells' number. Normal keratinocytes (HaCaT) were also not sensitive to compound **5** in 25 and 50 µM concentrations.

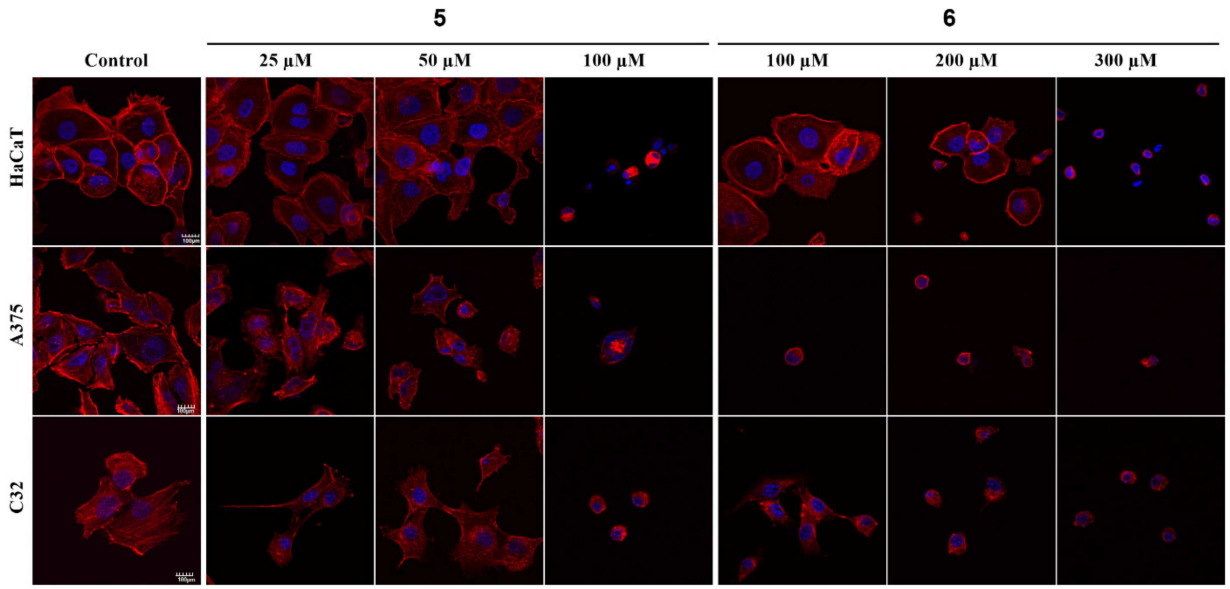

Figure 7. Immunofluorescence studies of C32, A375 and HaCaT cells' structure (60×) 24 h after the treatment with compounds **5** and **6**. DAPI (4′,6-diamidino-2-phenylindole) was used for nuclei staining (blue) and actin filaments were labeled with phallotoxin (red).

2.3. Molecular Docking Studies

Docking studies were performed to assess the binding affinity of compounds **3**–**12** and the reference drugs to the selected receptors: cMet (PDB code: 3RHK) [52], EGFR (PDB code: 5GTY) [53], HER2 (PDB code: 7JXH) [54] and hTrkA (PDB code: 6PL2) [55]. The four chosen receptors are well known for their importance in cancer progression and metastasis. The ligands denoted as M97 [52], 816 [53], VOY [54] and OOM [55] were re-docked to the receptors. The positions of the co-crystallized ligands with the lowest binding affinity values were selected and presented in Figure 8. Careful inspection of Figure 8 shows that the docking parameters were chosen appropriately, because in the case of the M97, 816, VOY and OOM ligands, the root-mean-square deviation (RMSD) values are relatively low and they are equal to: 0.832, 1.812, 2.006 and 1.200 Å, respectively.

After the validation of the docking protocol, compounds **3**–**12** were docked and their binding affinity was estimated—their performance was compared to the binding affinities of known inhibitors of the cMet, EGFR, HER2 and hTrkA receptors, namely: Erlotinib, Neratinib and Tepotinib (see Table 2).

Most of the compounds from the set of **3**–**12**, with regards to each of the receptors, obtained a lower binding affinity score than one of the reference drugs (Erlotinib)—the exceptions were only complexes with **8**-EGFR and **9**-HER2. The most interesting compounds, when the binding affinity to the chosen receptors is taken into consideration, were compounds **7** and **11**. Compound **7** had the best score of binding to the receptors EGFR and HER2, where it values were equal to −12.9 and −13.6 kcal/mol, respectively. In turn, compound **11** was bound in the most pronounced way by the cMet (−12.6 kcal/mol)

and hTrkA (−14.5 kcal/mol) receptors. The binding modes to the four receptors with compounds **7** and **11** are presented in Figure 9.

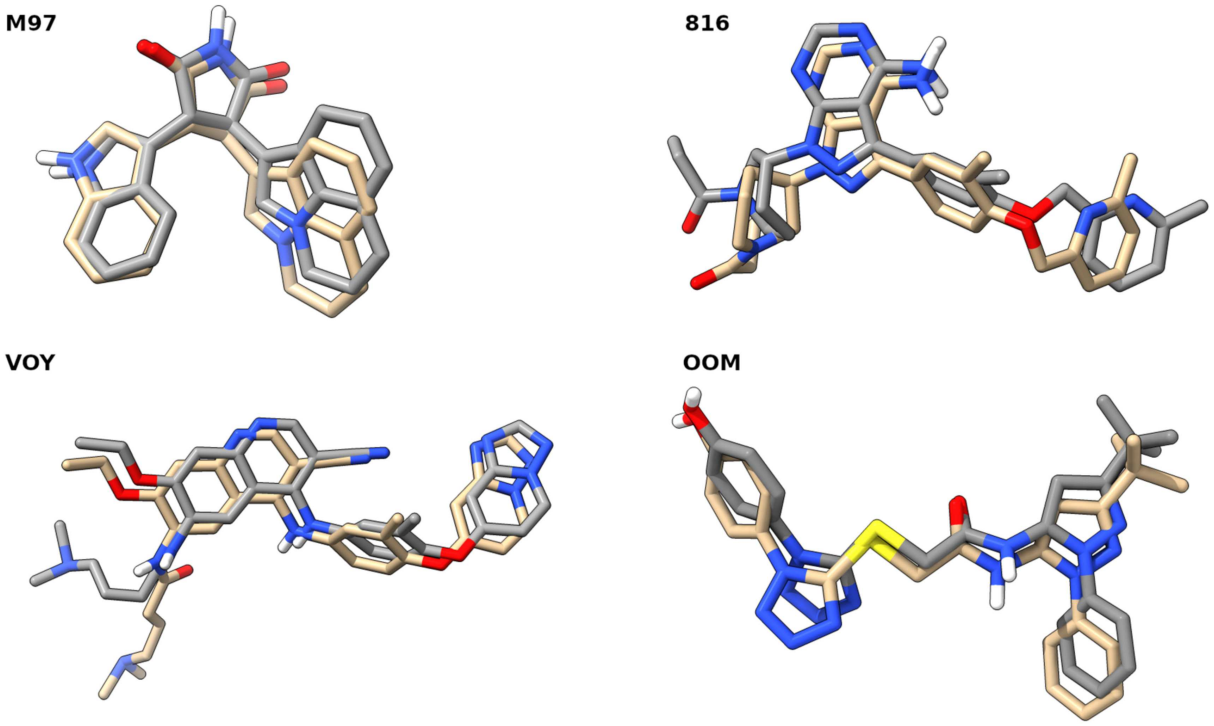

Figure 8. Superimposed structures obtained in re-docking experiment. M97, 816, VOY and OOM ligands where co-crystallized with the cMet (PDB code: 3RHK), EGFR (PDB code: 5GTY), HER2 (PDB code: 7JXH), hTrkA (PDB code: 6PL2), respectively. Color coding: beige—carbon atoms of the co-crystallized structures, grey—carbon atoms of the re-docked structures, blue—nitrogen, red—oxygen, yellow—sulfur, white—hydrogen. All-atom RMSD values are as follows: 0.832, 1.812, 2.006, 1.200 for M97, 816, VOY and OOM, respectively.

Table 2. Binding affinities of the investigated ligand-receptor complexes. Values given in kcal/mol.

Compound	cMET	EGRF	HER2	hTrkA
3	−11.8	−12.0	−12.2	−13.2
4	−12.1	−11.8	−12.9	−13.4
5	−12.1	−12.2	−12.5	−13.6
6	−11.4	−11.4	−12.1	−13.2
7	−11.9	−12.9	−13.6	−14.0
8	−11.6	−10.8	−11.8	−13.7
9	−9.7	−11.0	−10.3	−11.7
10	−11.1	−11.4	−12.2	−13.6
11	−12.6	−12.0	−12.3	−14.5
12	−10.6	−11.1	−11.2	−13.5
Erlotinib	−9.2	−10.9	−10.5	−10.4
Neratinib	−12.3	−13.1	−13.2	−14.2
Tepotinib	−13.7	−13.9	−13.5	−14.2

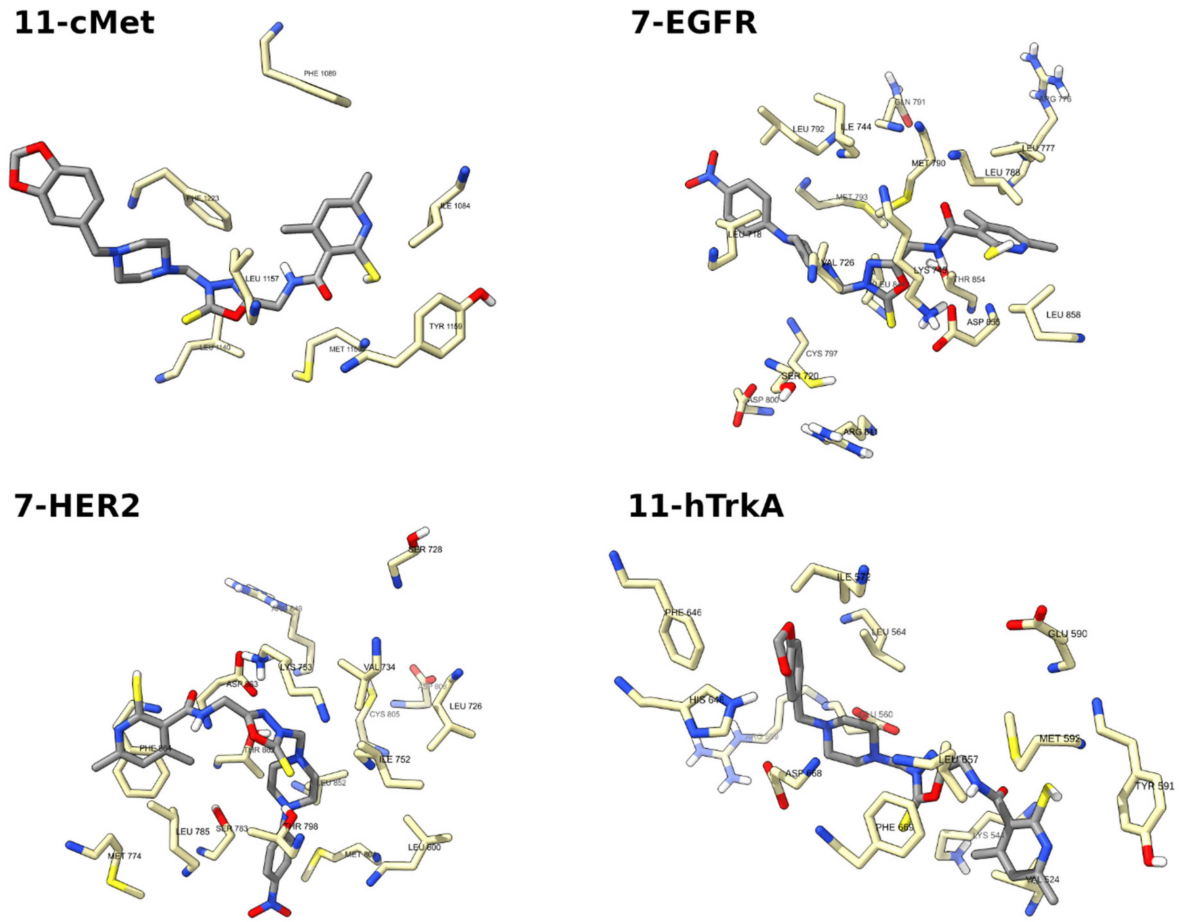

Figure 9. Binding modes of the ligand-receptor complexes. Only the best performing ligands (compounds **7** and **11** in our case) in terms of binding affinity are presented. Color coding: beige—carbon atoms of the amino acid residues, grey—carbon atoms of the docked ligand, blue—nitrogen, red—oxygen, yellow—sulfur, white—hydrogen.

It is visible that the flexible binding sites, depending on the receptor, varied in size. It is especially noticeable in the binding pocket of cMet, which had only **7** flexible amino acid residues. In the case of the remaining three receptors, the flexible parts consisted of 19 (for EGFR), 18 (for HER2) and 14 (for hTrkA) residues, respectively. In order to perform a more in-depth analysis of the binding modes of the abovementioned structures, 2D diagrams of the ligand–receptor interactions were prepared (see Figure 10).

An inspection of the presented diagrams shows that the **11**-cMet complex interactions are stabilized mainly by the presence of hydrogen bonds, in which the sulfur atom of the thiol group attached to pyridine and the carbonyl oxygen acts as an electron density donor to the Met1269 of the binding pocket. Other important interactions, such as Van der Waals with Tyr1159; π-alkyl with Ile1084, Phe1089, Leu1157 and Leu1140; and π-σ with Phe1223 are also present and stabilize the complex. For the complex of **11**-hTrkA, the interactions present in the binding pocket differ mainly by the contribution of many the Van der Waals contacts of Phe646, Phe669, Leu657, Ile572, Glu560 and Tyr591 to the stabilization of the examined compound. The binding of the ligand to the receptor is also stabilized by the π-σ interactions of Val524 with the aromatic ring of pyridine and the hydrogen bond formed by His648 (which acts as a proton donor) and the oxygen from the 1,3-benzodioxole moiety. As was the case with the former, π-alkyl interactions are also present (for more details, see Figure 10). Moreover, the binding affinity for this complex is equal to -14.5 kcal/mol. It is the lowest value among the studied, synthesized **3**–**12** and reference compounds (as it is shown in Table 2). In the case of the 7-EGFR complex, the most important contributions

to the binding affinity come from the presence of the hydrogen bond between the Asp668 and the hydrogen atom from the amide group of the compound **7** as well as from the π-σ interactions of **7** with the Leu718 and Met780 residues. A plethora of π-alkyl interactions with various residues is present as well. A totally different mode of binding exists in the case of the 7-HER2 complex—here, four different hydrogen bonds, one π-sulfur and two π-alkyl interactions are formed between the ligand and the binding site of the receptor. Two of the hydrogen bonds can be classified as weak hydrogen bonds, where the carbon atom of the Asp863 and the carbon atom from the methyl group attached to pyridine act as proton donors. Another two, conventional hydrogen bonds were formed between **7** and the residues Thr798 and Lys753, where amino acids act as proton donors. Additionally, contributions from the π-sulfur and π-alkyl interactions were noticed as well.

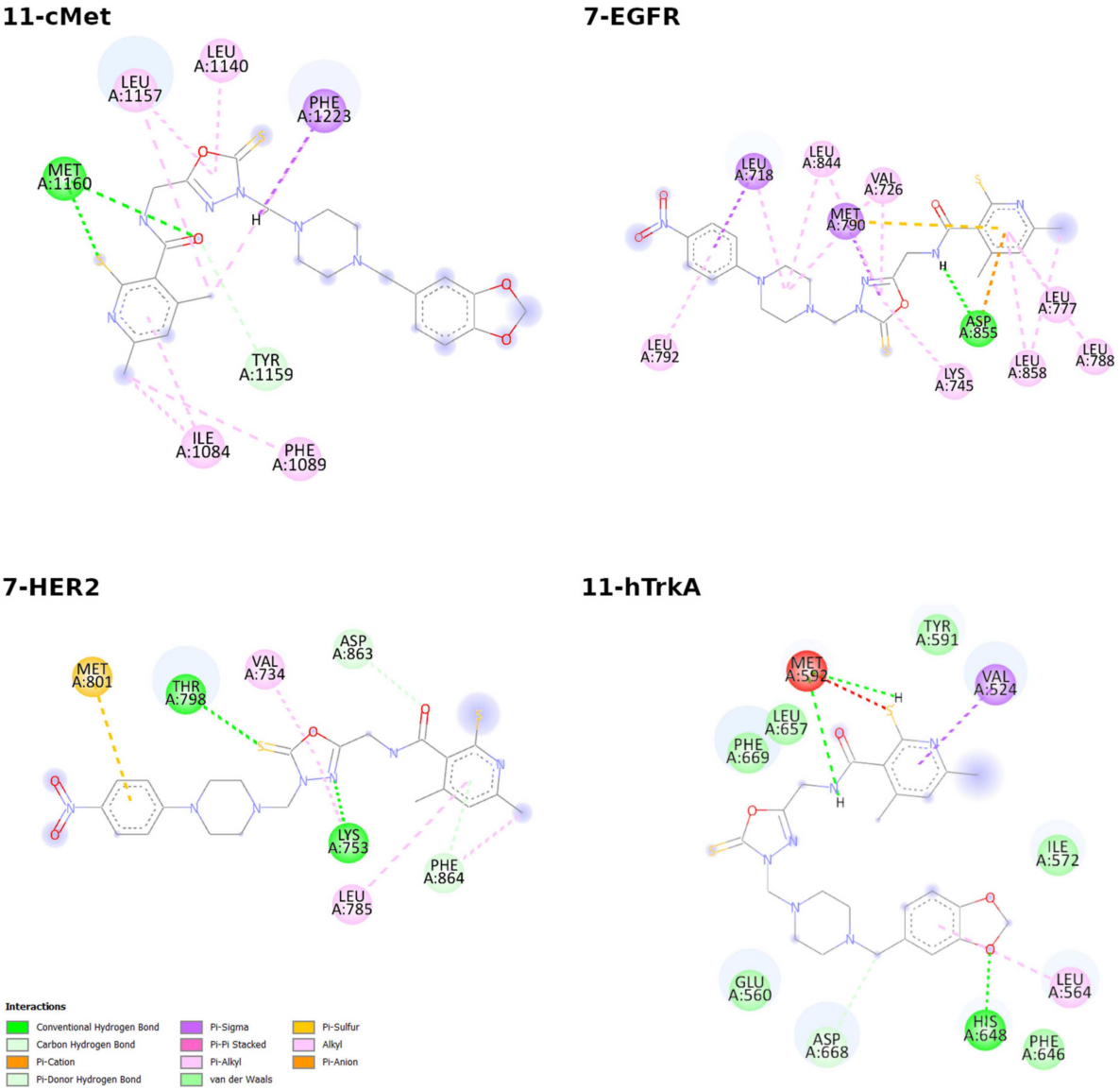

Figure 10. 2D diagrams of ligand-receptor interactions. Only the best performing ligands (compounds **7** and **11** in our case) in terms of binding affinity are shown.

As a supplement to our discussion of the ligand–receptor interactions, the Molecular Electrostatic Potential (MEP) maps of compounds **7** and **11** as well as Neratinib and Tepotinib were prepared (see Figure 11).

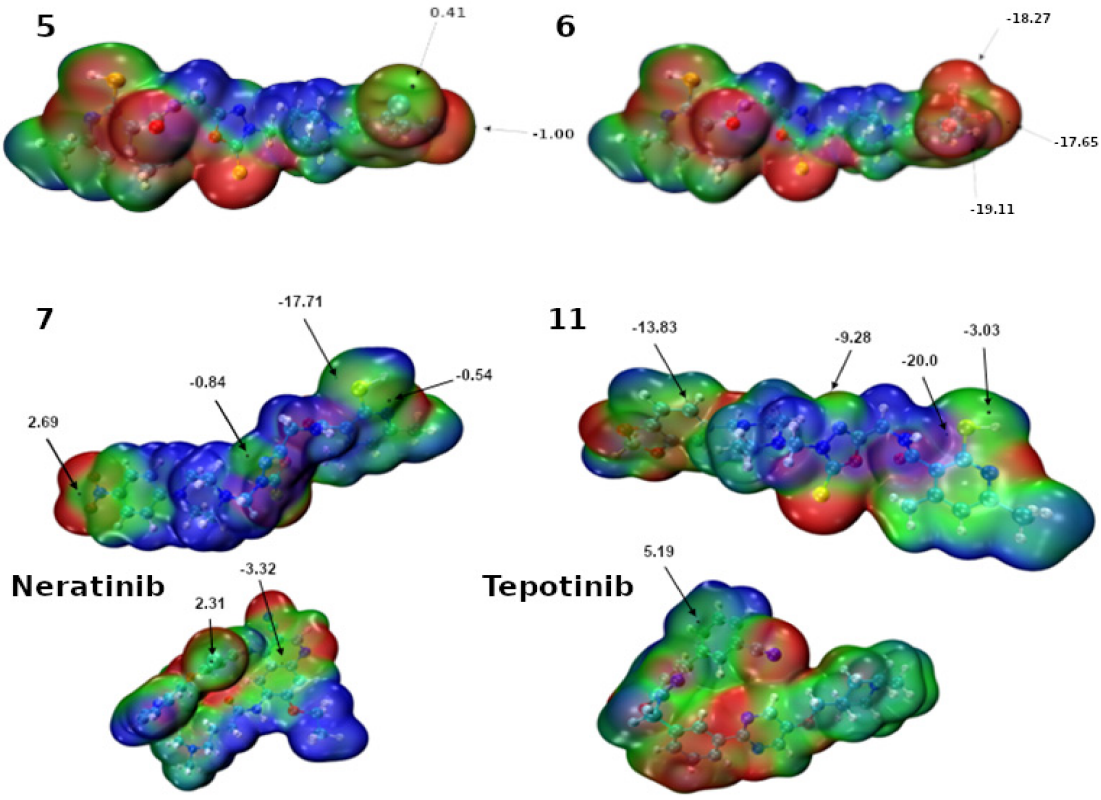

Figure 11. Molecular Electrostatic Potential (MEP) of **5**, **6**, **7** and **11** compounds as well as reference drugs: Neratinib and Tepotinib computed at the MN15/def2-TZVP level of theory. The isosurface was set from −0.001 a.u. to 0.001 a.u. Color coding: red—negative values, blue—positive values. Black dots and arrows mark the presence of V_{ext} (extremas on the MEP surface).

From the perspective of the detailed description of the possible interactions of the ligands with the binding pocket, one must also take into consideration the possible anisotropy of the charge density distribution—which is not taken into account by modern docking software [56]. The arrows depicted in Figure 11 point to the MEP extrema relevant to the analysis of the interactions involving the ligand. For compound **6**, only negative extrema are presented—in fact, there is no σ-hole or π-hole at the CF_3 substituent and at the center of the benzene ring, respectively. Due to that, CF_3 can act only as an electron density—which is a distinguishing feature between **5** and **6**, because in the case of compound **5**, we can observe two σ-holes (of magnitude 0.41 and 1 kcal/mol) on chlorine atoms attached to the benzene ring (in this manner, compound **5** can form two halogen bonds). With regards to compound **7**, it can be noted that four different extrema exist. One can observe the presence of a π-hole on the nitrogen atom of the nitro group, a σ-hole on the nitrogen from the 1,3,4-oxadiazole ring and a π-hole on the sulfur atom of the thiol group attached to the pyridine ring with 2.69, −0.84 and −0.54 kcal/mol MEP values, respectively. On the sulfur atom of the thiol group, at the opposite site, there is also present another extremum with a −17.71 kcal/mol value of the MEP. These numbers indicate that the first three abovementioned atoms can act as acceptors of the electron density and take a part in the σ- and π-hole interactions. Interestingly, on the sulfur atom of the thiol group, two distinct extrema were spotted; thus, this atom could act as a Lewis-acid as well as Lewis-base center in the intermolecular interactions. The analysis of the MEP corresponding to compound **11** is somewhat similar. In fact, the one important difference is the ability of the terminal phenyl ring to form π-hole interactions—on the basis of MEP analysis one can suppose that the quadrupole moment of the phenyl in compound **7** is higher compared to the same aromatic framework in compound **11**, due to presence of the NO_2 group (which is able to withdraw electrons). In the case of Neratinib, two spots were noticed—one σ-hole on

the chlorine atom (2.31 kcal/mol) and the π-hole at the pyridine (−3.32 kcal/mol). It is noteworthy that a similarly positioned π-hole (5.19 kcal/mol) is present in the structure of Tepotinib. In fact, both Neratinib and Tepotinib possess a highly electron-withdrawing –CN group strongly affecting the charge distribution of the molecules.

3. Materials and Methods

3.1. Chemistry

3.1.1. Instruments and Chemicals

All solvents, reagents and chemicals used during the experiments described in this paper were delivered by commercial suppliers (Alchem, Wrocław, Poland; Chemat, Gdańsk, Poland; Archem, Łany, Poland) and were used without further purification. Any dry solvents were received due to standard procedures. Reaction progress was monitored by the Thin-Layer Chromatography (TLC) technique, on TLC plates made of 60–254 silica gel, and was visualized by UV light at 254/366 nm. Melting points of final compounds were determined on an Electrothermal Mel-Temp 1101D apparatus (Cole-Parmer, Vernon Hills, IL, USA) using the open capillary method, no correction needed. ^{1}H NMR (300 MHz) and ^{13}C NMR (75 MHz) spectra were recorder using a Bruker 300 MHz NMR spectrometer (Bruker Analytische Messtechnik GmbH, Rheinstetten, Germany) in DMSO-d_6, with tetramethylsilane (TMS) as an internal reference. Chemical shifts (δ) were reported in ppm. In order to record and read spectra, the TopSpin 3.6.2. (Bruker Daltonik, GmbH, Bremen, Germany) program was used. FT-IR spectra were measured on a Nicolet iS50 FT-IR Spectrometer (Thermo Fisher Scientific, Waltham, MA, USA). Frequencies were reported in cm^{-1}. All samples were solid, and spectra were read by OMNIC Spectra 2.0 (Thermo Fisher Scientific, Waltham, MA, USA). Mass spectra (MS) were recorded using the Bruker Daltonics Compact ESI-Mass Spectrometer (Bruker Daltonik, GmbH, Bremen, Germany), operating in the positive ion mode with methanol as a solvent. Theoretical monoisotopic masses of ions were calculated (calcd.) using Bruker Compass Data Analysis 4.2 software (Bruker Daltonik GmbH, Bremen, Germany).

3.1.2. Preparation and Experimental Properties of Compounds **3**–**12**

The synthesis protocols and experimental data for compound **1** and **2** were already reported [46,47].

General Procedure for Preparation of Compounds **3**–**12**

0.16 mL of 36% formaldehyde was added to a solution of 0.001 mol of 4,6-dimethyl-*N*-[(5-sulfanylidene-4,5-dihydro-1,3,4-oxadiazol-2-yl)methyl]-2-sulfanylpyridine-3-carboxamide **2** in 30 mL of ethanol. The obtained mixture was stirred at room temperature for several minutes. Then, 0.001 mole of the appropriate piperazine derivative or morpholine was added to the flask. The resulting mixture was stirred for 4 h at room temperature and then left overnight. The obtained precipitate was filtered off and allowed to dry, then the obtained product was crystallized from ethanol.

4,6-Dimethyl-*N*-{[4-((4-phenylpiperazin-1-yl)methyl)-5-sulfanylidene-4,5-dihydro-1,3,4-oxadiazol-2-yl]methyl}-2-sulfanylpyridine-3-carboxamide **3**

Yield: 52.0%, m.p: 215–218 °C

FT-IR (selected lines, γ_{max}, cm^{-1}): 3193 (NH), 2926, 2824 (C-H aliph.), 1663 (C=O)

^{1}H NMR (300 MHz, DMSO-d_6): δ = 2.07 (s, 3H, CH_3), 2.26 (s, 3H, CH_3), 2.81–2.83 (m, 4H, $CH_{2\text{-piperazine}}$), 3.09–3.11 (m, 4H, $CH_{2\text{-piperazine}}$), 4.44–4.46 (d, 2H, CH_2, *J = 6 Hz*), 5.00 (s, 2H, CH_2), 6.48 (s, 1H, $H_{\text{-pyridine}}$), 6.73–6.78 (m, 1H, ArH), 6.89–6.91 (m, 2H, ArH), 7.15–7.20 (m, 2H, ArH), 8.84 (t, 1H, NH, *J = 6 Hz*), 13.29 (s, 1H, SH);

^{13}C NMR (75 MHz, DMSO-d_6): δ = 18.74, 19.32, 34.67, 48.76, 50.01, 69.96, 115.28, 116.13, 119.52, 129.43, 146.65, 148.52, 151.51, 167.45, 174.32

HRMS (ESI-MS) (*m/z*): calcd. for $C_{22}H_{26}N_6O_2S_2$ $[M+H]^+$: 471.1631; found: 471.1634

4,6-Dimethyl-*N*-{[4-((4-(2-chloro)phenylpiperazin-1-yl)methyl)-5-sulfanylidene-4,5-dihydro-1,3,4-oxadiazol-2-yl]methyl}-2-sulfanylpyridine-3-carboxamide **4**

Yield: 62.7%, m.p: 208–210 °C

FT-IR (selected lines, γ_{max}, cm^{-1}): 3193 (NH), 2827 (C-H aliph.), 1655 (C=O)

^{1}H NMR (300 MHz, DMSO-d_6): δ = 2.08 (s, 3H, CH_3), 2.27 (s, 3H, CH_3), 2.85–2.87 (m, 4H, $CH_{2\text{-piperazine}}$), 2.94–2.96 (m, 4H, $CH_{2\text{-piperazine}}$), 4.47–4.49 (d, 2H, CH_2, *J = 6 Hz*), 5.00 (s, 2H, CH_2), 6.49 (s, 1H, $H_{\text{-pyridine}}$), 7.01–7.03 (m, 1H, ArH), 7.14–7.16 (m, 1H, ArH), 7.26–7.28 (m, 1H, ArH), 7.36–7.38 (m, 1H, ArH), 8.86 (t, 1H, NH, *J = 6 Hz*), 13.28 (s, 1H, SH)

^{13}C NMR (75 MHz, DMSO-d_6): δ = 18.70, 19.39, 34.63, 50.25, 51.23, 70.28, 115.21, 115.26, 121.58, 124.46, 127.93, 128.52, 130.79, 146.87, 148.51, 151.62, 167.49, 174.59

HRMS (ESI-MS) (*m/z*): calcd. for $C_{22}H_{25}ClN_6O_2S_2$ $[M+H]^+$: 505.1242; found: 505.1224

4,6-Dimethyl-*N*-{[4-((4-(3,4-dichloro)phenylpiperazin-1-yl)methyl)-5-sulfanylidene-4,5-dihydro-1,3,4-oxadiazol-2-yl]methyl}-2-sulfanylpyridine-3-carboxamide **5**

Yield: 70.3%, m.p: 226–228 °C

FT-IR (selected lines, γ_{max}, cm^{-1}): 3158 (NH), 2834 (C-H aliph.), 1646 (C=O)

^{1}H NMR (300 MHz, DMSO-d_6): δ = 2.07 (s, 3H, CH_3), 2.26 (s, 3H, CH_3), 2.79–2.81 (m, 4H, $CH_{2\text{-piperazine}}$), 3.15–3.17 (m, 4H, $CH_{2\text{-piperazine}}$), 4.45–4.47 (d, 2H, CH_2, *J = 6 Hz*), 5.00 (s, 2H, CH_2), 6.48 (s, 1H, $H_{\text{-pyridine}}$), 6.89–6.93 (m, 1H, ArH), 7.09–7.10 (m, 1H, ArH), 7.34–7.37 (m, 1H, ArH), 8.81 (t, 1H, NH, *J = 6 Hz*), 13.27 (s, 1H, SH)

^{13}C NMR (75 MHz, DMSO-d_6): δ = 18.70, 19.45, 34.72, 48.00, 49.70, 70.02, 115.25, 116.06, 116.82, 120.19, 125.00 130.87, 146.73, 148.50, 151.30, 153.20, 167.56, 174.47

HRMS (ESI-MS) (*m/z*): calcd. for $C_{22}H_{24}Cl_2N_6O_2S_2$ $[M+H]^+$: 539.0852; found: 539.0836

4,6-Dimethyl-*N*-{[4-((4-(3-trifluoromethyl)phenylpiperazin-1-yl)methyl)-5-sulfanylidene-4,5-dihydro-1,3,4-oxadiazol-2-yl]methyl}-2-sulfanylpyridine-3-carboxamide **6**

Yield: 59.3%, m.p: 215–218 °C

FT-IR (selected lines, γ_{max}, cm^{-1}): 3164 (NH), 2835 (C-H aliph.), 1648 (C=O)

^{1}H NMR (300 MHz, DMSO-d_6): δ = 2.07 (s, 3H, CH_3), 2.26 (s, 3H, CH_3), 2.82–2.84 (m, 4H, $CH_{2\text{-piperazine}}$), 3.19–3.21 (m, 4H, $CH_{2\text{-piperazine}}$), 4.45-4.47 (d, 2H, CH_2, *J = 6 Hz*), 5.01 (s, 2H, CH_2), 6.48 (s, 1H, $H_{\text{-pyridine}}$), 7.04–7.06 (m, 1H, ArH), 7.13–7.21 (m, 1H, ArH), 7.36–7.42 (m, 1H, ArH), 8.83 (t, 1H, NH, *J* = 6 *Hz*), 13.27 (s, 1H, SH)

^{13}C NMR (75 MHz, DMSO-d_6): δ = 18.70, 19.37, 34.77, 48.10, 49.84, 70.28, 111.61, 115.21, 115.26, 119.51, 130.39, 136.66, 146.14, 148.57, 151.49, 167.78, 174.84

HRMS (ESI-MS) (*m/z*): calcd. for $C_{23}H_{25}F_3N_6O_2S_2$ $[M+H]^+$: 539.1505; found: 539.1534

4,6-Dimethyl-*N*-{[4-((4-(4-nitro)phenylpiperazin-1-yl)methyl)-5-sulfanylidene-4,5-dihydro-1,3,4-oxadiazol-2-yl]methyl}-2-sulfanylpyridine-3-carboxamide **7**

Yield: 67.3%, m.p: 221–223 °C

FT-IR (selected lines, γ_{max}, cm^{-1}): 3157 (NH), 2834 (C-H aliph.), 1647 (C=O)

^{1}H NMR (300 MHz, DMSO-d_6): δ = 2.04 (s, 3H, CH_3), 2.26 (s, 3H, CH_3), 2.80–2.82 (m, 4H, $CH_{2\text{-piperazine}}$), 3.44–3.46 (m, 4H, $CH_{2\text{-piperazine}}$), 4.42–4.44 (d, 2H, CH_2, *J = 6 Hz*), 5.02 (s, 2H, CH_2), 6.46 (s, 1H, $H_{\text{-pyridine}}$), 6.99–7.02 (d, 2H, ArH), 8.00–8.03 (d, 2H, ArH), 8.82 (t, 1H, NH, *J* = 6 *Hz*), 13.28 (s, 1H, SH)

^{13}C NMR (75 MHz, DMSO-d_6): δ= 18.68, 19.35, 34.50, 46.76, 49.65, 69.82, 106.70, 113.18, 115.19, 120.44, 126.17, 126.41, 127.67, 146.65, 148.59, 150.21, 167.46, 175.44

HRMS (ESI-MS) (*m/z*): calcd. for $C_{22}H_{25}N_7O_4S_2$ $[M+H]^+$: 516.1482; found: 516.1465

4,6-Dimethyl-*N*-{[4-((4-(2-methoxy)phenylpiperazin-1-yl)methyl)-5-sulfanylidene-4,5-dihydro-1,3,4-oxadiazol-2-yl]methyl}-2-sulfanylpyridine-3-carboxamide **8**

Yield: 64.0%, m.p: 207–210 °C

FT-IR (selected lines, γ_{max}, cm^{-1}): 3176 (NH), 2830 (C-H aliph.), 1653 (C=O)

^{1}H NMR (300 MHz, DMSO-d_6): δ = 2.09 (s, 3H, CH_3), 2.27 (s, 3H, CH_3), 2.81–2.83 (m, 4H, $CH_{2\text{-piperazine}}$), 2.91–2.93 (m, 4H, $CH_{2\text{-piperazine}}$), 3.73 (s, 3H, OCH_3), 4.47–4.49 (d, 2H, CH_2, *J = 6 Hz*), 4.99 (s, 2H, CH_2), 6.49 (s, 1H, $H_{\text{-pyridine}}$), 6.85–6.91 (m, 4H, ArH), 8.85 (t, 1H, NH, *J = 6 Hz*), 13.29 (s, 1H, SH)

^{13}C NMR (75 MHz, DMSO-d_6): δ = 18.70, 19.38, 34.64, 50.27, 50.36, 50.44, 55.68, 70.12, 112.18, 115.22, 118.49, 121.20, 123.00, 136.76, 141.49, 146.68, 148.49, 152.39, 152.45, 167.48, 174.41, 178.21

HRMS (ESI-MS) (*m/z*): calcd. for $C_{23}H_{28}N_6O_3S_2$ $[M+H]^+$: 501.1737; found: 501.1719

4,6-Dimethyl-*N*-{[4-(morpholinyl)methyl)-5-sulfanylidene-4,5-dihydro-1,3,4-oxadiazol-2-yl]methyl}-2-sulfanylpyridine-3-carboxamide **9**

Yield: 79.0%, m.p: 178–181 °C

FT-IR (selected lines, γ_{max}, cm^{-1}): 3167 (NH), 2859 (C-H aliph.), 1652 (C=O)

^{1}H NMR (300 MHz, DMSO-d_6): δ = 2.07 (s, 3H, CH_3), 2.27 (s, 3H, CH_3), 2.66–2.68 (m, 4H, $CH_{2\text{-morpholine}}$), 3.53–3.55 (m, 4H, $CH_{2\text{-morpholine}}$), 4.44-4.46 (d, 2H, CH_2, *J = 6 Hz*), 4.92 (s, 2H, CH_2), 6.49 (s, 1H, $H_{\text{-pyridine}}$), 8.84 (t, 1H, NH, *J = 6 Hz*), 13.23 (s, 1H, SH)

^{13}C NMR (75 MHz, DMSO-d_6): δ = 18.69, 19.37, 34.59, 43.20, 49.04, 50.35, 63.47, 66.45, 70.03, 115.22, 136.90, 146.64, 148.82, 167.54, 174.44

HRMS (ESI-MS) (*m/z*): calcd. for $C_{16}H_{21}N_5O_3S_2$ $[M+H]^+$: 396.1159; found: 396.1165

4,6-Dimethyl-*N*-{[4-((4-(pyrimidin-2-yl)piperazin-1-yl)methyl)-5-sulfanylidene-4,5-dihydro-1,3,4-oxadiazol-2-yl]methyl}-2-sulfanylpyridine-3-carboxamide **10**

Yield: 63.8%, m.p: 234–236 °C

FT-IR (selected lines, γ_{max}, cm^{-1}): 3285 (NH), 2971, 2926, 2830 (C-H aliph.), 1663 (C=O)

^{1}H NMR (300 MHz, DMSO-d_6): δ = 2.04 (s, 3H, CH_3), 2.26 (s, 3H, CH_3), 2.71–2.73 (m, 4H, $CH_{2\text{-piperazine}}$), 3.71-3.73 (m, 4H, $CH_{2\text{-piperazine}}$), 4.42–4.44 (d, 2H, CH_2, *J = 6 Hz*), 5.00 (s, 2H, CH_2), 6.47 (s, 1H, $H_{\text{-pyridine}}$), 6.57–6.61 (m, 1H, ArH), 8.31–8.33 (m, 2H, ArH), 8.80 (t, 1H, NH, *J = 6 Hz*), 13.27 (s, 1H, SH)

^{13}C NMR (75 MHz, DMSO-d_6): δ = 18.64, 19.38, 34.58, 43.53, 49.88, 70.06, 110.67, 115.17, 136.73, 146.56, 148.48, 158.38, 161.51, 167.44, 174.38

HRMS (ESI-MS) (*m/z*): calcd. for $C_{20}H_{24}N_8O_2S_2$ $[M+H]^+$: 473.1536; found: 473.1528

4,6-Dimethyl-*N*-{[4-((4-(1,3-benzodioxol-5-ylmethyl)piperazin-1-yl)methyl)-5-sulfanylidene-4,5-dihydro-1,3,4-oxadiazol-2-yl]methyl}-2-sulfanylpyridine-3-carboxamide **11**

Yield: 35.8%, m.p: 210–212 °C

FT-IR (selected lines, γ_{max}, cm^{-1}): 3155 (NH), 2911, 2839 (C-H aliph.), 1646 (C=O)

^{1}H NMR (300 MHz, DMSO-d_6): δ = 2.07 (s, 3H, CH_3), 2.27 (s, 3H, CH_3), 2.34–2.36 (m, 4H, $CH_{2\text{-piperazine}}$), 2.67–2.69 (m, 4H, $CH_{2\text{-piperazine}}$), 4.44–4.46 (d, 2H, CH_2, *J = 6 Hz*), 4.92 (s, 2H, CH_2), 5.96 (s, 2H, $CH_{2\text{-benzodioxole}}$), 6.48 (s, 1H, $H_{\text{-pyridine}}$), 6.69-6.72 (m, 1H, ArH), 6.80–6.82 (m, 2H, ArH), 8.80 (t, 1H, NH, *J = 6 Hz*), 13.27 (s, 1H, SH)

^{13}C NMR (75 MHz, DMSO-d_6): δ = 18.70, 19.40, 34.60, 49.82, 52.56, 61.88, 70.38, 101.24, 108.29, 109.54, 115.22, 122.52, 130.49, 136.80, 146.68, 147.65, 148.47, 167.45, 174.42

HRMS (ESI-MS) (*m/z*): calcd. for $C_{24}H_{28}N_6O_4S_2$ $[M+H]^+$: 529.1686; found: 529.1678

4,6-Dimethyl-*N*-{[4-((4-hexylpiperazin-1-yl)methyl)-5-sulfanylidene-4,5-dihydro-1,3,4-oxadiazol-2-yl]methyl}-2-sulfanylpyridine-3-carboxamide **12**

Yield: 31.3%, m.p: 279–283 °C

FT-IR (selected lines, γ_{max}, cm^{-1}): 3179 (NH), 2928, 2857 (C-H aliph.), 1642 (C=O)

^{1}H NMR (300 MHz, DMSO-d_6): δ = 0.83 (t, 3H, CH_3, *J = 6 Hz*), 1.20–1.24 (m, 6H, CH_2), 1.41–1.43 (m, 2H, CH_2), 2.08 (s, 3H, CH_3), 2.15–2.17 (m, 2H, CH_2), 2.27 (s, 3H, CH_3), 2.38–2.40 (m, 4H, $CH_{2\text{-piperazine}}$), 2.73-2.75 (m, 4H, $CH_{2\text{-piperazine}}$), 4.45-4.47 (d, 2H, CH_2, *J = 6 Hz*), 4.93 (s, 2H, CH_2), 6.49 (s, 1H, $H_{\text{-pyridine}}$), 8.86 (t, 1H, NH, *J = 6 Hz*), 13.29 (s, 1H, SH)

^{13}C NMR (75 MHz, DMSO-d_6): δ = 14.35, 18.70, 19.41, 22.46, 25.06, 26.76, 31.51, 34.64, 49.09, 52.49, 57.87, 69.79, 115.22, 115.31, 136.66, 146.66, 148.44, 167.54, 174.41

HRMS (ESI-MS) (*m/z*): calcd. for $C_{22}H_{34}N_6O_2S_2$ $[M+H]^+$: 479.2257; found: 479.2250

3.2. Biological Section

3.2.1. Cell Lines

The following cell lines were used in the study: human melanotic melanoma cell line A375 (CRL-1619™); human amelanotic melanoma cell line C32 (CRL-1585™); human glioblastoma SNB-19 (CRL-2219™); two breast adenocarcinoma cell lines: sensitive MCF-7/WT and resistant MCF-7/DX; and immortalized human keratinocyte from histologically normal skin HaCaT, purchased from the American Type Culture Collection (ATCC®). Breast cancer cell lines were a kind gift from the Department of Experimental and Clinical Radiobiology, Center of Oncology (Gliwice, Poland). Cells were cultured as a monolayer in

Dulbecco's Modified Eagle's Medium (DMEM, Sigma-Aldrich, St. Louis, MO, USA). The medium was supplemented with 10% fetal bovine serum (FBS, Sigma-Aldrich, St. Louis, MO, USA) and 1% of antibiotic (streptomycin/penicillin, Sigma-Aldrich, St. Louis, MO, USA). The cells were incubated at 37 °C in a humidified atmosphere containing 5% CO_2. The cell medium was changed 2–3 times per week. For the experimental protocols, cells were washed with phosphate-buffered saline (PBS) and removed by trypsinization (0.025% trypsin and 0.02% EDTA; Sigma-Aldrich, St. Louis, MO, USA).

3.2.2. MTT Cell Viability Assay

The evaluation of a potential cytotoxic action of the compounds was performed in monolayer culture on human cancer cell lines (A375, C32, SNB-19, MCF-7/WT and MCF-7/DX) and a normal cell line: HaCaT. Stock solutions were prepared in DMSO (dimethyl sulfoxide, Sigma Aldrich, St. Louis, MO, USA); and compound dilutions were performed in Dulbecco's Modified Eagle's Medium supplemented with 10% FBS (EURx, Gdansk, Poland), where DMSO concentration did not exceed more than 1% in the sample. Compounds were tested in the 25–300 μM concentration range. The cells were seeded in 96-well flat-bottom plates at a density of 3×10^4 cells/well, and cells were incubated for 24 h in a cell culture incubator for the cells to stick to the plate. After the incubation, the culture supernatants were removed, and to the monolayer cell cultures, appropriate dilutions of compounds in the culture medium (200 μL/well) were added and incubated for an additional 24 h to assess the influence of different concentrations of compounds. The cell viability was determined by measuring the metabolic activity using a 3-(4,5-dimethylthiazol-2-yl)-2,5-diphenyltetrazolium bromide (MTT assay, Sigma Aldrich, St. Louis, MO, USA). After exposure to the compounds, the medium of each well was replaced with 10 μL of 5 mg/mL MTT stock solution diluted in 90 μL phosphate-buffered saline (PBS). After 2 h of incubation, isopropanol with 0.04 M HCl was added (100 μL/well). The absorbance was measured by a multiwell scanning spectrophotometer at 560 nm (Glomax, Promega, GmbH, Walldorf, Germany). The experiments were performed in triplicate.

3.2.3. Clonogenic Assay

The cells were seeded in dilutions (1000 cells) on 6-well plates to assess the colony-forming properties after the therapy. Plates were placed in an incubator and left untouched for 10 days until colonies were observed in the control samples. After the incubation, DMEM was removed, and the cells were washed with PBS. Clones were stained with a 0.5% crystal violet mixture in 4% paraformaldehyde (PFA, Sigma-Aldrich, St. Louis, MO, USA) for 10 min. Afterward, the free stain was removed by washing with water and left to dry at room temperature. Next, only the eye-visible colonies (>~0.02 cm) were counted manually. The counting of the colonies was unbiased because the counting person was not familiar with the samples' IDs. The experiments were performed in triplicate.

3.2.4. Population Doubling Time

The population doubling time determines the dynamics of the cell culture development as the average time required for a cell to complete the cell cycle. In the case of cancer cells, population doubling time allows evaluation of the compounds' efficiency. In the case of increased growth of the cell culture, the compound has a regenerative potential called cell self-renewal.

A total of 3×10^5 A375, C32 and HaCaT cells were seeded in 35 mm culture dishes (Corning, New York, NY, USA). The cells were incubated at 37 °C in a humidified atmosphere containing 5% CO_2. After 24 h, the culture supernatants were removed, and appropriate dilutions of compounds in the culture medium were added and incubated for an additional 24 h or 72 h. The cells were collected using trypsin and counted using KOVA (KOVA® Glasstic Slide 10 with Grid Chamber, HYCOR Biomedical, Garden Grove, CA, USA) after 24 and 72 h.

3.2.5. Cell Death Evaluation by Neutral Comet Assay

The neutral comet assay method was used to detect DNA damage associated with exposure to the used compounds [57,58]. Slides with cells were submerged in precooled lytic solution (100 mM EDTA, 2.5 M NaCl, 10 mM Tris base, 1% Triton X-100, pH 10) at 4 °C for 60 min. After lysis and rinsing, slides were equilibrated in TBE solution (40 mM Tris/boric acid, 2 mM EDTA, pH 8.3); after that, electrophorese was set at 1.2 V/cm for 15 min. To visualize comets, Sytox Green staining was performed (Thermo Fisher Scientific, Waltham, MA, USA) for the fluorescent microscope. For scoring the comet patterns, about 50 nuclei from each slide were assessed. CometScore 2.0 software was used to analyze the comets. The cell death type was assessed by the visual inspection described by Cortes-Gutierrez et al. (class 0—not affected, class 1 and 2—early apoptosis/intermediate damages, class 3—late apoptosis). The data are presented on the histograms [51].

3.2.6. Fluorescent Staining of Actin Filaments

To visualize the actin filaments of the cells, confocal microscopy was used. The cells were incubated on cover glasses (24 × 24 mm, Thermo Fisher Scientific, Waltham, MA, USA) in 35 mm Petri dishes for 24 h with different concentrations (25–300 µM) of compounds. Control samples were prepared as well. Afterward, the cells were washed three times with PBS. Actin filaments were stained with Invitrogen™ Alexa Fluor™ 546 Phalloidin (2 µg/mL, A22283, Thermo Fisher Scientific, Waltham, MA, USA) with the manufacturer's standard protocol. To stain cell nuclei, samples were fixed with a DAPI (4′,6-diamidino-2-phenylindole) solution (Roti®-Mount FluorCare DAPI, Carl Roth GmbH, Karlsruhe, Germany). The cells were examined using a Laser Scanning Confocal Microscope Olympus FluoView FV1000 (LSCM, Olympus, Warszawa, Poland). An oil immersion lens with 60x magnification, NA: 1.35 (Olympus, Tokyo, Japan) was used to capture the images.

3.3. Molecular Modeling—Computational Methodology

The structures of four receptors denoted as: cMet (PDB code: 3RHK) [52], EGFR (PDB code: 5GTY) [53], HER2 (PDB code: 7JXH) [54] and hTrkA (PDB code: 6PL2) [55] were used in the flexible docking study. They were taken from the Protein Data Bank (PDB) [59]. Hydrogen atoms were added with the usage of the Reduce program [60] and the "prepare_receptor" script (from the ADFR software suite) [61]. Subsequently, the AutoDockTools 1.5.7 program [62] was used to examine the macromolecule and the ligand to prepare them for further docking study. Every of the selected receptors was co-crystallized with the ligand in the binding pocket and the docking protocol was assessed based on the root-mean-square deviation (RMSD) values between the docked and the crystallized structures. The literature ligands have the following codes in the PDB database: M97 [52], 816 [53], VOY [54] and OOM [55], and were co-crystallized with the abovementioned receptors. Our flexible docking protocol included 150 independent searches with 3,500,000 evaluations of the scoring function. Flexible amino acid residues were chosen manually and, as a result, the binding pocket for each examined receptor had a different dimension. The dimensions and centers of the grid boxes of cMet, EGFR, HER2 and hTrka were set to: 27 × 1827 × 27; (−5.75, 12.46, −1.62), 32.2527 × 29.2527 × 28.50; (−35.75, 16.34, −61.24), 26.5027 × 25.7527 × 20.5; (65.75, 11.19, 82.58) and 20.5027 × 25.7527 × 34.00; (−18.27, −24.54, −18.85), respectively. The grid box sizes were adjusted to include all amino acids considered in the flexible docking procedure and were centered on their co-crystallized inhibitors present in the resulting pdb files. The binding affinity of the experimentally obtained ligands (compounds **3**–**12**) was compared to the drugs available on the market: Erlotinib (PDB code: AQ4) [63], Neratinib (PDB code: HKI) [64] and Tepotinib (PDB code: 3E8) [65]. The structures of the medicines were also downloaded from the PDB (they are further denoted as reference drugs). In the next step, the ligands (compounds **3**−**12** synthesized especially for the study) and the reference drugs underwent quantum-chemical simulations based on Density Functional Theory (DFT) [66,67]. The energy minimization was performed at the MN15/def2-TZVP level of theory using the continuum solvation

model (IEF-PCM) with water as a solvent [68–70]. The harmonic frequencies were computed as well to confirm that the structures of the set of the studied compounds correspond with the minima on the Potential Energy Surface (PES)—no imaginary frequencies were found. For the set of compounds **3**–**12** and the reference drugs, the calculations of the Molecular Electrostatic Potential (MEP) were carried out using the DFT level of the theory mentioned above. The quantum-chemical simulations were performed with the Gaussian 16 Rev. C.0.1 suite of programs [71]. The Multiwfn and Visual Molecular Dynamics (VMD) 1.9.3 programs served for MEP calculations and visualization [72,73]. Subsequently, the "prepare_ligand" (from the ADFR software suite) script [61] was used to prepare ligands (in this case, the compounds denoted as **3**–**12** and the reference drugs) for the docking studies. The same docking protocol as in the case of the co-crystallized ligands was applied to estimate the binding affinities and the position of the ligand in the binding pocket of the selected receptors. The docking experiment and the ligand preparation were performed with the assistance of the AutoDock Flexible Receptor (ADFR) v1.2 suite of programs [74]. The 2D diagrams of the ligand–receptor interactions were generated in the BIOVIA Discovery Studio 2021 [75]. All visualizations of the binding pocket and the ligand positions were obtained with the ChimeraX 1.3 program [76].

4. Conclusions

In the present study, ten *N*-Mannich-base-type compounds **3**–**12** were synthesized for the first time, and their chemical structures were confirmed by detailed spectral analyses. All compounds were evaluated in vitro for their growth inhibitory activity on selected cancer cell lines: A375, C32, SNB-19, MCF-7/WT and MCF-7/DX. Two of the compounds (**5** and **6**) that displayed promising cytotoxic effect were further evaluated for anticancer activity on melanoma cells (A375 and C32) and human normal cells (keratinocytes) to explore their properties. The results of the MTT assay showed that the most significant cytotoxic effect was observed for compound **5** against A375 cells (IC_{50} = 80.79 μM). However, the highly cytotoxic impact of this compound on keratinocytes has to be considered as well. In the case of compound **6**, the anticancer effect was more selective to melanoma cell lines. A colony formation assay, population doubling time test and comet assay used in the neutral version, as well as fluorescent staining of actin filaments, proved the promising growth-inhibitory properties of compounds **5** and **6**. The results demonstrated the capability of the tested compounds to induce apoptosis and DNA damage in exposed melanoma cells; in particular, A375 cells were high sensitive to the genotoxic activity of compound **6**. Furthermore, this compound caused disturbing of the normal cytoskeleton organization by rearranging the F-actin microfilaments network in both melanoma cells at lower concentrations than those affecting normal keratinocytes.

However, the most promising compounds, from the perspective of the in silico flexible docking study to the selected receptors involved in cancer progression and metastasis (cMet, EGFR, HER2 and hTrkA) are compounds **7** and **11**. It is worth underlining that the binding affinities of the whole series of the synthesized compounds **3**–**12** are similar to or lower than the binding affinity of Erlotinib (one of the reference drugs). The MEP calculations revealed that compounds **3**–**12** are capable of interacting non-covalently. The interactions could be of the σ- and π-hole types.

Further research to investigate the mechanism of the anticancer effect of the tested compounds, including their implications in the cell cycle progression, as well as identify their molecular targets, are currently being investigated. Nevertheless, our present results constitute a foundation for further in vivo studies, which may lead to the selection of the most efficient compounds among the group of de novo synthesized *N*-Mannich bases of 1,3,4-oxadiazole based on a 4,6-dimethylpyridine core.

Supplementary Materials: The following supporting information can be downloaded at: https://www.mdpi.com/article/10.3390/ijms231911173/s1.

Author Contributions: Conceptualization, M.S. and P.Ś.; methodology, M.S., M.D.-Z., J.K., P.K.-W. and A.J.; software, A.J. and K.W.; validation, A.J. and K.W.; formal analysis, M.S., T.G., M.D.-Z., J.K., A.S., J.S., P.K.-W., N.R., K.W., A.J. and P.Ś.; investigation, M.S., T.G., M.D.-Z., A.S., P.K.-W., N.R., K.W., A.J. and P.Ś.; writing—original draft preparation, M.S., T.G., M.D.-Z., J.K., A.S., J.S., P.K.-W., N.R., K.W., A.J. and P.Ś.; writing—review and editing, M.S., J.K., J.S., A.J. and P.Ś.; visualization, M.S., A.S., K.W. and P.Ś.; supervision, P.Ś. and A.J.; project administration, P.Ś.; funding acquisition, P.Ś. All authors have read and agreed to the published version of the manuscript.

Funding: This research was funded by the Ministry of Health subvention according to the number SUBZ.D070.22.030 from the IT Simple system of Wroclaw Medical University.

Institutional Review Board Statement: Not applicable.

Informed Consent Statement: Not applicable.

Acknowledgments: A.J. and K.W. gratefully acknowledge the generous grants of CPU time and storage space provided by the Wrocław Centre for Networking and Supercomputing (WCSS), the Poznań Supercomputing and Networking Center (PSNC) and the Academic Computing Centre Cyfronet-Kraków (Prometheus supercomputer, part of the PL-Grid infrastructure). ^{1}H NMR, ^{13}C NMR, FT-IR and ESI-MS measurements were carried out in the Laboratory of Elemental Analysis and Structural Research, Faculty of Pharmacy, Wroclaw Medical University.

Conflicts of Interest: The authors declare no conflict of interest.

References

1. Cancer. Available online: https://www.who.int/news-room/fact-sheets/detail/cancer (accessed on 14 July 2022).
2. Hanahan, D.; Weinberg, R.A. Hallmarks of Cancer: The next Generation. *Cell* **2011**, *144*, 646–674. [CrossRef] [PubMed]
3. Side Effects of Cancer Treatment | CDC. Available online: https://www.cdc.gov/cancer/survivors/patients/side-effects-of-treatment.htm (accessed on 14 July 2022).
4. Assaraf, Y.G.; Brozovic, A.; Gonçalves, A.C.; Jurkovicova, D.; Linē, A.; Machuqueiro, M.; Saponara, S.; Sarmento-Ribeiro, A.B.; Xavier, C.P.R.; Vasconcelos, M.H. The Multi-Factorial Nature of Clinical Multidrug Resistance in Cancer. *Drug Resist. Updates* **2019**, *46*, 100645. [CrossRef] [PubMed]
5. Bukowski, K.; Kciuk, M.; Kontek, R. Mechanisms of Multidrug Resistance in Cancer Chemotherapy. *Int. J. Mol. Sci.* **2020**, *21*, 3233. [CrossRef] [PubMed]
6. Sochacka-Ćwikła, A.; Mączyński, M.; Regiec, A. FDA-Approved Small Molecule Compounds as Drugs for Solid Cancers from Early 2011 to the End of 2021. *Molecules* **2022**, *27*, 2259. [CrossRef]
7. Sigismund, S.; Avanzato, D.; Lanzetti, L. Emerging Functions of the EGFR in Cancer. *Mol. Oncol.* **2018**, *12*, 3–20. [CrossRef]
8. Massicano, A.V.F.; Marquez-Nostra, B.V.; Lapi, S.E. Targeting HER2 in Nuclear Medicine for Imaging and Therapy. *Mol. Imaging* **2018**, *17*, 153601211774538. [CrossRef]
9. Zhang, Y.; Xia, M.; Jin, K.; Wang, S.; Wei, H.; Fan, C.; Wu, Y.; Li, X.; Li, X.; Li, G.; et al. Function of the C-Met Receptor Tyrosine Kinase in Carcinogenesis and Associated Therapeutic Opportunities. *Mol. Cancer* **2018**, *17*, 45. [CrossRef]
10. Miao, Q.; Ma, K.; Chen, D.; Wu, X.; Jiang, S. Targeting Tropomyosin Receptor Kinase for Cancer Therapy. *Eur. J. Med. Chem.* **2019**, *175*, 129–148. [CrossRef]
11. Debela, D.T.; Muzazu, S.G.; Heraro, K.D.; Ndalama, M.T.; Mesele, B.W.; Haile, D.C.; Kitui, S.K.; Manyazewal, T. New Approaches and Procedures for Cancer Treatment: Current Perspectives. *SAGE Open Med.* **2021**, *9*, 205031212110343. [CrossRef]
12. Kottschade, L.A. The Future of Immunotherapy in the Treatment of Cancer. *Semin. Oncol. Nurs.* **2019**, *35*, 150934. [CrossRef]
13. Roman, G. Mannich Bases in Medicinal Chemistry and Drug Design. *Eur. J. Med. Chem.* **2015**, *89*, 743–816. [CrossRef]
14. Tugrak, M.; Gul, H.I.; Bandow, K.; Sakagami, H.; Gulcin, I.; Ozkay, Y.; Supuran, C.T. Synthesis and Biological Evaluation of Some New Mono Mannich Bases with Piperazines as Possible Anticancer Agents and Carbonic Anhydrase Inhibitors. *Bioorg. Chem.* **2019**, *90*, 103095. [CrossRef]
15. Ma, L.; Xiao, Y.; Li, C.; Xie, Z.L.; Li, D.D.; Wang, Y.T.; Ma, H.T.; Zhu, H.L.; Wang, M.H.; Ye, Y.H. Synthesis and Antioxidant Activity of Novel Mannich Base of 1,3,4-Oxadiazole Derivatives Possessing 1,4-Benzodioxan. *Bioorg. Med. Chem.* **2013**, *21*, 6763–6770. [CrossRef]
16. Palkar, M.B.; Singhai, A.S.; Ronad, P.M.; Vishwanathswamy, A.H.M.; Boreddy, T.S.; Veerapur, V.P.; Shaikh, M.S.; Rane, R.A.; Karpoormath, R. Synthesis, Pharmacological Screening and in Silico Studies of New Class of Diclofenac Analogues as a Promising Anti-Inflammatory Agents. *Bioorg. Med. Chem.* **2014**, *22*, 2855–2866. [CrossRef]
17. Köksal, M.; Gökhan, N.; Küpeli, E.; Yesilada, E.; Erdogan, H. Analgesic and Antiinflammatory Activities of Some New Mannich Bases of 5-Nitro-2-Benzoxazolinones. *Arch. Pharm. Res.* **2007**, *30*, 419–424. [CrossRef]
18. Szczukowski, Ł.; Krzyżak, E.; Wiatrak, B.; Jawień, P.; Marciniak, A.; Kotynia, A.; Świątek, P. New N-Substituted-1,2,4-Triazole Derivatives of Pyrrolo [3,4-d]Pyridazinone with Significant Anti-Inflammatory Activity—Design, Synthesis and Complementary In Vitro, Computational and Spectroscopic Studies. *Int. J. Mol. Sci.* **2021**, *22*, 11235. [CrossRef]

19. Patel, A.B.; Rohit, J.V. Development of 1,3,4-Thiadiazole and Piperazine Fused Hybrid Quinazoline Derivatives as Dynamic Antimycobacterial Agents. *Polycycl. Aromat. Compd.* **2021**, 1–12. [CrossRef]
20. Pandeya, S.N.; Sriram, D.; Nath, G.; De Clercq, E. Synthesis, Antibacterial, Antifungal and Anti-HIV Activities of Norfloxacin Mannich Bases. *Eur. J. Med. Chem.* **2000**, *35*, 249–255. [CrossRef]
21. Abrão, P.H.O.; Pizi, R.B.; de Souza, T.B.; Silva, N.C.; Fregnan, A.M.; Silva, F.N.; Coelho, L.F.L.; Malaquias, L.C.C.; Dias, A.L.T.; Dias, D.F.; et al. Synthesis and Biological Evaluation of New Eugenol Mannich Bases as Promising Antifungal Agents. *Chem. Biol. Drug Des.* **2015**, *86*, 459–465. [CrossRef]
22. Rybka, S.; Obniska, J.; Rapacz, A.; Filipek, B.; Żmudzki, P. Synthesis and Evaluation of Anticonvulsant Properties of New N-Mannich Bases Derived from Pyrrolidine-2,5-Dione and Its 3-Methyl-, 3-Isopropyl, and 3-Benzhydryl Analogs. *Bioorg. Med. Chem. Lett.* **2017**, *27*, 1412–1415. [CrossRef]
23. Kamiński, K.; Obniska, J.; Chlebek, I.; Wiklik, B.; Rzepka, S. Design, Synthesis and Anticonvulsant Properties of New N-Mannich Bases Derived from 3-Phenylpyrrolidine-2,5-Diones. *Bioorg. Med. Chem.* **2013**, *21*, 6821–6830. [CrossRef]
24. Kaur, P.; Wakode, S. Synthesis and In Vitro Evaluation of Anticancer Activity of Mannich Bases of Benzimidazole Derivatives. *Int. J. Sci. Res. ISSN* **2016**, *5*, 1096–1099.
25. Demirci, S.; Demirbaş, N. Anticancer Activities of Novel Mannich Bases against Prostate Cancer Cells. *Med. Chem. Res.* **2019**, *28*, 1945–1958. [CrossRef]
26. Sun, J.; Zhu, H.; Yang, Z.M.; Zhu, H.L. Synthesis, Molecular Modeling and Biological Evaluation of 2-Aminomethyl-5-(Quinolin-2-Yl)-1,3,4-Oxadiazole-2(3H)-Thione Quinolone Derivatives as Novel Anticancer Agent. *Eur. J. Med. Chem.* **2013**, *60*, 23–28. [CrossRef]
27. Savariz, F.C.; Foglio, M.A.; Goes Ruiz, A.L.T.; Da Costa, W.F.; De Magalhães Silva, M.; Santos, J.C.C.; Figueiredo, I.M.; Meyer, E.; De Carvalho, J.E.; Sarragiotto, M.H. Synthesis and Antitumor Activity of Novel 1-Substituted Phenyl 3-(2-Oxo-1,3,4-Oxadiazol-5-Yl) β-Carbolines and Their Mannich Bases. *Bioorg. Med. Chem.* **2014**, *22*, 6867–6875. [CrossRef]
28. Sun, J.; Ren, S.Z.; Lu, X.Y.; Li, J.J.; Shen, F.Q.; Xu, C.; Zhu, H.L. Discovery of a Series of 1,3,4-Oxadiazole-2(3H)-Thione Derivatives Containing Piperazine Skeleton as Potential FAK Inhibitors. *Bioorg. Med. Chem.* **2017**, *25*, 2593–2600. [CrossRef]
29. Luczynski, M.; Kudelko, A. Synthesis and Biological Activity of 1,3,4-Oxadiazoles Used in Medicine and Agriculture. *Appl. Sci.* **2022**, *12*, 3756. [CrossRef]
30. Bąchor, U.; Drozd-Szczygieł, E.; Bąchor, R.; Jerzykiewicz, L.; Wieczorek, R.; Mączyński, M. New Water-Soluble Isoxazole-Linked 1,3,4-Oxadiazole Derivative with Delocalized Positive Charge. *RSC Adv.* **2021**, *11*, 29668–29674. [CrossRef]
31. Verma, S.K.; Verma, R.; Verma, S.; Vaishnav, Y.; Tiwari, S.P.; Rakesh, K.P. Anti-Tuberculosis Activity and Its Structure-Activity Relationship (SAR) Studies of Oxadiazole Derivatives: A Key Review. *Eur. J. Med. Chem.* **2021**, *209*, 112886. [CrossRef] [PubMed]
32. Boström, J.; Hogner, A.; Llinàs, A.; Wellner, E.; Plowright, A.T. Oxadiazoles in Medicinal Chemistry. *J. Med. Chem.* **2012**, *55*, 1817–1830. [CrossRef]
33. Rana, K.; Salahuddin; Sahu, J.K. Significance of 1,3,4-Oxadiazole Containing Compounds in New Drug Development. *Curr. Drug Res. Rev.* **2021**, *13*, 90–100. [CrossRef] [PubMed]
34. Hughes, T.V.; Xu, G.; Wetter, S.K.; Connolly, P.J.; Emanuel, S.L.; Karnachi, P.; Pollack, S.R.; Pandey, N.; Adams, M.; Moreno-Mazza, S.; et al. A Novel 5-[1,3,4-Oxadiazol-2-Yl]-N-Aryl-4,6-Pyrimidine Diamine Having Dual EGFR/HER2 Kinase Activity: Design, Synthesis, and Biological Activity. *Bioorg. Med. Chem. Lett.* **2008**, *18*, 4896–4899. [CrossRef] [PubMed]
35. Liu, K.; Lu, X.; Zhang, H.J.; Sun, J.; Zhu, H.L. Synthesis, Molecular Modeling and Biological Evaluation of 2-(Benzylthio)-5-Aryloxadiazole Derivatives as Anti-Tumor Agents. *Eur. J. Med. Chem.* **2012**, *47*, 473–478. [CrossRef] [PubMed]
36. Akhtar, M.J.; Siddiqui, A.A.; Khan, A.A.; Ali, Z.; Dewangan, R.P.; Pasha, S.; Yar, M.S. Design, Synthesis, Docking and QSAR Study of Substituted Benzimidazole Linked Oxadiazole as Cytotoxic Agents, EGFR and ErbB2 Receptor Inhibitors. *Eur. J. Med. Chem.* **2017**, *126*, 853–869. [CrossRef]
37. Osmaniye, D.; Görgülü, Ş.; Sağlık, B.N.; Levent, S.; Özkay, Y.; Kaplancıklı, Z.A. Synthesis and Biological Evaluation of Novel 1,3,4-oxadiazole Derivatives as Anticancer Agents and Potential EGFR Inhibitors. *J. Heterocycl. Chem.* **2022**, *59*, 518–532. [CrossRef]
38. Ibrahim, H.A.; Awadallah, F.M.; Refaat, H.M.; Amin, K.M. Molecular Docking Simulation, Synthesis and 3D Pharmacophore Studies of Novel 2-Substituted-5-Nitro-Benzimidazole Derivatives as Anticancer Agents Targeting VEGFR-2 and c-Met. *Bioorg. Chem.* **2018**, *77*, 457–470. [CrossRef]
39. Tian, C.; Huang, S.; Xu, Z.; Liu, W.; Li, D.; Liu, M.; Zhu, C.; Wu, L.; Jiang, X.; Ding, H.; et al. Design, Synthesis, and Biological Evaluation of β-Carboline 1,3,4-Oxadiazole Based Hybrids as HDAC Inhibitors with Potential Antitumor Effects. *Bioorg. Med. Chem. Lett.* **2022**, *64*, 128663. [CrossRef]
40. Zhang, F.; Wang, X.L.; Shi, J.; Wang, S.F.; Yin, Y.; Yang, Y.S.; Zhang, W.M.; Zhu, H.L. Synthesis, Molecular Modeling and Biological Evaluation of N-Benzylidene-2-((5-(Pyridin-4-Yl)-1,3,4-Oxadiazol-2-Yl)Thio)Acetohydrazide Derivatives as Potential Anticancer Agents. *Bioorg. Med. Chem.* **2014**, *22*, 468–477. [CrossRef]
41. Alzhrani, Z.M.M.; Alam, M.M.; Neamatallah, T.; Nazreen, S. Design, Synthesis and in Vitro Antiproliferative Activity of New Thiazolidinedione-1,3,4-Oxadiazole Hybrids as Thymidylate Synthase Inhibitors. *J. Enzyme Inhib. Med. Chem.* **2020**, *35*, 1116–1123. [CrossRef]
42. Tantak, M.P.; Malik, M.; Klingler, L.; Olson, Z.; Kumar, A.; Sadana, R.; Kumar, D. Indolyl-α-Keto-1,3,4-Oxadiazoles: Synthesis, Anti-Cell Proliferation Activity, and Inhibition of Tubulin Polymerization. *Bioorg. Med. Chem. Lett.* **2021**, *37*, 127842. [CrossRef]

43. Tagad, H.D.; Hamada, Y.; Nguyen, J.T.; Hamada, T.; Abdel-Rahman, H.; Yamani, A.; Nagamine, A.; Ikari, H.; Igawa, N.; Hidaka, K.; et al. Design of Pentapeptidic BACE1 Inhibitors with Carboxylic Acid Bioisosteres at P1′ and P4 Positions. *Bioorg. Med. Chem.* **2010**, *18*, 3175–3186. [CrossRef]
44. Goldberg, K.; Groombridge, S.; Hudson, J.; Leach, A.G.; MacFaul, P.A.; Pickup, A.; Poultney, R.; Scott, J.S.; Svensson, P.H.; Sweeney, J. Oxadiazole Isomers: All Bioisosteres Are Not Created Equal. *MedChemComm* **2012**, *3*, 600–604. [CrossRef]
45. Li, Y.T.; Wang, J.H.; Pan, C.W.; Meng, F.F.; Chu, X.Q.; Ding, Y.H.; Qu, W.Z.; Li, H.Y.; Yang, C.; Zhang, Q.; et al. Syntheses and Biological Evaluation of 1,2,3-Triazole and 1,3,4-Oxadiazole Derivatives of Imatinib. *Bioorg. Med. Chem. Lett.* **2016**, *26*, 1419–1427. [CrossRef]
46. Świątek, P.; Glomb, T.; Dobosz, A.; Gębarowski, T.; Wojtkowiak, K.; Jezierska, A.; Panek, J.J.; Świątek, M.; Strzelecka, M. Biological Evaluation and Molecular Docking Studies of Novel 1,3,4-Oxadiazole Derivatives of 4,6-Dimethyl-2-Sulfanylpyridine-3-Carboxamide. *Int. J. Mol. Sci.* **2022**, *23*, 549. [CrossRef]
47. Świątek, P.; Saczko, J.; Rembiałkowska, N.; Kulbacka, J. Synthesis of New Hydrazone Derivatives and Evaluation of Their Efficacy as Proliferation Inhibitors in Human Cancer Cells. *Med. Chem.* **2019**, *15*, 903–910. [CrossRef]
48. Ahmed, E.M.; Bandopadhyay, G.; Coyle, B.; Grabowska, A. A HIF-Independent, CD133-Mediated Mechanism of Cisplatin Resistance in Glioblastoma Cells. *Cell. Oncol.* **2018**, *41*, 319–328. [CrossRef]
49. Suberu, J.O.; Romero-Canelón, I.; Sullivan, N.; Lapkin, A.A.; Barker, G.C. Comparative Cytotoxicity of Artemisinin and Cisplatin and Their Interactions with Chlorogenic Acids in MCF7 Breast Cancer Cells. *ChemMedChem* **2014**, *9*, 2791–2797. [CrossRef]
50. Elias, S.T.; Borges, G.A.; Rêgo, D.F.; E Silva, L.F.O.; Avelino, S.; Neto, J.N.D.M.; Simeoni, L.A.; Guerra, E.N.S. Combined Paclitaxel, Cisplatin and Fluorouracil Therapy Enhances Ionizing Radiation Effects, Inhibits Migration and Induces G0/G1 Cell Cycle Arrest and Apoptosis in Oral Carcinoma Cell Lines. *Oncol. Lett.* **2015**, *10*, 1721–1727. [CrossRef]
51. Cortés-Gutiérrez, E.I.; Hernández-Garza, F.; García-Pérez, J.O.; Dávila-Rodríguez, M.I.; Aguado-Barrera, M.E.; Cerda-Flores, R.M. Evaluation of DNA Single and Double Strand Breaks in Women with Cervical Neoplasia Based on Alkaline and Neutral Comet Assay Techniques. *J. Biomed. Biotechnol.* **2012**, *2012*, 385245. [CrossRef]
52. Eathiraj, S.; Palma, R.; Volckova, E.; Hirschi, M.; France, D.S.; Ashwell, M.A.; Chan, T.C.K. Discovery of a Novel Mode of Protein Kinase Inhibition Characterized by the Mechanism of Inhibition of Human Mesenchymal-Epithelial Transition Factor (c-Met) Protein Autophosphorylation by ARQ 197. *J. Biol. Chem.* **2011**, *286*, 20666–20676. [CrossRef]
53. Hu, C.; Wang, A.; Wu, H.; Qi, Z.; Li, X.; Yan, X.E.; Chen, C.; Yu, K.; Zou, F.; Wang, W.; et al. Discovery and Characterization of a Novel Irreversible EGFR Mutants Selective and Potent Kinase Inhibitor CHMFL-EGFR-26 with a Distinct Binding Mode. *Oncotarget* **2017**, *8*, 18359–18372. [CrossRef] [PubMed]
54. Son, J.; Jang, J.; Beyett, T.S.; Eum, Y.; Haikala, H.M.; Verano, A.; Lin, M.; Hatcher, J.M.; Kwiatkowski, N.P.; Eser, P.; et al. A Novel HER2-Selective Kinase Inhibitor Is Effective in HER2 Mutant and Amplified Non-Small Cell Lung Cancer. *Cancer Res.* **2022**, *82*, 1633–1645. [CrossRef] [PubMed]
55. Subramanian, G.; Bowen, S.J.; Zhu, Y.; Roush, N.; Zachary, T.; Javens, C.; Williams, T.; Janssen, A.; Gonzales, A. Type 2 Inhibitor Leads of Human Tropomyosin Receptor Kinase (HTrkA). *Bioorg. Med. Chem. Lett.* **2019**, *29*, 126624. [CrossRef] [PubMed]
56. Pecina, A.; Haldar, S.; Fanfrlík, J.; Meier, R.; Řezáč, J.; Lepšík, M.; Hobza, P. SQM/COSMO Scoring Function at the DFTB3-D3H4 Level: Unique Identification of Native Protein-Ligand Poses. *J. Chem. Inf. Model.* **2017**, *57*, 127–132. [CrossRef] [PubMed]
57. Collins, A.R. The Comet Assay. Principles, Applications, and Limitations. In *Methods in Molecular Biology*; Humana Press: Clifton, NJ, USA, 2002; pp. 163–177. [CrossRef]
58. Nadin, S.B.; Vargas-Roig, L.M.; Ciocca, D.R. A Silver Staining Method for Single-Cell Gel Assay. *J. Histochem. Cytochem.* **2001**, *49*, 1183–1186. [CrossRef]
59. RCSB PDB: Homepage. Available online: https://www.rcsb.org/ (accessed on 27 June 2022).
60. Word, J.M.; Lovell, S.C.; Richardson, J.S.; Richardson, D.C. Asparagine and Glutamine: Using Hydrogen Atom Contacts in the Choice of Side-Chain Amide Orientation. *J. Mol. Biol.* **1999**, *285*, 1735–1747. [CrossRef] [PubMed]
61. Downloads—ADFR. Available online: https://ccsb.scripps.edu/adfr/downloads/ (accessed on 27 June 2022).
62. Forli, S.; Huey, R.; Pique, M.E.; Sanner, M.F.; Goodsell, D.S.; Olson, A.J. Computational Protein-Ligand Docking and Virtual Drug Screening with the AutoDock Suite. *Nat. Protoc.* **2016**, *11*, 905–919. [CrossRef] [PubMed]
63. Park, J.H.; Liu, Y.; Lemmon, M.A.; Radhakrishnan, R. Erlotinib Binds Both Inactive and Active Conformations of the EGFR Tyrosine Kinase Domain. *Biochem. J.* **2012**, *448*, 417–423. [CrossRef]
64. Sogabe, S.; Kawakita, Y.; Igaki, S.; Iwata, H.; Miki, H.; Cary, D.R.; Takagi, T.; Takagi, S.; Ohta, Y.; Ishikawa, T. Structure-Based Approach for the Discovery of Pyrrolo [3,2-d]Pyrimidine-Based EGFR T790M/L858R Mutant Inhibitors. *ACS Med. Chem. Lett.* **2013**, *4*, 201–205. [CrossRef]
65. Dorsch, D.; Schadt, O.; Stieber, F.; Meyring, M.; Grädler, U.; Bladt, F.; Friese-Hamim, M.; Knühl, C.; Pehl, U.; Blaukat, A. Identification and Optimization of Pyridazinones as Potent and Selective C-Met Kinase Inhibitors. *Bioorg. Med. Chem. Lett.* **2015**, *25*, 1597–1602. [CrossRef]
66. Hohenberg, P.; Kohn, W. Inhomogeneous Electron Gas. *Phys. Rev.* **1964**, *136*, B864–B871. [CrossRef]
67. Kohn, W.; Sham, L.J. Self-Consistent Equations Including Exchange and Correlation Effects. *Phys. Rev.* **1965**, *140*, A1133–A1138. [CrossRef]

68. Yu, H.S.; He, X.; Li, S.L.; Truhlar, D.G. MN15: A Kohn-Sham Global-Hybrid Exchange-Correlation Density Functional with Broad Accuracy for Multi-Reference and Single-Reference Systems and Noncovalent Interactions. *Chem. Sci.* **2016**, *7*, 5032–5051. [CrossRef]
69. Weigend, F.; Ahlrichs, R. Balanced Basis Sets of Split Valence, Triple Zeta Valence and Quadruple Zeta Valence Quality for H to Rn: Design and Assessment of Accuracy. *Phys. Chem. Chem. Phys.* **2005**, *7*, 3297–3305. [CrossRef]
70. Cossi, M.; Barone, V.; Cammi, R.; Tomasi, J. Ab Initio Study of Solvated Molecules: A New Implementation of the Polarizable Continuum Model. *Chem. Phys. Lett.* **1996**, *255*, 327–335. [CrossRef]
71. Frisch, M.J.; Trucks, G.W.; Schlegel, H.B.; Scuseria, G.E.; Robb, M.A.; Cheeseman, J.R.; Scalmani, G.; Barone, V.; Mennucci, B.; Petersson, G.A. *Gaussian 16 Revision C.0.1*; Gaussian, Inc.: Wallingford, CT, USA, 2016.
72. Lu, T.; Chen, F. Multiwfn: A Multifunctional Wavefunction Analyzer. *J. Comput. Chem.* **2012**, *33*, 580–592. [CrossRef]
73. Humphrey, W.; Dalke, A.; Schulten, K. VMD: Visual Molecular Dynamics. *J. Mol. Graph.* **1996**, *14*, 33–38. [CrossRef]
74. Ravindranath, P.A.; Forli, S.; Goodsell, D.S.; Olson, A.J.; Sanner, M.F. AutoDockFR: Advances in Protein-Ligand Docking with Explicitly Specified Binding Site Flexibility. *PLoS Comput. Biol.* **2015**, *11*, e1004586. [CrossRef]
75. *DSV: Discover Studio Visualiser, V21.1.0.20298*; BIOVIA, Dassault Systèmes: San Diego, CA, USA, 2020.
76. Pettersen, E.F.; Goddard, T.D.; Huang, C.C.; Meng, E.C.; Couch, G.S.; Croll, T.I.; Morris, J.H.; Ferrin, T.E. UCSF ChimeraX: Structure Visualization for Researchers, Educators, and Developers. *Protein Sci.* **2021**, *30*, 70–82. [CrossRef]

SUPPLEMENTARY MATERIALS

Synthesis, Anticancer Activity and Molecular Docking Studies of Novel *N*-Mannich Bases of 1,3,4-Oxadiazole Based on 4,6-Dimethylpyridine Scaffold

Małgorzata Strzelecka [1], Teresa Glomb [1,*], Małgorzata Drąg-Zalesińska [2], Julita Kulbacka [3], Anna Szewczyk [3,4], Jolanta Saczko [3], Paulina Kasperkiewicz-Wasilewska [5], Nina Rembiałkowska[3], Kamil Wojtkowiak[6], Aneta Jezierska [6] and Piotr Świątek [1,*]

[1] Department of Medicinal Chemistry, Faculty of Pharmacy, Wroclaw Medical University, Borowska 211, 50-556 Wroclaw, Poland
[2] Division of Histology and Embryology, Department of Human Morphology and Embryology, Faculty of Medicine, Wroclaw Medical University, Chałubińskiego 6a, 50-368 Wroclaw, Poland
[3] Department of Molecular and Cellular Biology, Faculty of Pharmacy, Wroclaw Medical University, Borowska 211, 50-556 Wroclaw, Poland
[4] Department of Animal Developmental Biology, Institute of Experimental Biology, University of Wroclaw, Sienkiewicza 21, 50-335 Wroclaw, Poland
[5] Department of Bioorganic Chemistry, Faculty of Chemistry, Wroclaw University of Science and Technology, Wybrzeże Wyspiańskiego 27, 50-370 Wroclaw, Poland
[6] Faculty of Chemistry, University of Wroclaw, F. Joliot-Curie 14, 50-383 Wroclaw, Poland

***** Correspondence: piotr.swiatek@umw.edu.pl (P.Ś.); teresa.glomb@umw.edu.pl (T.G.); Tel.: +48-717840391

Table S1. NMR spectra of new compounds

3
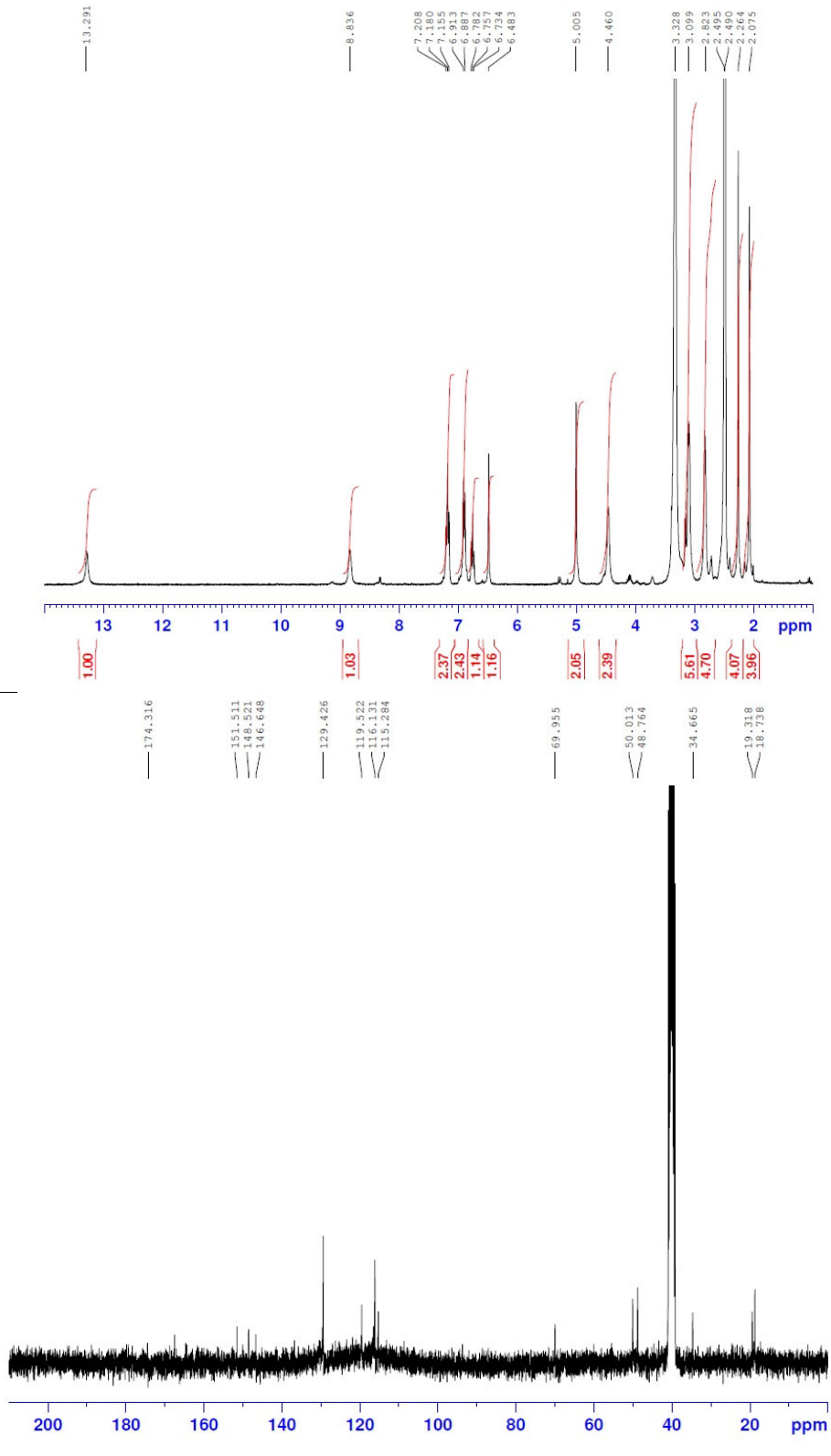

4

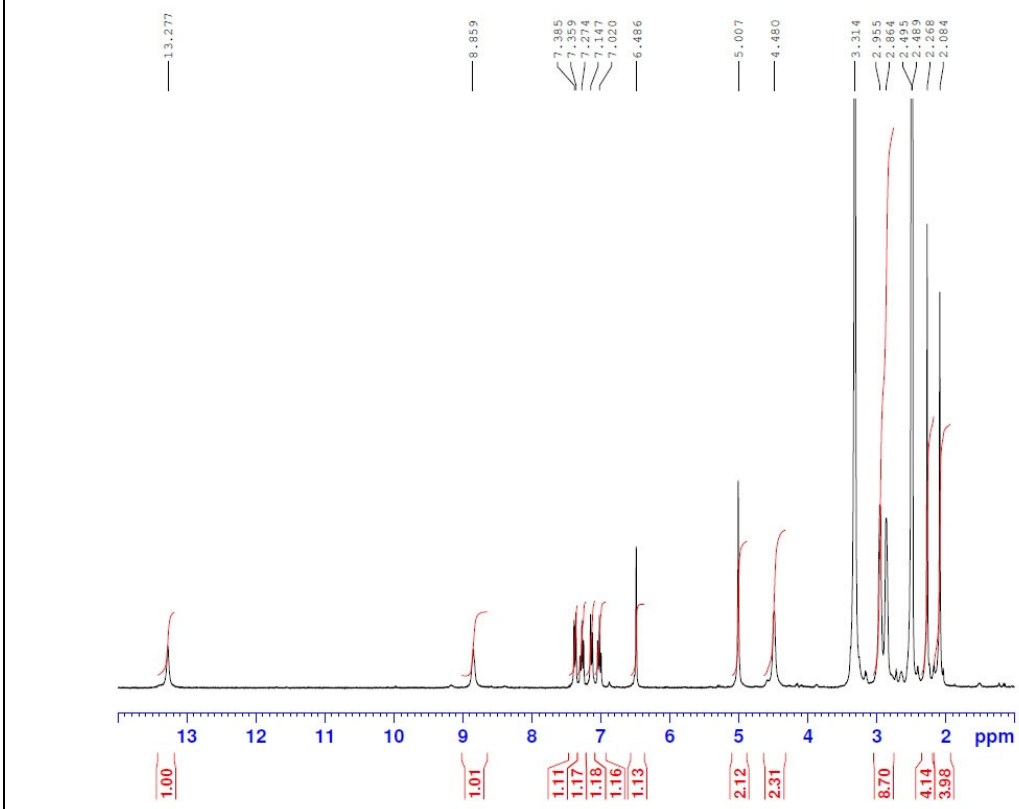
13.277
8.859
7.385
7.359
7.274
7.147
7.020
6.486
5.007
4.480
3.314
2.955
2.864
2.485
2.483
2.268
2.084
13 12 11 10 9 8 7 6 5 4 3 2 ppm
1.00
1.01
1.11
1.17
1.18
1.16
1.13
2.12
2.31
8.70
4.14
3.98

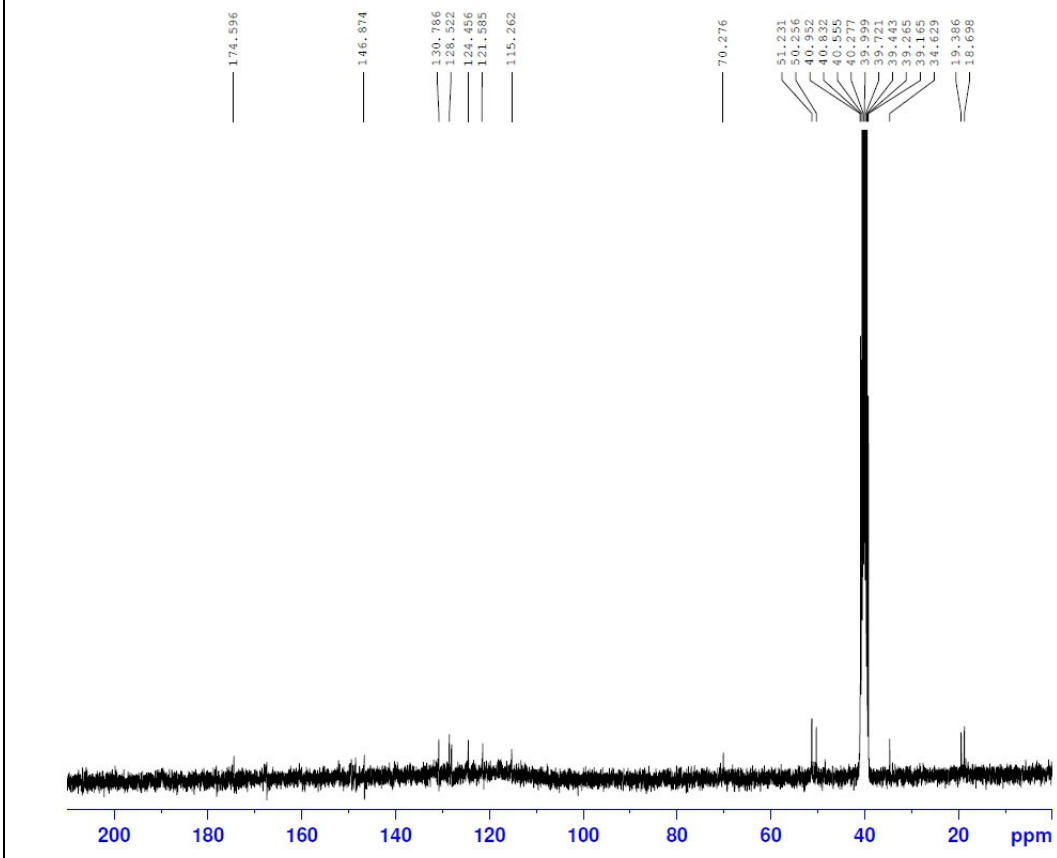
174.596
146.874
130.786
128.522
124.456
121.585
115.262
70.276
51.231
50.256
40.952
40.832
40.555
40.277
39.999
39.721
39.443
39.265
39.165
34.629
19.386
18.698
200 180 160 140 120 100 80 60 40 20 ppm

5

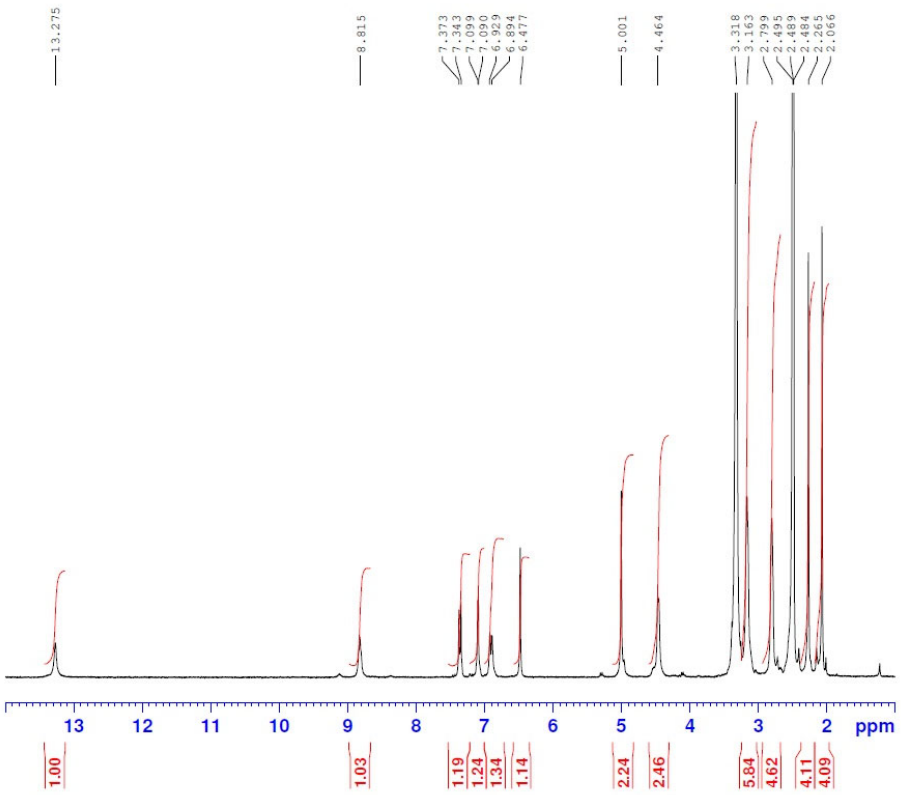
13.275
8.815
7.373
7.343
7.099
7.090
6.929
6.894
6.477
5.001
4.464
3.318
3.163
2.799
2.495
2.489
2.484
2.265
2.066
13 12 11 10 9 8 7 6 5 4 3 2 ppm
1.00
1.03
1.19
1.24
1.34
1.14
2.24
2.46
5.84
4.62
4.11
4.09

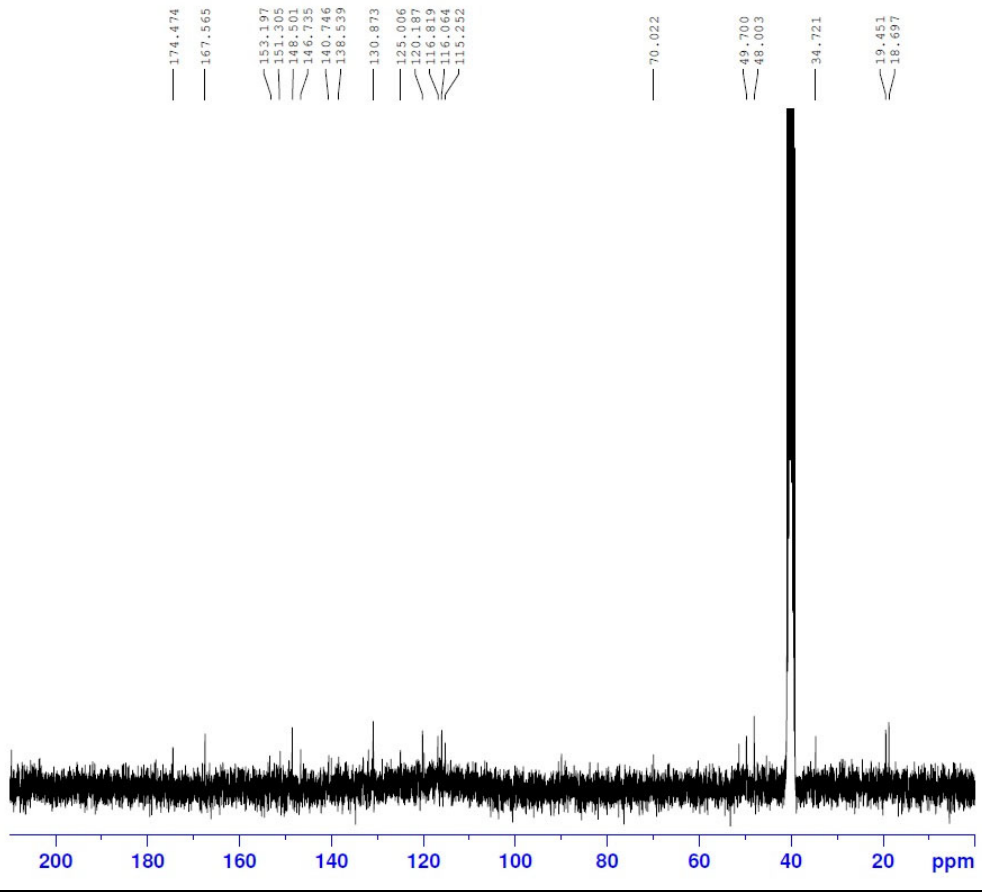
174.474
167.565
153.197
151.305
148.501
146.735
140.746
138.539
130.873
125.006
120.187
116.819
116.064
115.252
70.022
49.700
48.003
34.721
19.451
18.697
200 180 160 140 120 100 80 60 40 20 ppm

6

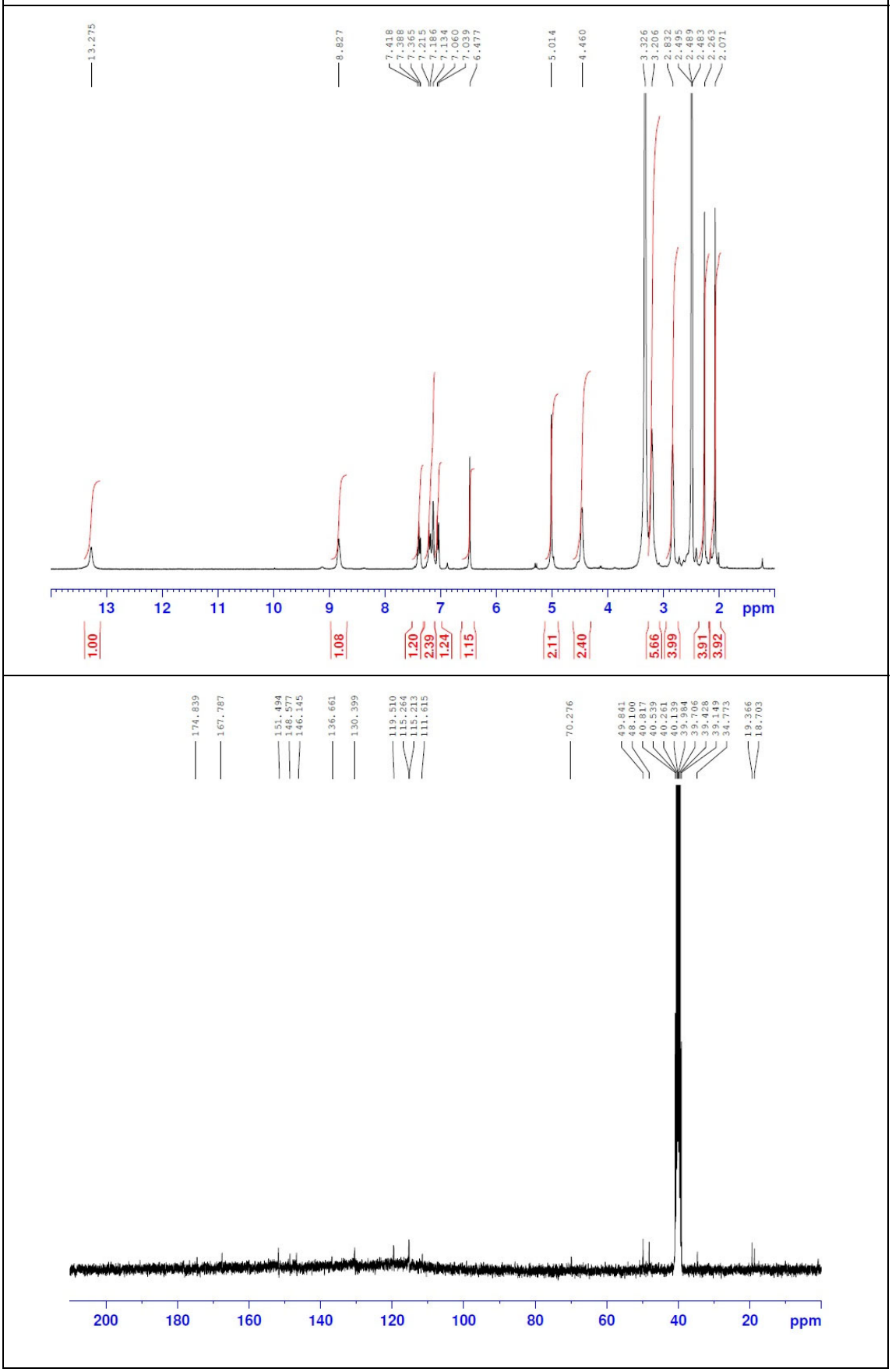
13.275
8.827
7.418
7.388
7.365
7.215
7.186
7.134
7.060
7.039
6.477
5.014
4.460
3.326
3.206
2.832
2.495
2.489
2.483
2.263
2.071
13 12 11 10 9 8 7 6 5 4 3 2 ppm
1.00
1.08
1.20
2.39
1.24
1.15
2.11
2.40
5.66
3.99
3.91
3.92
174.839
167.787
151.494
148.577
146.145
136.661
130.399
119.510
115.264
115.213
111.615
70.276
49.841
48.100
40.817
40.539
40.261
40.139
39.984
39.706
39.428
39.149
34.773
19.366
18.703
200 180 160 140 120 100 80 60 40 20 ppm

7

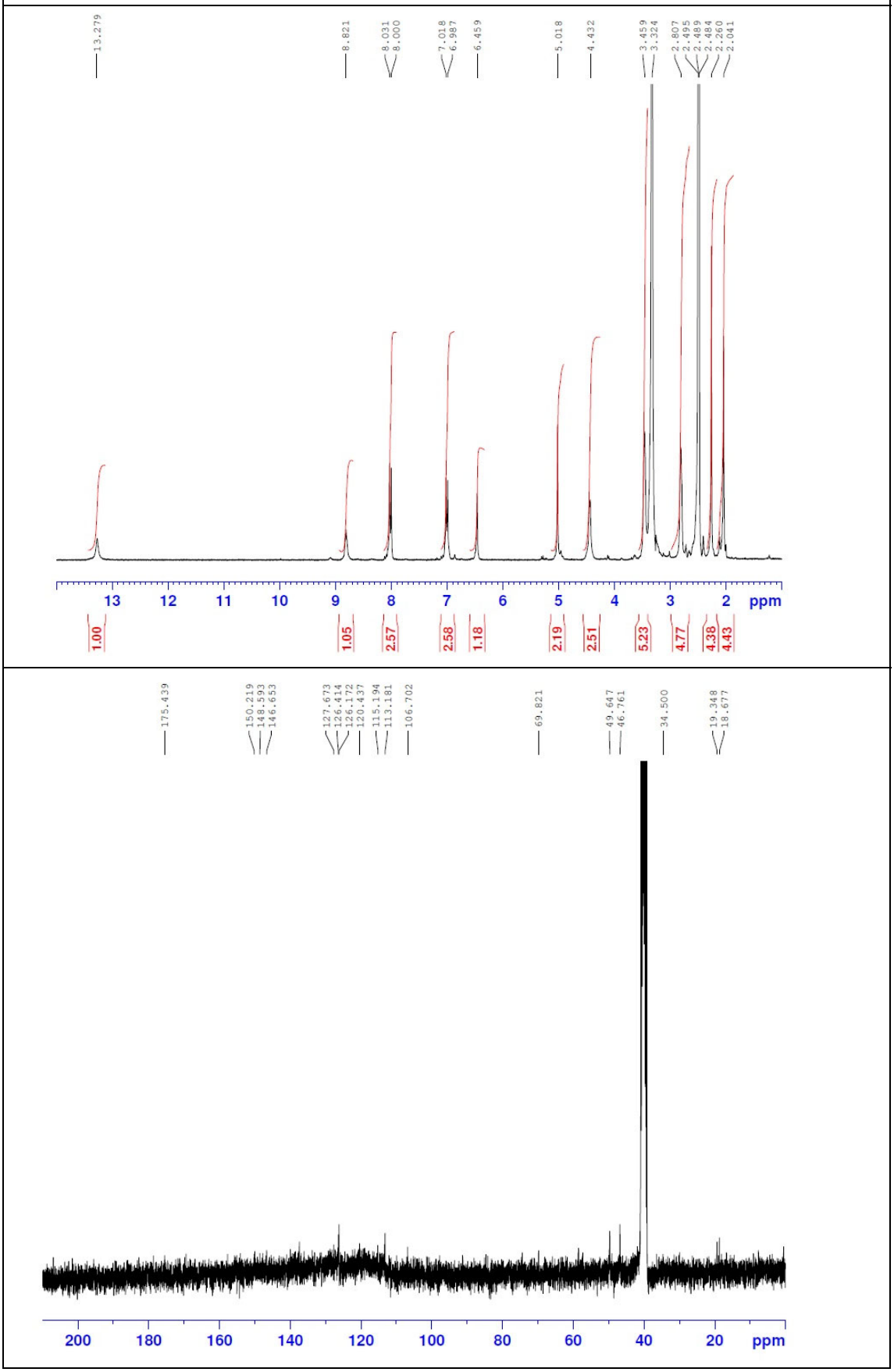
13.279
8.821
8.031
8.000
7.018
6.987
6.459
5.018
4.432
3.459
3.324
2.807
2.495
2.489
2.484
2.260
2.041
13 12 11 10 9 8 7 6 5 4 3 2 ppm
1.00 1.05 2.57 2.58 1.18 2.19 2.51 5.23 4.77 4.38 4.43
175.439
150.219
148.593
146.653
127.673
126.414
126.172
120.437
115.194
113.181
106.702
69.821
49.647
46.761
34.500
19.348
18.677
200 180 160 140 120 100 80 60 40 20 ppm

8

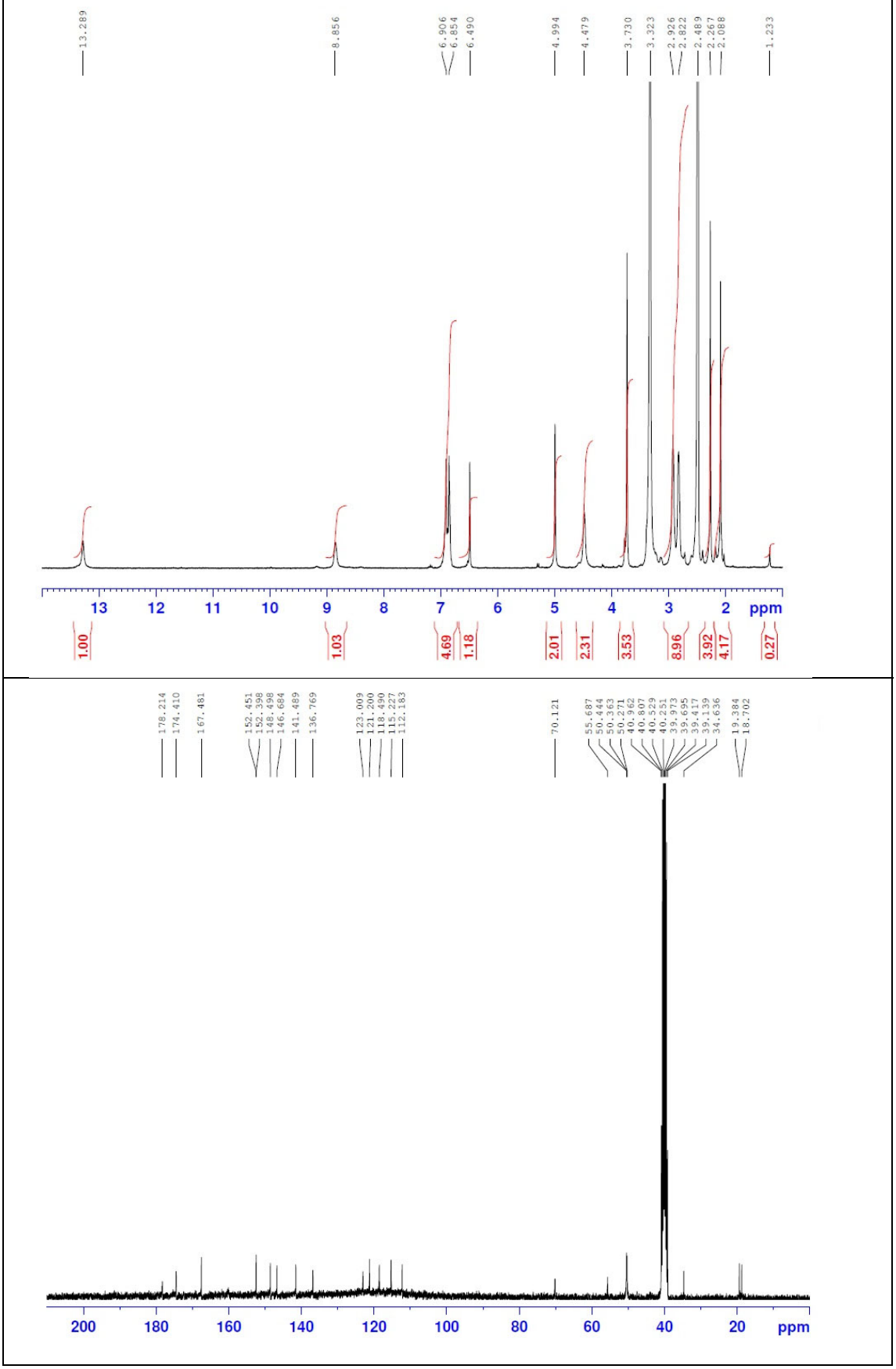
13.289
8.856
6.906
6.854
6.490
4.994
4.479
3.730
3.323
2.926
2.822
2.489
2.267
2.088
1.233
13 12 11 10 9 8 7 6 5 4 3 2 ppm
1.00
1.03
4.69
1.18
2.01
2.31
3.53
8.96
3.92
4.17
0.27
178.214
174.410
167.481
152.451
152.398
148.498
146.684
141.489
136.769
123.009
121.200
118.490
115.227
112.183
70.121
55.687
50.444
50.363
50.271
40.962
40.837
40.629
40.253
39.973
39.695
39.417
39.139
34.636
19.384
18.702
200 180 160 140 120 100 80 60 40 20 ppm

9

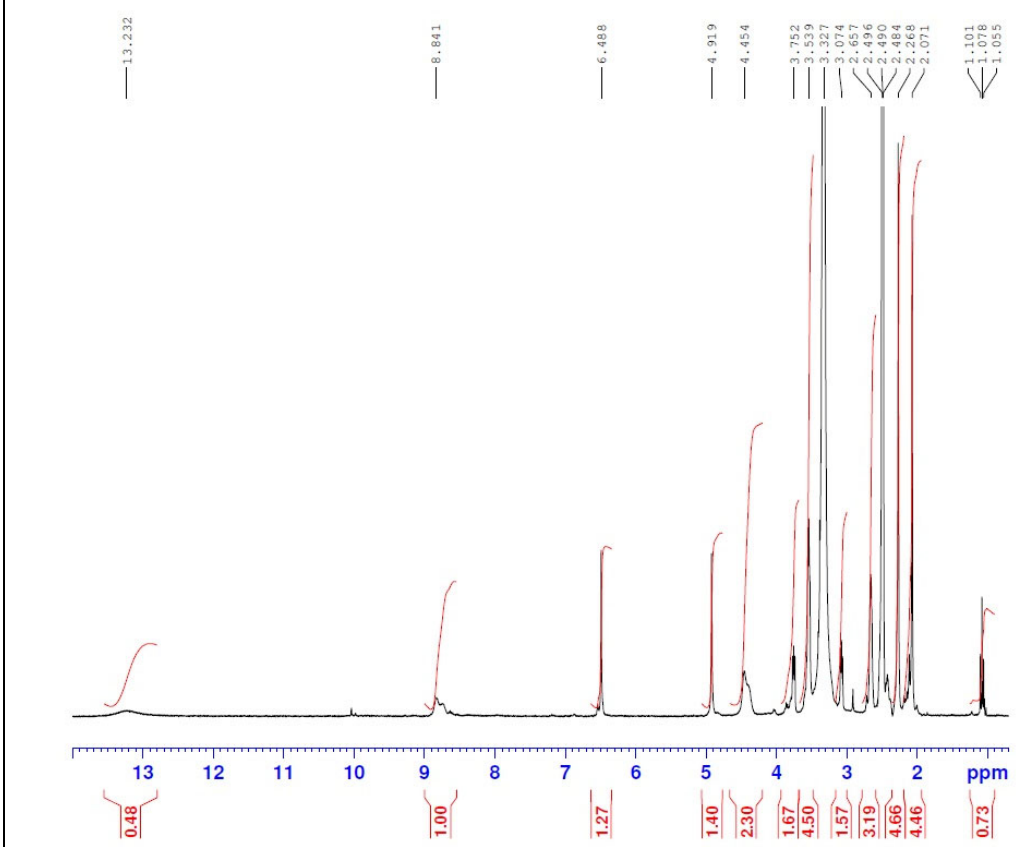
13.232
8.841
6.488
4.919
4.454
3.752
3.539
3.327
3.074
2.657
2.496
2.490
2.484
2.268
2.071
1.101
1.078
1.055
13 12 11 10 9 8 7 6 5 4 3 2 ppm
0.48
1.00
1.27
1.40
2.30
1.67
4.50
1.57
3.19
4.66
4.46
0.73

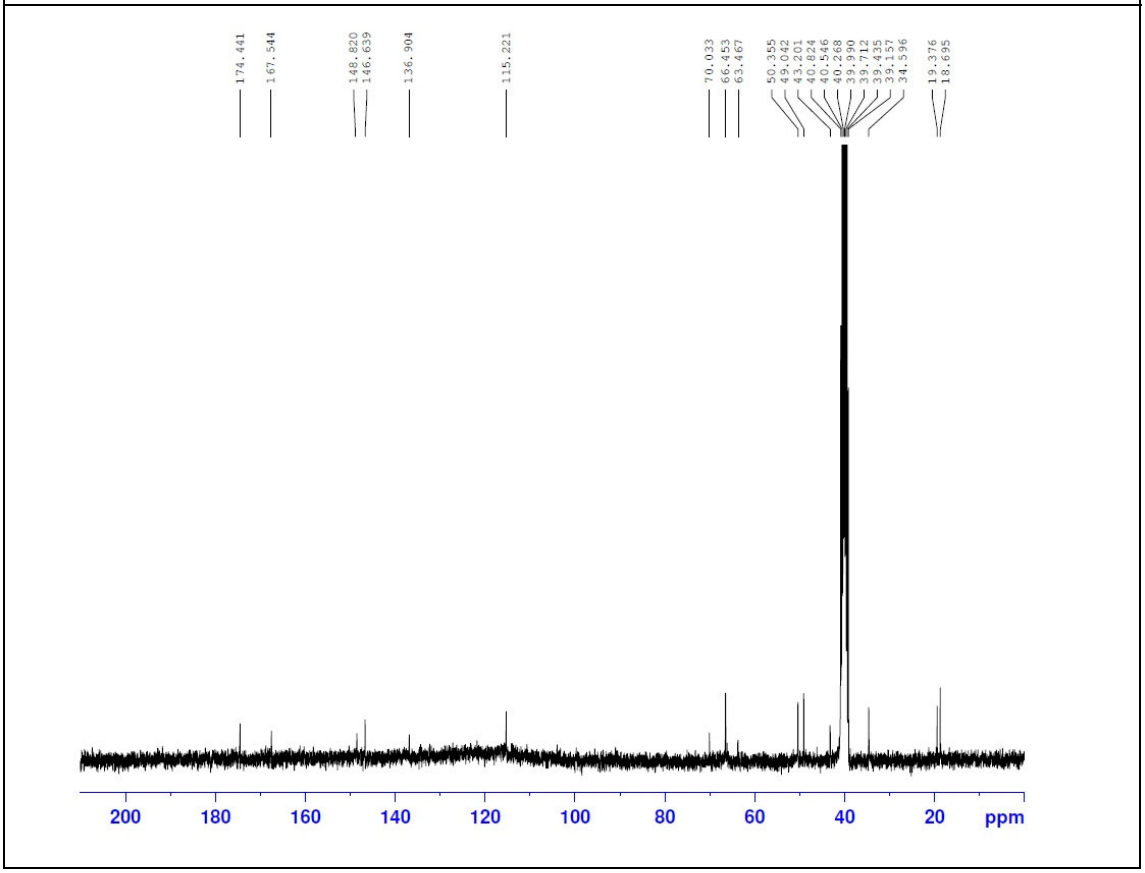
174.441
167.544
148.820
146.639
136.904
115.221
70.033
66.453
63.467
50.355
49.042
43.201
40.824
40.546
40.268
39.990
39.712
39.435
39.157
34.596
19.376
18.695
200 180 160 140 120 100 80 60 40 20 ppm

10

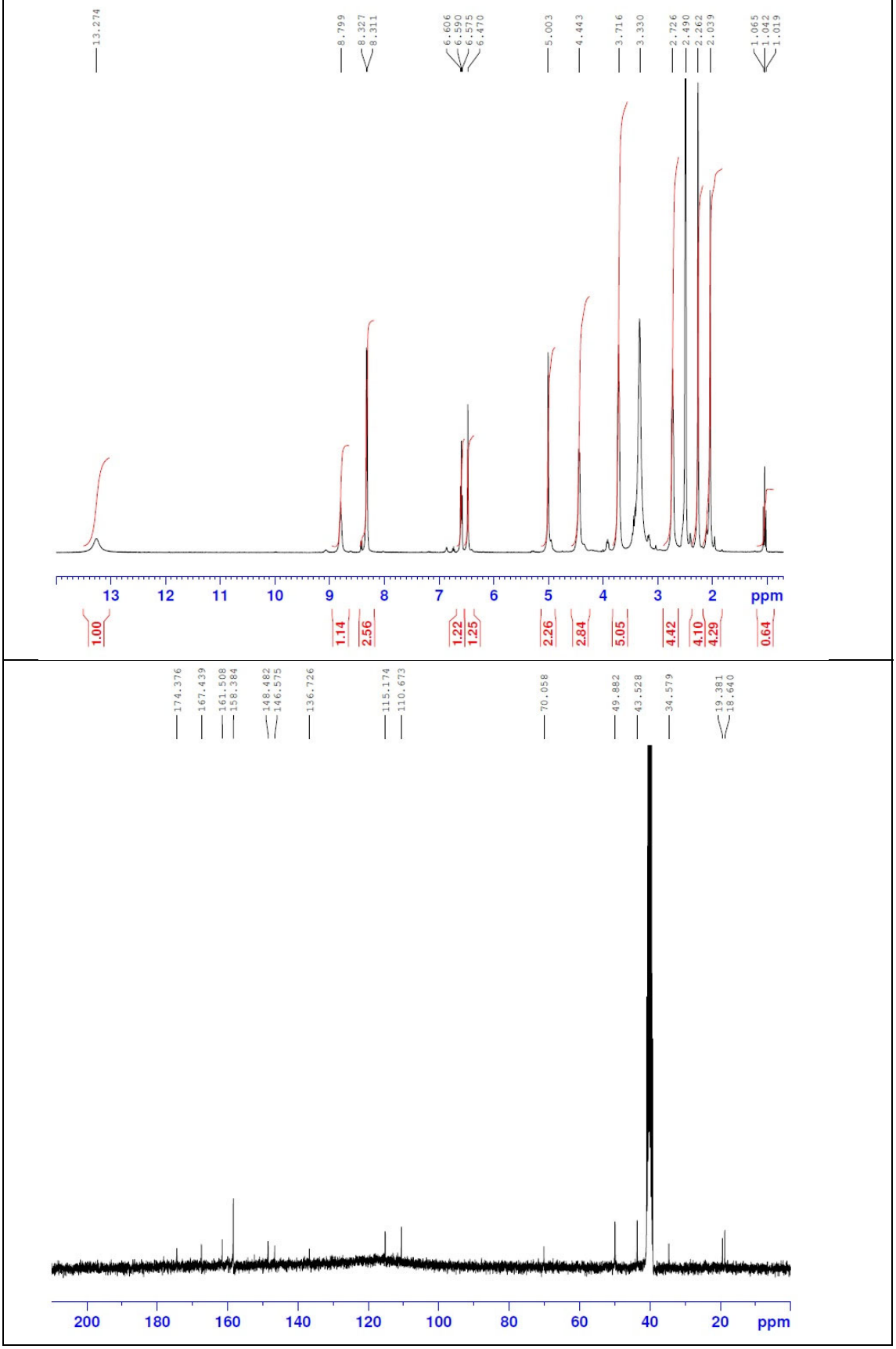
13.274
8.799
8.327
8.311
6.606
6.590
6.575
6.470
5.003
4.443
3.716
3.330
2.726
2.490
2.262
2.039
1.065
1.042
1.019
13 12 11 10 9 8 7 6 5 4 3 2 ppm
1.00
1.14
2.56
1.22
1.25
2.26
2.84
5.05
4.42
4.10
4.29
0.64
174.376
167.439
161.508
158.384
148.482
146.575
136.726
115.174
110.673
70.058
49.882
43.528
34.579
19.381
18.640
200 180 160 140 120 100 80 60 40 20 ppm

11

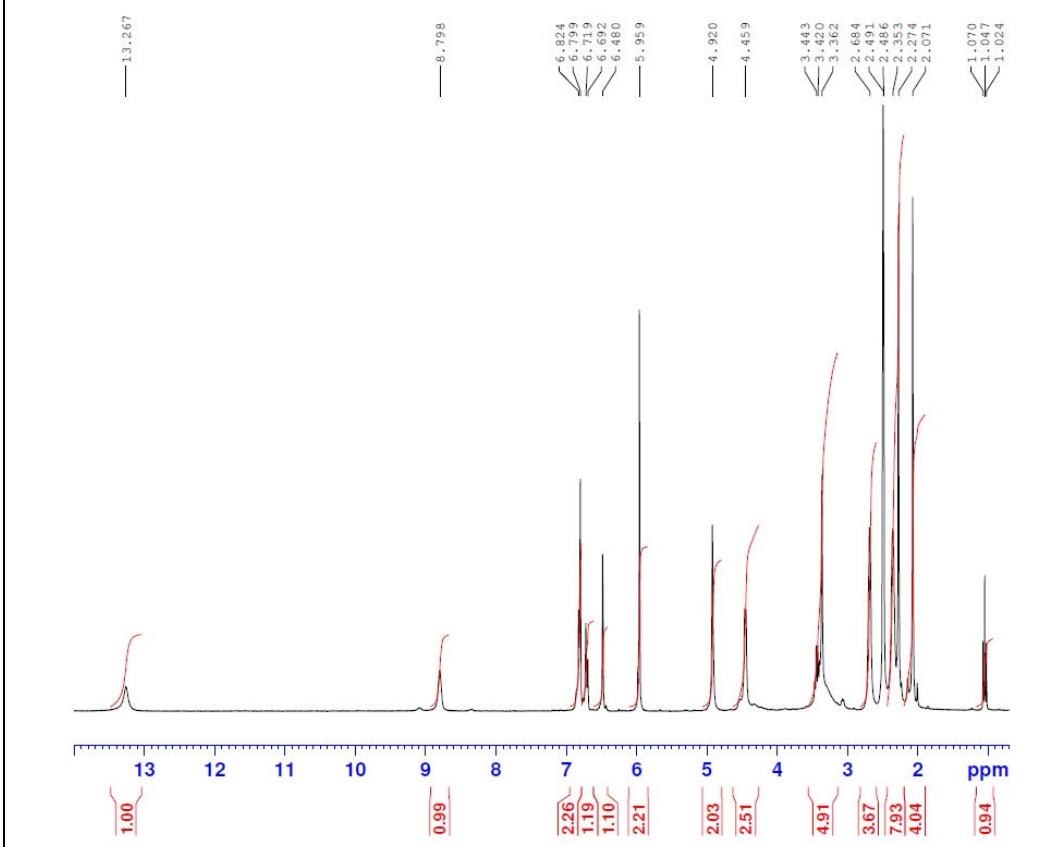
13.267
8.798
6.824
6.799
6.719
6.692
6.480
5.959
4.920
4.459
3.443
3.420
3.362
2.684
2.491
2.486
2.353
2.274
2.071
1.070
1.047
1.024
13 12 11 10 9 8 7 6 5 4 3 2 ppm
1.00
0.99
2.26
1.19
1.10
2.21
2.03
2.51
4.91
3.67
7.93
4.04
0.94

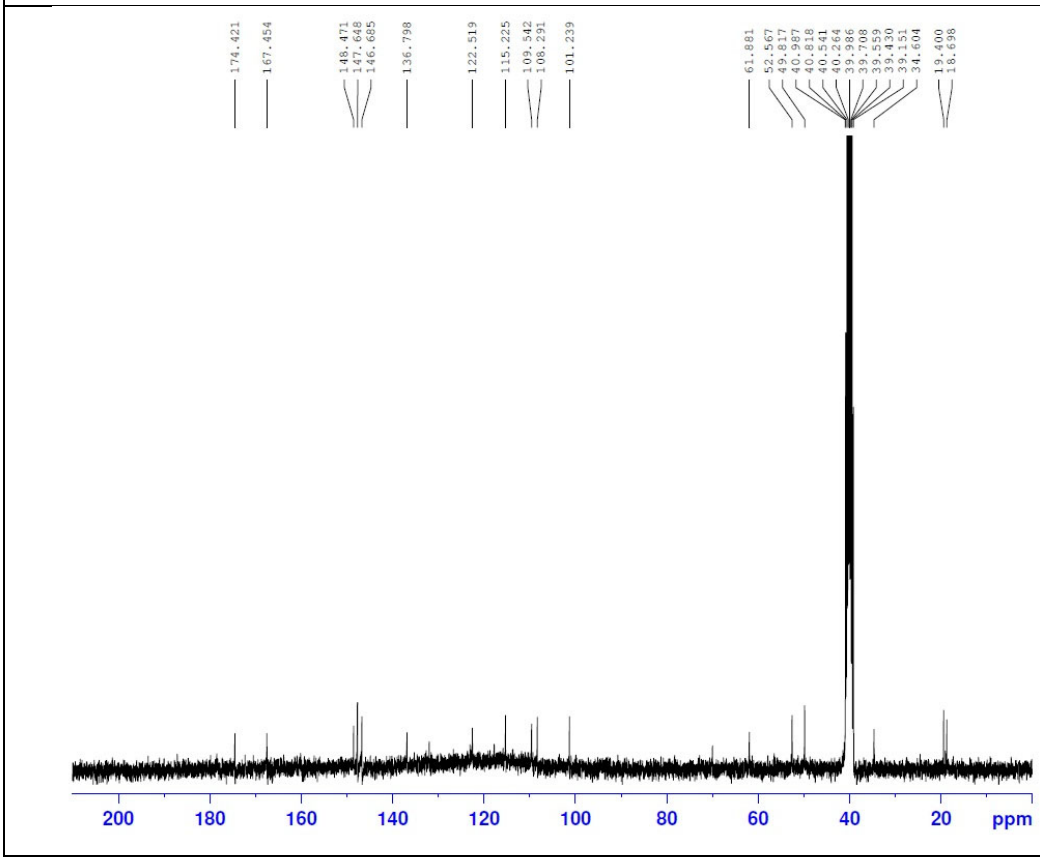
174.421
167.454
148.471
147.648
146.685
136.798
122.519
115.225
109.542
108.291
101.239
61.801
52.567
49.817
40.987
40.818
40.541
40.264
39.986
39.708
39.430
39.153
38.875
34.604
19.400
18.698
200 180 160 140 120 100 80 60 40 20 ppm

12

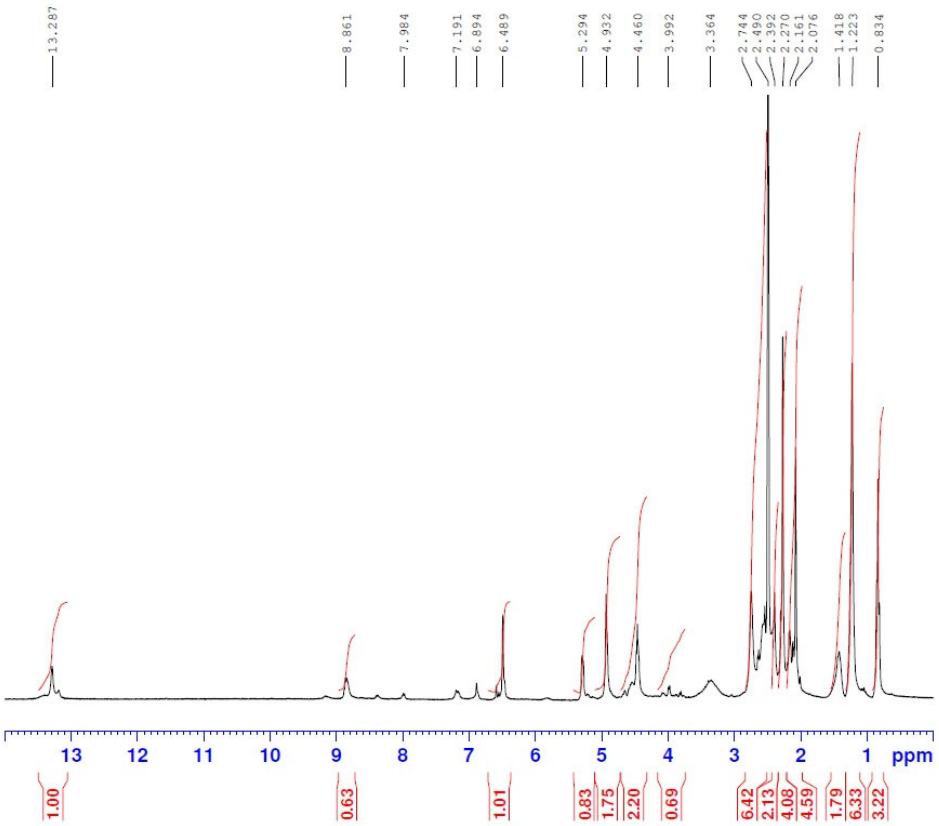
13.287
8.861
7.984
7.191
6.894
6.489
5.294
4.932
4.460
3.992
3.364
2.744
2.490
2.392
2.270
2.161
2.076
1.418
1.223
0.834
13 12 11 10 9 8 7 6 5 4 3 2 1 ppm
1.00
0.63
1.01
0.83
1.75
2.20
0.69
6.42
2.13
4.08
4.59
1.79
6.33
3.22

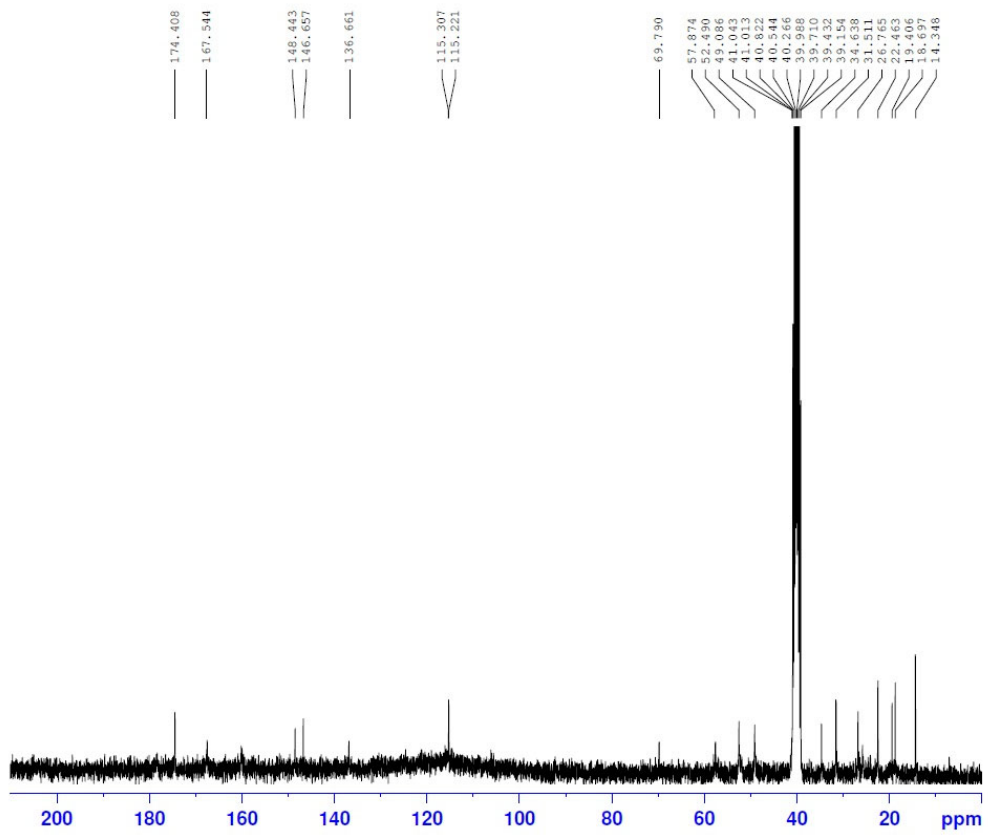
174.408
167.544
148.443
146.657
136.661
115.307
115.221
69.790
57.874
52.490
49.086
41.043
40.822
40.544
40.266
39.988
39.710
39.432
39.154
34.638
31.511
26.765
22.463
19.406
18.697
14.348
200 180 160 140 120 100 80 60 40 20 ppm

PUBLIKACJA P3

WRAZ Z MATERIAŁAMI UZUPEŁNIAJĄCYMI

ISSN 0045-2068

ELSEVIER

BIO-ORGANIC CHEMISTRY

MECHANISMS FOR BIOLOGY

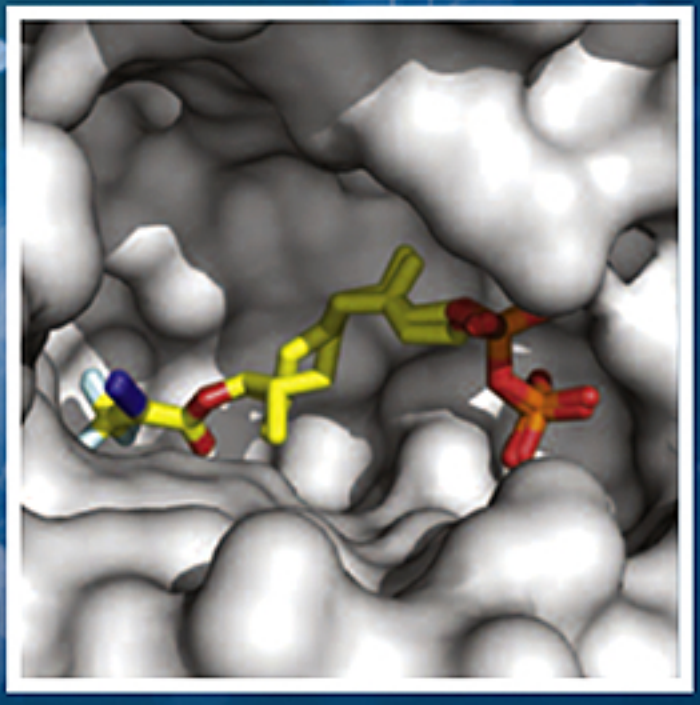

Available online at www.sciencedirect.com

ScienceDirect

Bioorganic Chemistry 139 (2023) 106758

Contents lists available at ScienceDirect

Bioorganic Chemistry

journal homepage: www.elsevier.com/locate/bioorg

New Schiff bases derived from dimethylpyridine-1,2,4-triazole hybrid as cytotoxic agents targeting gastrointestinal cancers: Design, synthesis, biological evaluation and molecular docking studies

Małgorzata Strzelecka [a,*], Benita Wiatrak [b], Paulina Jawień [c], Żaneta Czyżnikowska [d], Piotr Świątek [a,*]

[a] Department of Medicinal Chemistry, Faculty of Pharmacy, Wroclaw Medical University, Borowska 211, 50-556 Wroclaw, Poland
[b] Department of Pharmacology, Wroclaw Medical University, J. Mikulicza-Radeckiego 2, 50-345 Wroclaw, Poland
[c] Department of Biostructure and Animal Physiology, Wroclaw University of Environmental and Life Sciences, Norwida 25/27, 50-375 Wroclaw, Poland
[d] Department of Basic Chemical Sciences, Faculty of Pharmacy, Wroclaw Medical University, Borowska 211a, 50-556 Wroclaw, Poland

ARTICLE INFO

Keywords:
Dimethylpyridine
1,2,4-triazole
Schiff bases
Anticancer activity
P-glycoprotein inhibition
Apoptosis induction
Molecular docking

ABSTRACT

In this research, a series of novel hybrid structures of dimethylpyridine-1,2,4-triazole Schiff bases were designed, synthesized, and evaluated for their *in vitro* cytotoxic potency on several human gastrointestinal cancer cells (EPG, Caco-2, LoVo, LoVo/Dx, HT29) and normal colonic epithelial cells (CCD 841 CoN). Schiff base **4h** was the most potent compound against gastric EPG cancer cells (CC_{50} = 12.10 ± 3.10 μM), being 9- and 21-fold more cytotoxic than 5-FU and cisplatin, respectively. Moreover, it was not toxic to normal cells. Regarding the cytotoxicity against colorectal cancer cells, compounds **4d** and **4l** exhibited good activity against HT29 cells (CC_{50} = 52.80 ± 2.80 μM and 61.40 ± 10.70 μM, respectively), and were comparable to or more potent than cisplatin and 5-FU. Also, they were less toxic to normal cells with a higher selectivity index (SI, CCD 841 CoN/HT29 = 4.20 and 2.85, respectively) than reference drugs (SI, CCD 841 CoN/HT29 < 1). Selected Schiff bases were subjected to the P-glycoprotein inhibition assay. Schiff bases **4d**, **4e**, and **4l** influenced P-gp efflux function, significantly increasing the accumulation of rhodamine 123 in colon cancer cell lines. Further mechanistic studies showed that compound **4l** induced apoptotic cell death through a caspase-dependent mechanism and by regulating the p53-MDM2 signaling pathway in HT29 cells. Also, physicochemical predictions of compounds **4d**, **4e**, **4h**, and **4i** were examined *in silico*. The results revealed that the compounds possessed promising drug-likeness profiles.

1. Introduction

Cancer is one of the leading causes of mortality and exerts a major health problem globally. It was estimated that 19.3 million new cases of cancer and almost 10.0 million cancer-related deaths were reported in 2020 [1]. Of all types of tumors, gastrointestinal cancers represent an important percentage, and their incidence is expected to increase more rapidly than other types of tumors due to unhealthy lifestyles and dietary habits [2,3]. According to global statistics, colorectal cancer and gastric cancer are in the top most frequently diagnosed tumors worldwide, and are the second and fourth leading causes of death among cancer patients, respectively [4]. The majority of patients newly diagnosed with gastrointestinal cancer are aged 65 and over. However, there is an increasing burden and worse outcome of digestive cancer in young adults, who represent the main proportion of contributors to the economy and their family care [3]. The continual increase in cancer cases as well as the resistance of cancer cells to the existing drugs have driven the search for novel anticancer drugs with better potency, selectivity, and low toxicity.

1,2,4-Triazole derivatives have gained broad attention due to their diverse biological activities such as antifungal [5–7], antibacterial [8–10], antiviral [11,12], antiparasitic [13,14], analgesic and anti-inflammatory [15–17] as well as anticonvulsant [18–20]. Moreover, numerous 1,2,4-triazoles have been specially designed to target specific pathways involved in cancer pathogenesis [21–27]. Letrozole, anastrozole, and vorozole (Fig. 1A) are 1,2,4-triazole-based drugs clinically

* Corresponding authors.
E-mail addresses: malgorzata.strzelecka@umw.edu.pl (M. Strzelecka), piotr.swiatek@umw.edu.pl (P. Świątek).

https://doi.org/10.1016/j.bioorg.2023.106758
Received 19 June 2023; Received in revised form 13 July 2023; Accepted 29 July 2023
Available online 31 July 2023
0045-2068/© 2023 The Authors. Published by Elsevier Inc. This is an open access article under the CC BY license (http://creativecommons.org/licenses/by/4.0/).

used as first-line therapies for the treatment of breast cancer in postmenopausal women. It is worth mentioning that several research groups reported the anticancer activity of 4-(arylidene-amino)-4*H*-1,2,4-triazole-3-thione/thiol derivatives (Fig. 1B). The indolyl-triazole Schiff base **I** exhibited potent cytotoxic activity against human breast adenocarcinoma (MCF-7) cells through apoptosis activation and VEGFR2 inhibition [28]. The triazole-piperazine hybrid **II** showed an excellent anticancer effect in both *in vitro* and *in vivo* models by triggering the mitochondrial pathway of apoptosis in the human osteosarcoma cell line (Cal72) [29]. Investigation on Schiff bases bearing a 3,4,5-trimethoxyphenyl ring and 1,2,4-triazole-3-thiol provided a potent anticancer agent **III**, which exhibited better cytotoxic activity against colon adenocarcinoma cell line (HT29) compared to reference drug doxorubicin, and it was able to strongly inhibit tubulin polymerization [30]. Schiff base derivative **IV** based on the naproxen scaffold showed remarkable antitumor activity, especially against colon cancer cell lines (HCT-116 and Caco-2) when compared to doxorubicin [31]. Furthermore, *in vitro* COX-1/COX-2 inhibition assay showed that this compound exhibited effective COX-2 inhibition.

In our recently published works, we demonstrated that 4,6-dimethyl-2-sulfanylpyridine derivatives (Fig. 1C) containing differently substituted 1,3,4-oxadiazole moiety (series A and B) exhibited potent anticancer activity against various cancer cell lines [32,33]. In particular, *N*-acylhydrazone derivatives (series A), in which an arylidene amino group can be found, displayed significant cytotoxicity against colon cancer cell line (LoVo) with the inhibitory concentrations (IC_{50}) in the range of 6.33–9.63 μM.

Guided by the aforementioned data regarding the wide spectrum of medicinal applications, especially anticancer properties of various arylidene derivatives of 4-amino-1,2,4-triazole, and as a continuation of our research interests in the scope of synthesis and biological evaluation of novel, potential anticancer molecules, we designed the new compounds as a hybrid structure of dimethylpyridine core with Schiff bases derived from the 4-amino-1,2,4-triazole-3-thiole moiety (Fig. 1D). The molecular hybridization of biologically active molecules is one of a powerful tool for drug discovery and appeared as a novel strategy to identify potential drug molecules against various diseases, including cancer [34–36]. Synthesized derivatives have been evaluated for their potential cytotoxicity against a panel of gastrointestinal cancer cells: gastric cancer (EPG) and four colorectal cancers (Caco-2, HT29, LoVo, and its drug-resistant subline LoVo/Dx,). The cytotoxic effects of tested compounds on non-cancerous cells were evaluated using normal colonic

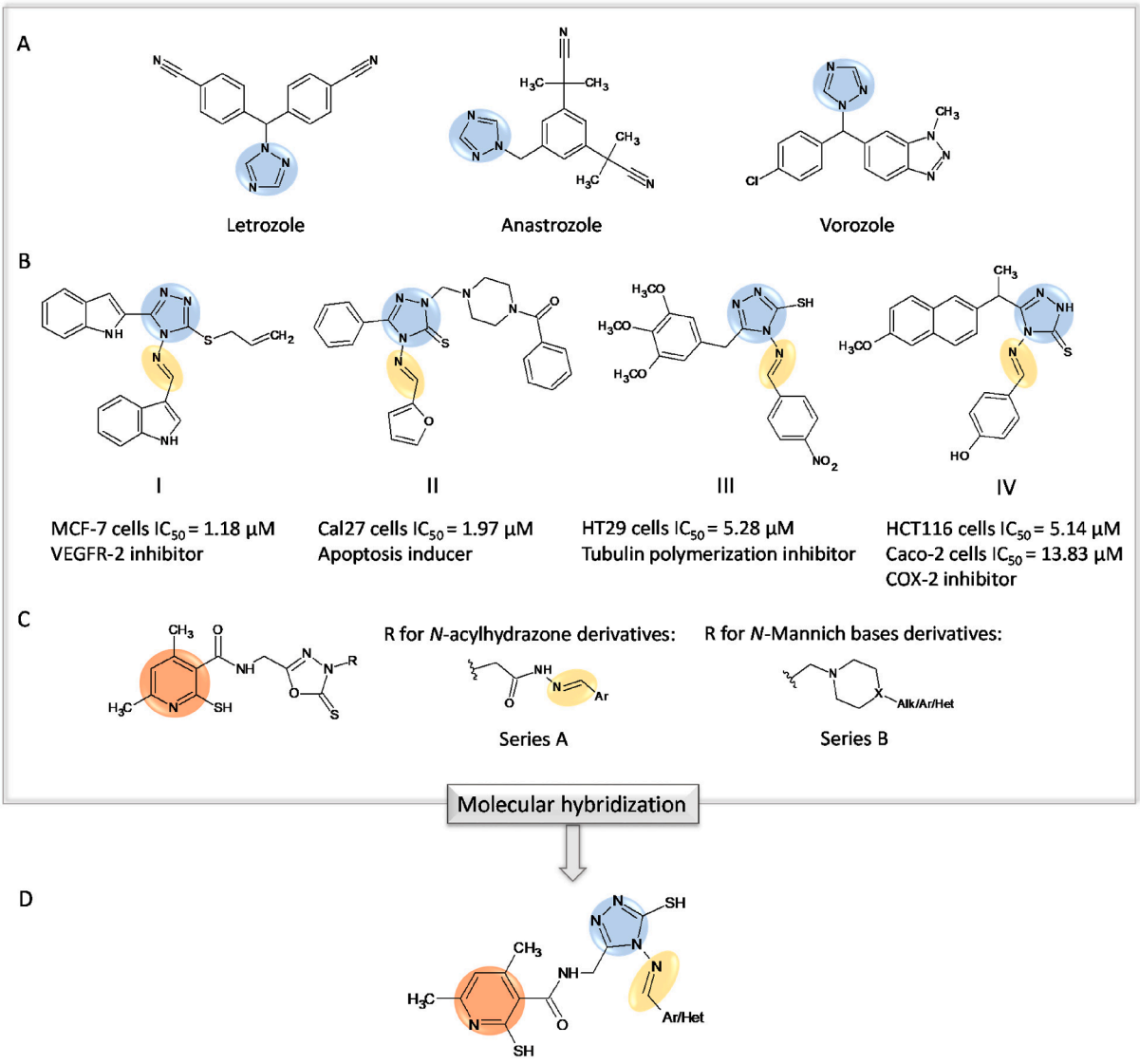

Fig. 1. (A) 1,2,4-triazole-based anticancer drugs; (B) Selected arylidene amino-1,2,4-triazole derivatives as anticancer agents with identified molecular mechanisms of action; (C) Structure of our previously reported compounds with anticancer activity; (D) Design strategy of dimethylpyridine-based target compounds.

epithelial cells (CCD 841 CoN). The most active compounds were selected for further studies concerning their mechanism of action.

2. Results and discussion

2.1. Chemistry

The synthetic route leading to the formation of the target derivatives is outlined in Scheme 1. The structures of compounds **3** and **4a-n** were confirmed by FTIR, ^{1}H NMR, ^{13}C NMR, and HRMS, and all the analytical data were documented in the Supplementary data. The starting material *N*-(2-hydrazinyl-2-oxoethyl)-4,6-dimethyl-2-sulfanylpyridine-3-carboxamide (**1**) was prepared according to the protocol published previously [37]. The key intermediate in the present study, 4,6-dimethyl-*N*-[(4-amino-5-sulfanyl-4*H*-1,2,4-triazol-3-yl)methyl]-2-sulfanylpyridine-3-carboxamide (**3**) was synthesized in two steps employing salt formation and cyclization. Firstly, the reaction of acid hydrazide **1** with carbon disulfide in an ethanolic solution of potassium hydroxide at room temperature yielded potassium dithiocarbazate salt (**2**). Subsequently, the treatment of compound **2** with hydrazine hydrate in refluxing ethanol afforded the corresponding 1,2,4-triazole derivative **3**. The FTIR spectrum of **3** demonstrated broad bands at approximately 3475 cm^{-1} and 3190 cm^{-1} corresponding to NH_2 and NH groups, respectively, and other bands at the range of 1647–1573 cm^{-1} indicating the presence of C═O, C═N, and C═C fragments. An absorption band at 2770 cm^{-1} which corresponds to the SH groups from the 1,2,4-triazole core may suggest that in solid state compound **3** exist as triazole thiol form. When considering the ^{1}H NMR spectrum of compound **3**, a singlet signal integrating two protons was recorded at δ 5.68 ppm, which confirmed the presence of the NH_2 group (for the primary amine of the 1,2,4-triazole ring), additionally, a triplet signal was found at δ 8.60 ppm integrating one proton, corresponding to the NH from the amide fragment. The signals referred to SH protons from the pyridine and triazole rings resonated at 13.31 ppm and 13.56 ppm, respectively.

The synthesis of the title Schiff bases **4a-n** was carried out by the reaction of compound **3** with various aromatic and heteroaromatic aldehydes in the presence of a catalytic amount of glacial acetic acid in refluxing ethanol. In the FTIR spectra, characteristic bands are visible: for the NH group in the range of 3100–3210 cm^{-1}, for aromatic rings in the range of 3014–3058 cm^{-1}, and C═N, C═O and C═C fragments in the range of 1543–1644 cm^{-1}. The disappearance of a broad band at 3475 cm^{-1} ascribed to the NH_2 group from the 1,2,4-triazole ring of compound **3** confirms the formation of Schiff bases. It is known that compounds having arylidene amino structure may exist as E/Z geometrical isomers about CH = N double bond [38]. According to the literature [38,39], the compounds containing imine bonds are present in higher percentages in deuterated dimethyl sulfoxide (DMSO-d_6) solution in the form of geometrical E isomer about CH = N double bond. In the present study, based on the spectral data obtained in the DMSO-d_6 solution, it can be assumed that the observed signals belong to E isomers. The ^{1}H NMR and ^{13}C NMR spectra of compounds **4a-n** displayed the presence of the distinctive signals in the regions of 9.45–10.72 ppm and 152.16–162.34 ppm, respectively, which are identified with the protons and carbon atoms of azomethine group, while the signal of NH_2 of the 4-amino-1,2,4-triazole disappeared. In the ^{1}H NMR spectrum, aromatic protons of Schiff bases were observed at 6.75–8.32 ppm (the presence of the characteristic pattern of *para*-substituted aromatic rings was detected). Also, the increase in the resonance peak numbers of the aromatic ring carbons in the ^{13}C NMR spectrum confirmed the condensation. Further, the signals of the protons of the SH groups appeared in the 13.21–14.00 ppm region. Mass spectral analysis was carried out and the molecular ion peaks (M + 1) were found to be in correlation with the corresponding calculated molecular mass, confirming the structure of synthesized molecules. Additionally, the obtained data supported the formation of 1,2,4-triazole-Schiff base derivatives with $[M + Na]^+$ and $[M + K]^+$ ion peaks.

2.2. Biological evaluation

2.2.1. In vitro cytotoxicity

In the present study, previously prepared hydrazide **1**, the newly synthesized 4-amino-1,2,4-triazole-3-thiol derivative **3,** and its Schiff bases **4a-n** were evaluated for their possible anti-proliferative efficacy against five human cancer cell lines: gastric (EPG) and colorectal (Caco-2, HT29, LoVo, LoVo/Dx), and one normal cell line (human colonic epithelial cells CCD 841 CoN) using the 3-(4,5-dimethylthiazol-2-yl)-2,5-diphenyl-2*H*-tetrazolium bromide (MTT) colorimetric assay. Cisplatin and 5-fluorouracil (5-FU) were used as positive controls. The results were expressed as the cytotoxic concentration (CC_{50} ± SD) that causes a 50% reduction in viable cells (Table 1).

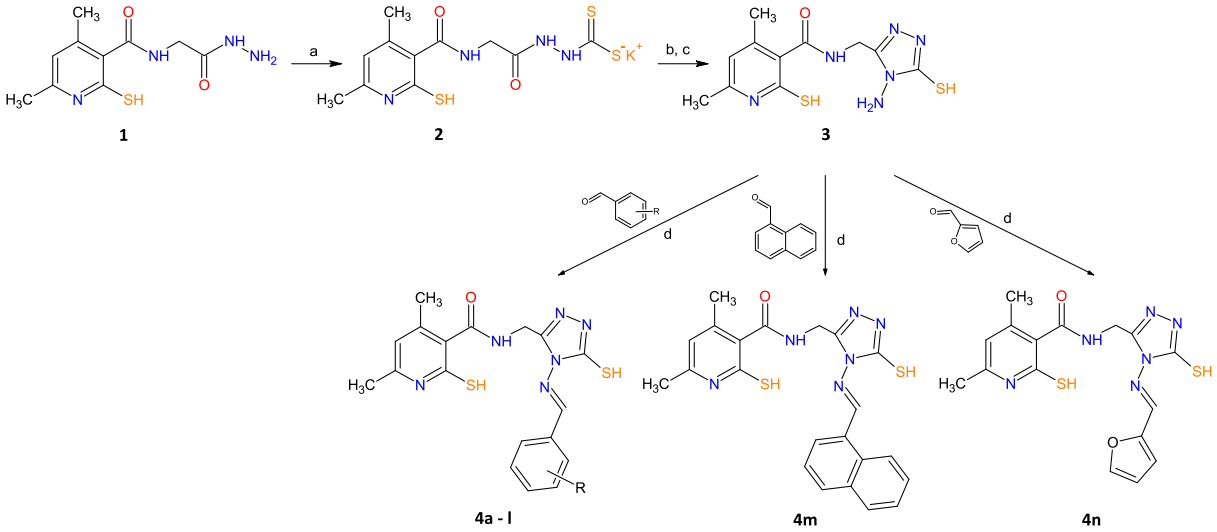

4a: R = H, **4b**: R = 2-OC_2H_5, **4c**: R = 4-CH_3, **4d**: R = 4-CF_3,
4e: R = 4-F, **4f**: R = 3-Cl, **4g**: R = 4-NO_2, **4h**: R = 4-OCH_3,
4i: R = 2-OH, **4j**: R = 3-OH, **4k**: R = 4-$N(CH_3)_2$, **4l**: R = 4-$N(C_2H_5)_2$

Scheme 1. General procedure for preparation of target compounds **4a-n**. Reagents and conditions: (a) CS_2, KOH, EtOH/stirring/5h; (b) hydrazine hydrate, EtOH/reflux/7h; (c) HCl; (d) EtOH/reflux/4h.

Table 1
Cytotoxic activities of compounds 1, 3, and 4a-n and reference drugs against the selected cell lines evaluated in the MTT assay, and presented as the cytotoxic concentration (CC_{50} ± SD) that causes a 50% reduction in viable cells. SD is the standard deviation. SI is the selectivity index, which is the ratio of the cytotoxic concentration (CC_{50}) against healthy cells (CCD 841 CoN) to the cytotoxic concentration against cancer cells.

Comp.	CCD 841 CoN	EPG		Caco-2		LoVo		LoVo/Dx		HT29	
	CC_{50} ± SD[a] (μM)	CC_{50} ± SD[a] (μM)	SI	CC_{50} ± SD[a] (μM)	SI	CC_{50} ± SD[a] (μM)	SI	CC_{50} ± SD[a] (μM)	SI	CC_{50} ± SD[a] (μM)	SI
1	Non-toxic[b]	483,70 ± 9,10	≫1[c]	189,10 ± 3,90	≫1[c]	203,80 ± 4,90	≫1[c]	518,00 ± 5,2	≫1[c]	502,30 ± 2,9	≫1[c]
3	438,20 ± 4,70	156,30 ± 3,50	2.80	165,90 ± 2,70	2.64	211,40 ± 5,10	2.07	286,40 ± 7,3	1.53	261,90 ± 3,4	1.67
4a	643,00 ± 5,40	147,80 ± 7,20	4.35	129,90 ± 5,20	4.95	171,50 ± 7,10	3.75	389,50 ± 1,8	1.65	356,70 ± 7,8	1.80
4b	425,50 ± 6,20	98,80 ± 4,70	4.31	107,30 ± 7,20	3.97	122,50 ± 2,90	3.47	273,30 ± 2,4	1.56	247,70 ± 8,1	1.72
4c	168,00 ± 1,80	93,10 ± 4,30	1.80	125,10 ± 3,70	1.34	115,40 ± 3,30	1.45	102,70 ± 3,7	1.63	95,30 ± 6,7	1.76
4d	221,7 ± 3,40	46,2 ± 4,70	4.80	70,30 ± 5,6	3.15	124,40 ± 6,1	1.78	159,6 ± 4,1	1.39	52,8 ± 2,8	4.20
4e	377,80 ± 3,50	62,50 ± 6,70	6.04	84,60 ± 4,00	4.46	108,10 ± 5,80	3.49	313,60 ± 2,8	1.20	85,30 ± 6,9	4.43
4f	452,70 ± 2,90	99,00 ± 3,80	4.57	85,20 ± 7,40	5.31	126,90 ± 3,80	3.57	216,30 ± 9,1	2.09	193,00 ± 5,3	2.34
4g	451,50 ± 3,40	129,00 ± 4,10	3.50	145,30 ± 8,20	3.11	223,10 ± 9,00	2.02	316,40 ± 10,7	1.43	298,70 ± 4,2	1.51
4h	Non-toxic[b]	12,10 ± 3,10	≫1[c]	118,00 ± 9,10	≫1[c]	264,40 ± 10,10	≫1[c]	374,90 ± 1,7	≫1[c]	361,40 ± 2,5	≫1
4i	427,60 ± 4,20	109,10 ± 5,20	3.92	127,70 ± 7,40	3.35	203,30 ± 5,70	2.10	279,70 ± 2,7	1.53	255,80 ± 6,8	1.67
4j	368,60 ± 6,70	78,60 ± 6,70	4.69	97,00 ± 1,90	3.80	254,10 ± 2,80	1.45	118,20 ± 3,4	3.12	99,00 ± 4,3	3.72
4k	619,40 ± 8,10	136,70 ± 3,80	4.53	122,10 ± 3,70	5.07	142,80 ± 3,40	4.34	233,00 ± 3,4	2.66	201,60 ± 1,9	3.07
4l	175,10 ± 9,00	58,30 ± 4,10	3.00	146,60 ± 3,10	1.19	162,10 ± 3,70	1.08	131,80 ± 9,7	1.33	61,40 ± 10,7	2.85
4m	492,10 ± 3,70	92,80 ± 7,30	5.30	133,40 ± 4,40	3.69	212,20 ± 1,70	2.32	135,50 ± 6,4	3.63	116,80 ± 5,1	4.21
4n	218,70 ± 7,40	186,40 ± 7,20	1.17	130,00 ± 4,80	1.68	160,40 ± 4,70	1.36	218,50 ± 4,9	1.00	204,90 ± 4,9	1.07
Cisplatin	14,50 ± 2,90	261,50 ± 4,60	0.05	136,40 ± 5,00	0.11	27,40 ± 2,70	0.53	47,80 ± 6,1	0.30	52,80 ± 7,1	0.27
5-FU	61,62 ± 3,70	111,20 ± 3,50	0.55	169,60 ± 3,70	0.36	72,20 ± 1,80	0.85	225,70 ± 2,7	0.27	428,50 ± 2,7	0.14

[a] CC_{50} values were estimated from a 4-parameter logistic model with a Hill slope. Six concentrations of the tested solutions were used (i.e. 1, 5, 10, 50, 150 and 500 μM); [b] No toxicity was observed in the tested concentration range of 1–500μ; [c] ≫ 1 means a very high value due to the lack of cytotoxic effect of the test compound on healthy CCD 841 CoN cells.

In general, it was found that EPG cells were the most sensitive to the synthesized compounds of all cancer cell lines, and Schiff bases **4b-f**, **4h**, **4j**, **4l**, and **4 m** exhibited higher activity against EPG with CC_{50} values ranging from 12.10 to 99.00 μM when compared to 5-FU and cisplatin (111.20 μM and 261.50 μM, respectively). It is noteworthy that the presence of an azomethine group with different substituted phenyl rings or naphthalene core within a series of Schiff bases (**4a-m**) was advantageous in cytotoxic activities against EPG in comparison to the parent compound **3**. Only for heteroaromatic derivative **4n**, the introduction of the furanyl methylidene group leads to a reduction in activity against the EPG cell line. Schiff base **4h** with a methoxy group at the para position of the phenyl ring displayed the highest cytotoxicity against EPG with the CC_{50} value of 12.1 μM.

Regarding activity against colon cancer cell lines, compounds **4d** and **4e** containing trifluoromethyl and fluorine groups at the para position of the phenyl ring, respectively, revealed the most significant anticancer activities against both Caco-2 (CC_{50} = 70.3 μM and 84.6 μM, respectively) and HT29 (CC_{50} = 52.8 μM and 85.3 μM, respectively), and were more potent or comparable to the reference drugs. In addition, Schiff base **4l** with 4-diethylaminophenyl moiety showed good activity against HT29 (CC_{50} = 61.4 μM) but was much less active against Caco-2 (CC_{50} = 146.6 μM). Also, compounds **4c** and **4j** with 4-methyl- and 3-hydroxyphenyl moieties, respectively, exhibited good inhibition of HT29 cell viability (CC_{50} values 95.3 and 99.00 μM, respectively). Moreover, compounds **4j** and also **4f** with the 3-chlorophenyl group had good inhibitory effects on Caco-2 cells (CC_{50} values 85.2 and 97.00 μM, respectively). The other tested compounds exhibited moderate to weak cytotoxic activities against Caco-2 and HT29 cell lines. Cytotoxicity evaluation against LoVo and LoVo/Dx discovered that these cancer cells were the most insensitive among the tested cancer cell lines. Indeed, none of the tested compounds turned out to be more potent than the cisplatin, and only six compounds **4c**, **4d**, **4j**, and **4l-n** exhibited higher activity than 5-FU against LoVo/Dx subline, but still 2- to 3-times lower than cisplatin. Interestingly, compounds **4c**, **4j**, **4l**, and **4 m** break through the multidrug-resistance of LoVo/Dx cells (CC_{50} values against LoVo/Dx vs LoVo: 102.7 μM vs 115.4 μM, 118.2 μM vs 254.1 μM, 131.8 μM vs 162.1 μM, 135.5 μM vs 212.2 μM, respectively), which may suggest their possible anticancer potential against drug-resistant cancer cells.

Further evaluation of the cytotoxic effect on normal non-cancerous cell line (CCD 841 CoN) was performed to predict their safety and selectivity. Results showed a promising safety profile of test compounds to normal cells with CC_{50} values in the range of 168.0 to 643.0 μM when compared to cisplatin and 5-FU (CC_{50} = 14.5 μM and 61.61 μM, respectively). Moreover, compounds **1** and **4h** were non-toxic to normal CCD 841 CoN cells. Additionally, the selectivity index (SI) was calculated as the ratio of CC_{50} of the tested compounds on the normal cell line vs CC_{50} of the same compounds on cancerous cells. None of the compounds had SI value inferior to 1, and what is more, for compounds **4f**, **4k** and **4m** there was found SI value superior to 2 on all the tested cell lines which suggested that those compounds exhibited selectivity against cancer cell lines.

2.2.2. *Structure-activity relationship*

Based on the results of anti-cancer studies, it was possible to establish some structure–activity relationships (SAR), which are graphically presented in Fig. 2. The obtained results showed that among the tested compounds, the hydrazide derivative **1** displayed the lowest antitumor activity against cancer cell lines, except for LoVo cells. This reveals the importance of cyclization of the starting hydrazide into the corresponding 1,2,4-triazole ring among dimethylpyridine derivatives in improving anticancer potential. The substituent of the phenyl ring in the series of benzylidene Schiff bases, depending on the position of the substituent and electron-receiving/donating and steric characteristics, had a diverse impact on the ability to inhibit cancer cell viability. In general, the *para*-fluorinated derivatives (**4d** and **4e**) showed the most potent cytotoxic activity against selected cell lines which might be because of the electron-receiving ability of halogens. On the other hand, substitution with strong electronegative nitro moiety at the *para* position of the phenyl ring (**4g**) leads to a reduction in activity which could be due to the polar nature of this group. *Para*-methyl substitution (**4c**) displayed good activity against all the tested cancer cells, especially for LoVo and LoVo/Dx cell lines. Substitution on the hydroxyl group at the *meta* position of the phenyl ring (**4j**) exhibited satisfactory cytotoxic activity whereas its substitution at the *ortho* position (**4i**) significantly reduced the effect of its analog against EPG, CaCo-2, LoVo/Dx, and HT29 cell lines, suggesting that hydroxyl group is favored at *o*-position. Also, in the case of *para*-dialkylamino substituted Schiff bases, the presence of bulky diethylamino group (**4l**) increased anticancer activity against EPG, LoVo/Dx, and HT29 cells when compared with

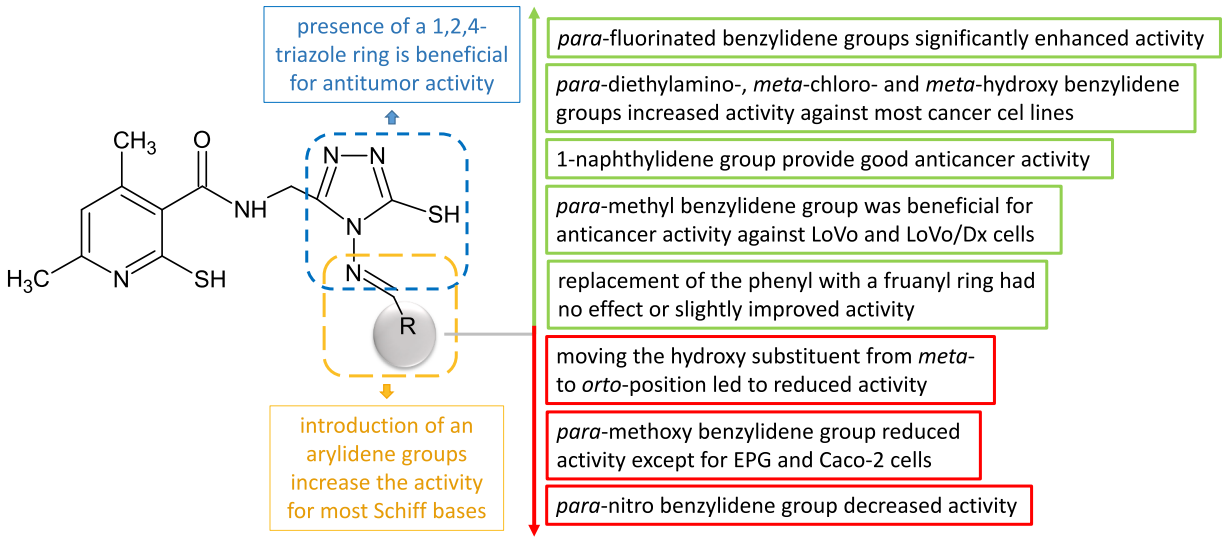

Fig. 2. Summarized SAR of the novel compounds.

dimethylamino derivative (**4k**). Regarding the Schiff bases with ether groups, the presence of a *para*-methoxy substituent at the phenyl ring (**4h**) provided excellent to moderate activity against EPG and Caco-2 cell lines while it was one of the least active Schiff bases against other cancer cells. On the other hand, an *ortho*-ethoxy substituent in compound **4b** exerted good growth inhibition potency toward most cancer cell lines. Finally, replacing the phenyl (**4a**) with a furanyl ring (**4n**) did not improve or slightly improved the activity, while the introduction of a larger group, namely 1-naphthyl moiety (**4m**) markedly increased activity against EPG, LoVo/Dx, and HT29 cell lines.

2.2.3. The P-glycoprotein inhibition potential

P-glycoprotein (P-gp) is a member of the ATP-binding cassette (ABC) superfamily, which transports various molecules across cellular membranes to reduce their accumulation in cells [40]. Although ABC transporters have important physiologic functions, clinical insensitivity to a wide range of different chemotherapeutic agents, attributed to an elevated expression of P-gp, may be associated with lower remission and lower survival rates in cancer patients [41]. This contributes to the development of multidrug resistance (MDR) and represents a major cause of cancer treatment failure. Moreover, it has been reported that P-gp plays a role in cancer cells MDR not only by participating in the efflux of intracellular cytotoxic agents but also by inhibiting tumor necrosis factor-related apoptosis-inducing ligand (TRAIL)-mediated [42] and caspase-related [43,44] pathways of apoptosis. In order to identify putative MDR inhibitors among the selected compounds (**4d**, **4e**, and **4l**), that exhibited the most promising anti-colon cancer activity, an assay based on the measurement of intracellular accumulation of rhodamine 123 (a fluorescent P-gp substrate analog) in P-gp-expressing cell lines (HT29, LoVo, and LoVo/Dx) was applied. The fluorescence of rhodamine 123 (Rh-123), after an accumulation and efflux period was quantified by spectrofluorimetry and the results are depicted in Fig. 3. Verapamil was used as a positive control for P-gp inhibition [45].

As shown in Fig. 3a, the untreated LoVo/Dx cells poorly accumulated Rh-123 when compared to the sensitive parental LoVo cells as well as HT29 cell line, thus reflecting the difference in fluorescent dye efflux depending on the level of P-gp expression. The presence of the reference P-gp inhibitor, verapamil, significantly increased the intracellular fluorescence in LoVo/Dx cells, while its potency on two other colon cancer cell lines was almost unnoticeable. Both HT29 and sensitive LoVo cells express P-gp, but at a considerably lower level than LoVo/Dx cells, thus the P-gp inhibition effect was much more pronounced in LoVo/Dx cell line. For selected Schiff bases, all compounds were found to increase Rh-123 accumulation in all of the tested cell lines, and LoVo cells showed the highest intracellular fluorescence intensity. In Fig. 3b, the results have been normalized to control untreated cells and expressed as E/E0 (E - mean fluorescence intensity of the appropriate compound, and E0 - control). The highest accumulation of Rh-123 occurred after incubation of the LoVo/Dx cells with compounds in the order: **4l** > **4d** > **4e**, with E/E0 values = 5.1, 4.7, and 3.6, respectively. However, their potency in increasing Rh-123 accumulation in LoVo/Dx cells was lower than that of the reference verapamil, measured in the same cellular model. It is noteworthy that in the case of sensitive colon cancer cell lines (HT29 and LoVo), the intracellular fluorescence intensity of Rh-123 after treatment with the tested Schiff bases increased 1.83- to even 3.9-fold, and was higher than verapamil, measured in the same cellular model. These differences in results may be related to the fact that Rh-123 is also a substrate of other multidrug resistance-associated proteins [44]. These findings urge the need for additional studies.

2.2.4. Apoptosis analysis

Since apoptosis is a process of programmed cell death, it has a critical

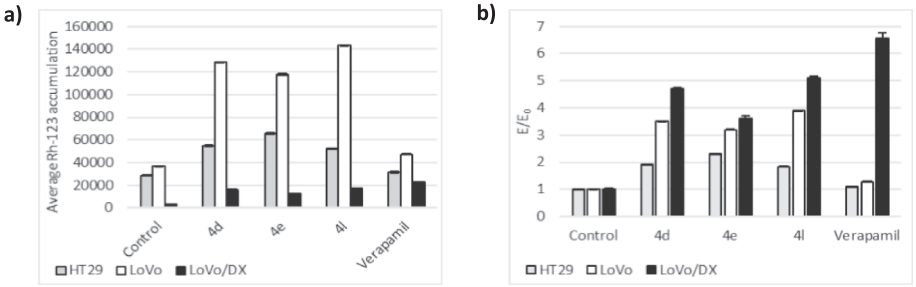

Fig. 3. Influence of compounds **4d**, **4e**, and **4l** on rhodamine 123 accumulation in HT29, LoVo, and LoVo/Dx cancer cells. The mean fluorescence intensity of accumulated Rh-123 dye (a), expressed as a fluorescence arbitrary unit, of untreated or treated HT29, LoVo, and LoVo/Dx cells populations is presented as well as E/E_0 values (b) which means the results normalized to control untreated cells (E is the result for the measured sample, and E_0 is the result for the control). Verapamil was used as a positive control.

effect on tissue homeostasis [46]. It is distinguished from death by necrosis by the absence of an associated inflammatory response [47]. Apoptosis is regarded as a defense mechanism against cancer proliferation, and many anticancer drugs are designed to induce tumor cell apoptosis [48].

Annexin–V/Propidium iodide staining assay was performed to evaluate the apoptosis-inducing effect of compounds **4d**, **4e**, and **4l** on HT29 cells to find a plausible reason for their cytotoxic activity. Doxorubicin was used as a positive control. The obtained results (Fig. 4) revealed that all tested compounds exhibited pro-apoptotic activity at a concentration of 1 μM, although it was weaker compared to doxorubicin. The percent of apoptotic cells increased from 6.73% in untreated control cells to 36.73%, 41.95%, and 50.60% in cells treated with compounds **4e**, **4d**, and **4l**, respectively. This means an almost 5.5- to 7.5-fold increase in apoptotic cells compared to the control. In parallel, an increase in necrotic cell percentage from 2.40 (control cells) to 6.70% (**4e**), 10.40% (**4d**), and 11.70% (**4l**) was noticed. These encouraged outcomes have promoted us to further investigate the effect of the best apoptotic agent – compound **4l** on variant apoptotic markers.

2.2.5. *Impact of **4l** on apoptotic markers - p53 protein and caspase-3*

The effect of compound **4l** on p53 protein and caspase-3 levels were investigated in the HT29 cell with the use of appropriate human enzyme-linked immunosorbent assay (ELISA) kits. The p53 protein, also known as a tumor suppressor, is a transcription factor that prevents the outgrowth of aberrant cells by inducing cell cycle arrest, DNA repair, or programmed death. Loss of its normal function leads to a disruption of the mechanisms controlling cell proliferation and survival, which contributes to the development of neoplasms [49]. The activation or stabilization of p53 helps the cancer cell normalize p53-controlled physiological processes and enhances apoptotic function [50,51]. The effect of compound **4l** on the p53 protein level was assessed and compared with the reference doxorubicin (Table 2). The results revealed a 2.48-fold increase in the concentration of p53 when compared with untreated control cells, however, it was lower than for doxorubicin (4.23-fold increase in p53 concentration).

On the other hand, the sequential activation of proteolytic caspases is considered as one of the important keys in the cellular apoptosis process. Stimulation of caspase-3 by both intrinsic (mitochondria-mediated) and extrinsic (cell death receptor-mediated) cellular pathways activates the endonuclease leading to the degradation of chromosomal DNA, chromatin condensation, and disintegration of the cell into apoptotic bodies [52–54]. Considering the important role of caspase-3 in the apoptotic process, we evaluated the effects of compound **4l** on the level of this protein in HT29 cells. The results showed that the tested compound afforded a marked increase in caspase-3 level (20.67-fold) compared to the control cells, however, this effect was lower compared to doxorubicin (30.67-fold increase in the level of caspase-3). According to the obtained results, it can be safely concluded that compound **4l** may cause apoptosis *via* a p53 pathway and caspase-dependent mechanism.

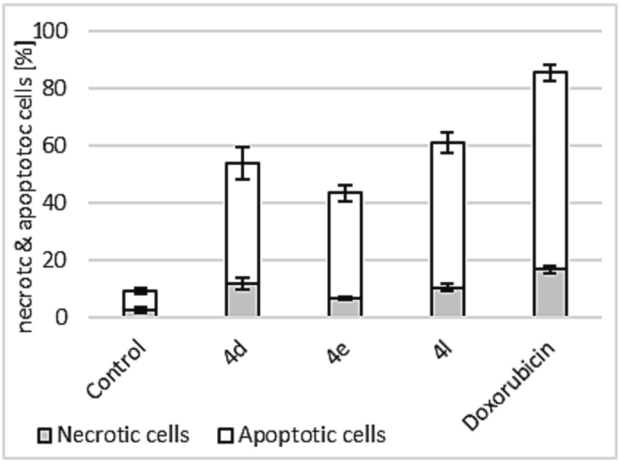

Fig. 4. Effect of compounds **4d**, **4e**, and **4l** on the level of apoptotic and necrotic HT29 cells after 24 h of incubation. Doxorubicin was used as reference drug.

Table 2
Effects of compound **4l** and doxorubicin on the levels of p53 and caspase-3 proteins in HT29 cell line.

Comp. [1 μM]	HT29 cell line			
	p53		caspase-3	
	Conc. ± SD [U/ml]	Fold change	Conc. ± SD [ng/ml]	Fold change
Control	1,80 ± 0,06	1	0,03 ± 0,08	1
4l	4,46 ± 0,11	2.48	0,62 ± 0,11	20.67
Doxorubicin	7,62 ± 0,17	4.23	0,92 ± 0,23	30.67

2.2.6. *Effect of **4l** on IL-6 level*

Interleukin-6 (IL-6) is a pro-inflammatory cytokine that has an important role in cancer progression and therapeutic resistance through inhibition of cancer cell apoptosis and stimulation of tumour-promoting factors such as proliferation, angiogenesis, etc. [55,56]. An increased expression of IL-6 has been detected and associated with an unfavourable prognosis in patients with various types of cancer including both sporadic and colitis-associated colorectal cancer [57]. Therefore, inhibiting IL-6 signaling or minimizing the level of IL-6 can be a potential therapeutic strategy for those cancers which are characterized by overproduction of IL-6 [58,59].

In this study, the effect of compound **4l** on the level of IL-6 was determined using ELISA assay. The quantity of IL-6 in untreated and compound **4l**-treated HT29 cells was assessed. As shown in Table 3, compound **4l** slightly decreased IL-6 protein level.

2.3. *Molecular docking studies*

2.3.1. *Docking study inside caspase-3 protein binding active site*

Our experimental data obtained from the caspase-3 activation assay showed that compound **4l** induces apoptosis through caspase-3 in HT29 cell lines. Therefore, we try to obtain the possibility of its binding to the active site of caspase-3. Based on the previous studies we choose to our investigation crystal structure of caspase-3 taken from Protein Data Bank (PDBID:1RE1) [60]. The validation of re-docking procedure was performed by docking of nicotinic acid aldehyde into the protein and comparison of its position with the crystal. We also calculated the root mean square deviation (RMSD) on the LigRMSD web server (RMSD = 0.79 Å) [61]. According to molecular docking **4l** can bind in the same place as the reference compound and makes similar contacts in this positively charged site (Fig. 5a). As presented in Fig. 5b the interactions with positively charged and polar amino acid residues Arg179, Arg341 and Gln283 were identified. Additionally, the interactions with crucial catalytic Cys285 and Gly238 via hydrogen bonds are possible. Next π-sulfur and π-stacking interactions with His237 and Tyr388 are formed. The approximate value of free energy of binding in this case is hardly equal −6 kcal/mol. These experimental data suggest a worthy explanation for the pro-apoptotic activity of compound **4l** as a caspase-3

Table 3
Effects of compound **4l** on the level of interleukin-6 in HT29 cell line.

Comp. [1 μM]	HT29 cell line
	IL-6 Conc. ± SD [pg/ml]
Control	9,30 ± 0,20
4l	8,10 ± 0,34

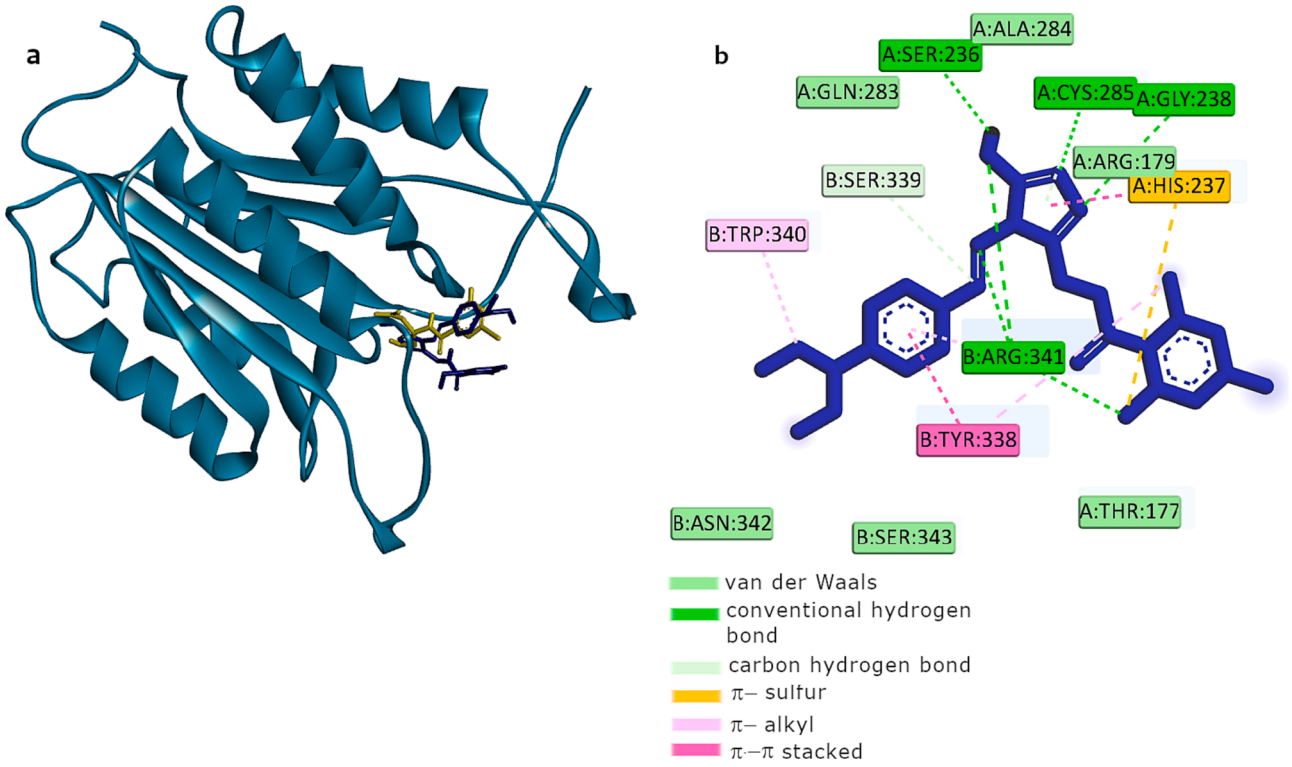

Fig. 5. a) Docking pose of **4l** (navy blue) and nicotinic acid aldehyde inhibitor (yellow) in the active centre of caspase-3b) intermolecular interactions of **4l** with caspase-3. (For interpretation of the references to colour in this figure legend, the reader is referred to the web version of this article.)

activator and are in accordance with the literature [54].

2.3.2. Docking study inside MDM2 protein binding active site

It is commonly known that the p53 pathways is inactivated due to the overexpression of main endogenous factor protein MDM2. This negative protein regulator binds to the p53 directly and inhibits of p53 transcriptional activity and enhancement of p53 degradation via the ubiquitin–proteasome pathway. Pavletich et al. established that hydrophobic pockets of MDM2 are responsible for interactions with three keys amino acids of p53. Pocket surrounding of Leu26 is defined by Val53, Tyr100 and Thr101 amino acids of MDM2. The Trp23 residue of p53 interacts with Leu54, Gly58, Tyr60, Phe91, Ser92 and Val93 of MDM2. Finally, Phe19 is localized in close proximity of Met62, Arg65, Tyr67, Glu69, His73, Ile74, Val75, and Val93 of MDM2 [62]. It is also

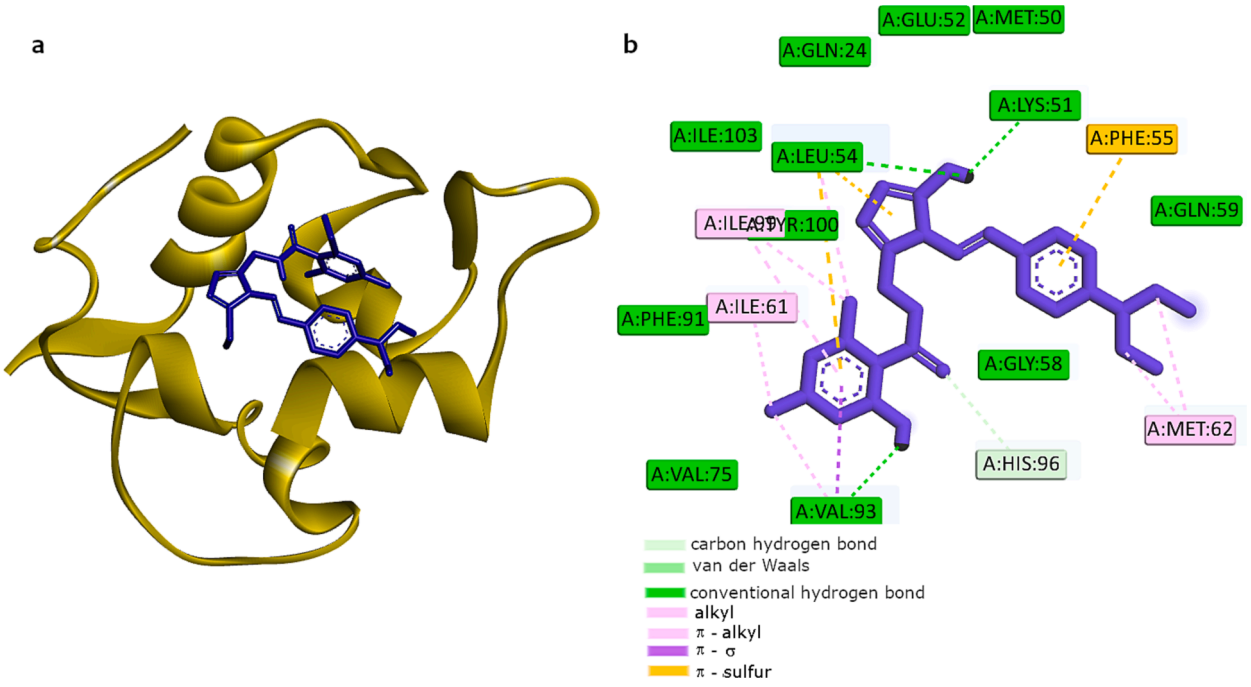

Fig. 6. a) docking pose of **4l** in the active centre of MDM2 b) intermolecular interactions of **4l** with MDM-2 protein.

recognized that MDM2 inhibitors induce apoptosis and p53 upregulation but not p53 phosphorylation. Our experimental data obtained from the p53 activation assay showed that compound **4l** increased the level of p53 protein in HT29 cell lines. Therefore, we decided to determine the ability of **4l** to bind to MDM2. The structural data of the protein were taken from Protein Data Bank (PDB ID:3JZK) [63]. The root-mean-square deviation between the predicted and the native poses of co-crystalized ligand chromenotriazolopyrimidine, small potent inhibitor of MDM2 protein were found to be 0.64 Å. As can be observed in Fig. 6a, compound **4l** partially penetrate binding site of Phe19 and interacts with Met62, Val75 and Val93. Additionally, it makes the interactions with Leu54, Gly58, Phe91 and Val93 in the Trp23 of p53 binding domain. Finally, is also surrounded by amino acids responsible for Leu26 binding such as Glu52, Leu54 and Tyr100. As presented in Fig. 6b the main stabilizing factors are van der Waals interactions. Beside three hydrogen bonds are also possible.

2.4. *In-silico prediction of physicochemical and drug-likeness properties*

It should be remembered that pre-clinical and clinical trials are time-consuming and responsible for most of the cost of drug development. Therefore, drug-likeness of compounds should be determined as early as possible in the design process. Recently, *in silico* ADMET predictors based on empirical and computational approaches have become useful and very popular tools. It should be noted that currently available methods do not fully replace experimental studies, however, they allow to determine the most promising candidates [64,65]. It is widely known that simple physicochemical properties of molecules such as molecular weight (MW), the number of hydrogen bond donors (nHD) and acceptors (nHA), hydrophobicity and polarity of compounds can affect their *in vivo* behavior and influence their efficiency to molecular target. According to data obtained from many predictive models molecular weight and topological surface area influence very important processes such membrane diffusion, blood-barrier penetration or elimination from the organism [66,67]. Another important factors is the octanol/water partition coefficient. High lipophilic compounds can be trapped into bilayer due to the poor penetration of membranes. On the other hand, low lipophilicity decreased of permeability [68]. We analyzed properties of four compounds (**4d**, **4e**, **4h**, and **4l**) and presented them in Table 4. As can be seen all compounds meet criteria of Lipinski rule.

The side effects of drugs are often related to their interactions with cytochrome P450 (CYP). We analyzed the affinity to five isoforms of CYP which are responsible for metabolism of>80% of clinically used drugs [69]. Data collected in Table 5 indicate that all compounds exhibit inhibitory activity towards CYP2C19. All of them are characterized by low blood–brain barrier permeability and low gastrointestinal absorption. The interaction of drugs with the membrane P-glycoprotein (P-gp) is quite important factor affecting the absorption process and their transport out of the cells. According to the results our compounds exhibit probability of inhibition of P-gp protein, which is consistent with *in vitro* studies. All data were obtained *in silico* using SwissADME tool and based on comprehensive database ADMETlab [70,71].

3. Conclusion

Exploration of novel hybrid structures of dimethylpyridine-1,2,4-triazole Schiff bases was undergone. These compounds were designed and synthesized through efficient synthetic routes, and their structures were confirmed using NMR, FTIR, and HRMS. All synthesized compounds as well as their hydrazide precursor were assessed by MTT assay for their *in vitro* cytotoxic activity on a panel of gastrointestinal cancer cells: gastric cancer (EPG) and colorectal cancers (Caco-2, HT29, LoVo, LoVo/Dx,). Some of the Schiff bases exhibited good to significant inhibition of cancer cell viability compared to 5-FU and cisplatin. Compound **4h** showed remarkable cytotoxic activity against EPG cells (CC_{50} = 12.10 ± 3.10 μM) while **4d**, **4e**, and **4l** were the most active against HT29 cell line (CC_{50} = 52.8 ± 2.8 μM, 85.3 ± 6.9 μM, 61.40 ± 10.7 μM, respectively). Besides, all of the tested compounds exhibited a promising safety profile when evaluated against normal colonic epithelial cells (CCD 841 CoN) compared to reference drugs. The elucidation of SAR revealed that fluorinated electron-withdrawing groups (-CF_3 and -F) contribute to the enhanced anticancer activity. Selected Schiff bases were subjected to further biological evaluations. Compounds **4d**, **4e**, and **4l** showed an inhibitory effect on P-glycoprotein activity, particularly in the drug-resistant LoVo/Dx cell subline. Moreover, they induced the apoptosis of HT29 cells in Annexin–V/Propidium iodide assay. According to ELISA assay analysis, compound **4l** was found to exert its considerable pro-apoptotic activity through a significant increase of the caspase-3 and p53 protein levels. Subsequent IL-6 level studies showed that Schiff base **4l** slightly decreased the concentration of this pro-inflammatory cytokine in HT29 cells. The results of *in silico* molecular docking studies proved a valuable binding affinity of compound **4l** to MDM2 protein, suggesting that the p53-MDM2 pathway may be involved in **4l**-induced apoptosis in HT29 cancer cells. Moreover, compound **4l** exhibited good fitting interactions inside the active site of caspase-3 protein, confirming a possible mode of action by activating caspase-3. Thus, from the present study, it can be concluded that compound **4l** can be regarded as a promising anti-colon cancer agent that may provide important leads for the design of potent P-glycoprotein inhibitors which exhibit also apoptosis-promoting properties.

4. Experimental

4.1. *Chemistry*

4.1.1. *General comments*

All solvents and chemical reagents were purchased from commercial suppliers (Chemat, Gdańsk, Poland; Alchem, Wrocław, Poland;) and were used without further purification. Dry solvents were received according to the standard procedures. Progress of the reactions was monitored by thin layer chromatography (TLC) on silica gel-coated aluminum sheets (Silica Gel 60 F_{254}). Spots on the TLC plates were visualized using an ultraviolet lamp. The melting points of all of the new compounds were determined on the Electrothermal Mel-Temp 1101D apparatus (Cole-Parmer, Vernon Hills, IL, USA) using the open capillary

Table 4
Physicochemical properties and medicinal chemistry of compounds **4d, 4e, 4h** and **4l**.

	Physicochemical properties									
Comp.	MW[a]	HBA[b]	HBD[c]	TPSA[d]	NROTB[e]	logP[f]	logS[g]	Fsp3[h]	Lipinski Rule	Abbott bioavailability score[i]
4d	466.50	8	1	162.7	7	2.6	−4.8	0.21	accepted	0.55
4e	416.50	6	1	162.7	6	1.9	−4.1	0.17	accepted	0.55
4 h	428.53	6	1	171.9	7	1.5	−4.0	0.21	accepted	0.55
4l	469.63	5	1	165.9	9	1.9	−4.6	0.32	accepted	0.55

[a] MW: molecular weight (optimal 100–600); [b] HBA: hydrogen bond acceptors (optimal 0–12); [c] HBD: hydrogen bond donors (optimal 0–7); [d] TPSA: topological polar surface area (optimal ⟨140); [e] NROTB: number of rotatable bonds (0–11); [f] LogP: Log of the octanol/water partition coefficient (optimal 0–3); [g] logS: solubility (insoluble < -10 < poorly < -6 < moderately < -4 < soluble < -2 < very < 0 highly); [h] Fsp3: number of sp3 hybridized carbons/total carbon count; [I] Abbott bioavailability score: probability of F > 10% in rat;

Table 5
Absorption and distribution of compounds **4d, 4e, 4h and 4l**.

Comp.	Parameter								
	Gastrointestinal absorption	P-gp substrate	P-gp inhibitor	CYP1A2 inhibitor	CYP2C19 inhibitor	CYP2C9 inhibitor	CYP2D6 inhibitor	CYP3A4 inhibitor	Blood-Brain Barrier Penetration
4d	low	no	yes	no	yes	yes	no	no	no
4e	low	no	yes	no	yes	no	no	no	no
4h	low	no	yes	no	yes	yes	no	no	no
4l	low	no	yes	no	yes	yes	no	no	no

method and were uncorrected. The ^{1}H NMR (300 MHz) and ^{13}C NMR (75 MHz) spectra were recorded on the Bruker 300 MHz NMR spectrometer (Bruker Analytische Messtechnik GmbH, Rheinstetten, Germany). The samples were dissolved in DMSO-d_6, and tetramethylsilane (TMS) was used as an internal reference. Chemical shifts (δ) were reported in ppm and multiplicities of NMR signals are designated as s (singlet), d (doublet), t (triplet), q (quartet), and m (multiplet, for unresolved lines). To record and read spectra, TopSpin 3.6.2. (Bruker Daltonik, GmbH, Bremen, Germany) program was used. The infrared (IR) spectra were determined on the Nicolet iS50 FT-IR Spectrometer (Thermo Fisher Scientific, Waltham, MA, USA). The samples were applied as solids and the frequencies were reported in cm^{-1}. Spectra were read by OMNIC Spectra 2.0 (Thermo Fisher Scientific, Waltham, MA, USA). Mass spectra (MS) were recorded using the Bruker Daltonics Compact ESI-Mass Spectrometer (Bruker Daltonik, GmbH, Bremen, Germany), operating in the positive ion mode. The analyzed compounds were dissolved in a methanol/isopropanol/water mixture. Aryl acid hydrazide 1 was prepared as previously described [37].

A patent application for the synthesis method and compounds application of **4d**, **4e** and **4h** described in this paper has been submitted [P.444904].

*4.1.2. Synthesis of compound **3***

General procedure for the synthesis of 4,6-dimethyl-*N*-[(4-amino-5-sulfanyl-4*H*-1,2,4-triazol-3-yl)methyl]- 2-sulfanylpyridine-3-carboxamide **3**.

Hydrazid **1** (0.005 mol) and potassium hydroxide (0.01 mol) were suspended in absolute ethanol (30 mL). Carbon disulfide (0,01 mol) was then added dropwise and the reaction mixture was stirred at room temperature for 5 h. The solid of potassium salt of aryl dithiocarbazinic acid **2** was filtered off, washed with diethyl ether and dried. Thus obtained (in quantitative yield) potassium salt **2** was used in the next step without further purification.

A mixture of the potassium dithiocarbazinate **2**, hydrazine hydrate (2 eq.) and ethanol (30 mL) was heated under reflux for 7 h. Hydrogen sulphide gas was evolved and a light green, homogenous solution was obtained. The reaction mixture was then cooled to room temperature and acidified with 3 M hydrochloric acid. The resulting precipitate was filtered, dried and recrystallized from aquenous ethanol 95%.

Pale yellow solid (55%); m.p.: 278–280 °C. **FT-IR** (selected lines, γ_{max}, cm^{-1}): 3480 (br, NH_2), 3189 (NH), 3034 (C—H ar.), 2930 (C—H aliph.), 2770 (SH), 1647 (C═O), 1618 (C═N), 1573 (C═C). **^{1}H NMR** (300 MHz, DMSO-d_6): δ = 2.08 (s, 3H, $CH_{3\text{-pyridine}}$), 2.27 (s, 3H, $CH_{3\text{-pyridine}}$), 4.41–4.42 (d, 2H, CH_2, J = 5.4 Hz), 5.68 (br s, 2H, NH_2), 6.50 (s, 1H, $H_{\text{-pyridine}}$), 8.60 (t, 1H, NH), 13.31 (s, 1H, SH), 13.56 (s, 1H, SH). **^{13}C NMR** (75 MHz, DMSO-d_6): δ = 18.70, 19.57, 34.00, 115.48, 137.06, 146.87, 148.41, 149.55, 166.04, 167.01, 173.85.

*4.1.3. General procedure for preparation of Schiff base type derivatives of 4,6-dimethyl-N-[(4-amino-5-sulfanyl-4H-1,2,4-triazol-3-yl)methyl)- 2-sulfanylpyridine-3-carboxamide **4a-n***

A mixture of 1,2,4-triazole **3** (0,01 mol), appropriate aromatic aldehydes (0,01 mol) and glacial acetic acid (1.5 mL) in the presence of absolute ethanol (25 mL) was stirred and refluxed for 4 h. Precipitated arylidene derivatives were filtered off, washed with ethanol, dried and recrystallized from aquenous ethanol 95% to get the target compounds **4a-n**.

4a 4,6-dimethyl-*N*-[(4-{(E)-[(phenyl)methylidene]amino}-5-sulfanyl-4*H*-1,2,4-triazol-3-yl)methyl)-2-sulfanylpyridine-3-carboxamide.

Pale Yellow solid (75%); m.p.: 280–282 °C. **FT-IR** (selected lines, γ_{max}, cm^{-1}): 3170 (NH), 3019 (C—H ar.), 2836 (C—H aliph.), 2702 (SH), 1615 (C═O), 1573 (C═C)**. ^{1}H NMR** (300 MHz, DMSO-d_6): δ = 1.97 (s, 3H, $CH_{3\text{-pyridine}}$), 2.24 (s, 3H, $CH_{3\text{-pyridine}}$), 4.50–4.51 (d, J = 5.4 Hz, 2H, CH_2), 6.43 (s, 1H, $H_{\text{-pyridine}}$), 7.50–7.60 (m, 3H, ArH), 7.92–7.94 (m, 2H, ArH), 8.63 (t, 1H, NH), 9.98 (s, 1H, N = CH), 13.22 (s, 1H, SH), 13.89 (s, 1H, SH). **^{13}C NMR** (75 MHz, DMSO-d_6): δ = 18.67, 19.43, 34.34, 115.29, 129.26 (2xC), 129.50 (2xC), 132.71, 133.17, 137.14, 146.69, 148.26, 148.90, 162.05, 163.80, 167.09, 174.50. **HR-MS** calculated for $C_{18}H_{18}N_6OS_2$ $[M + K]^+$ 437.0615, found: 437.0593.

4b 4,6-dimethyl-*N*-[(4-{(E)-[(2-ethoxyphenyl)methylidene]amino}-5-sulfanyl-4*H*-1,2,4-triazol-3-yl)methyl)-2-sulfanylpyridine-3-carboxamide.

Light yellow solid (65%); m.p.: 320 °C decomp. **FT-IR** (selected lines, γ_{max}, cm^{-1}): 3210 (NH), 3041 (C—H ar.), 2901 (C—H aliph.), 2759 (SH), 1635 (C═O), 1620 (C═N), 1573 (C═C), 1257 (Ar-O-CH_2). **^{1}H NMR** (300 MHz, DMSO-d_6): δ = 1.34 (t, J = 1.2 Hz, 3H, $CH_2\underline{CH_3}$), 1.97 (s, 3H, $CH_{3\text{-pyridine}}$), 2.24 (s, 3H, $CH_{3\text{-pyridine}}$), 4.12 (q, J = 6.9 Hz, 2H, $\underline{CH_2}CH_3$), 4.49–4.51 (d, J = 6 Hz, 2H, CH_2), 6.43 (s, 1H, $H_{\text{-pyridine}}$), 7.02–7.17 (m, 2H, ArH), 7.51–7.54 (m, 1H, ArH), 8.05 (d, J = 7.8 Hz, 1H, ArH), 8.61 (t, 1H, NH), 10.43 (s, 1H, N = CH), 13.22 (s, 1H, SH), 13.87 (s, 1H, SH). **^{13}C NMR** (75 MHz, DMSO-d_6): δ = 15.05, 18.66, 19.41, 34.34, 64.68, 113.74, 115.16, 121.10, 121.26, 127.22, 134.76, 137.07, 146.54, 148.22, 149.08, 158.42, 159.09, 162.00, 167.03, 174.57. **HR-MS** calculated for $C_{20}H_{22}N_6O_2S_2$ $[M + K]^+$ 481.0877, found: 481.0875.

4c 4,6-dimethyl-*N*-[(4-{(E)-[(4-methylphenyl)methylidene]amino}-5-sulfanyl-4*H*-1,2,4-triazol-3-yl)methyl)-2-sulfanylpyridine-3-carboxamide.

Light yellow solid (72%); m.p.:281–283 °C. **FT-IR** (selected lines, γ_{max}, cm^{-1}): 3101 (NH), 3043 (C—H ar.), 2920 (C—H aliph.), 2738 (SH), 1637 (C═O), 1599 (C═N), 1577 (C═C). **^{1}H NMR** (300 MHz, DMSO-d_6): δ = 1.97 (s, 3H, $CH_{3\text{-pyridine}}$), 2.24 (s, 3H, $CH_{3\text{-pyridine}}$), 2.38 (s, 3H, CH_3), 4.48–4.50 (d, J = 5.1 Hz, 2H, CH_2), 6.43 (s, 1H, $H_{\text{-pyridine}}$), 7.33 (d, J = 7.8 Hz, 2H, ArH), 7.80 (d, J = 7.5 Hz, 2H, ArH), 8.64 (t, J = 5.1 Hz, 1H, NH), 9.90 (s, 1H, N = CH), 13.22 (s, 1H, SH), 13.88 (s, 1H, SH). **^{13}C NMR** (75 MHz, DMSO-d_6): δ = 18.67, 19.45, 21.73, 34.27, 115.18, 129.27 (2xC), 129.97, 130.09 (2xC), 137.04, 143.37, 146.59, 148.24, 148.86, 162.13, 163.86, 167.04, 174.45. **HR-MS** calculated for $C_{19}H_{20}N_6OS_2$ $[M + Na]^+$ 435.1032, found: 435.1012.

4d 4,6-dimethyl-*N*-[(4-{(E)-[(4-trifluoromethylphenyl)methylidene]amino}-5-sulfanyl-4*H*-1,2,4-triazol-3-yl)methyl)-2-sulfanylpyridine-3-carboxamide.

Pale Yellow solid (60%); m.p.: 270–272 °C. **FT-IR** (selected lines, γ_{max}, cm^{-1}): 3187 (NH), 3041 (C—H ar.), 2850 (C—H aliph.), 2739 (SH), 1685 (C═O), 1618 (C═N), 1575 (C═C), 1322 (CF_3). **^{1}H NMR** (300 MHz, DMSO-d_6): δ = 1.96 (s, 3H, $CH_{3\text{-pyridine}}$), 2.24 (s, 3H, $CH_{3\text{-pyridine}}$), 4.52–4.54 (d, J = 5.1 Hz, 2H, CH_2), 6.43 (s, 1H, $H_{\text{-pyridine}}$), 7.87–8.18 (m, 4H, ArH), 8.67 (t, 1H, NH), 10.28 (s, 1H, N = CH), 13.22 (s, 1H, SH), 13.98 (s, 1H, SH). **^{13}C NMR** (75 MHz, DMSO-d_6): δ = 18.66, 19.41, 34.23, 114.69, 115.19, 118.67, 126.37, 129.77, 129.91, 133.34, 137.02, 137.08, 146.56, 148.28, 149.14, 160.49, 162.23, 167.05, 174.43. **HR-**

MS calculated for $C_{19}H_{17}F_3N_6OS_2$ [M + H]$^+$ 467.0930, found: 467.0919.

4e 4,6-dimethyl-*N*-[(4-{(E)-[(4-fluorophenyl)methylidene]amino}-5-sulfanyl-4*H*-1,2,4-triazol-3-yl)methyl)-2-sulfanylpyridine-3-carboxamide.

White solid (51%); m.p.: 262–265 °C. **FT-IR** (selected lines, γ_{max}, cm^{-1}): 3204 (NH), 3038 (C—H ar.)), 2834 (C—H aliph.), 2731 (SH), 1617 (C═O), 1600 (C═N), 1577 (C═C), 1186 (C-F). **^{1}H NMR** (300 MHz, DMSO-d_6): δ = 1.98 (s, 3H, $CH_{3\text{-pyridine}}$), 2.23 (s, 3H, $CH_{3\text{-pyridine}}$), 4.54 (d, J = 5.4 Hz, 2H, CH_2), 6.43 (s, 1H, $H_{\text{-pyridine}}$), 8.21 (d, J = 9.0 Hz, 2H, ArH), 8.32 (d, J = 9.0 Hz, 2H, ArH,), 8.66 (m, 1H, NH), 10.37 (s, 1H, N = CH), 13.25 (s, 1H, SH), 13.99 (s, 1H, SH). **^{13}C NMR** (75 MHz, DMSO-d_6): δ = 18.70, 19.57, 34.01, 115.48, 116.39, 116.68, 130.84, 130.88, 131.09, 131. 21, 137.05, 146.88, 148.41, 149.56, 160.86, 166.05, 167.01, 174.02. **HR-MS** calculated for $C_{18}H_{17}FN_6OS_2$ [M + K]$^+$ 455.0521, found: 455.0518.

4f 4,6-dimethyl-*N*-[(4-{(E)-[(3-chlorophenyl)methylidene]amino}-5-sulfanyl-4*H*-1,2,4-triazol-3-yl)methyl)-2-sulfanylpyridine-3-carboxamide.

Light yellow solid (57%); m.p.: 276–278 °C. **FT-IR** (selected lines, γ_{max}, cm^{-1}): 3170 (NH), 3021 (C—H ar.), 2889 (C—H aliph.), 2738 (SH), 1614 (C═O), 1575 (C═C), 687 (C-Cl). **^{1}H NMR** (300 MHz, DMSO-d_6): δ = 1.98 (s, 3H, $CH_{3\text{-pyridine}}$), 2.24 (s, 3H, $CH_{3\text{-pyridine}}$), 4.51–4.53 (d, J = 5.4 Hz, 2H, CH_2), 6.44 (s, 1H, $H_{\text{-pyridine}}$), 7.53–7.67 (m, 2H, ArH), 7.87–8.02 (m, 2H, ArH), 8.65 (m, 1H, NH), 10.08 (s, 1H, N = CH), 13.22 (s, 1H, SH), 13.94 (s, 1H, SH). **^{13}C NMR** (75 MHz, DMSO-d_6): δ = 18.67, 19.77, 34.60, 115.11, 128.19, 128.30, 131.53, 132.61, 134.35, 134.85, 137.09, 146.63, 148.37, 149.03, 161.64, 162.22, 167.03, 174.57. **HR-MS** calculated for $C_{18}H_{17}ClN_6OS_2$ [M + K]$^+$ 471.0225, found: 471.0207.

4g 4,6-dimethyl-*N*-[(4-{(E)-[(4-nitrophenyl)methylidene]amino}-5-sulfanyl-4*H*-1,2,4-triazol-3-yl)methyl)-2-sulfanylpyridine-3-carboxamide.

Yellow solid (46%); m.p.: 254–6 °C. **FT-IR** (selected lines, γ_{max}, cm^{-1}): 3590, 3174 (NH), 3056 (C—H ar.), 2932 (C—H aliph.), 2745 (SH), 1635 (C═O), 1576 (C═C), 1515 (NO_2), 1343 (NO_2). **^{1}H NMR** (300 MHz, DMSO-d_6): δ = 1.98 (s, 3H, $CH_{3\text{-pyridine}}$), 2.26 (s, 3H, $CH_{3\text{-pyridine}}$), 4.54 (d, J = 5.4 Hz, 2H, CH_2), 6.43 (s, 1H, $H_{\text{-pyridine}}$), 8.21 (d, J = 9.0 Hz, 2H, ArH,), 8.33 (d, J = 8.7 Hz, 2H, ArH,), 8.66 (t, J = 5.4 Hz, 1H, NH), 10.37 (s, 1H, N = CH), 13.22 (s, 1H, SH), 13.99 (s, 1H, SH). **^{13}C NMR** (75 MHz, DMSO-d_6): δ = 18.66, 19.43, 34.33, 115.20, 124.50 (2xC), 130.35 (2xC), 137.00, 138.76, 146.59, 148.29, 149.19, 149.90, 159.72, 162.25, 167.07, 174.57. **HR-MS** calculated for $C_{18}H_{17}N_7O_3S_2$ [M + K]$^+$ 482.0466, found: 482.0446.

4h 4,6-dimethyl-*N*-[(4-{(E)-[(4-methoxyphenyl)methylidene]amino}-5-sulfanyl-4*H*-1,2,4-triazol-3-yl)methyl)-2-sulfanylpyridine-3-carboxamide.

White solid (68%); m.p.: 278–280 °C. **FT-IR** (selected lines, γ_{max}, cm^{-1}): 3181 (NH), 3016 (C—H ar.), 2840 (C—H aliph.), 2732 (SH), 1617 (C═O), 1598 (C═N), 1574 (C═C). **^{1}H NMR** (300 MHz, DMSO-d_6): δ = 1.98 (s, 3H, $CH_{3\text{-pyridine}}$), 2.24 (s, 3H, $CH_{3\text{-pyridine}}$), 3.84 (s, 3H, OCH_3), 4.47 (d, J = 5.4 Hz, 2H, CH_2), 6.43 (s, 1H, $H_{\text{-pyridine}}$), 7.06 (d, J = 9.0 Hz, 2H, ArH), 7.86 (d, J = 9.0 Hz, 2H, ArH), 8.63 (t, 1H, NH), 9.76 (s, 1H, N = CH), 13.22 (s, 1H, SH), 13.84 (s, 1H, SH). **^{13}C NMR** (75 MHz, DMSO-d_6): δ = 18.67, 19.45, 34.33, 56.01, 114.50 (2xC), 115.19, 125.08, 131.25 (2xC), 137.04, 146.58, 148.24, 148.73, 162.11, 163.28, 164.05, 167.03, 174.45. **HR-MS** calculated for $C_{19}H_{20}N_6O_2S_2$ [M + K]$^+$ 467.0721, found: 467.0710.

4i 4,6-dimethyl-*N*-[(4-{(E)-[(2-hydroxyphenyl)methylidene]amino}-5-sulfanyl-4*H*-1,2,4-triazol-3-yl)methyl)-2-sulfanylpyridine-3-carboxamide.

White solid (58%); m.p.: 265–270 °C. **FT-IR** (selected lines, γ_{max}, cm^{-1}): 3163 (NH), 3014 (C—H ar.), 2828 (C—H aliph.), 2710 (SH), 1617 (C═O), 1571 (C═C). **^{1}H NMR** (300 MHz, DMSO-d_6): δ = 1.97 (s, 3H, $CH_{3\text{-pyridine}}$), 2.24 (s, 3H, $CH_{3\text{-pyridine}}$), 4.48 (d, J = 5.4 Hz 2H, CH_2), 6.43 (s, 1H, $H_{\text{-pyridine}}$), 6.91–7.02 (m, 2H, ArH), 7.40 (m, 1H, ArH), 7.92 (d, J = 7.8 Hz, 1H, ArH), 8.63 (t, 1H, NH), 10.16 (s, 1H, N = CH), 10.46 (s, 1H, OH), 13.23 (s, 1H, SH), 13.85 (s, 1H, SH). **^{13}C NMR** (75 MHz, DMSO-d_6): δ = 18.67, 19.41, 34.60, 115.18, 117.05, 118.87, 119.88, 128.00, 134.76, 137.05, 146.57, 148.23, 148.86, 158.95, 160.72, 162.07, 167.06, 174.83. **HR-MS** calculated for $C_{18}H_{18}N_6O_2S_2$ [M + K]$^+$ 453.0564, found: 453.0587.

4j 4,6-dimethyl-*N*-[(4-{(E)-[(3-hydroxyphenyl)methylidene]amino}-5-sulfanyl-4*H*-1,2,4-triazol-3-yl)methyl)-2-sulfanylpyridine-3-carboxamide.

White solid (77%); m.p.: 274–275 °C. **FT-IR** (selected lines, γ_{max}, cm^{-1}): 3320 (Ar-OH), 3135 (NH), 2870 (C—H aliph.), 2731 (SH), 1645 (C═O), 1623 (C═N), 1581 (C═C), 1230 (OH). **^{1}H NMR** (300 MHz, DMSO-d_6): δ = 1.98 (s, 3H, $CH_{3\text{-pyridine}}$), 2.23 (s, 3H, $CH_{3\text{-pyridine}}$), 4.4 (d, J = 4.8 Hz, 2H, CH_2), 6.43 (s, 1H, $H_{\text{-pyridine}}$), 6.96–6.99 (m, 1H, ArH), 7.31–7.36 (m, 3H, ArH), 8.63 (m, 1H, NH), 9.82 (s, 1H, N = CH), 9.83 (s, 1H, OH), 13.22 (s, 1H, SH), 13.87 (s, 1H, SH). **^{13}C NMR** (75 MHz, DMSO-d_6): δ = 18.66, 19.44, 34.26, 114.58, 115.20, 120.38, 120.89, 130.60, 133.81, 137.02, 146.62, 148.26, 148.88, 158.23, 162.12, 164.11, 167.08, 174.43. **ESI-MS** calculated for $C_{18}H_{18}N_6O_2S_2$ [M + H]$^+$ 453.0564, found: 453.0573.

4k 4,6-dimethyl-*N*-[(4-{(E)-[(4-dimethylaminophenyl)methylidene]amino}-5-sulfanyl-4*H*-1,2,4-triazol-3-yl)methyl)-2-sulfanylpyridine-3-carboxamide.

Orange solid (72%); m.p.: 276–278 °C. **FT-IR** (selected lines, γ_{max}, cm^{-1}): 3098 (C—H ar.), 2915 (C—H aliph.), 2738 (SH), 1637 (C═O), 1611 (C═N), 1584 (C═C). **^{1}H NMR** (300 MHz, DMSO-d_6): δ = 1.99 (s, 3H, $CH_{3\text{-pyridine}}$), 2.24 (s, 3H, $CH_{3\text{-pyridine}}$), 3.03 (s, 6H, $N(CH_3)_2$), 4.44 (d, J = 5.4 Hz, 2H, CH_2), 6.43 (s, 1H, $H_{\text{-pyridine}}$), 6.76 (d, J = 9.0 Hz, 2H, ArH), 7.69 (d, J = 8.7 Hz, 2H, ArH,), 8.60 (t, J = 5.4 Hz, 1H, NH), 9.45 (s, 1H, N = CH), 13.22 (s, 1H, SH), 13.74 (s, 1H, SH). **^{13}C NMR** (75 MHz, DMSO-d_6): δ = 18.67, 19.49, 34.27, 111.92 (2xC), 115.20, 119.20, 130.99 (2xC), 137.06, 146.63, 148.21, 148.57, 153.58, 162.11, 165.25, 167.01, 174.44. **HR-MS** calculated for $C_{20}H_{23}N_7OS_2$ [M + K]$^+$ 480.1037, found: 480.1024.

4l 4,6-dimethyl-*N*-[(4-{(E)-[(4-diethylaminophenyl)methylidene]amino}-5-sulfanyl-4*H*-1,2,4-triazol-3-yl)methyl)-2-sulfanylpyridine-3-carboxamide.

Yellow solid (53%); m.p.: 320–322 °C. **FT-IR** (selected lines, γ_{max}, cm^{-1}): 3094 (NH), 2971 (C—H ar.), 2929 (C—H aliph.), 2738 (SH), 1638 (C═O), 1610 (C═N), 1583 (C═C). **^{1}H NMR** (300 MHz, DMSO-d_6): δ = 1.04–1.14 (m, 6H, $2xCH_2\underline{CH_3}$), 2.00 (s, 3H, $CH_{3\text{-pyridine}}$), 2.24 (s, 3H, $CH_{3\text{-pyridine}}$), 3.38–3.43 (m, 4H, $2x\underline{CH_2}CH_3$), 4.43 (d, J = 5.4 Hz, 2H, CH_2), 6.44 (s, 1H, $H_{\text{-pyridine}}$), 6.72 (d, J = 9.0 Hz, 2H, ArH), 7.66 (d, J = 9.0 Hz, 2H, ArH,), 8.59 (t, 1H, NH), 9.37 (s, 1H, N = CH), 13.22 (s, 1H, SH), 13.72 (s, 1H, SH). **^{13}C NMR** (75 MHz, DMSO-d_6): δ = 12.83 (2xC), 18.66, 19.49, 34.60, 44.37 (2xC), 111.43 (2xC), 115.21, 118.43, 131.36 (2xC), 137.06, 146.62, 148.21, 148.53, 151.18, 162.34, 165.46, 167.28, 174.50. **HR-MS** calculated for $C_{22}H_{27}N_7OS_2$ [M + K]$^+$ 508.1350, found: 508.1377.

4m 4,6-dimethyl-*N*-[(4-{(*E*)-[(naphthalene-1-yl)methylidene]amino}-5-sulfanyl-4*H*-1,2,4-triazol-3-yl)methyl)-2-sulfanylpyridine-3-carboxamide.

Pale yellow solid (73%); m.p.: 318–322 °C. **FT-IR** (selected lines, γ_{max}, cm^{-1}): 3122 (NH), 3058 (C—H ar.), 2955 (C—H aliph.), 1644 (C═O), 1620 (C═N), 1583 (C═C). **^{1}H NMR** (300 MHz, DMSO-d_6): δ = 1.96 (s, 3H, $CH_{3\text{-pyridine}}$), 2.23 (s, 3H, $CH_{3\text{-pyridine}}$), 4.58 (d, J = 5.4 Hz, 2H, CH_2), 6.41 (s, 1H, $H_{\text{-pyridine}}$), 7.64–7.72 (m, 3H, ArH), 8.06 (d, J = 8.4 Hz, 1H, ArH), 8.18 (d, J = 8.4 Hz, 1H, ArH), 8.27 (d, J = 7.2 Hz, 1H, ArH), 8.58 (d, J = 8.4 Hz, 1H, ArH), 8.68 (t, 1H, NH), 10.72 (s, 1H, N = CH), 13.26 (s, 1H, SH), 14.00 (s, 1H, SH). **^{13}C NMR** (75 MHz, DMSO-d_6): δ = 18.66, 19.44, 34.37, 115.18, 124.09, 126.06, 127.07, 128.22, 128.51, 129.18, 129.44, 131.41, 133.46, 133.83, 137.03, 146.59, 148.25, 148.92, 162.09, 163.21, 167.11, 174.45. **HR-MS** calculated for $C_{22}H_{20}N_6OS_2$ [M + H]$^+$ 487.0772, found: 487.0760.

4n 4,6-dimethyl-N-[(4-{[(furan-2yl)methylidene]amino}-5-sulfanyl-4*H*-1,2,4-triazol-3-yl)methyl)- 2-sulfanylpyridine-3-carboxamide.

Pale brown solid (73%); m.p.: 291–294 °C. **FT-IR** (selected lines,

γ_{max}, cm^{-1}): 3181 (NH), 3052 (C—H ar.), 2844 (C—H aliph.), 2736 (SH), 1620 (C═O), 1574 (C═C). **^{1}H NMR** (300 MHz, DMSO-d_6): $\delta = 2.00$ (s, 3H, $CH_{3\text{-pyridine}}$), 2.24 (s, 3H, $CH_{3\text{-pyridine}}$), 4.40 (d, $J = 5.4$ Hz, 2H, CH_2), 6.44 (s, 1H, $H_{\text{-pyridine}}$), 6.76 (q, $J = 1.8$ Hz, 1H, ArH), 7.35 (m, 1H, ArH), 8.04 (m, 1H, ArH), 8.60 (t, 1H, NH), 9.81 (s, 1H, N = CH), 13.22 (s, 1H, SH), 13.88 (s, 1H, SH). **^{13}C NMR** (75 MHz, DMSO-d_6): $\delta = 18.67$, 19.36, 34.34, 113.45, 115.20, 120.35, 137.06, 146.66, 147.82, 148.26, 148.42, 148.82, 152.16, 162.34, 167.07, 174.83. **HR-MS** calculated for $C_{16}H_{16}N_6O_2S_2$ $[M + K]^+$ 427.0394, found: 427.0408.

4.2. Biological activity

4.2.1. Cell lines and conditions

The *in vitro* study was conducted using a panel of gastrointestinal cancer cells: human gastric cancer (EPG) and human colorectal cancers (Caco-2, LoVo, LoVo/Dx, and HT29). All human cancer cell lines were purchased from the European Collection of Authenticated Cell Cultures (ECACC). The cytotoxic effects of tested compounds on normal cells were evaluated using human normal colonic epithelial cells (CCD 841 CoN) obtained from the American Type Culture Collection (ATCC). All the studied cell lines were cultured in the recommended media. The HT29 cell line was grown in modified McCoy's 5a medium, the Caco-2 and CCD 841 CoN cell lines were incubated in Minimal Eagle medium (MEM), the LoVo and LoVo/Dx cell lines were grown in Dulbecco's modified Eagle medium/F-12 nutrient mix (DMEM/F −12). Gastric cancer (EPG) cells were cultured in RPMI-1640. All media were supplemented with 10% fetal bovine serum (FBS) and antibiotics (penicillin and streptomycin). All cell lines were incubated in a CO_2-incubator under 5% CO_2, 95% humidity conditions at 37 °C, with both morphology and confluence assessed twice a week. When the confluence was>70%, the cell lines were detached from the surface of the bottle with TrypLE solution and then used in the assays or reduced. Cells were collected into prepared tubes and centrifuged at 1000 × g at room temperature for 5 min. The supernatant was removed and fresh media appropriate for cell lines was added, then cells were counted using a Burker cell and resuspended to a cell density of 10,000 cells per well for MTT determination and detection of apoptotic and necrotic cell counts. In the rhodamine 123 accumulation assay, cells were seeded at a density of 30,000 cells per well. To assess p53 and caspase-3 proteins levels, and cytokine IL-6 level, cell lines were seeded at a density of 500,000 per well. After inoculation, the culture plates were left overnight in a CO_2-incubator to allow the cells to adhere to the surface of the wells. The supernatant was then removed and the tested compounds were added for 24 h, followed by bioassays.

4.2.2. Tested compounds

All newly synthesized compounds were dissolved in DMSO. Verapamil was dissolved in methanol. Doxorubicin was prepared in deionized water, 5-fluorouracil and cisplatin were dissolved in physiological saline. All compounds were solvents up to a concentration of 10 mM. Cytostatic drugs and new compounds were prepared at concentrations from 1 to 500 μM in media recommended for the cell line prepared for the biological assay.

4.2.3. Viability assay

All the synthetized compounds and cytostatic drugs (5-fluorouracil and cisplatine) were evaluated in MTT assay. After 24 h of incubation with tested compounds the supernatant were removed from the culture on the 96-well plates. The 1 mg/ml MTT solution was added for 2 h in 5% CO_2, 95 % humidity at 37 °C. The supernatant was then removed. The violet crystal was dissolved in isopropanol for 30 min by shaking. The absorbance was measured at 570 nm.

4.2.4. Rh-123 assay

To estimate the glycoprotein-P activity the Rh-123 assay was performed. The assay was carried out on HT29, LoVo and LoVo/Dx cells for compounds **4d**, **4e**, and **4l**. Verapamil was used as a positive control. The solution of Rh-123 at a concentration of 10 mM in a 1:1 DMSO-water mixture was prepared. Solutions of tested compounds (50 μM) in nutrient broth (without FBS) were added to the wells of culture plate at a volume of 100 μl/well. The plates were incubated with tested compounds for 24 h. Then, Rh-123 was added to the wells to a final concentration of 12.5 μM and incubated for 60 min. After incubation, the supernatant was removed and the cells were dissolved (150 μl/well) in 20 mM Tris-HCl pH 7.7 containing 0.2% sodium dodecyl sulfate (SDS). The fluorescence was measured in ex. 485 nm/em538 nm by using a microplate reader.

4.2.5. Detection of apoptosis

The HT29 cells were grown in 96-well plates for 24 h. The detection of apoptosis was carried out for compounds **4d**, **4e**, and **4l**, and doxorubicin in concentrations of 1 μM. The Annexin-V conjugated with fluorescein and propidium iodide in PBS with Mg^{2+} and Ca^{2+} ions (Thermo Fisher Scientific, Waltham, MA, USA) was applied after 24 h incubation cells with tested compounds. So that all cells (live and dead) could be counted, 10 μM Hoechst was added to stain the cell nuclei. The incubation lasted 20 min at 37 °C. Pictures were taken using a fluorescence microscope. Images were taken from each well using an EVOS FL fluorescence microscope in three replication for each compound. The open ImageJ space was used to analyze the number of cells.

4.2.6. Preparation of cell lysates for human caspase 3 (active) ELISA Kit (KHO1091) and p53 human ELISA Kit (BMS256)

The HT29 lysate treated with compound **4l** was used to evaluate caspase-3 protein levels. HT29 cells were harvested by centrifugation (non-adherent cells) and scraping from the culture flasks (adherent cells), and then the cells were washed twice with cold PBS. The supernatant was removed and discarded, and the cell pellet was collected. The cell pellet was then lysed in a cell extraction vessel for 30 min on ice and centrifuged every 10 min. The lysate was transferred to microfuge tubes and centrifuged at 13,000 rpm for 10 min at 4 °C. The supernatant was transferred to clean microfuge tubes.

Lysate for evaluating of level of p53 protein was prepared with HT29 cells after treatment with compound **4l**. The cells were washed 2 times with approximately 400 μl of washing buffer per well. The washing buffer was left in the wells for approximately 15 s prior to aspiration. Care was taken not to scratch the surface of the microwells. After the final rinsing step, the wells were emptied. An absorbent swab was used to remove excess Wash Buffer. Standard dilutions were applied to the microwell plate.

The following kits: Human Caspase 3 (active) ELISA Kit (KHO1091), p53 Human ELISA Kit (BMS256), were used according to the manufacturer's instructions.

4.2.7. Cytokine (IL-6) levels

Cytokine (IL-6) level was assessed for cells treated with compound **4l** on HT29 cells. IL-6 level was measured in the supernatant according to the instructions of the manufacturer of the ELISA kits. The level of IL-6 (Abcam) was done according to the manufacturer's instructions.

4.2.8. Statistical analysis

All results are presented as the mean ± SD (standard deviation) relative to the respective control (E/E_0), where E is the mean of result for the measured sample, and E_0 is the mean of result for control. The control was the cell culture incubated only with the appropriate medium without the tested compounds or control drugs. The statistical evaluation was performed using the Statistica v13.3 and GraphPad PRISM software. All graphs were prepared in Microsoft Excel. The data had a normal distribution and equality of variance, so a one-way ANOVA with post-hoc Tukey's was conducted. The point of significance was set at $p < 0.05$. Biological assays were carried out in three independent replicates, and each replicate used four samples. Three repetitions were made

for the ELISA determinations. For the assessment of cytotoxicity, mathematical models were developed in the Statistica program, on the basis of which the CC_{50} was determined. The CC_{50} is the concentration that inhibits 50% of cell viability.

4.3. Molecular modeling

We adopted density functional theory (DFT) and polarizable continuum model model (PCM) to optimize the **4l** structure [72 Quantum Tomasi 2005]. During calculations standard protocol of AutoDock4.2 program and Lamarckian genetic algorithm with local search were used [73 Morris, G.M.; Huey, R.; Lindstrom, W.; Sanner, M.F.; Belew, R.K.; Goodsell, D.S.; Olson, A.J. AutoDock4 and AutoDockTools4: Automated docking with selective receptor flexibility. J. Comput. Chem. 2009, 30, 2785–2791]. Previous studies have shown that it is the most efficient and reliable algorithm of AutoDock4.2. Physicochemical properties, ADME activity were evaluated based on Swiss Institute Bioinformatics tool and based on comprehensive database ADMETlab [70,71]. The obtained results were visualized using a BIOVIA Discovery Studio visualizer [74 BIOVIA, Dassault Systèmes, Discovery Studio Visualizer, v21.1.0.20298, San Diego: Dassault Systèmes, 2020].

Funding

The investigation was supported by the Ministry of Health subvention according to the number SUB.D070.22.030 from the IT Simple system of Wroclaw Medical University.

Declaration of Competing Interest

The authors declare that they have no known competing financial interests or personal relationships that could have appeared to influence the work reported in this paper.

Data availability

Data will be made available on request.

Acknowledgments

Żaneta Czyżnikowska is grateful for the allocation of the CPU time at the Wroclaw Center of Networking and Supercomputing (WCSS). Additionally, the authors would like to thank Hanna Czapor-Irzabek from the Laboratory of Elemental Analysis and Structural Research (Faculty of Pharmacy of the Wroclaw Medical University) for performing HR-MS.

Appendix A. Supplementary data

Supplementary data to this article can be found online at https://doi.org/10.1016/j.bioorg.2023.106758.

References

[1] H. Sung, J. Ferlay, R.L. Siegel, M. Laversanne, I. Soerjomataram, A. Jemal, F. Bray, Global Cancer Statistics 2020: GLOBOCAN Estimates of Incidence and Mortality Worldwide for 36 Cancers in 185 Countries, CA Cancer J. Clin. 71 (3) (2021) 209–249, https://doi.org/10.3322/caac.21660.

[2] V. Kayamba, Nutrition and Upper Gastrointestinal Cancers: An Overview of Current Understandings. *Seminars in Cancer Biology*, Academic Press August 1 (2022) 605–616, https://doi.org/10.1016/j.semcancer.2021.03.004.

[3] J. Li, Digestive Cancer Incidence and Mortality among Young Adults Worldwide in 2020: A Population-Based Study, World J. Gastrointest. Oncol. 14 (1) (2022) 278–294, https://doi.org/10.4251/wjgo.v14.i1.278.

[4] https://www.who.int/news-room/fact-sheets/detail/cancer.

[5] E. Güzel, U. Acar Çevik, A.E. Evren, H.E. Bostancı, Ü.D. Gül, U. Kayış, Y. Özkay, Z. A. Kaplancıklı, Synthesis of Benzimidazole-1,2,4-Triazole Derivatives as Potential Antifungal Agents Targeting 14α-Demethylase, ACS Omega (2022), https://doi.org/10.1021/acsomega.2c07755.

[6] S. Sun, J. Yan, L. Tai, J. Chai, H. Hu, L. Han, A. Lu, C. Yang, M. Chen, Novel (Z)/(E)-1,2,4-Triazole Derivatives Containing Oxime Ether Moiety as Potential Ergosterol Biosynthesis Inhibitors: Design, Preparation, Antifungal Evaluation, and Molecular Docking, Mol. Divers. 27 (1) (2023) 145–157, https://doi.org/10.1007/s11030-022-10412-w.

[7] Y.N. Cheng, Z.H. Jiang, L.S. Sun, Z.Y. Su, M.M. Zhang, H.L. Li, Synthesis of 1, 2, 4-Triazole Benzoyl Arylamine Derivatives and Their High Antifungal Activities, Eur. J. Med. Chem. 200 (2020), https://doi.org/10.1016/j.ejmech.2020.112463.

[8] H.A. Hofny, M.F.A. Mohamed, H.A.M. Gomaa, S.A. Abdel-Aziz, B.G.M. Youssif, N. A. El-koussi, A.S. Aboraia, Design, Synthesis, and Antibacterial Evaluation of New Quinoline-1,3,4-Oxadiazole and Quinoline-1,2,4-Triazole Hybrids as Potential Inhibitors of DNA Gyrase and Topoisomerase IV, Bioorg. Chem. 112 (2021), https://doi.org/10.1016/j.bioorg.2021.104920.

[9] P. Yang, J.B. Luo, Z.Z. Wang, L.L. Zhang, J. Feng, X.B. Xie, Q.S. Shi, X.G. Zhang, Synthesis, Molecular Docking, and Evaluation of Antibacterial Activity of 1,2,4-Triazole-Norfloxacin Hybrids, Bioorg. Chem. 115 (2021), https://doi.org/10.1016/j.bioorg.2021.105270.

[10] J. Zhang, S. Wang, Y. Ba, Z. Xu, 1,2,4-Triazole-Quinoline/Quinolone Hybrids as Potential Anti-Bacterial Agents, Elsevier Masson SAS July 15, Eur. J. Med. Chem. (2019) 1–8, https://doi.org/10.1016/j.ejmech.2019.04.033.

[11] H.A.M. Goma'a, M.A. Ghaly, L.A. Abou-zeid, F.A. Badria, I.A. Shehata, M.M. El-Kerdawy, Synthesis, Biological Evaluation and In Silico Studies of 1,2,4-Triazole and 1,3,4-Thiadiazole Derivatives as Antiherpetic Agents, ChemistrySelect 4 (21) (2019) 6421–6428, https://doi.org/10.1002/slct.201900814.

[12] X. Jiang, P.P. Sharma, B. Rathi, X. Ji, L. Hu, Z. Gao, D. Kang, Z. Wang, M. Xie, S. Xu, X. Zhang, E. De Clercq, S. Cocklin, C. Pannecouque, A. Dick, X. Liu, P. Zhan, Discovery of Novel 1,2,4-Triazole Phenylalanine Derivatives Targeting an Unexplored Region within the Interprotomer Pocket of the HIV Capsid Protein, J. Med. Virol. 94 (12) (2022) 5975–5986, https://doi.org/10.1002/jmv.28064.

[13] M.S. Shaykoon, A.A. Marzouk, O.M. Soltan, A.S. Wanas, M.M. Radwan, A. M. Gouda, B.G.M. Youssif, M. Abdel-Aziz, Design, Synthesis and Antitrypanosomal Activity of Heteroaryl-Based 1,2,4-Triazole and 1,3,4-Oxadiazole Derivatives, Bioorg. Chem. 100 (2020), https://doi.org/10.1016/j.bioorg.2020.103933.

[14] F. Eyaane Meva, T.J. Prior, D.J. Evans, S. Shah, C.F. Tamngwa, H.G.L. Belengue, R. E. Mang, J. Munro, T. Qahash, M. Llinás, Anti-Inflammation and Antimalarial Profile of 5-Pyridin-2-Yl-1H-[1,2,4]Triazole-3-Carboxylic Acid Ethyl Ester as a Low Molecular Intermediate for Hybrid Drug Synthesis, Res. Chem. Intermed. 48 (2) (2022) 885–898, https://doi.org/10.1007/s11164-021-04607-3.

[15] M. Zaheer, M. Zia-Ur-Rehman, R. Munir, N. Jamil, S. Ishtiaq, R.S. Zaib Saleem, M. R.J. Elsegood, (Benzylideneamino)Triazole-Thione Derivatives of Flurbiprofen: An Efficient Microwave-Assisted Synthesis and in Vivo Analgesic Potential, ACS Omega 6 (46) (2021) 31348–31357, https://doi.org/10.1021/acsomega.1c05222.

[16] A.H. Abdelazeem, A.G.S. El-Din, H.H. Arab, M.T. El-Saadi, S.M. El-Moghazy, N. H. Amin, Design, Synthesis and Anti-Inflammatory/Analgesic Evaluation of Novel Di-Substituted Urea Derivatives Bearing Diaryl-1,2,4-Triazole with Dual COX-2/SEH Inhibitory Activities, J. Mol. Struct. (2021, 1240.), https://doi.org/10.1016/j.molstruc.2021.130565.

[17] A. Avci, H. Taşci, Ü. Kandemir, Ö.D. Can, N. Gökhan-Kelekçi, B. Tozkoparan, Synthesis, Characterization, and in Vivo Pharmacological Evaluation of Novel Mannich Bases Derived from 1,2,4-Triazole Containing a Naproxen Moiety, Bioorg. Chem. 100 (2020), 103892, https://doi.org/10.1016/j.bioorg.2020.103892.

[18] B. Kaproń, J.J. Łuszczki, A. Siwek, T. Karcz, G. Nowak, M. Zagaja, M. Andres-Mach, A. Stasiłowicz, J. Cielecka-Piontek, J. Kocki, T. Plech, Preclinical Evaluation of 1,2,4-Triazole-Based Compounds Targeting Voltage-Gated Sodium Channels (VGSCs) as Promising Anticonvulsant Drug Candidates, Bioorg. Chem. 94 (2020), https://doi.org/10.1016/j.bioorg.2019.103355.

[19] M. Song, R. Yan, Y. Zhang, D. Guo, N. Zhou, X.Q. Deng, Design, Synthesis, and Anticonvulsant Effects Evaluation of Nonimidazole Histamine H3 Receptor Antagonists/Inverse Agonists Containing Triazole Moiety, J. Enzyme Inhib. Med. Chem. 35 (1) (2020) 1310–1321, https://doi.org/10.1080/14756366.2020.1774573.

[20] K.K. Verma, U.K. Singh, J. Jain, Design, Synthesis and Biological Activity of Some 4, 5-Disubstituted-2, 4- Dihydro-3H-1, 2, 4- Triazole-3-Thione Derivatives, Cent. Nerv. Syst. Agents Med. Chem. 19 (3) (2019) 197–205, https://doi.org/10.2174/1871524919666190722144424.

[21] H. Cai, X. Huang, S. Xu, H. Shen, P. Zhang, Y. Huang, J. Jiang, Y. Sun, B. Jiang, X. Wu, H. Yao, J. Xu, Discovery of Novel Hybrids of Diaryl-1,2,4-Triazoles and Caffeic Acid as Dual Inhibitors of Cyclooxygenase-2 and 5-Lipoxygenase for Cancer Therapy, Eur. J. Med. Chem. 108 (2016) 89–103, https://doi.org/10.1016/j.ejmech.2015.11.013.

[22] H.A.M. El-Sherief, B.G.M. Youssif, S.N.A. Bukhari, M. Abdel-Aziz, H.M. Abdel-Rahman, Novel 1,2,4-Triazole Derivatives as Potential Anticancer Agents: Design, Synthesis, Molecular Docking and Mechanistic Studies, Bioorg. Chem. 76 (2018) 314–325, https://doi.org/10.1016/j.bioorg.2017.12.013.

[23] M. Zengin, O. Unsal Tan, R.K. Arafa, A. Balkan, Design and Synthesis of New 2-Oxoquinoxalinyl-1,2,4-Triazoles as Antitumor VEGFR-2 Inhibitors, Bioorg. Chem. 121 (2022), https://doi.org/10.1016/j.bioorg.2022.105696.

[24] F. Naaz, F. Ahmad, B.A. Lone, Y.R. Pokharel, N.K. Fuloria, S. Fuloria, M. Ravichandran, L. Pattabhiraman, S. Shafi, M. Shahar Yar, Design and Synthesis of Newer 1,3,4-Oxadiazole and 1,2,4-Triazole Based Topsentin Analogues as Anti-Proliferative Agent Targeting Tubulin, Bioorg. Chem. 95 (2020), https://doi.org/10.1016/j.bioorg.2019.103519.

[25] L. Yurttaş, A.E. Evren, A. Kubilay, H.E. Temel, Synthesis of New 1,2,4-Triazole Derivatives and Investigation of Their Matrix Metalloproteinase-9 (Mmp-9) Inhibition Properties. *Acta*, Pharm. Sci. 59 (2) (2021) 215–232, https://doi.org/10.23893/1307-2080.APS.05913.

[26] A. Turky, A.H. Bayoumi, F.F. Sherbiny, K. El-Adl, H.S. Abulkhair, Unravelling the Anticancer Potency of 1,2,4-Triazole-N-Arylamide Hybrids through Inhibition of STAT3: Synthesis and in Silico Mechanistic Studies, Mol. Divers. 25 (1) (2021) 403–420, https://doi.org/10.1007/s11030-020-10131-0.

[27] H.A.M. Gomaa, H.A.M. El-Sherief, S. Hussein, A.M. Gouda, O.I.A. Salem, K. S. Alharbi, A.M. Hayallah, B.G.M. Youssif, Novel 1,2,4-Triazole Derivatives as Apoptotic Inducers Targeting P53: Synthesis and Antiproliferative Activity, Bioorg. Chem. 105 (2020), https://doi.org/10.1016/j.bioorg.2020.104369.

[28] M.S. Nafie, A.T.A. Boraei, Exploration of Novel VEGFR2 Tyrosine Kinase Inhibitors via Design and Synthesis of New Alkylated Indolyl-Triazole Schiff Bases for Targeting Breast Cancer, Bioorg. Chem. 122 (2022), https://doi.org/10.1016/j.bioorg.2022.105708.

[29] C.B. Mishra, R.K. Mongre, S. Kumari, D.K. Jeong, M. Tiwari, Novel Triazole-Piperazine Hybrid Molecules Induce Apoptosis via Activation of the Mitochondrial Pathway and Exhibit Antitumor Efficacy in Osteosarcoma Xenograft Nude Mice Model, ACS Chem. Biol. 12 (3) (2017) 753–768, https://doi.org/10.1021/acschembio.6b01007.

[30] A. Ameri, G. Khodarahmi, H. Forootanfar, F. Hassanzadeh, G.H. Hakimelahi, Hybrid Pharmacophore Design, Molecular Docking, Synthesis, and Biological Evaluation of Novel Aldimine-Type Schiff Base Derivatives as Tubulin Polymerization Inhibitor, Chem. Biodivers. 15 (3) (2018), https://doi.org/10.1002/cbdv.201700518.

[31] W.M. El-Husseiny, M.A.A. El-Sayed, N.I. Abdel-Aziz, A.S. El-Azab, Y.A. Asiri, A.A. M. Abdel-Aziz, Structural Alterations Based on Naproxen Scaffold: Synthesis, Evaluation of Antitumor Activity and COX-2 Inhibition, and Molecular Docking, Eur. J. Med. Chem. 158 (2018) 134–143, https://doi.org/10.1016/j.ejmech.2018.09.007.

[32] P. Świątek, T. Glomb, A. Dobosz, T. Gębarowski, K. Wojtkowiak, A. Jezierska, J. J. Panek, M. Świątek, M. Strzelecka, Biological Evaluation and Molecular Docking Studies of Novel 1,3,4-Oxadiazole Derivatives of 4,6-Dimethyl-2-Sulfanylpyridine-3-Carboxamide, Int. J. Mol. Sci. 23 (1) (2022), https://doi.org/10.3390/ijms23010549.

[33] M. Strzelecka, T. Glomb, M. Drąg-Zalesińska, J. Kulbacka, A. Szewczyk, J. Saczko, P. Kasperkiewicz-Wasilewska, N. Rembiałkowska, K. Wojtkowiak, A. Jezierska, Ś. P. Synthesis, Anticancer Activity and Molecular Docking Studies of Novel N-Mannich Bases of 1,3,4-Oxadiazole Based on 4,6-Dimethylpyridine Scaffold, Int. J. Mol. Sci. (2022) 23 (19), https://doi.org/10.3390/ijms231911173.

[34] Singh, A. K.; Kumar, A.; Singh, H.; Sonawane, P.; Paliwal, H.; Thareja, S.; Pathak, P.; Grishina, M.; Jaremko, M.; Emwas, A. H.; Yadav, J. P.; Verma, A.; Khalilullah, H.; Kumar, P. Concept of Hybrid Drugs and Recent Advancements in Anticancer Hybrids. *Pharmaceuticals*. MDPI September 1, 2022. 10.3390/ph15091071.

[35] Ł. Szczukowski, E. Krzyżak, B. Wiatrak, P. Jawień, A. Marciniak, A. Kotynia, P. Świątek, New N-substituted-1,2,4-triazole Derivatives of Pyrrolo[3,4-d] Pyridazinone with Significant Anti-inflammatory Activity—Design, Synthesis and Complementary in Vitro, Computational and Spectroscopic Studies, Int. J. Mol. Sci. 22 (20) (2021), https://doi.org/10.3390/ijms222011235.

[36] T. Glomb, B. Wiatrak, K. Gębczak, T. Gębarowski, D. Bodetko, Ż. Czyżnikowska, P. Świątek, New 1,3,4-oxadiazole Derivatives of Pyridothiazine- 1,1-dioxide with Anti-inflammatory Activity, Int. J. Mol. Sci. 21 (23) (2020) 1–22, https://doi.org/10.3390/ijms21239122.

[37] P. Świątek, J. Saczko, N. Rembiałkowska, J. Kulbacka, Synthesis of New Hydrazone Derivatives and Evaluation of Their Efficacy as Proliferation Inhibitors in Human Cancer Cells, Med. Chem. (Los. Angeles). 15 (8) (2019) 903–910, https://doi.org/10.2174/1573406415666190128100524.

[38] E. Wyrzykiewicz, D. Prukała, New Isomeric N-Substituted Hydrazones of 2-, 3-and 4-Pyridinecarboxaldehydes, J. Heterocycl. Chem. 35 (2) (1998) 381–387, https://doi.org/10.1002/jhet.5570350221.

[39] H. Bayrak, A. Demirbas, S.A. Karaoglu, N. Demirbas, Synthesis of Some New 1,2,4-Triazoles, Their Mannich and Schiff Bases and Evaluation of Their Antimicrobial Activities, Eur. J. Med. Chem. 44 (3) (2009) 1057–1066, https://doi.org/10.1016/j.ejmech.2008.06.019.

[40] R.W. Johnstone, A.A. Ruefli, K.M. Tainton, M.J. Smyth, A Role for P-Glycoprotein in Regulating Cell Death. *Leukemia and Lymphoma*, Harwood Academic Publishers GmbH, 2000, pp. 1–11.

[41] Bukowski, K.; Kciuk, M.; Kontek, R. Mechanisms of Multidrug Resistance in Cancer Chemotherapy. *International Journal of Molecular Sciences*. MDPI AG May 2, 2020. 10.3390/ijms21093233.

[42] P.S. Souza, J.P. Madigan, J.P. Gillet, K. Kapoor, S.V. Ambudkar, R.C. Maia, M. M. Gottesman, K. Leung Fung, Expression of the Multidrug Transporter P-Glycoprotein Is Inversely Related to That of Apoptosis-Associated Endogenous TRAIL, Exp. Cell Res. 336 (2) (2015) 318–328, https://doi.org/10.1016/j.yexcr.2015.06.005.

[43] Y. Zu, Z. Yang, S. Tang, Y. Han, J. Ma, Effects of P-Glycoprotein and Its Inhibitors on Apoptosis in K562 Cells, Molecules 19 (9) (2014) 13061–13075, https://doi.org/10.3390/molecules190913061.

[44] M.Z. El-Readi, S.Y. Eid, A.A. Abdelghany, H.S. Al-Amoudi, T. Efferth, M. Wink, Resveratrol Mediated Cancer Cell Apoptosis, and Modulation of Multidrug Resistance Proteins and Metabolic Enzymes, Phytomedicine 55 (2019) 269–281, https://doi.org/10.1016/j.phymed.2018.06.046.

[45] E. Jouan, M. Le Vée, A. Mayati, C. Denizot, Y. Parmentier, O. Fardel, Evaluation of P-Glycoprotein Inhibitory Potential Using a Rhodamine 123 Accumulation Assay, Pharmaceutics 8 (2) (2016), https://doi.org/10.3390/pharmaceutics8020012.

[46] R.S.Y. Wong, Apoptosis in Cancer: From Pathogenesis to Treatment, J. Exp. Clin. Cancer Res. (2011), https://doi.org/10.1186/1756-9966-30-87.

[47] V. Nikoletopoulou, M. Markaki, K. Palikaras, N. Tavernarakis, Crosstalk between Apoptosis, Necrosis and Autophagy. *Biochimica et Biophysica Acta - Molecular*, Cell Res. (December 2013) 3448–3459, https://doi.org/10.1016/j.bbamcr.2013.06.001.

[48] Jan, R.; Chaudhry, G. e. S. Understanding Apoptosis and Apoptotic Pathways Targeted Cancer Therapeutics. *Advanced Pharmaceutical Bulletin*. Tabriz University of Medical Sciences 2019, pp 205–218. 10.15171/apb.2019.024.

[49] Gupta, A.; Shah, K.; Oza, M. J.; Behl, T. Reactivation of P53 Gene by MDM2 Inhibitors: A Novel Therapy for Cancer Treatment. *Biomedicine and Pharmacotherapy*. Elsevier Masson SAS January 1, 2019, pp 484–492. 10.1016/j.biopha.2018.10.155.

[50] T. Gębarowski, B. Wiatrak, K. Gębczak, B. Tylińska, K. Gąsiorowski, Effect of New Olivacine Derivatives on P53 Protein Level, Pharmacol. Reports 72 (1) (2020) 214–224, https://doi.org/10.1007/s43440-019-00004-1.

[51] B.Y. Sheikh, M.M.R. Sarker, M.N.A. Kamarudin, G. Mohan, Antiproliferative and Apoptosis Inducing Effects of Citral via P53 and ROS-Induced Mitochondrial-Mediated Apoptosis in Human Colorectal HCT116 and HT29 Cell Lines, Biomed. Pharmacother. 96 (2017) 834–846, https://doi.org/10.1016/j.biopha.2017.10.038.

[52] M. Zhou, X. Liu, Z. Li, Q. Huang, F. Li, C.Y. Li, Caspase-3 Regulates the Migration, Invasion and Metastasis of Colon Cancer Cells, Int. J. Cancer 143 (4) (2018) 921–930, https://doi.org/10.1002/ijc.31374.

[53] F.F. Ahmed, A.A. Abd El-Hafeez, S.H. Abbas, D. Abdelhamid, M. Abdel-Aziz, New 1,2,4-Triazole-Chalcone Hybrids Induce Caspase-3 Dependent Apoptosis in A549 Human Lung Adenocarcinoma Cells, Eur. J. Med. Chem. 151 (2018) 705–722, https://doi.org/10.1016/j.ejmech.2018.03.073.

[54] A.E. El Mansouri, A. Oubella, M. Maatallah, M.Y. AitItto, M. Zahouily, H. Morjani, H.B. Lazrek, Design, Synthesis, Biological Evaluation and Molecular Docking of New Uracil Analogs-1,2,4-Oxadiazole Hybrids as Potential Anticancer Agents, Bioorganic Med. Chem. Lett. 30 (19) (2020), https://doi.org/10.1016/j.bmcl.2020.127438.

[55] Setrerrahmane, S.; Xu, H. Tumor-Related Interleukins: Old Validated Targets for New Anti-Cancer Drug Development. *Molecular Cancer*. BioMed Central Ltd. September 19, 2017. 10.1186/s12943-017-0721-9.

[56] T. Nagasaki, M. Hara, H. Nakanishi, H. Takahashi, M. Sato, H. Takeyama, Interleukin-6 Released by Colon Cancer-Associated Fibroblasts Is Critical for Tumour Angiogenesis: Anti-Interleukin-6 Receptor Antibody Suppressed Angiogenesis and Inhibited Tumour-Stroma Interaction, Br. J. Cancer 110 (2) (2014) 469–478, https://doi.org/10.1038/bjc.2013.748.

[57] M.J. Waldner, S. Foersch, M.F. Neurath, Interleukin-6 - A Key Regulator of Colorectal Cancer Development, Int. J. Biol. Sci. (2012) 1248–1253, https://doi.org/10.7150/ijbs.4614.

[58] S. Han, A.J. Jeong, H. Yang, K. Bin Kang, H. Lee, E.H. Yi, B.H. Kim, C.H. Cho, J. W. Chung, S.H. Sung, S.K. Ye, Ginsenoside 20(S)-Rh2 Exerts Anti-Cancer Activity through Targeting IL-6-Induced JAK2/STAT3 Pathway in Human Colorectal Cancer Cells, J. Ethnopharmacol. 194 (2016) 83–90, https://doi.org/10.1016/j.jep.2016.08.039.

[59] M.A.A. Fathi, A.A. Abd El-Hafeez, D. Abdelhamid, S.H. Abbas, M.M. Montano, M. Abdel-Aziz, 1,3,4-Oxadiazole/Chalcone Hybrids: Design, Synthesis, and Inhibition of Leukemia Cell Growth and EGFR, Src, IL-6 and STAT3 Activities, Bioorg. Chem. 84 (2019) 150–163, https://doi.org/10.1016/j.bioorg.2018.11.032.

[60] A. Oubella, A.E. El Mansouri, M. Fawzi, A. Bimoussa, Y. Laamari, A. Auhmani, H. Morjani, A. Robert, A. Riahi, M. Youssef Ait Itto, Thiazolidinone-Linked 1,2,3-Triazoles with Monoterpenic Skeleton as New Potential Anticancer Agents: Design, Synthesis and Molecular Docking Studies, Bioorg. Chem. 115 (2021), 105184, https://doi.org/10.1016/J.BIOORG.2021.105184.

[61] J.L. Velázquez-Libera, F. Durán-Verdugo, A. Valdés-Jiménez, A. Valdés-Jiménez, G. Núñez-Vivanco, J. Caballero, LigRMSD: A Web Server for Automatic Structure Matching and RMSD Calculations among Identical and Similar Compounds in Protein-Ligand Docking, Bioinformatics 36 (9) (2020) 2912–2914, https://doi.org/10.1093/bioinformatics/btaa018.

[62] Kussie, P. H.; Gorina, S.; Marechal, V.; Elenbaas, B.; Moreau, J.; Levine, A. J.; Pavletich, N. P. Structure of the MDM2 Oncoprotein Bound to the P53 Tumor Suppressor Transactivation Domain. *Science (80-.)*. **1996**, *274* (5289), 948–953. 10.1126/SCIENCE.274.5289.948.

[63] J.G. Allen, M.P. Bourbeau, G.E. Wohlhieter, M.D. Bartberger, K. Michelsen, R. Hungate, R.C. Gadwood, R.D. Gaston, B. Evans, L.W. Mann, M.E. Matison, S. Schneider, X. Huang, D. Yu, P.S. Andrews, A. Reichelt, A.M. Long, P. Yakowec, E. Y. Yang, T.A. Lee, J.D. Oliner, Discovery and Optimization of Chromenotriazolopyrimidines as Potent Inhibitors of the Mouse Double Minute 2-Tumor Protein 53 Protein-Protein Interaction, J. Med. Chem. 52 (22) (2009) 7044–7053, https://doi.org/10.1021/JM900681H/SUPPL_FILE/JM900681H_SI_001.PDF.

[64] S.Q. Pantaleão, P.O. Fernandes, J.E. Gonçalves, V.G. Maltarollo, K.M. Honorio, Recent Advances in the Prediction of Pharmacokinetics Properties in Drug Design Studies: A Review, ChemMedChem 17 (1) (2022), https://doi.org/10.1002/CMDC.202100542.

[65] J. Dulsat, B. López-Nieto, R. Estrada-Tejedor, J.I. Borrell, Evaluation of Free Online ADMET Tools for Academic or Small Biotech Environments, *Molecules*. MDPI (January 1, 2023.), https://doi.org/10.3390/molecules28020776.

[66] D.E. Clark, In Silico Prediction of Blood-Brain Barrier Permeation, Drug Discov. Today 8 (20) (2003) 927–933, https://doi.org/10.1016/S1359-6446(03)02827-7.

[67] C.A. Lipinski, Rule of Five in 2015 and beyond: Target and Ligand Structural Limitations, Ligand Chemistry Structure and Drug Discovery Project Decisions, Adv. Drug Deliv. Rev. 101 (2016) 34–41, https://doi.org/10.1016/J.ADDR.2016.04.029.

[68] Waring, M. J. Lipophilicity in Drug Discovery. *https://doi.org/10.1517/17460441003605098* **2010**, *5* (3), 235–248. 10.1517/17460441003605098.

[69] J. Vrbanac, R. Slauter, ADME in Drug Discovery, in: A Comprehensive Guide to Toxicology in PreclinicAl Drug Development, Academic Press, 2013, pp. 3–30, https://doi.org/10.1016/B978-0-12-387815-1.00002-2.
[70] A. Daina, O. Michielin, V. Zoete, SwissADME: A Free Web Tool to Evaluate Pharmacokinetics, Drug-Likeness and Medicinal Chemistry Friendliness of Small Molecules, Sci. Rep. (2017) 7, https://doi.org/10.1038/srep42717.
[71] G. Xiong, Z. Wu, J. Yi, L. Fu, Z. Yang, C. Hsieh, M. Yin, X. Zeng, C. Wu, A. Lu, X. Chen, T. Hou, D. Cao, ADMETlab 2.0: An Integrated Online Platform for Accurate and Comprehensive Predictions of ADMET Properties, Nucleic Acids Res. 49 (W1) (2021) W5–W14, https://doi.org/10.1093/nar/gkab255.

SUPPLEMENTARY MATERIAL

New Schiff bases derived from dimethylpyridine-1,2,4-triazole hybrid as cytotoxic agents targeting gastrointestinal cancers: Design, synthesis, biological evaluation and molecular docking studies

Małgorzata Strzelecka[a,*], Benita Wiatrak[b], Paulina Jawień[c], Żaneta Czyżnikowska[d], Piotr Świątek[a,*]

[a] *Department of Medicinal Chemistry, Faculty of Pharmacy, Wroclaw Medical University, Borowska 211, 50-556 Wroclaw, Poland*
[b] *Department of Pharmacology, Wroclaw Medical University, J. Mikulicza-Radeckiego 2, 50-345 Wroclaw, Poland*
[c] *Department of Biostructure and Animal Physiology, Wroclaw University of Environmental and Life Sciences, Norwida 25/27, 50-375 Wroclaw, Poland*
[d] *Department of Inorganic Chemistry, Faculty of Pharmacy, Wroclaw Medical University, Borowska 211a, 50-556 Wroclaw, Poland*

[*] *Correspondence: malgorzata.strzelecka@umw.edu.pl (M. Strzelecka), piotr.swiatek@umw.edu.pl (P. Świątek)*

Table of contents:

Table S1. Visualizations of Nuclear Magnetic Resonance (NMR) spectra of compounds 3 and 4a-n (DMSO-d*6*) 2

Table S2. Visualizations of Fourier-Transform Infrared (FT-IR) spectra of compounds 3 and 4a-n …….18

Table S3. Visualizations of High Resolution Mass Spectrometry (HRMS) spectra of compounds 4a-m …….. 22

Table S4. Rhodamine-123 assay for compounds 4d, 4e, and 4l 27

Table S5. Detection of apoptosis for compounds 4d, 4e, and 4l 27

Table S1. Visualizations of Nuclear Magnetic Resonance (NMR) spectra of compounds 3 and 4a-n (DMSO-d*6*).

Comp.	^{1}H and ^{1}C NMR spectra
3	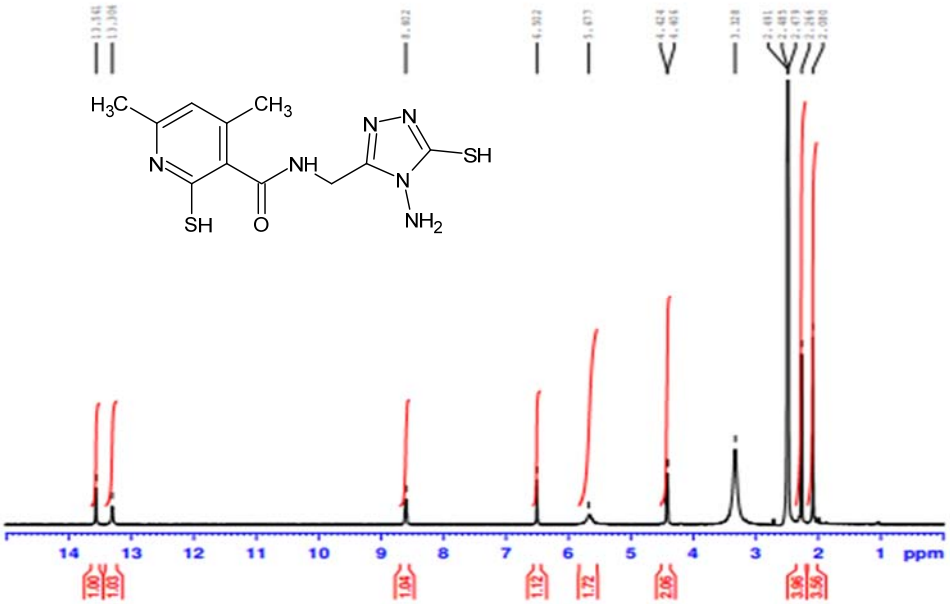 ^{1}H NMR of 3 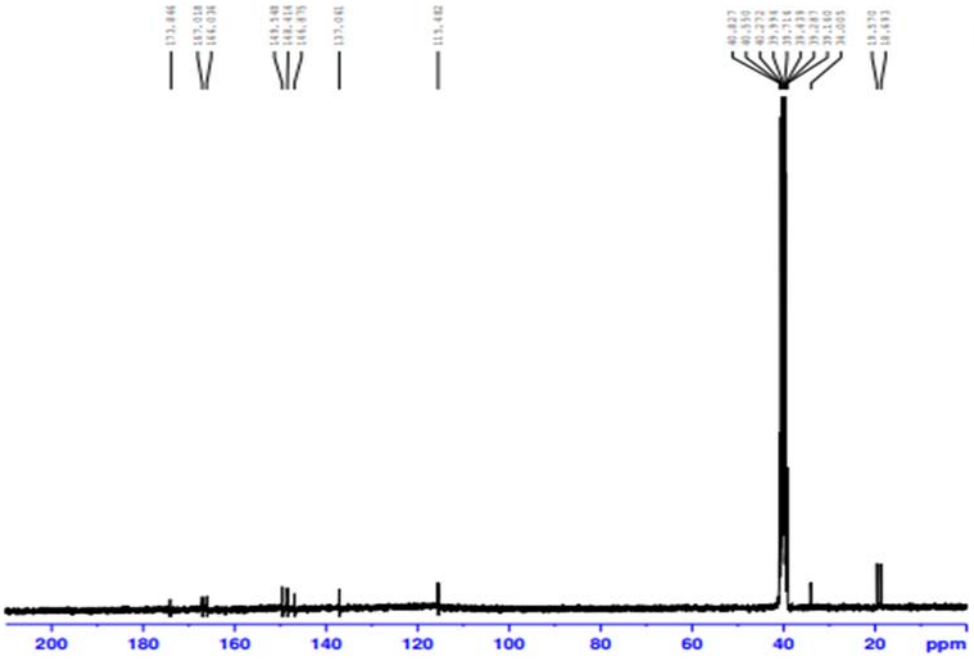 ^{1}C NMR of 3

4a

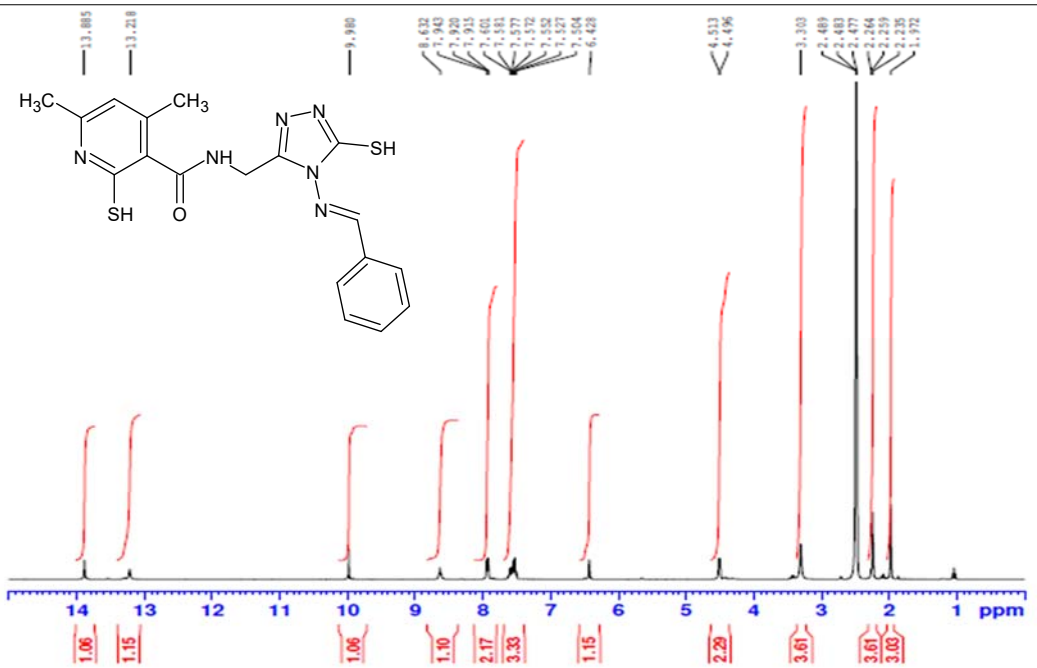

^{1}H NMR of 4a

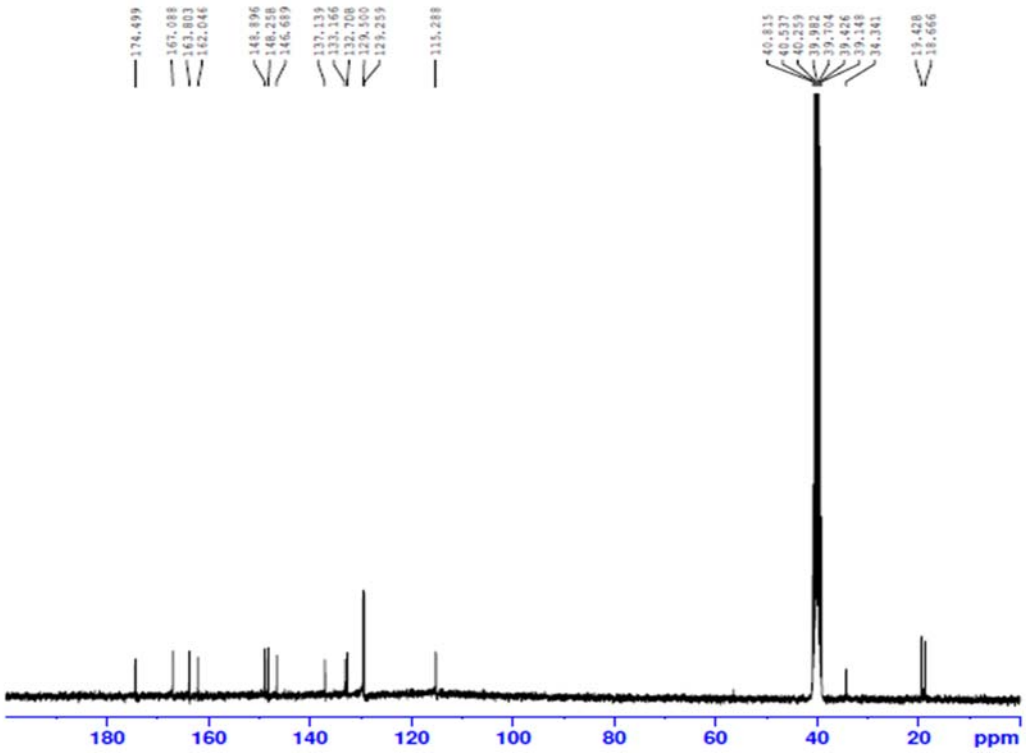

^{1}C NMR of 4a

4b

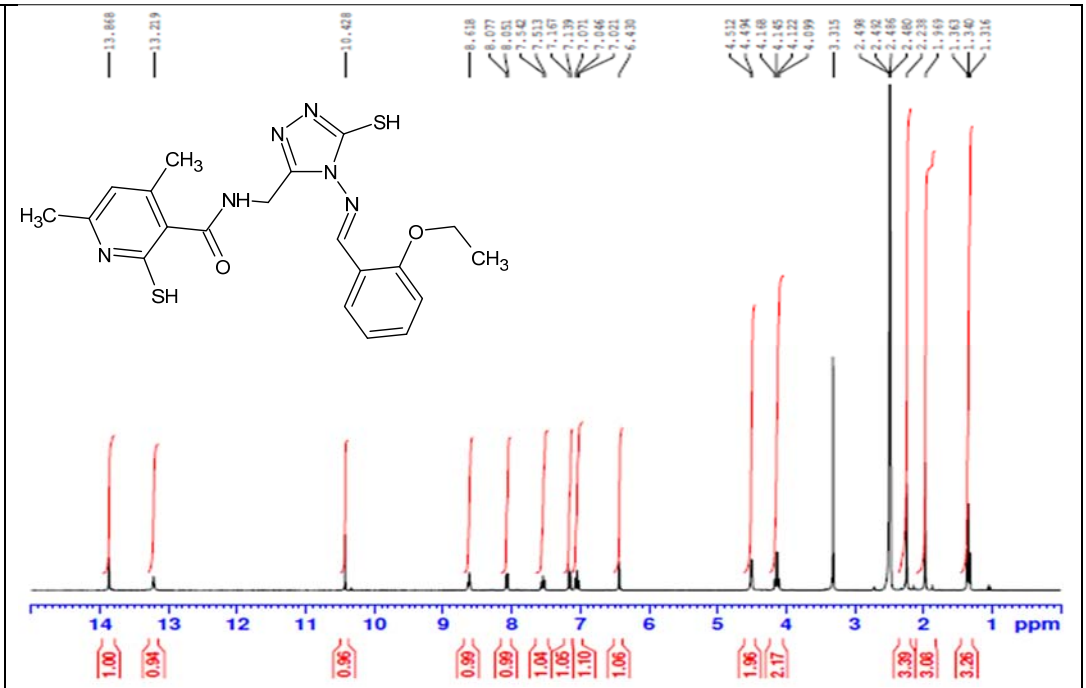

^{1}H NMR of 4b

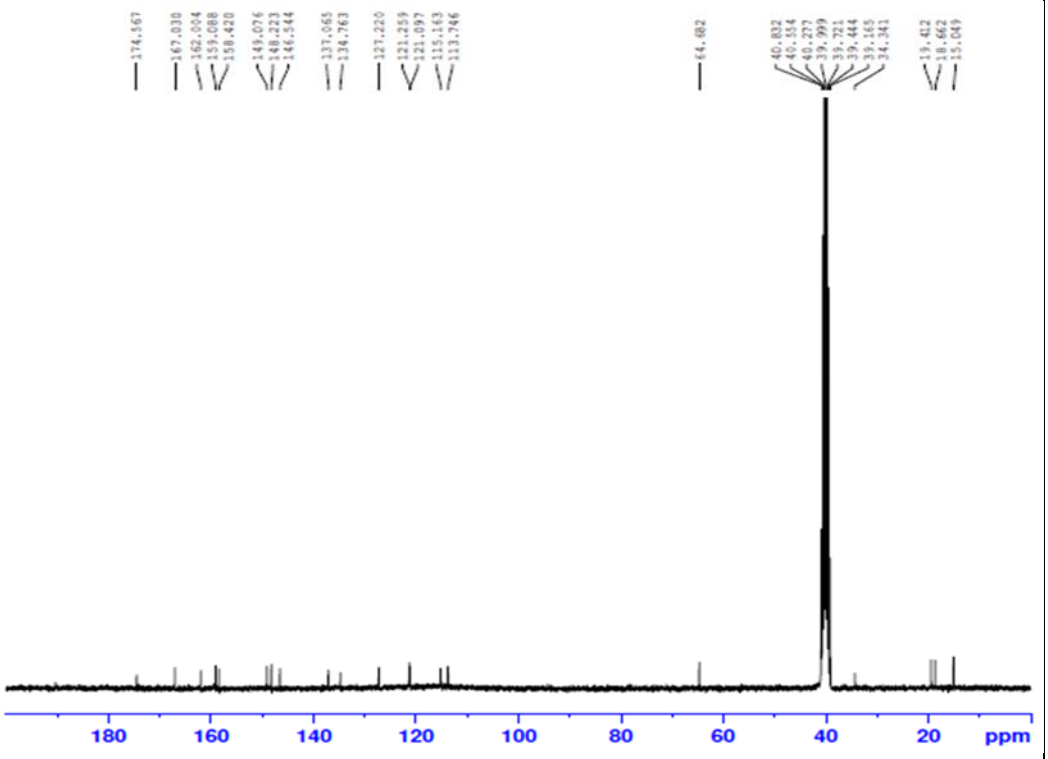

^{1}C NMR of 4b

4c

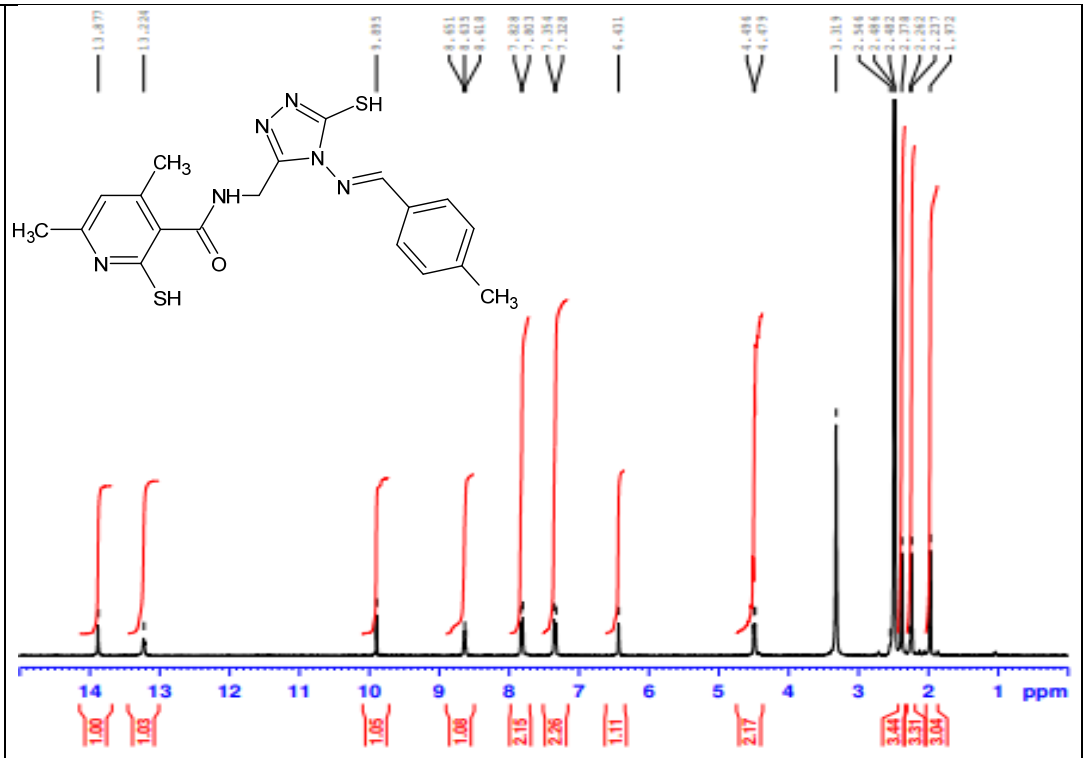

^{1}H NMR of 4c

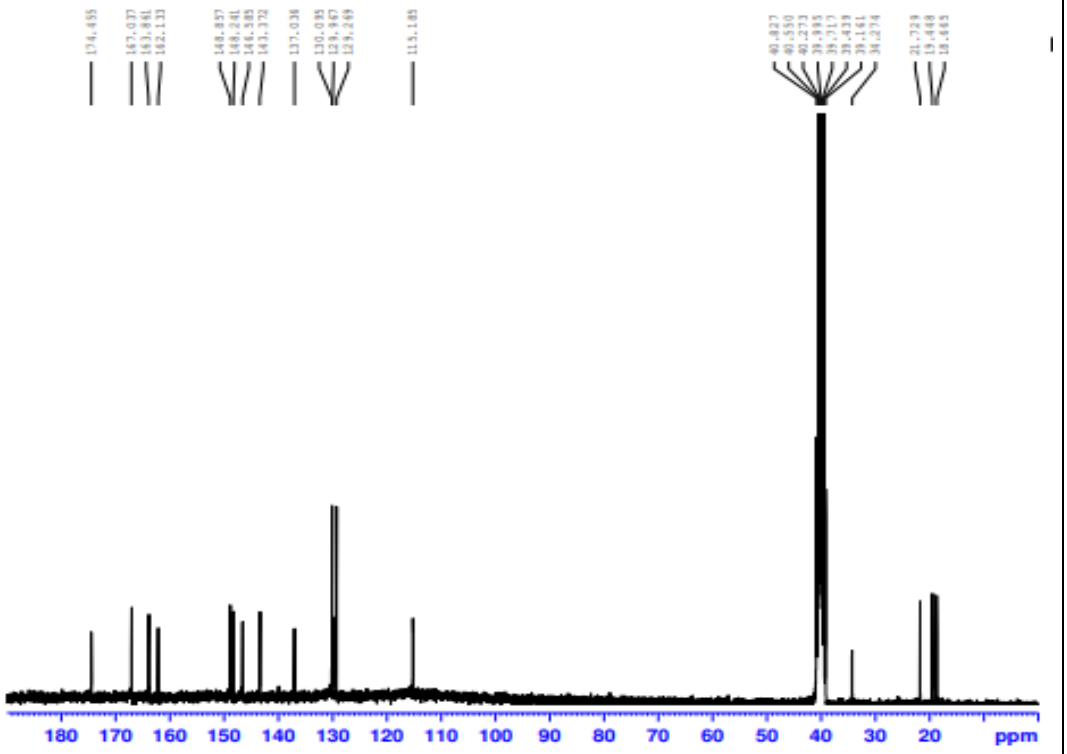

^{1}C NMR for 4c

4d

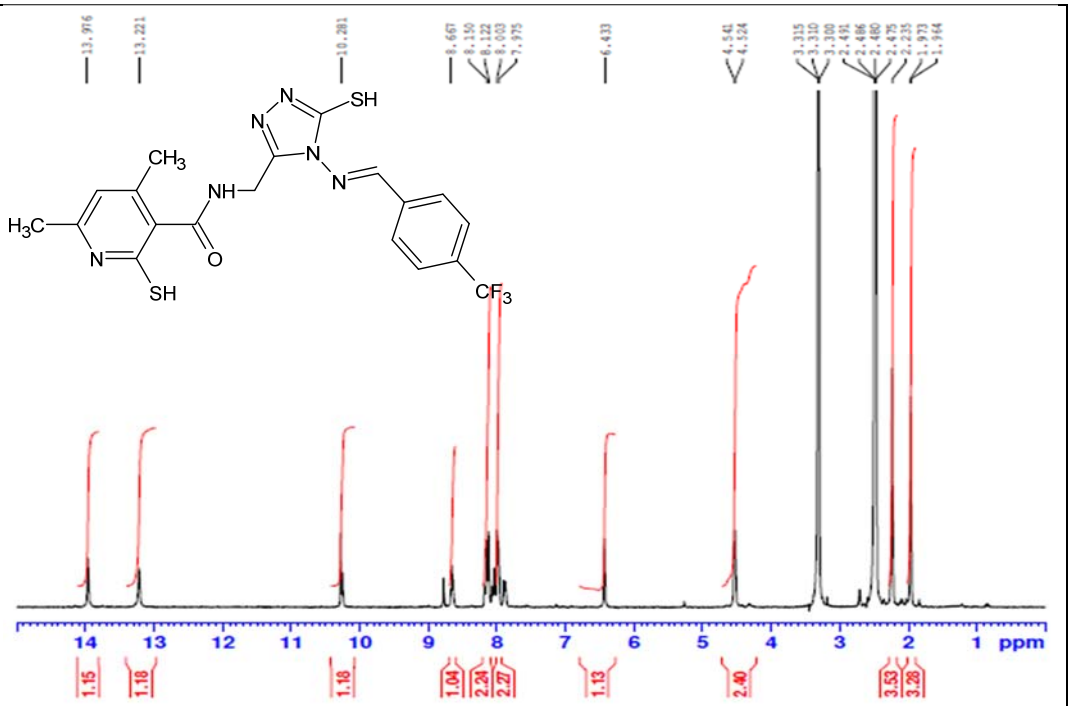

^{1}H NMR for 4d

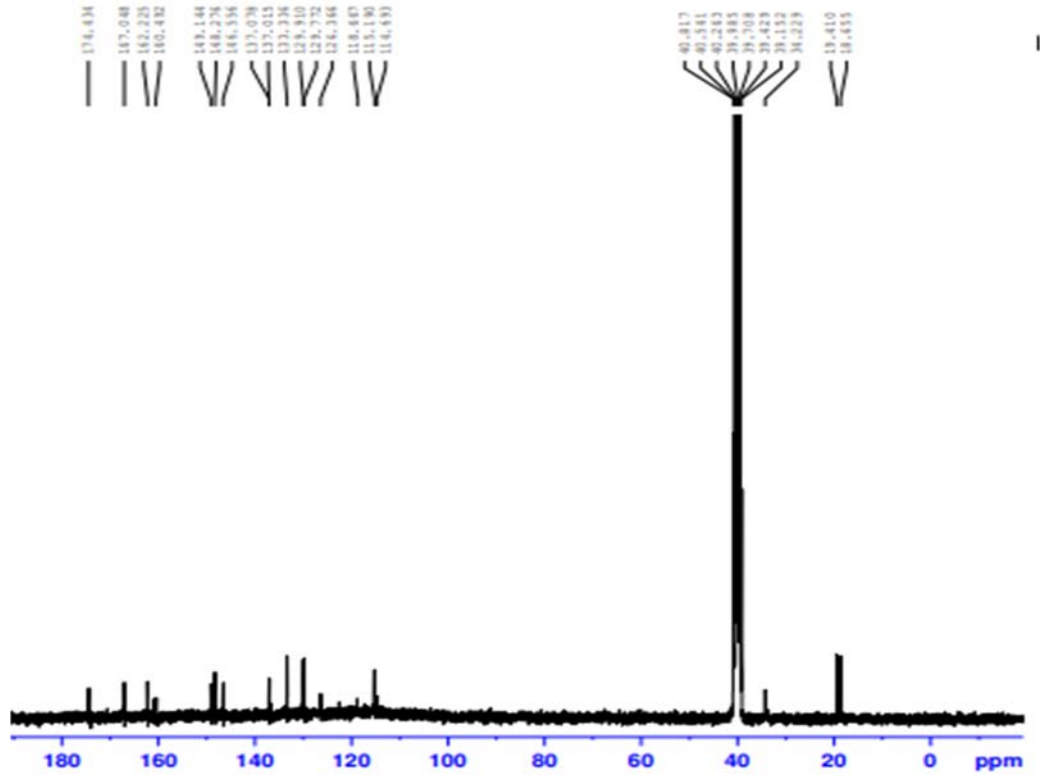

^{1}C NMR for 4d

4e

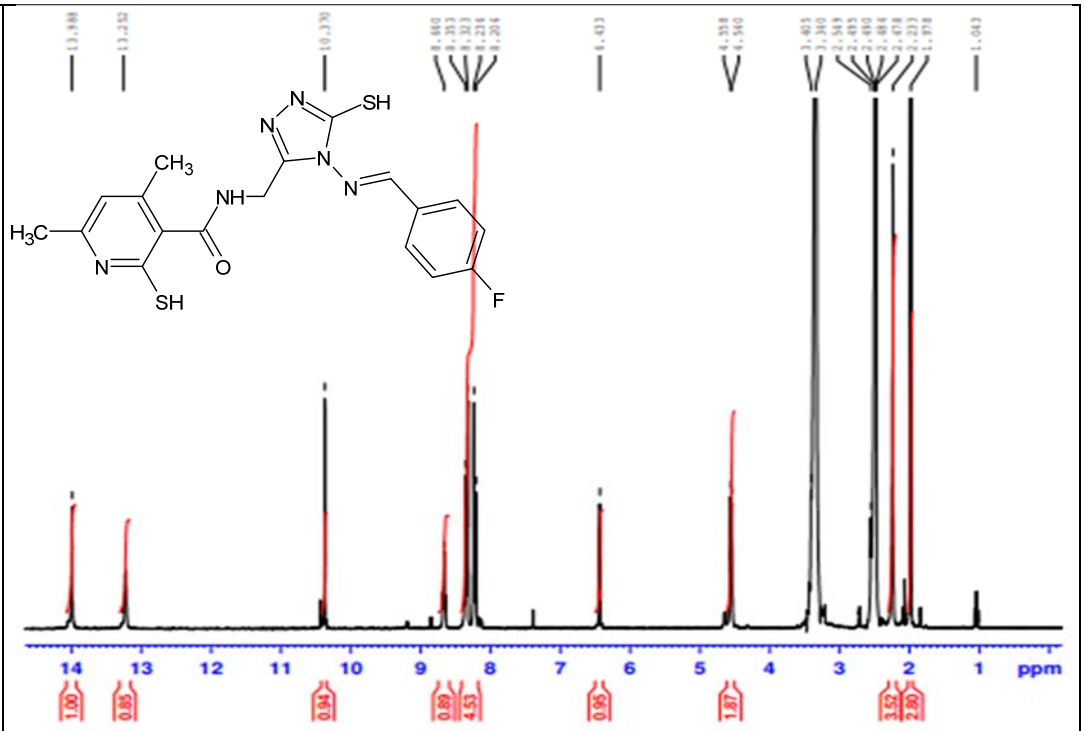

^{1}H NMR for 4e

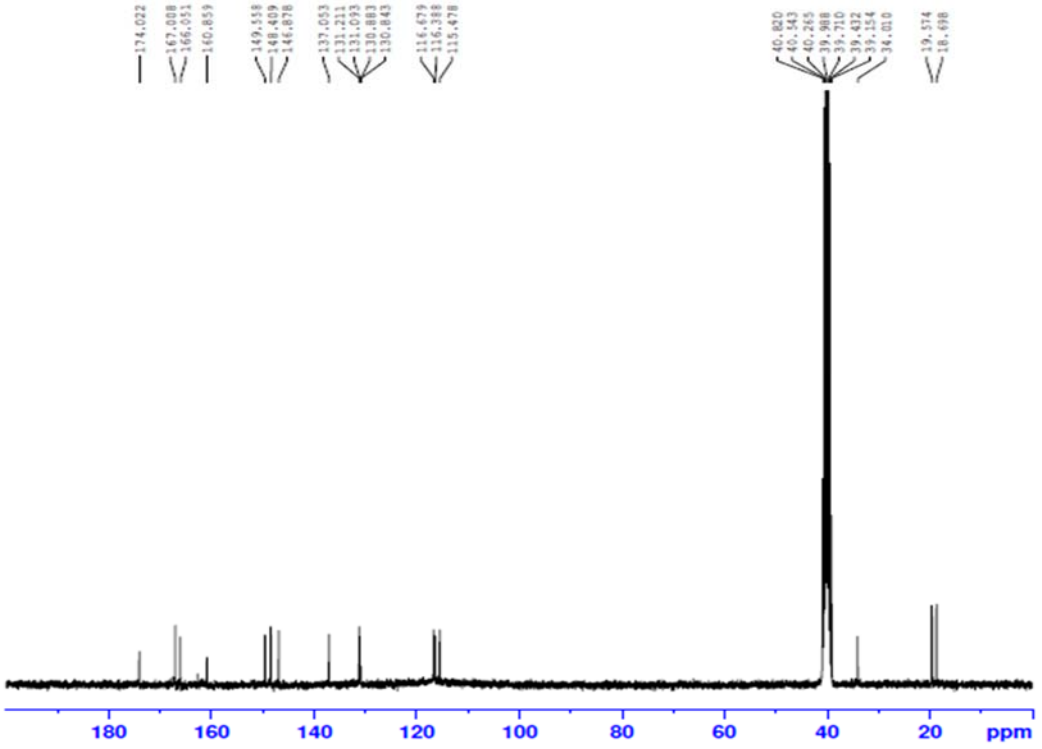

^{1}C NMR for 4e

4f

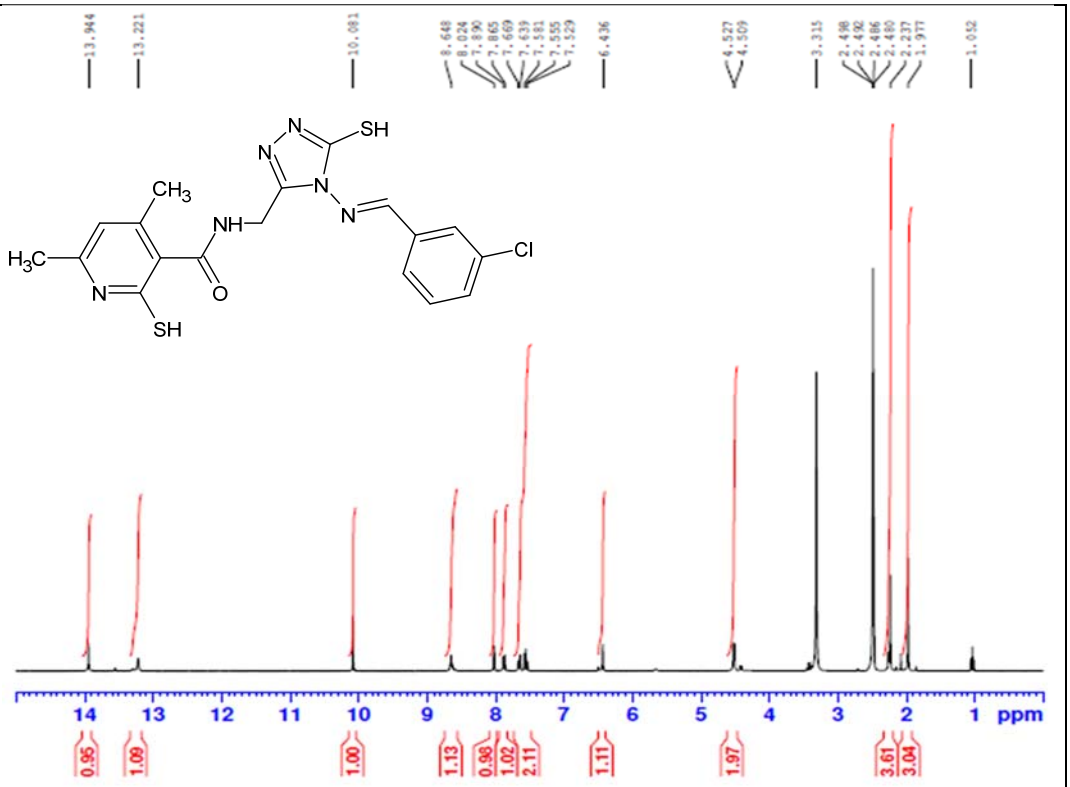

^{1}H NMR for 4f

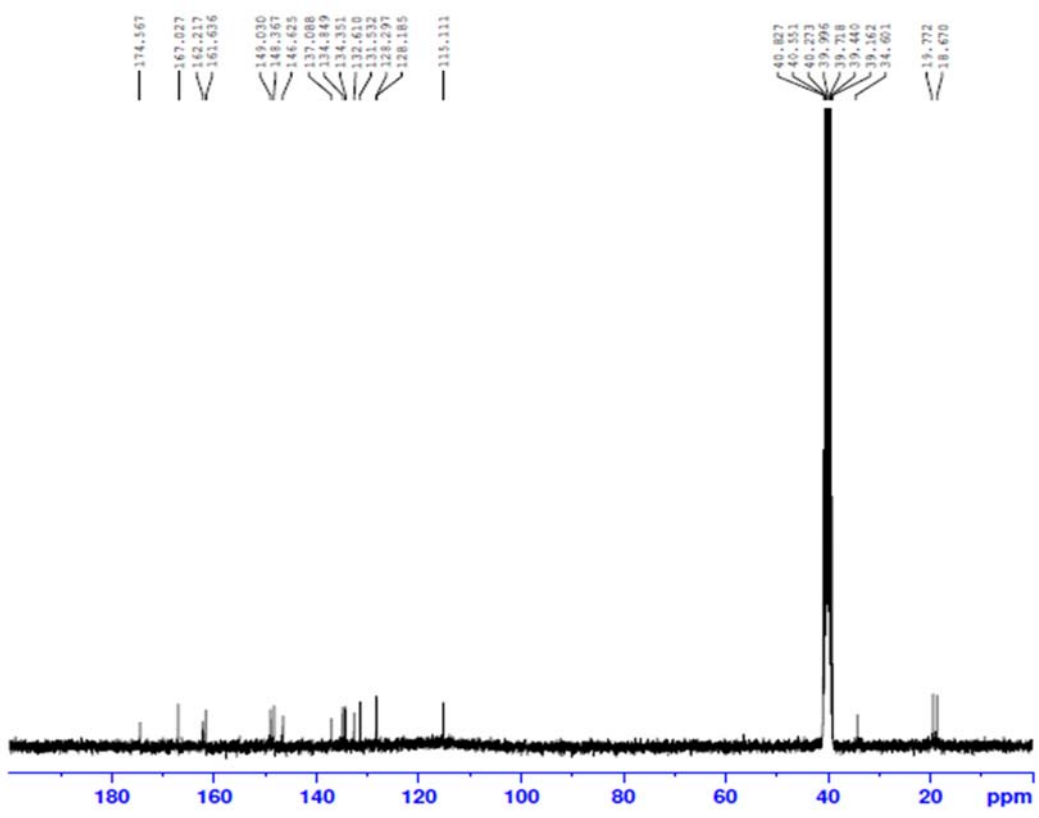

^{1}C NMR for 4f

4g

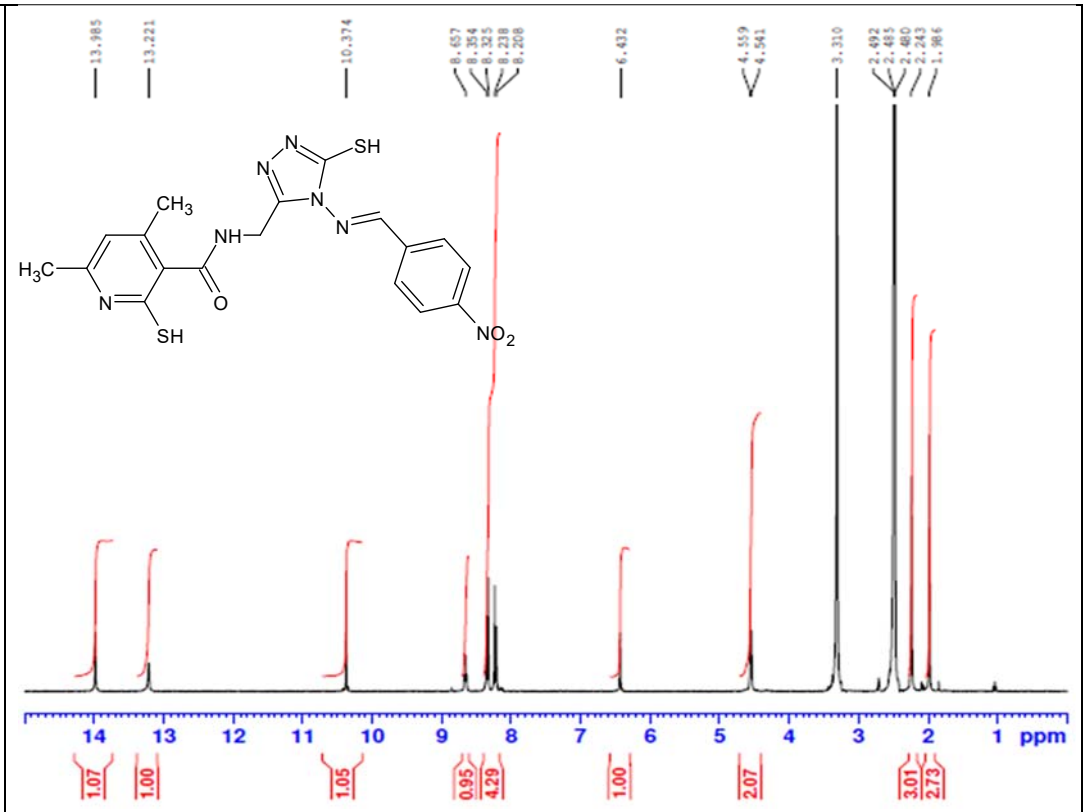

^{1}H NMR for 4g

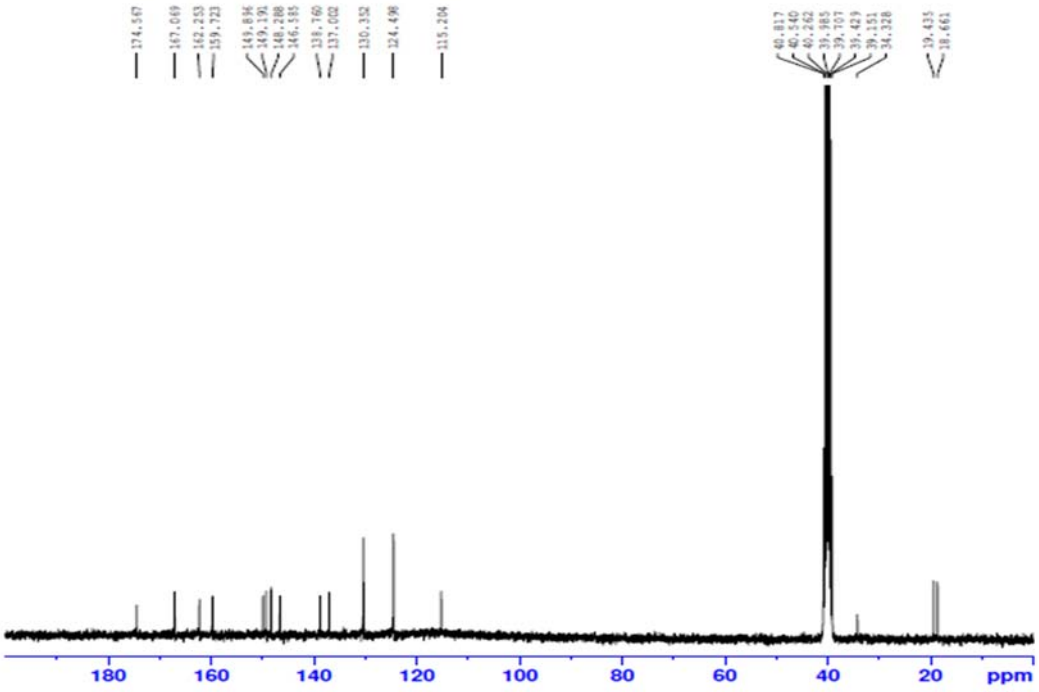

^{1}C NMR for 4g

4h

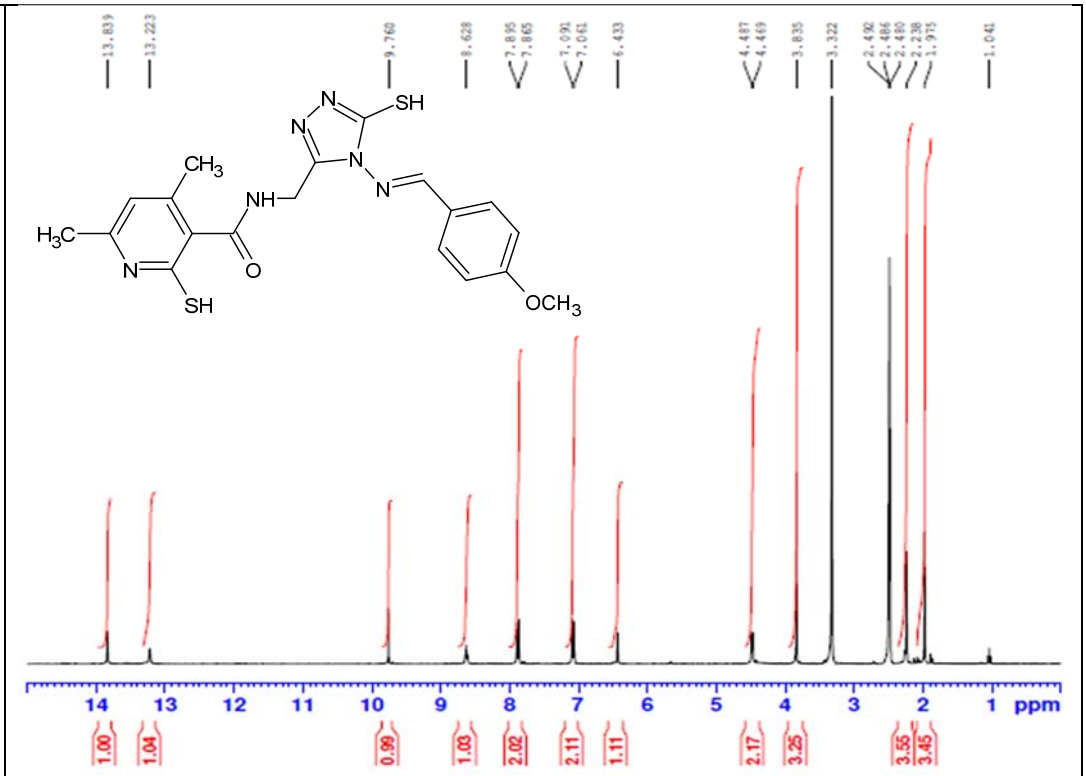

^{1}H NMR for 4h

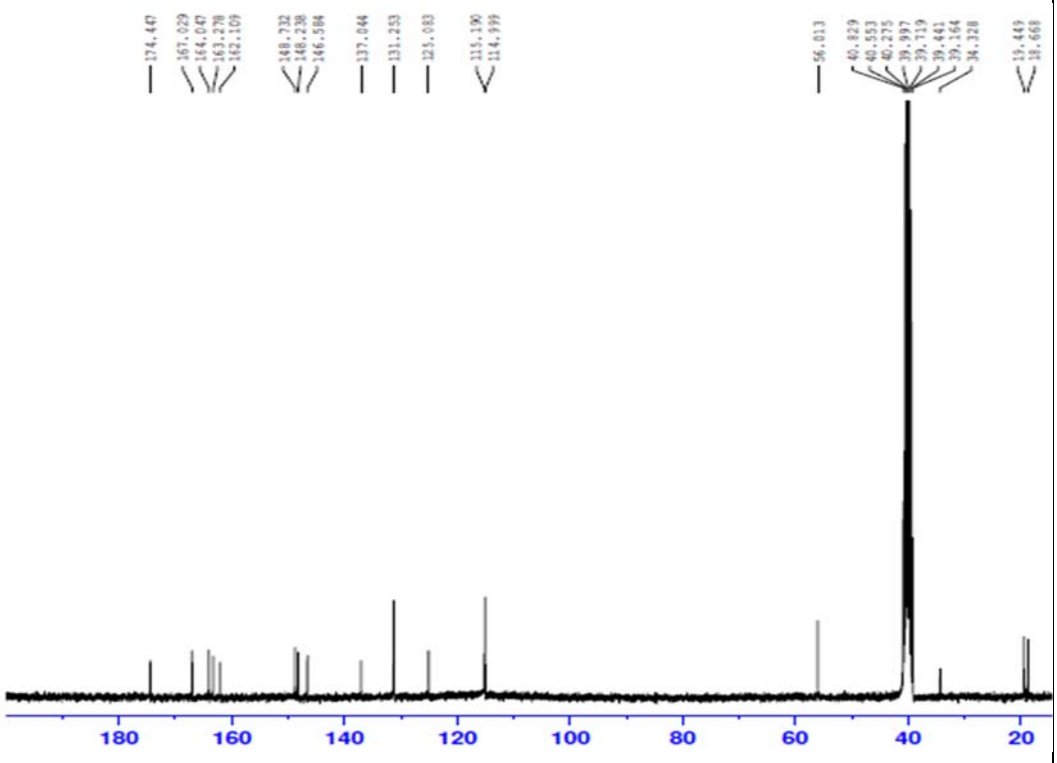

^{1}C NMR for 4h

4i	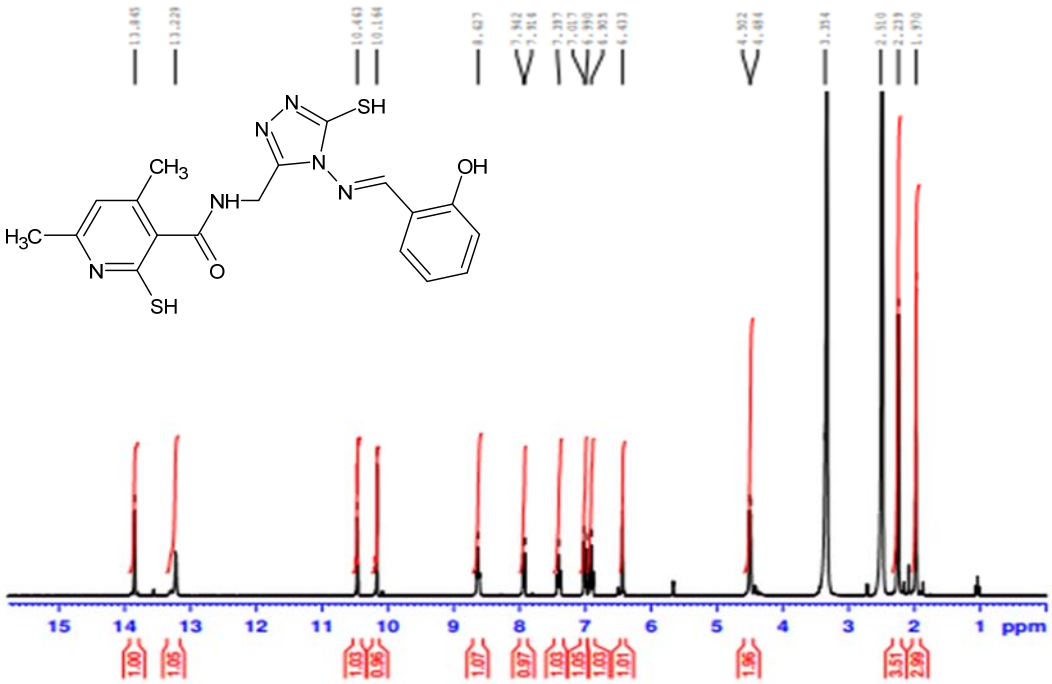 ^{1}H NMR for 4i 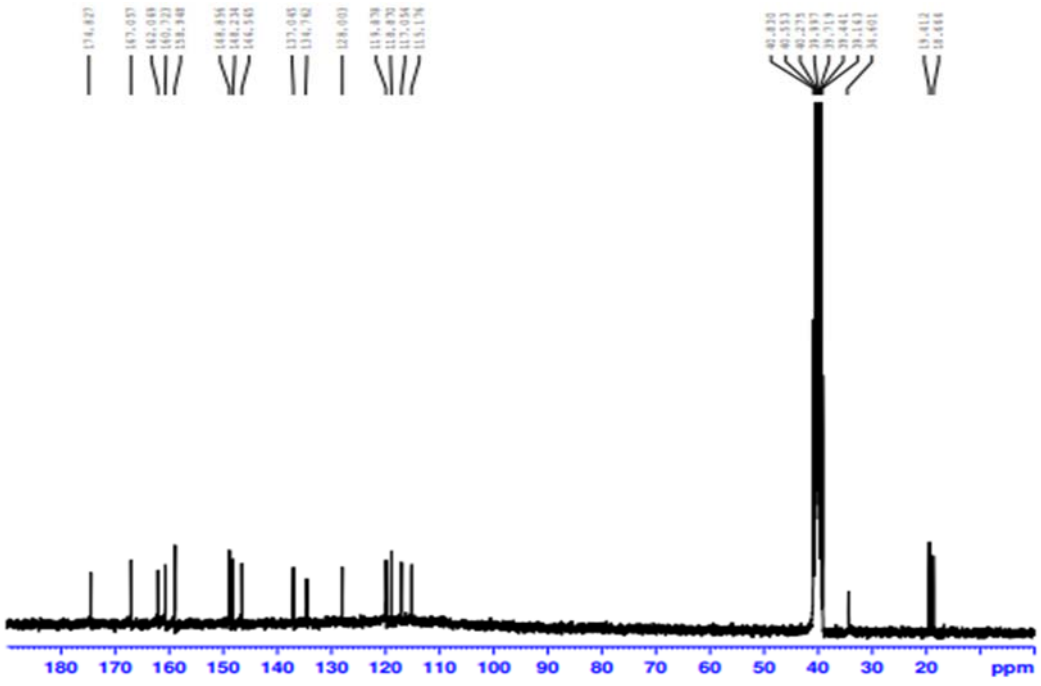 ^{1}C NMR for 4i

4j

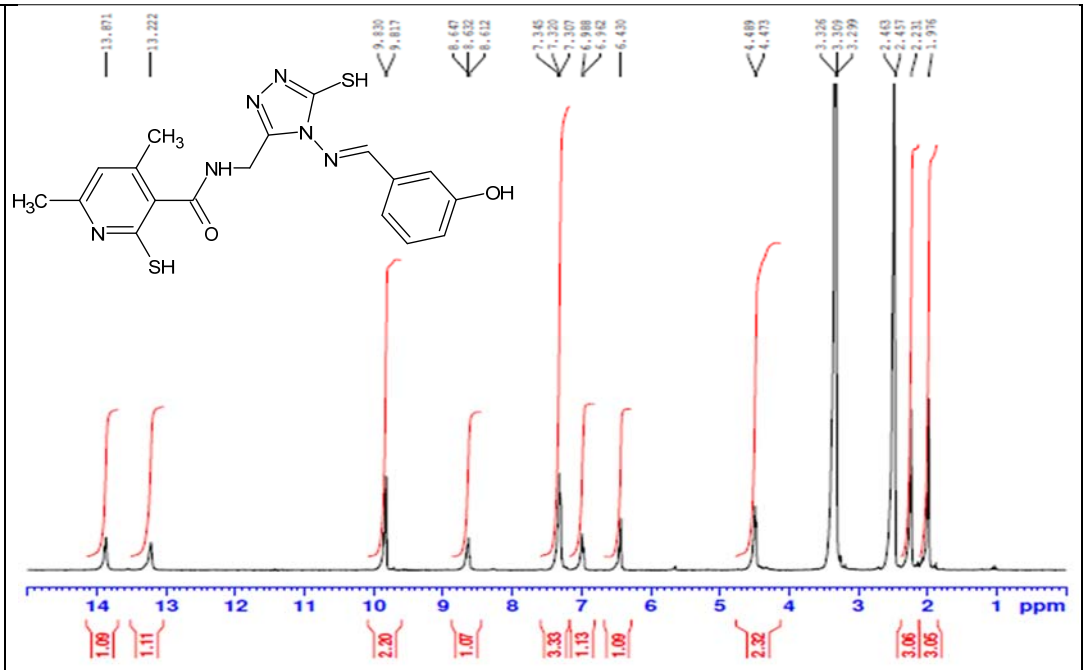

^{1}H NMR for 4j

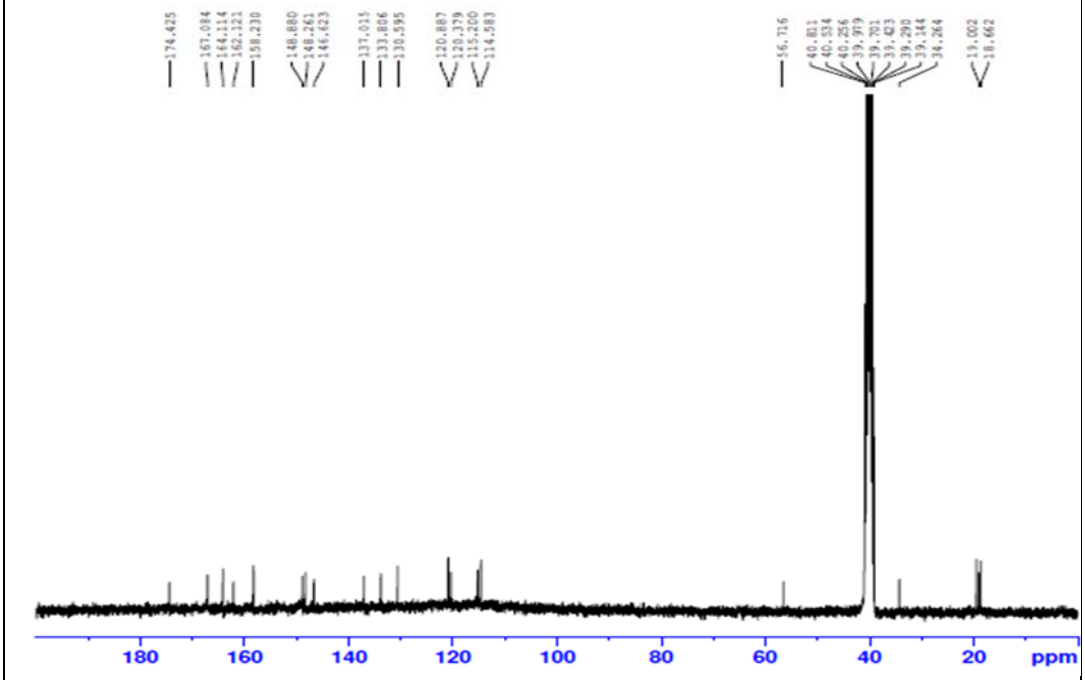

^{1}C NMR for 4j

4k

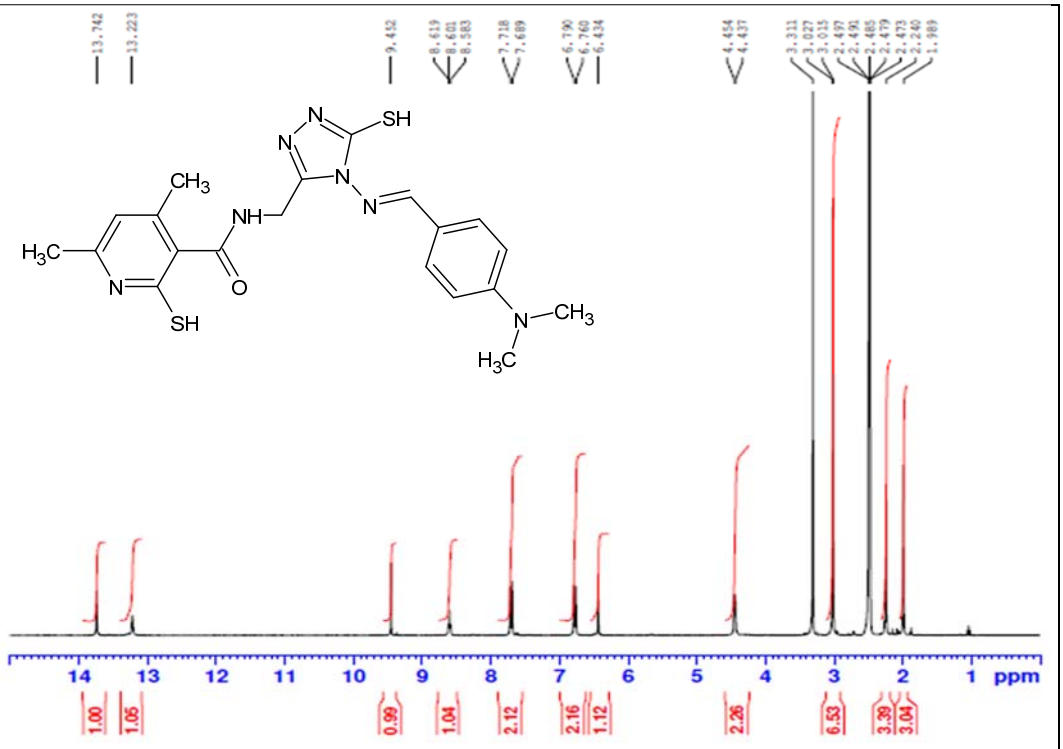

^{1}H NMR for 4k

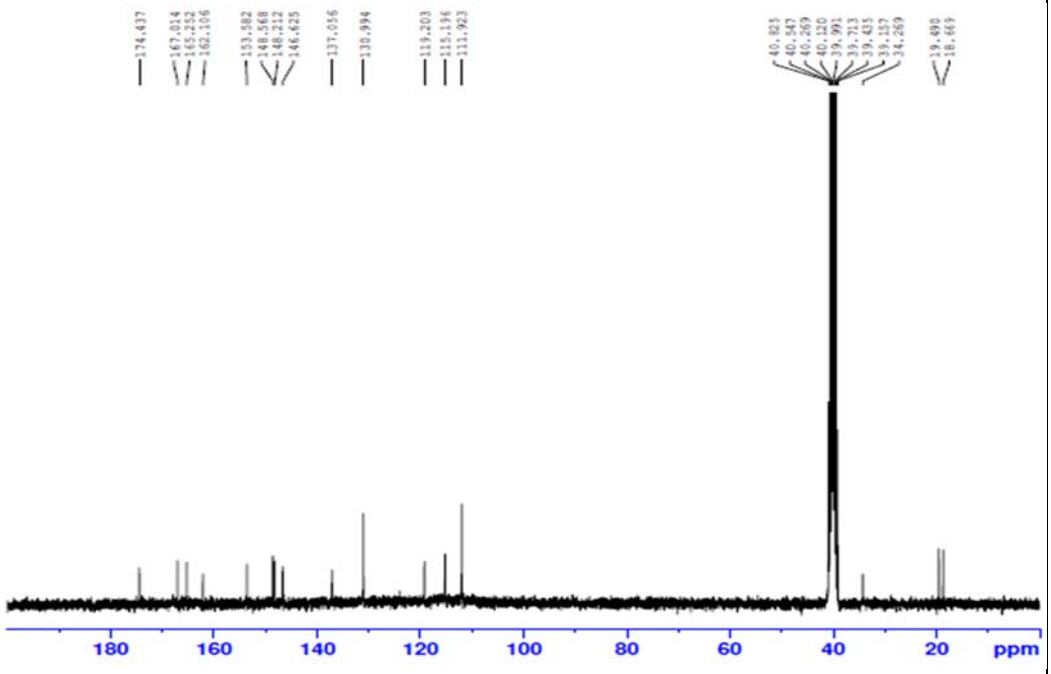

^{1}C NMR for 4k

41

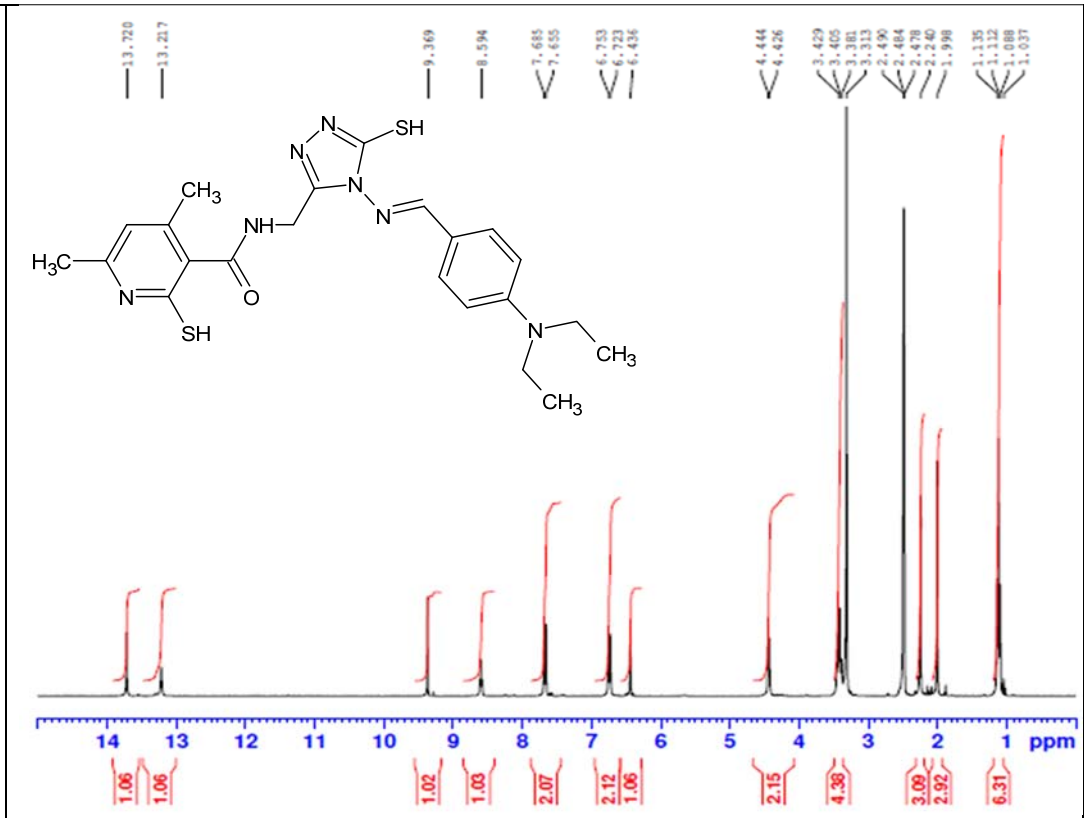

^{1}H NMR for 41

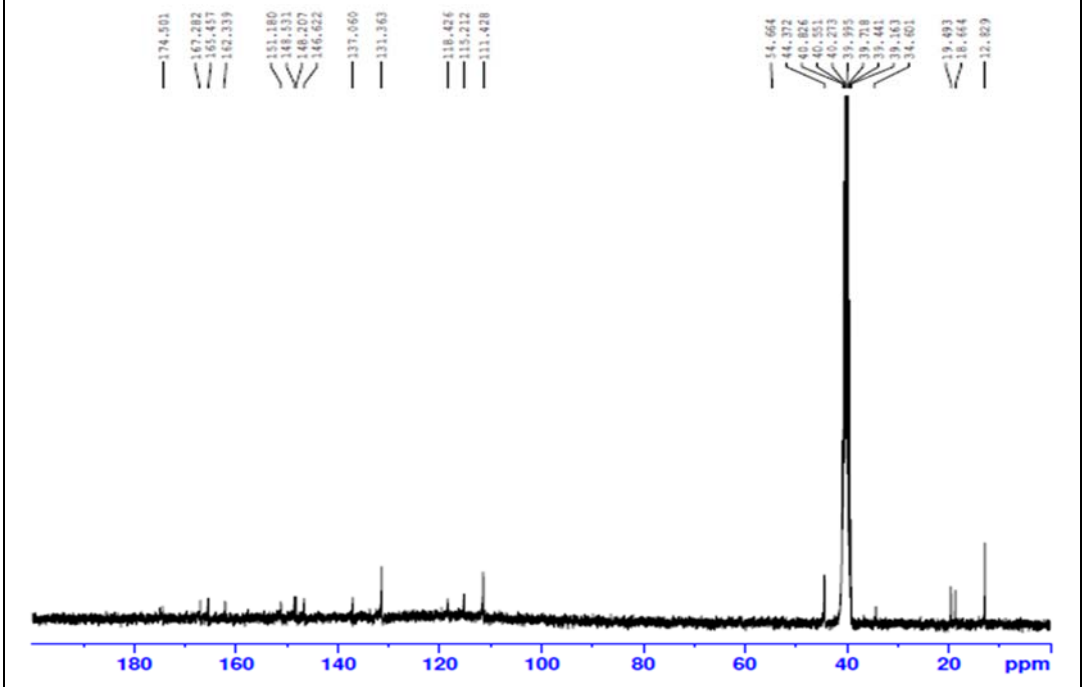

^{1}C NMR for 41

4m

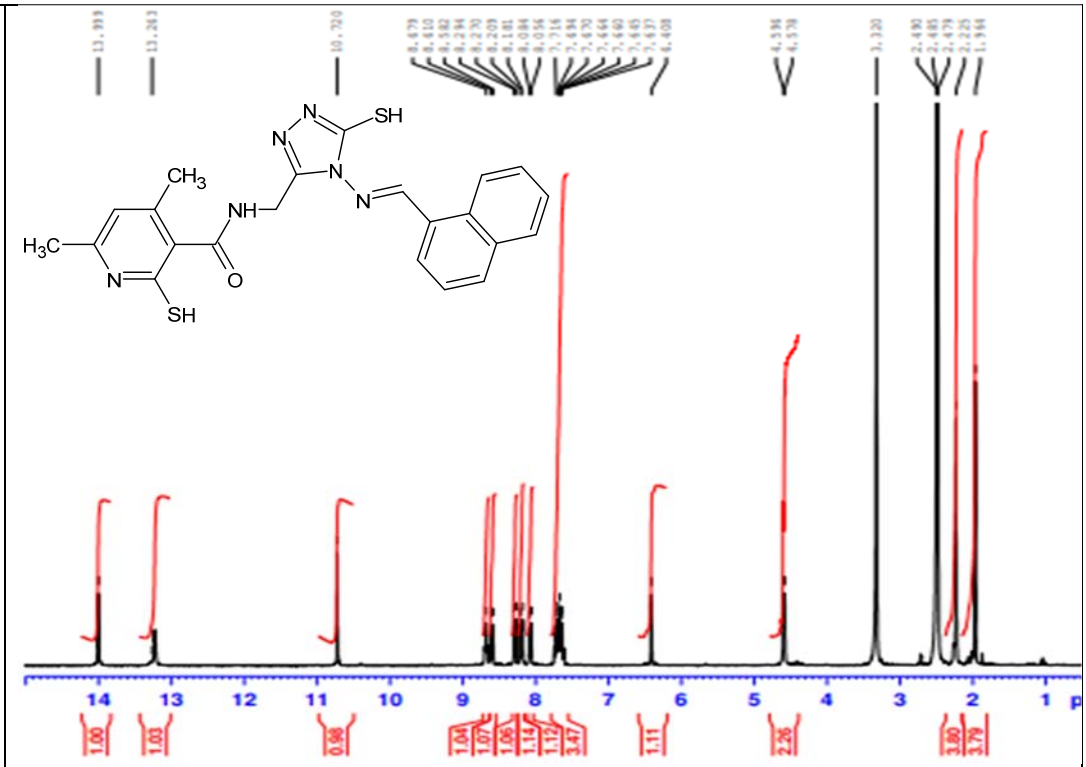

^{1}H NMR for 4m

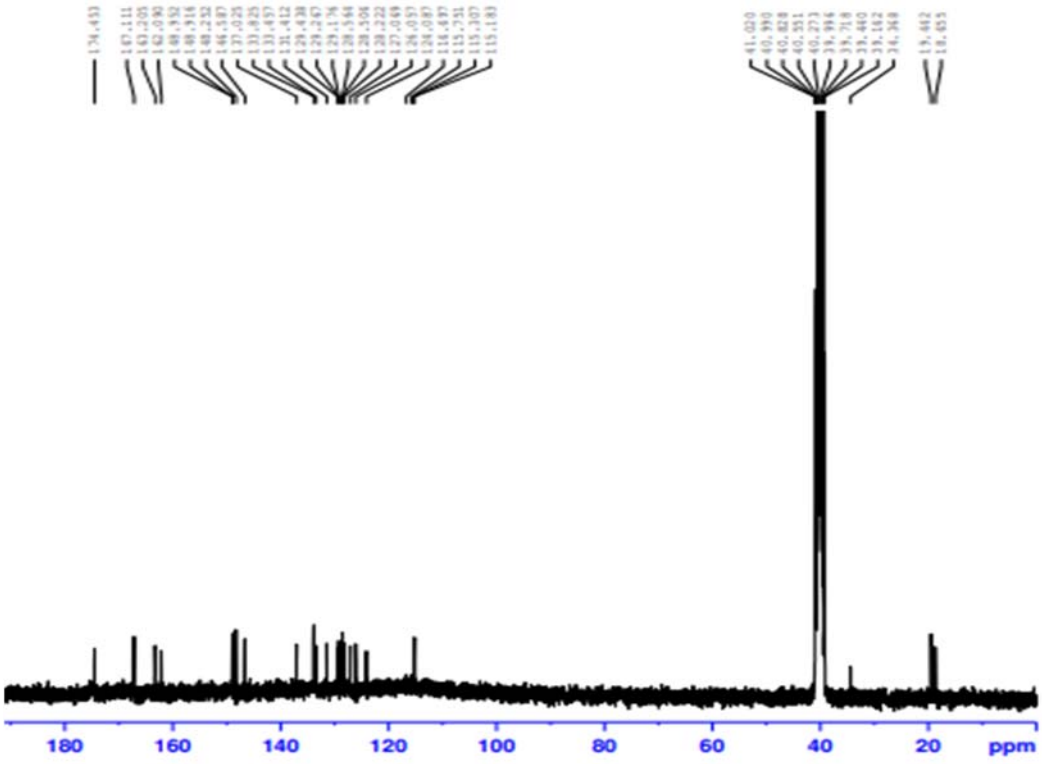

^{1}C NMR for 4m

4n

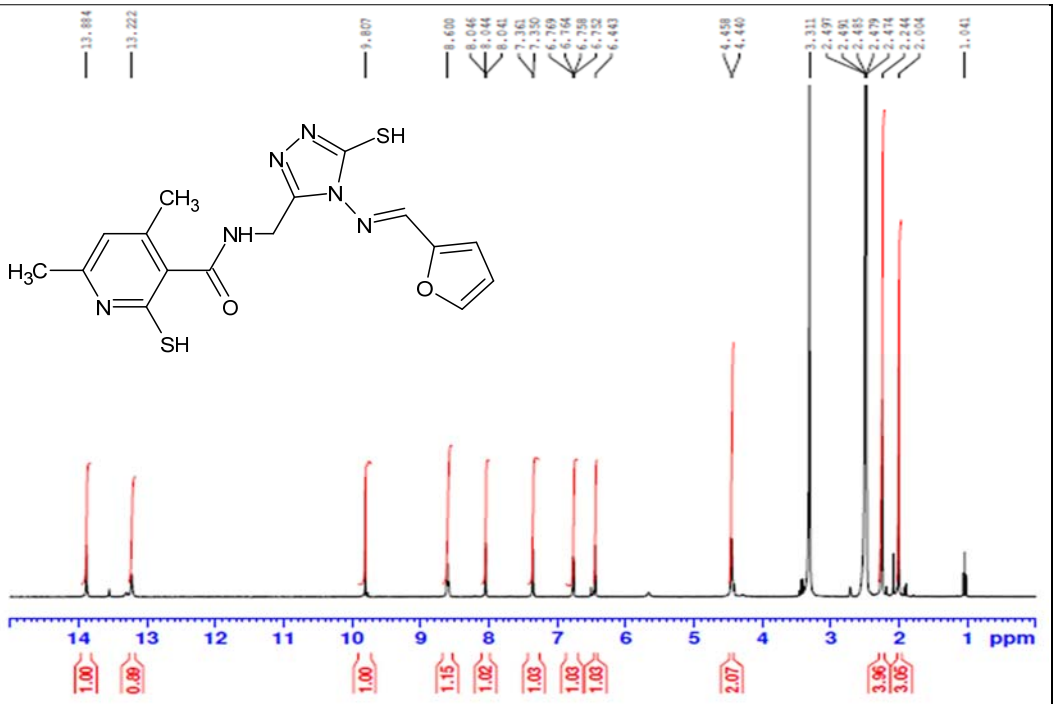

^{1}H NMR for 4n

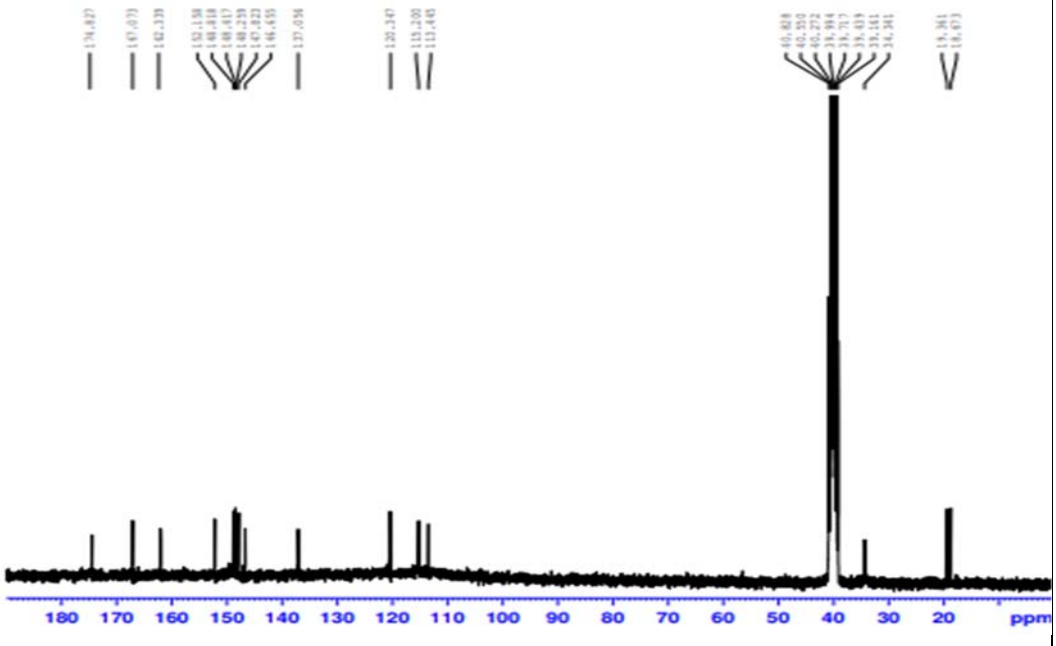

^{1}C NMR for 4n

Table S2. Visualizations of Fourier-Transform Infrared (FT-IR) spectra of compounds 3 and 4a-n.

Comp.	ATR-FTIR spectra
3	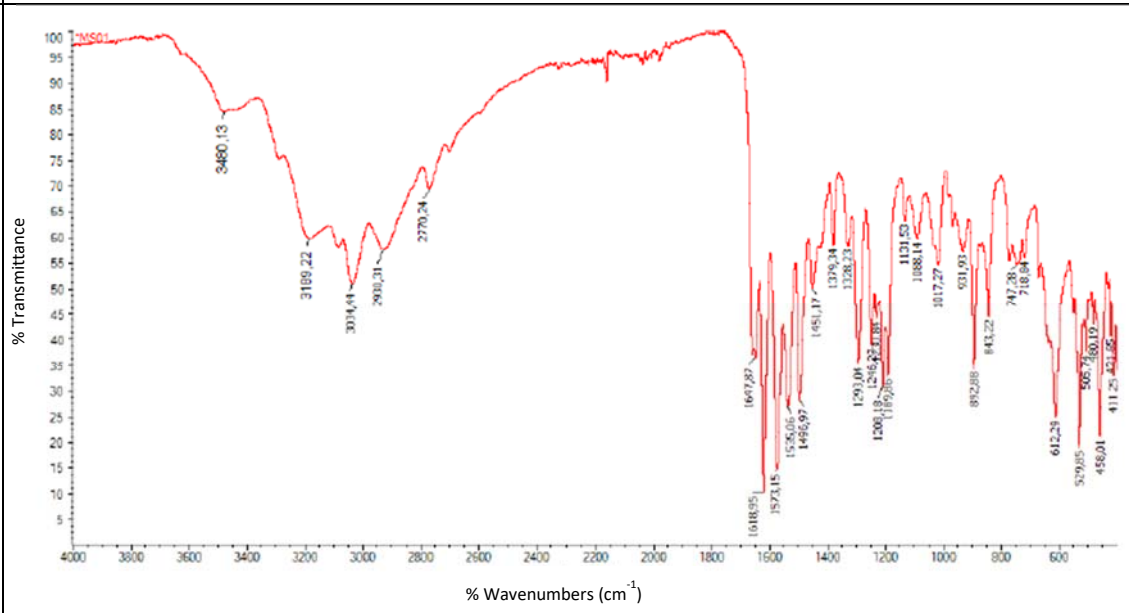
4a	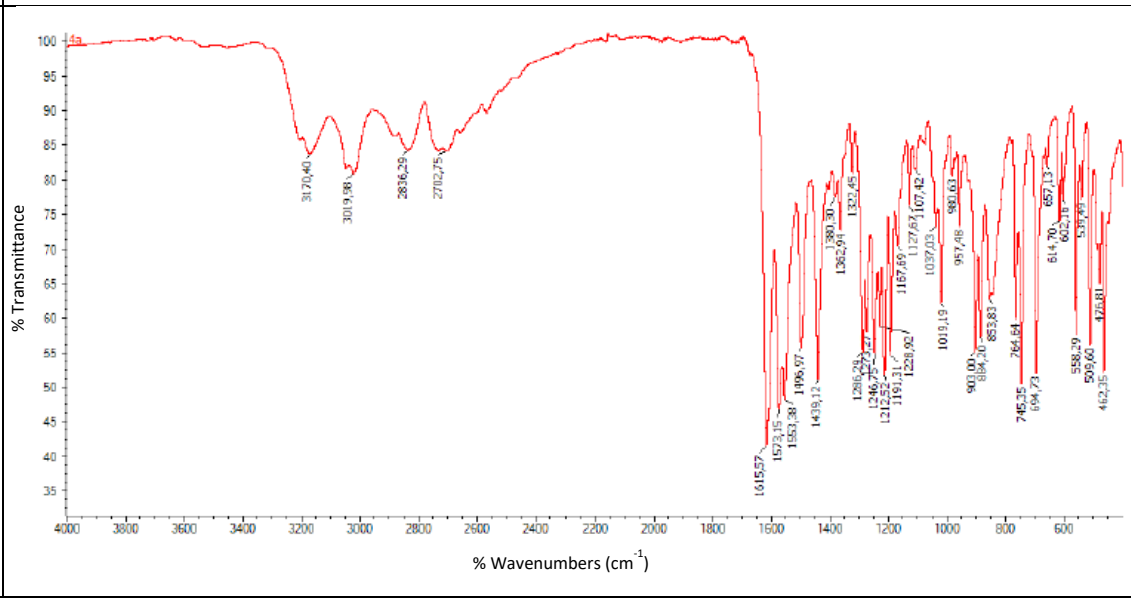

4b	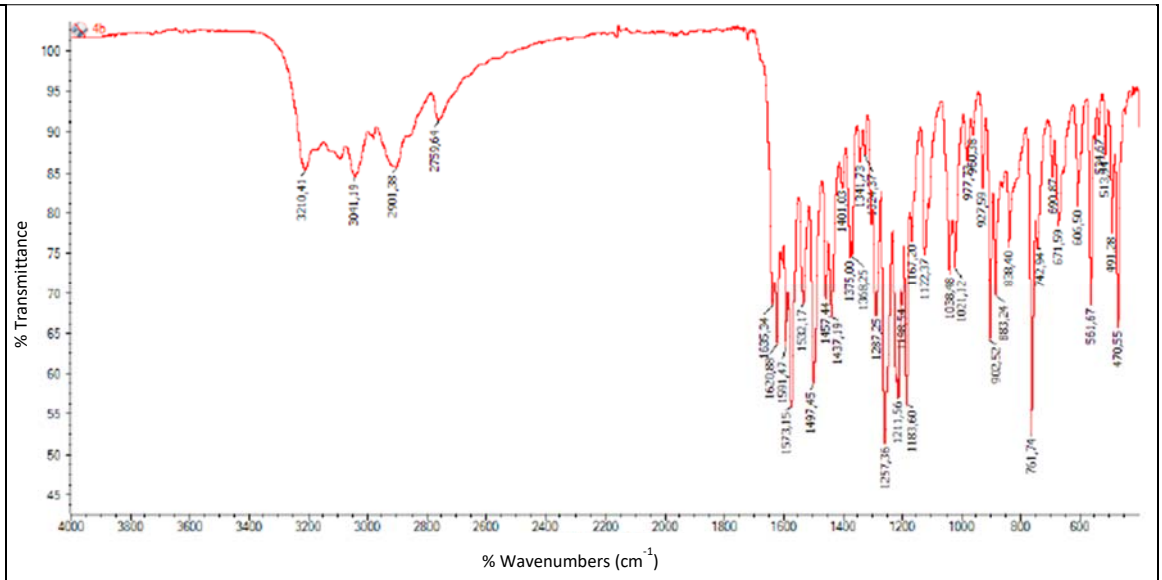 % Transmittance % Wavenumbers (cm-1)
4c	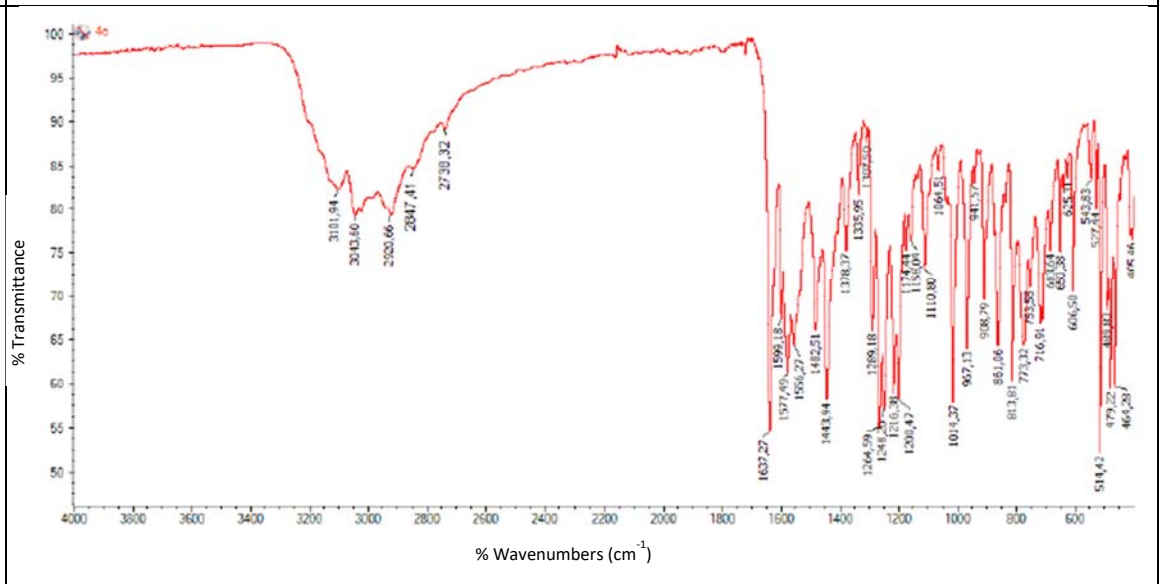 % Transmittance % Wavenumbers (cm-1)
4d	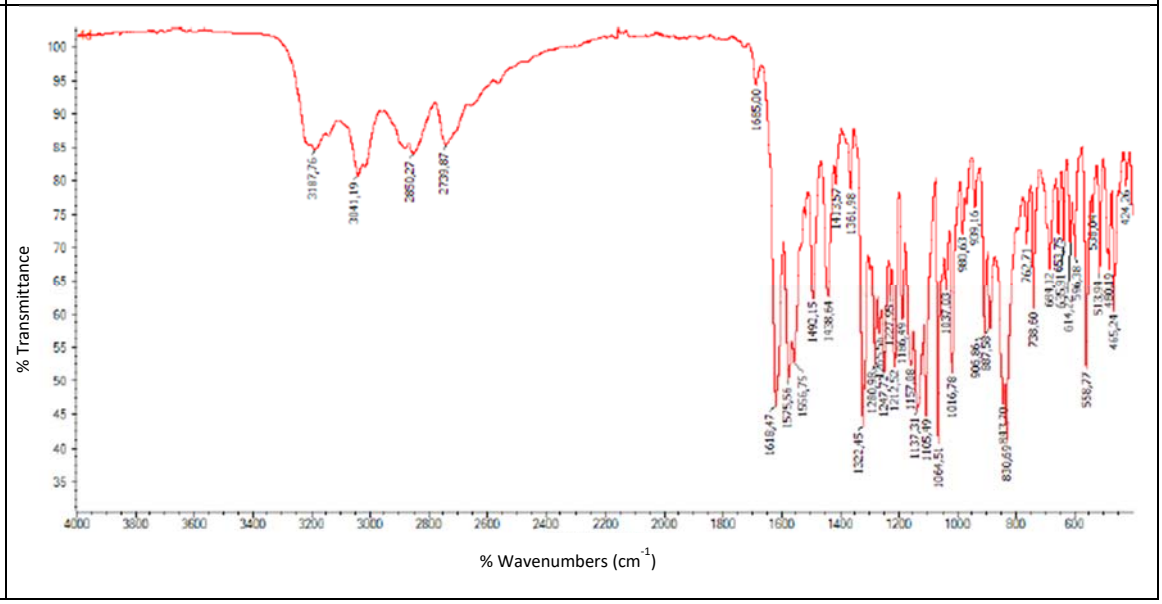 % Transmittance % Wavenumbers (cm-1)

4e	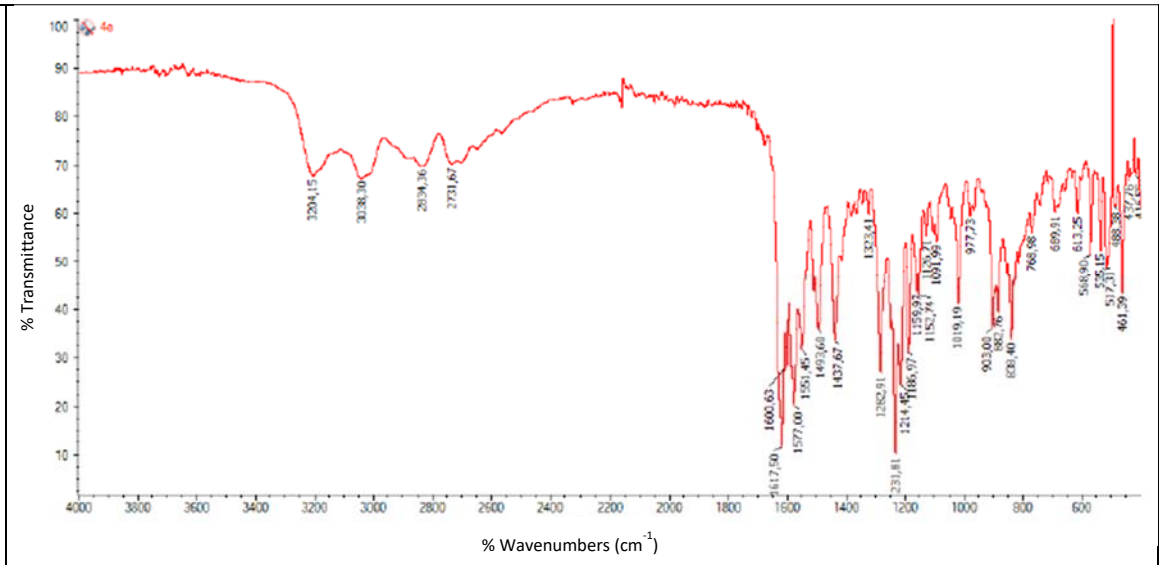 % Transmittance % Wavenumbers (cm-1)
4f	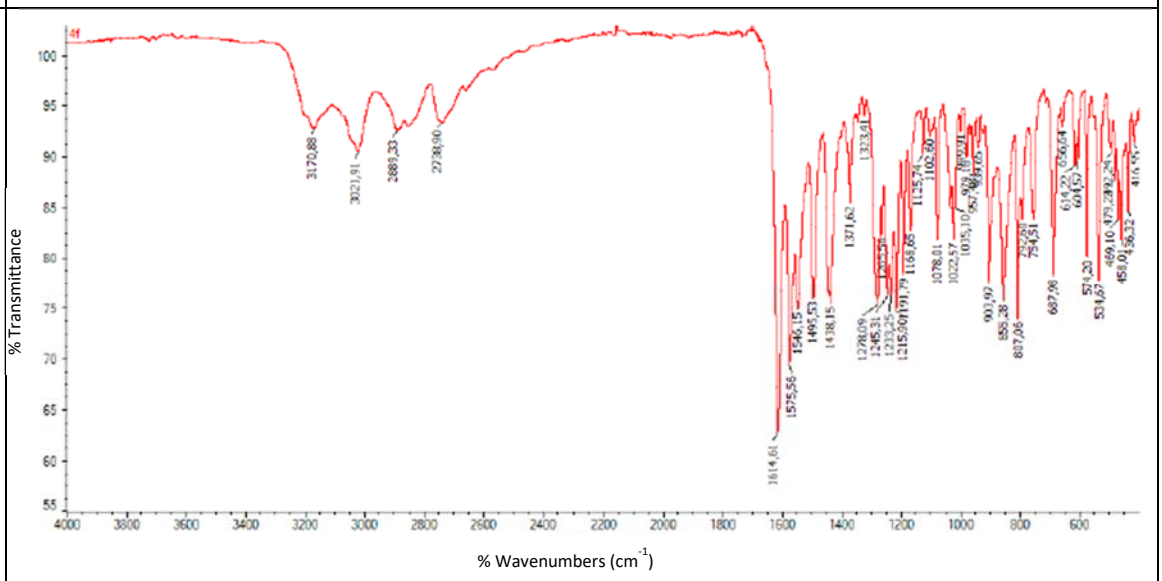 % Transmittance % Wavenumbers (cm-1)
4g	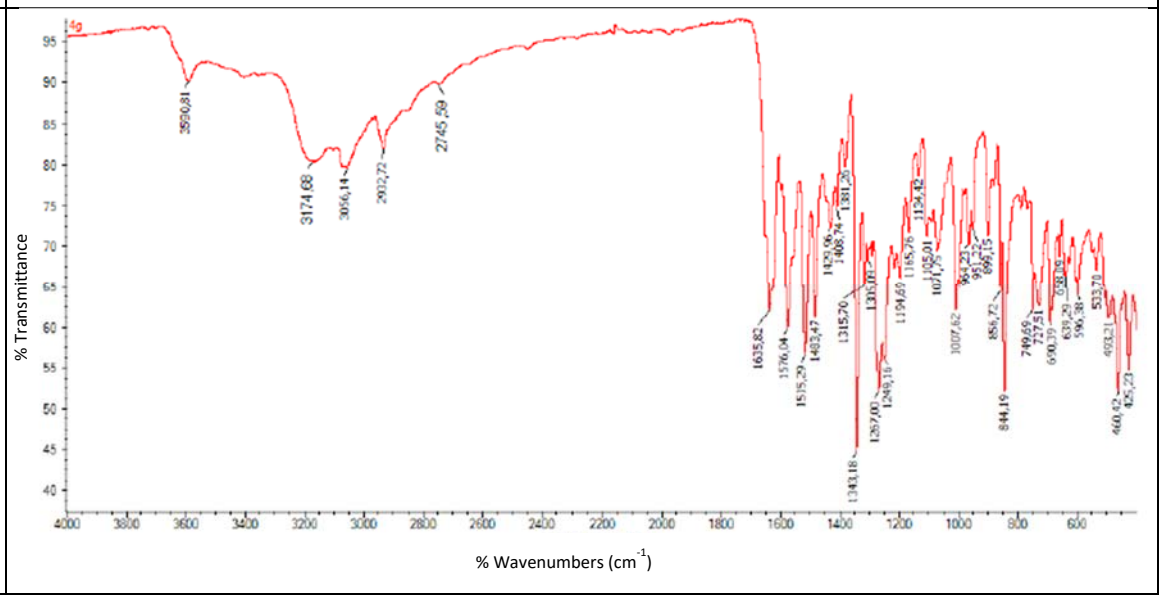 % Transmittance % Wavenumbers (cm-1)

4h	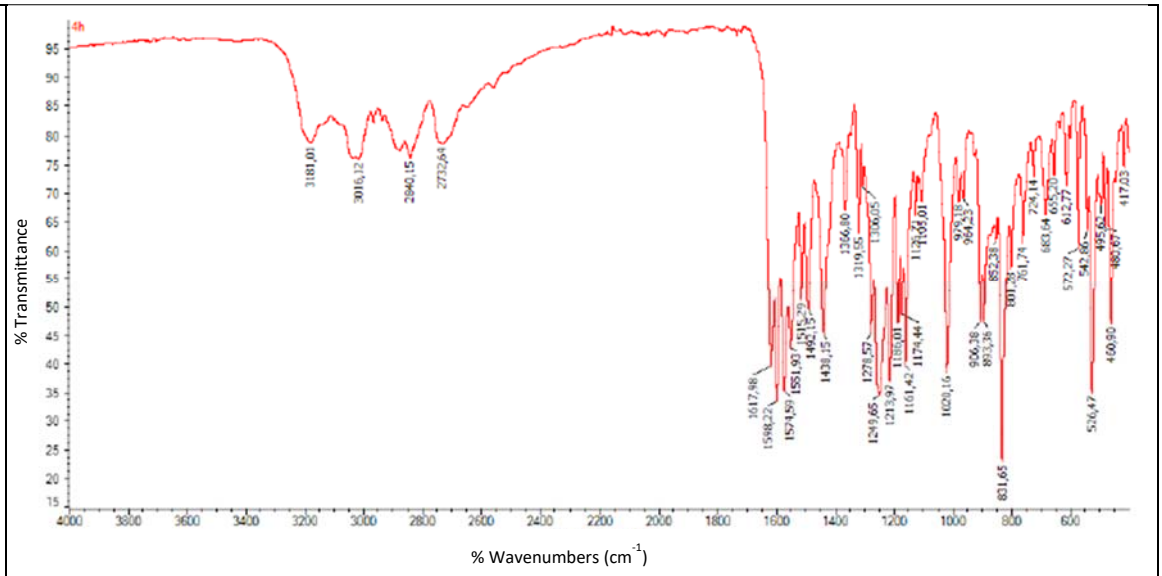 4h % Transmittance % Wavenumbers (cm-1)
4i	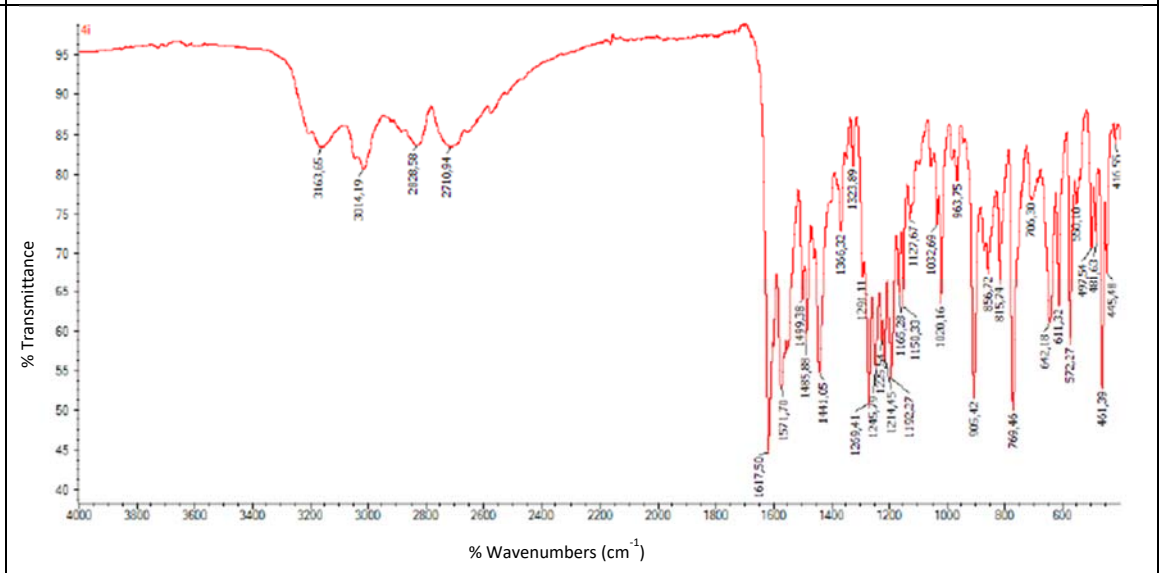 4i % Transmittance % Wavenumbers (cm-1)
4j	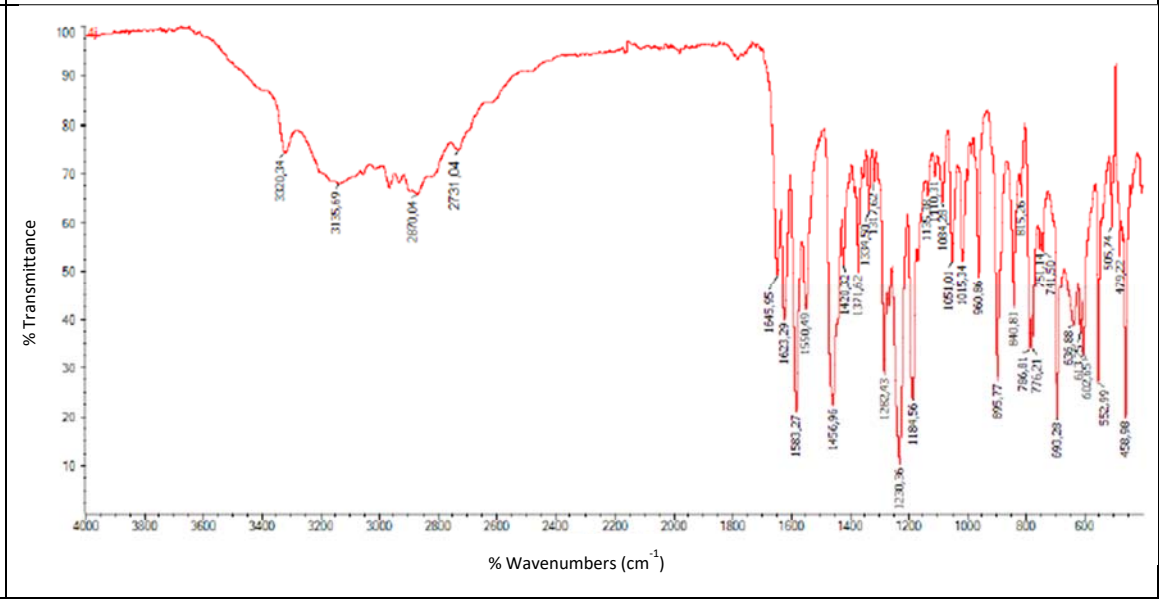 4j % Transmittance % Wavenumbers (cm-1)

4k	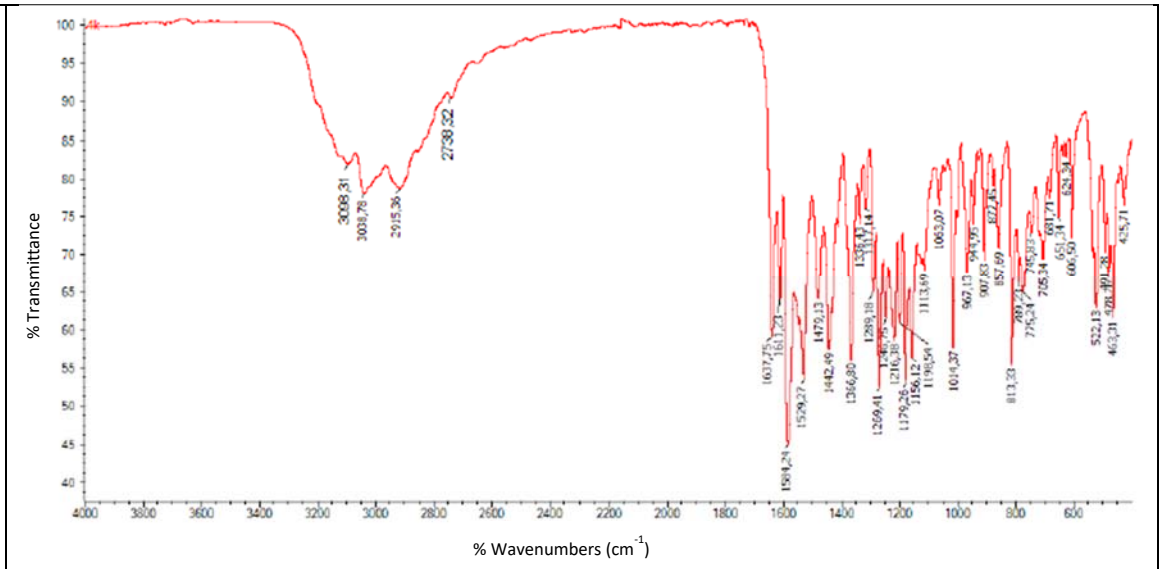 % Transmittance % Wavenumbers (cm-1)
4l	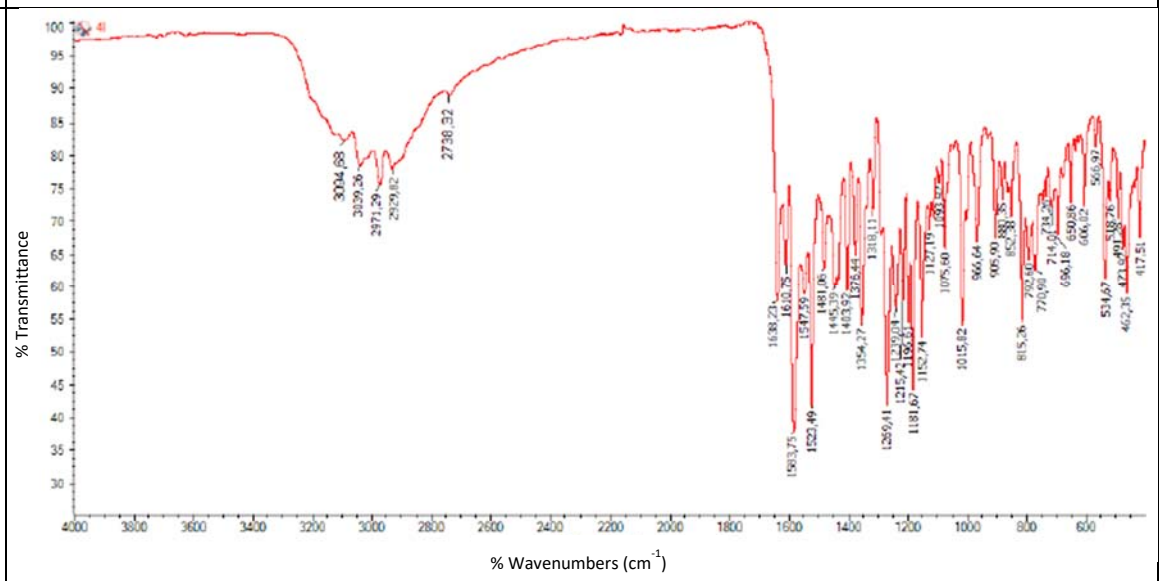 % Transmittance % Wavenumbers (cm-1)
4m	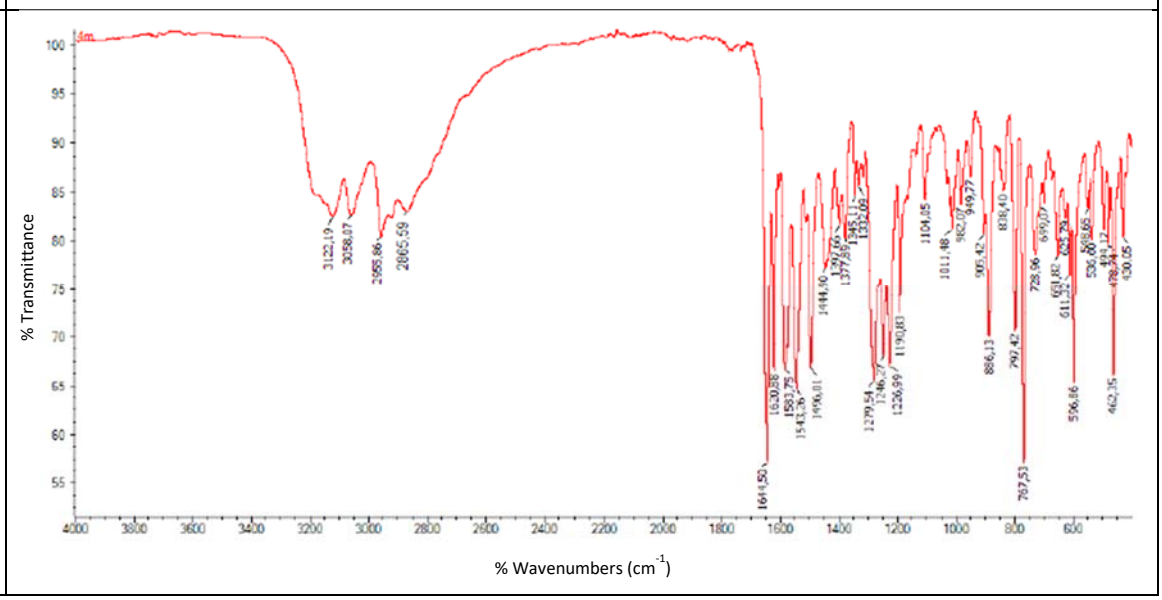 % Transmittance % Wavenumbers (cm-1)

4n	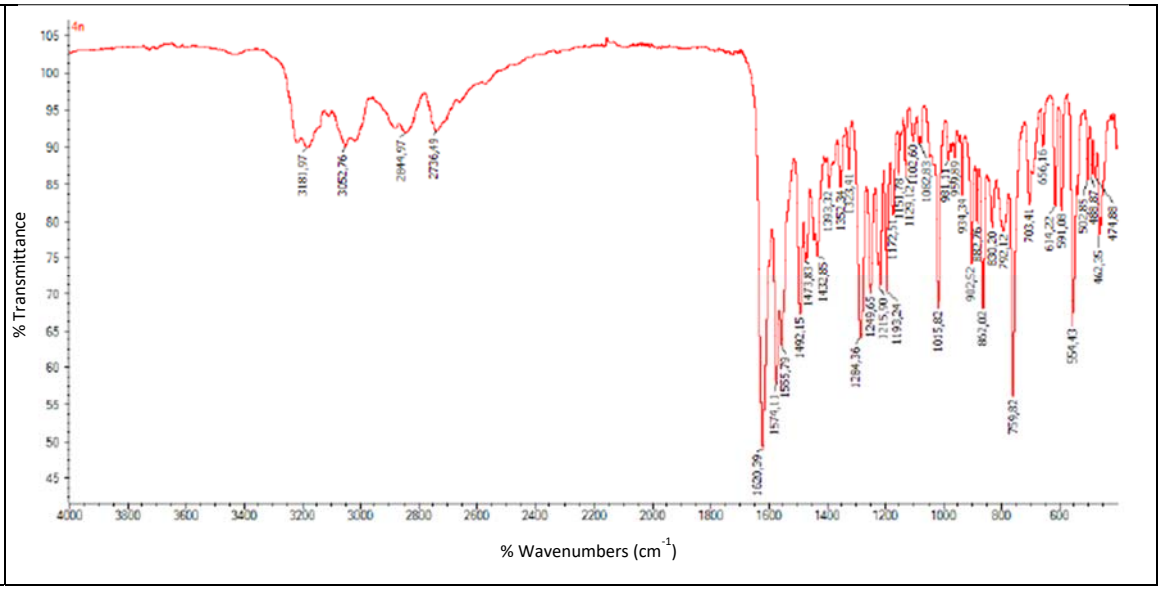

Table S3. Visualizations of High Resolution Mass Spectrometry (HRMS) spectra of compounds 4a-m.

Comp.	HRMS spectra
4a	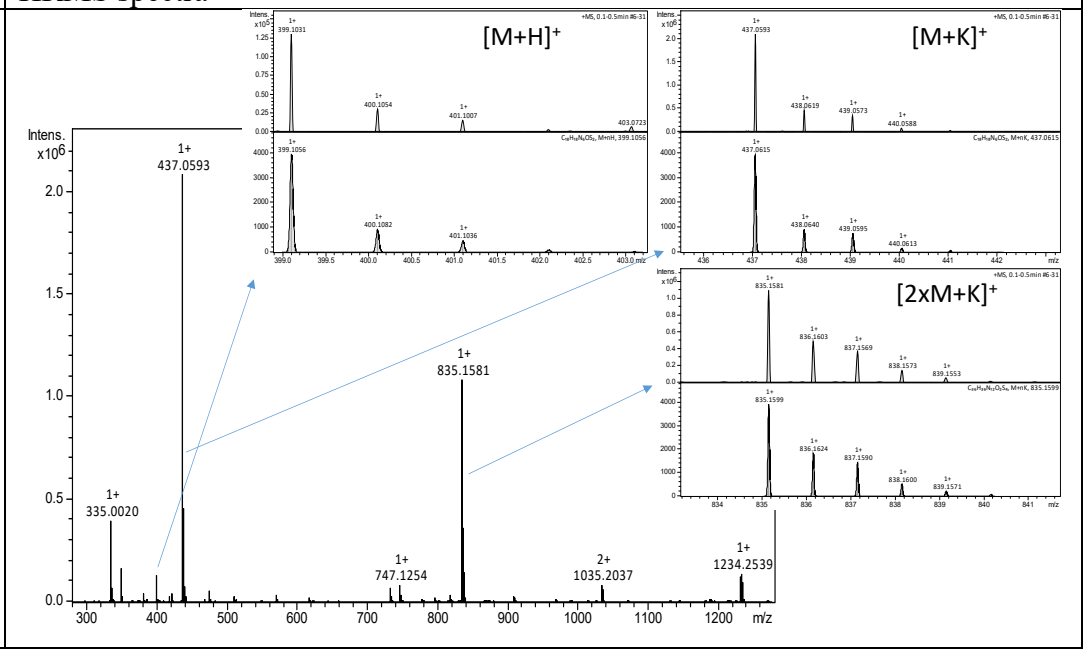

4b

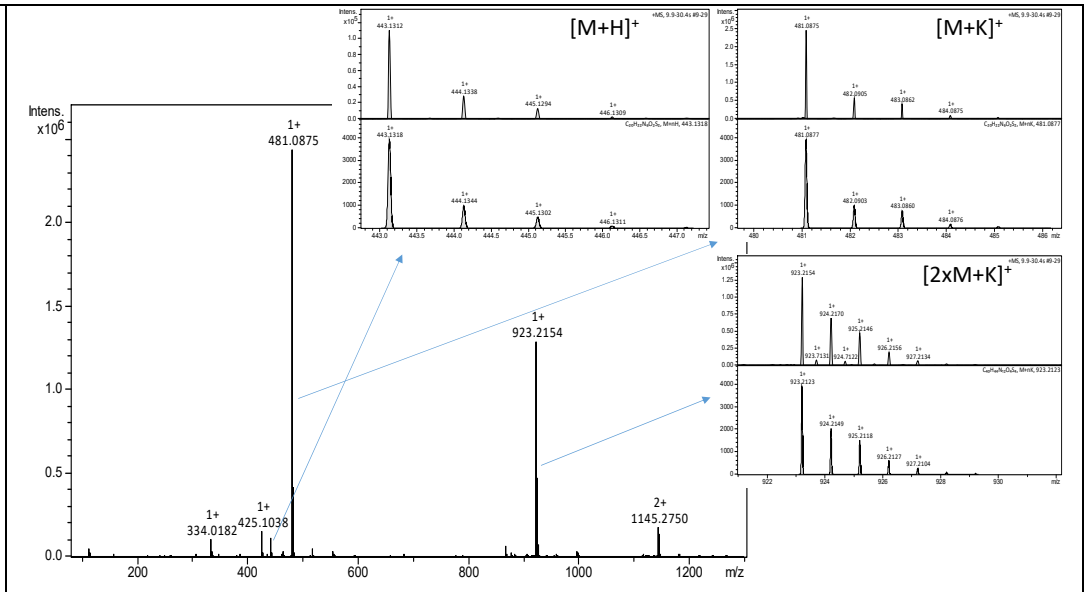
[M+H]+
[M+K]+
[2xM+K]+
Intens.
x10^6
1+
481.0875
1+
923.2154
1+
334.0182
1+
425.1038
2+
1145.2750
m/z

4c

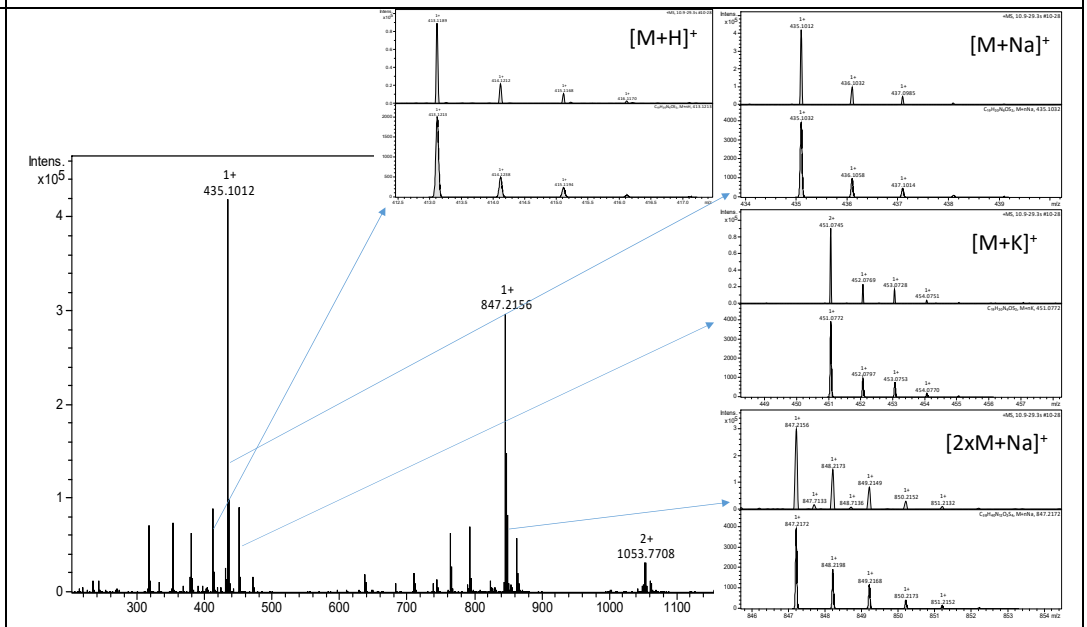
[M+H]+
[M+Na]+
[M+K]+
[2xM+Na]+
Intens.
x10^5
1+
435.1012
1+
847.2156
2+
1053.7708

4d

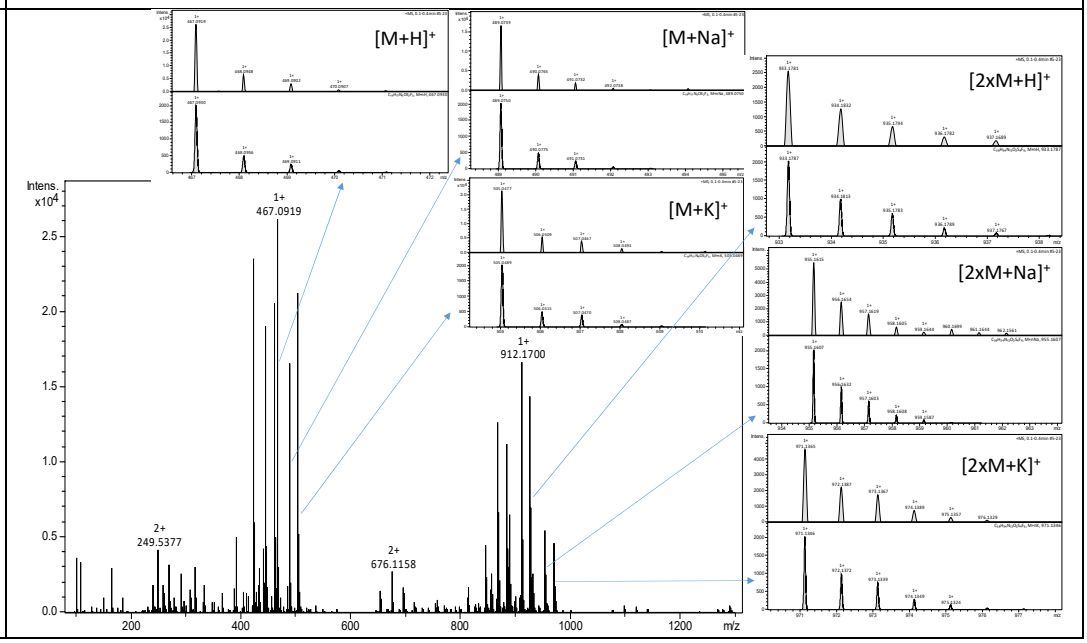
[M+H]+
[M+Na]+
[M+K]+
[2xM+H]+
[2xM+Na]+
[2xM+K]+
Intens.
x10^4
1+
467.0919
1+
912.1700
2+
249.5377
2+
676.1158
m/z

4e

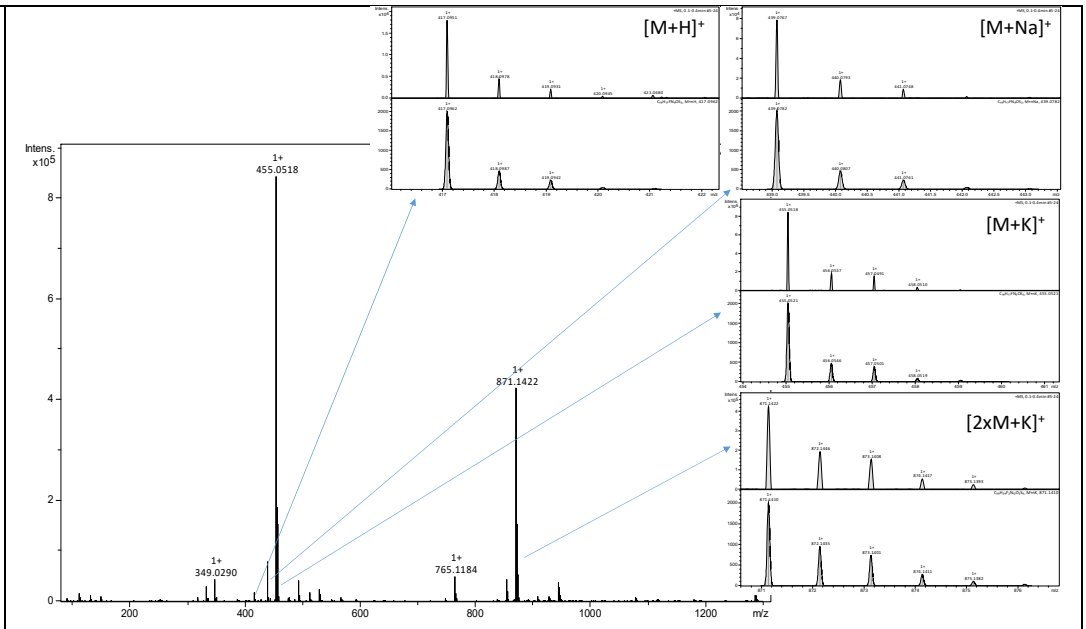
[M+H]+
[M+Na]+
[M+K]+
[2xM+K]+
Intens.
x10^5
1+
455.0518
1+
871.1422
1+
349.0290
1+
765.1184
m/z

4f

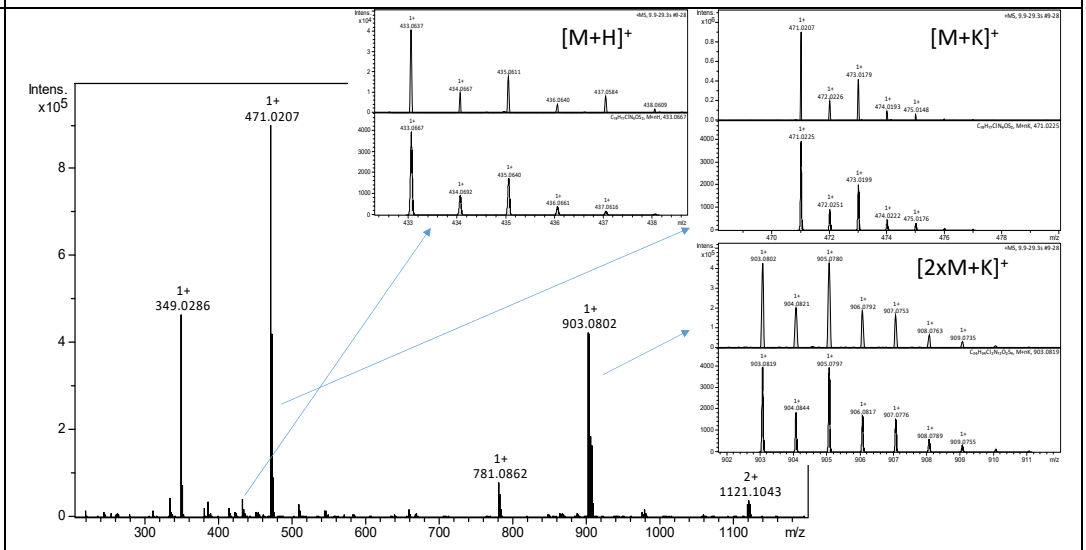
[M+H]+
[M+K]+
[2xM+K]+
Intens.
x10^5
1+
471.0207
1+
349.0286
1+
903.0802
1+
781.0862
2+
1121.1043
m/z

4g

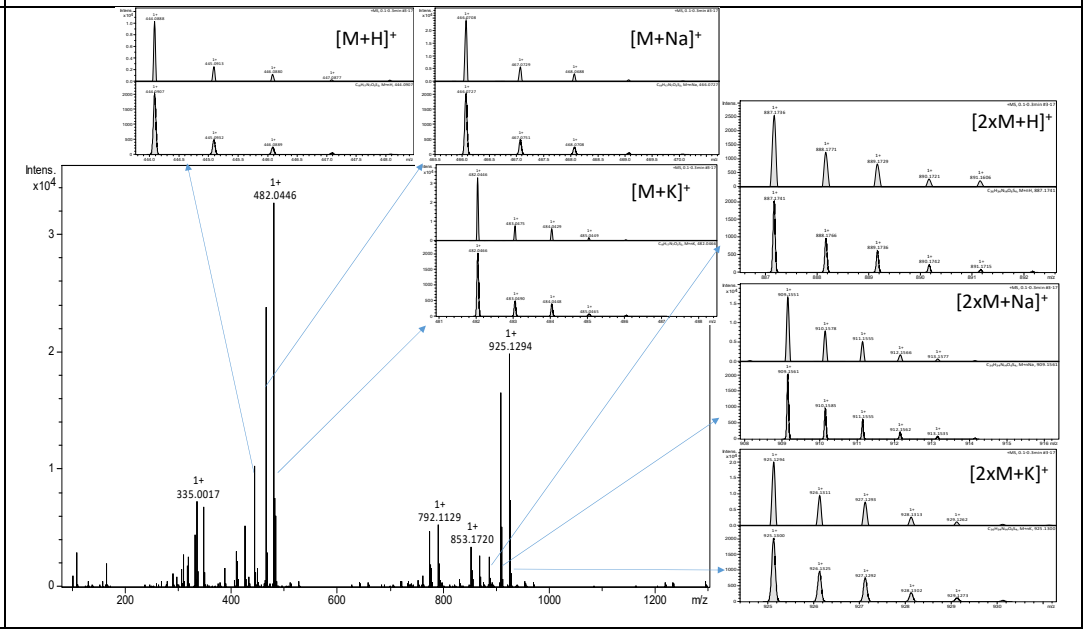
[M+H]+
[M+Na]+
[M+K]+
[2xM+H]+
[2xM+Na]+
[2xM+K]+
Intens.
x10^4
1+
482.0446
1+
925.1294
1+
335.0017
1+
792.1129
1+
853.1720
m/z

4h

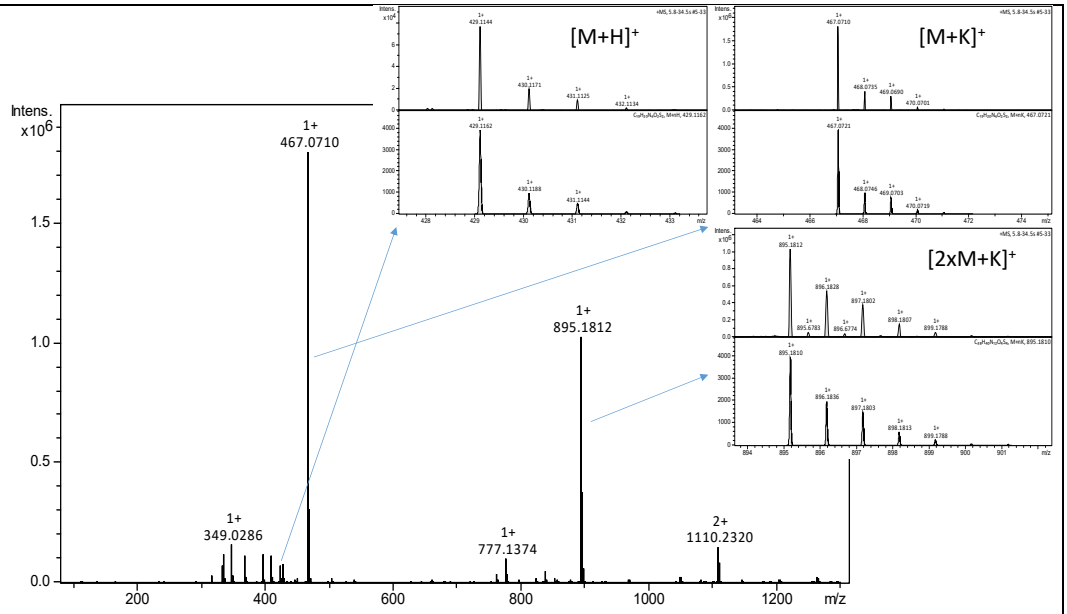
Intens.
x10^6
1+
467.0710
1+
895.1812
1+
349.0286
1+
777.1374
2+
1110.2320
m/z
[M+H]+
[M+K]+
[2xM+K]+

4i

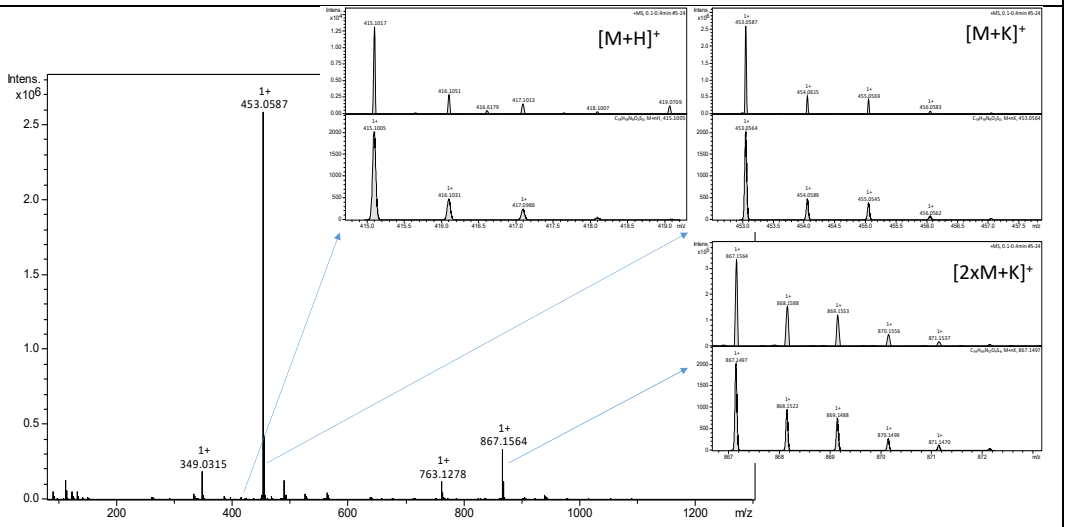
Intens.
x10^6
1+
453.0587
1+
349.0315
1+
763.1278
1+
867.1564
m/z
[M+H]+
[M+K]+
[2xM+K]+

4j

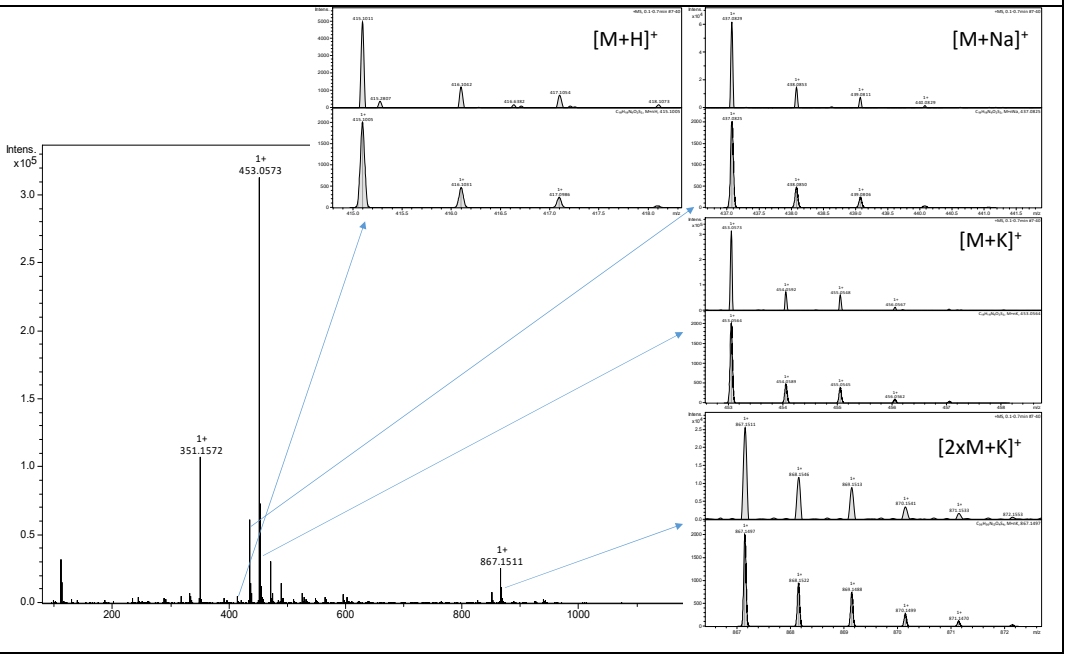
Intens.
x10^5
1+
453.0573
1+
351.1572
1+
867.1511
[M+H]+
[M+Na]+
[M+K]+
[2xM+K]+

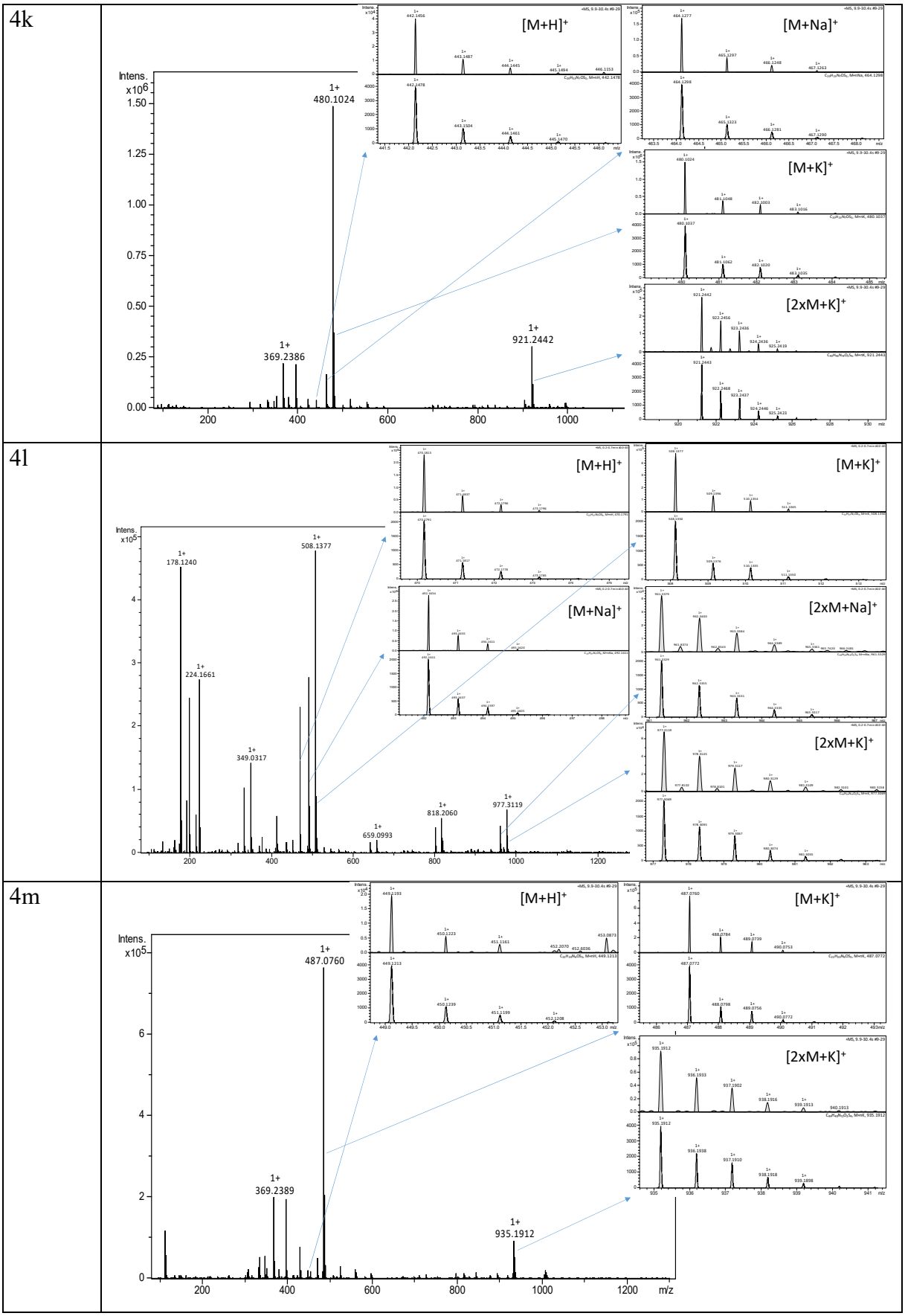
4k
Intens.
x10^6
1.50
1.25
1.00
0.75
0.50
0.25
0.00
1+
480.1024
1+
369.2386
1+
921.2442
200
400
600
800
1000
[M+H]+
[M+Na]+
[M+K]+
[2xM+K]+
4l
Intens.
x10^5
1+
178.1240
1+
508.1377
1+
224.1661
1+
349.0317
1+
659.0993
1+
818.2060
1+
977.3119
0
1
2
3
4
200
400
600
800
1000
1200
[M+H]+
[M+K]+
[M+Na]+
[2xM+Na]+
[2xM+K]+
4m
Intens.
x10^5
1+
487.0760
1+
369.2389
1+
935.1912
0
2
4
6
200
400
600
800
1000
1200
m/z
[M+H]+
[M+K]+
[2xM+K]+

4n	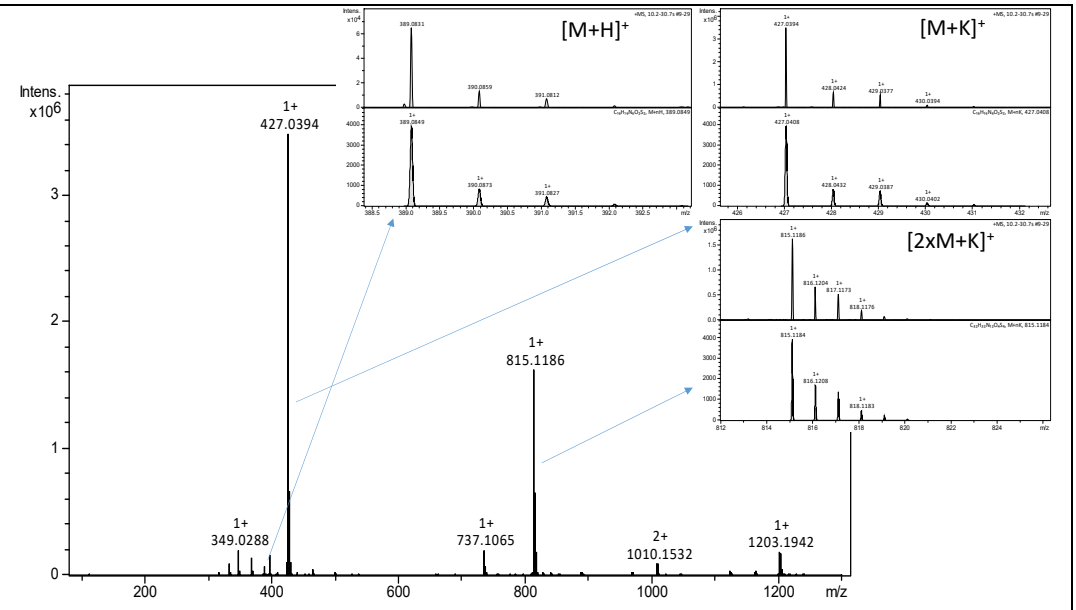

Table S4. Rhodamine-123 assay for compounds 4d, 4e, and 4l.

Compounds [50 µM]	Fluorescence (a.u.)					
	HT-29		LoVo		LoVo/DX	
	mean	SD	mean	SD	mean	SD
Control	28516.00	487	36713.00	287	3420.00	98
4d	54750.72	431	128495.50	462	16074.00	164
4e	65586.80	621	117481.60	832	12312.00	351
4l	52184.28	563	143180.70	425	17442.00	231
Verapamil	31306.00	612	46992.00	452	22492.20	581

Table S5. Detection of apoptosis for compounds 4d, 4e, and 4l.

Compounds [1 µM]	HT29				
	Live cells	Apoptotic cells		Necrotic cells	
	Mean [%]	Mean [%]	SD	Mean [%]	SD
Control	90.87	6.73	0.95	2.40	1.10
4d	46.35	41.95	5.67	11.70	2.20
4e	56.67	36.73	2.74	6.70	0.62
4l	39.00	50.60	3.60	10.40	1.50
Doxorubicin	14.55	68.75	2.90	16.70	1.30

OŚWIADCZENIA WSPÓŁAUTORÓW

PUBLIKACJI P1, P2 I P3

Wrocław, 9.02.2024r.
(miejscowość, data)

Mgr Małgorzata Strzelecka
(tytuł, imię i nazwisko)

Katedra i Zakład Chemii Leków
Wydział Farmaceutyczny
Uniwersytet Medyczny im. Piastów Śląskich we Wrocławiu
ul. Borowska 211a, 50-556 Wrocław
(miejsce zatrudnienia)

OŚWIADCZENIE AUTORA

Oświadczam, że w pracach:

1. Piotr Świątek, Teresa Glomb, Agnieszka Dobosz, Tomasz Gębarowski, Kamil Wojtkowiak, Aneta Jezierska, Jarosław J. Panek, Małgorzata Świątek, Małgorzata Strzelecka, 2022, Biological Evaluation and Molecular Docking Studies of Novel 1,3,4-Oxadiazole Derivatives of 4,6-Dimethyl-2-sulfanylpyridine-3-carboxamide. International Journal of Molecular Sciences, 23, art. 549.

(autorzy, rok wydania, tytuł, czasopismo lub wydawca, tom, strony)

mój udział polegał na: współopracowaniu koncepcji i planu wykonywanych badań, zsyntetyzowaniu tytułowych związków oraz potwierdzeniu ich tożsamości metodami spektralnymi, interpretacji oraz opisaniu wyników przeprowadzonych badań, współtworzeniu początkowej wersji manuskryptu oraz redagowaniu wersji finalnej, uwzględniającej sugestie recenzentów;

2. Małgorzata Strzelecka, Teresa Glomb, Małgorzata Drąg-Zalesińska, Julita Kulbacka, Anna Szewczyk, Jolanta Saczko, Paulina Kasperkiewicz-Wasilewska, Nina Rembiałkowska, Kamil Wojtkowiak, Aneta Jezierska, Piotr Świątek, 2022, Synthesis, Anticancer Activity and Molecular Docking Studies of Novel N-Mannich Bases of 1,3,4-Oxadiazole Based on 4,6-Dimethylpyridine Scaffold. International Journal of Molecular Sciences, 23, art. 11173.

(autorzy, rok wydania, tytuł, czasopismo lub wydawca, tom, strony)

mój udział polegał na: mój udział polegał na: współopracowaniu koncepcji i planu wykonywanych badań, zsyntetyzowaniu tytułowych związków oraz potwierdzeniu ich tożsamości metodami spektralnymi, interpretacji oraz opisaniu wyników przeprowadzonych badań, współtworzeniu początkowej wersji manuskryptu oraz redagowaniu wersji finalnej, uwzględniającej sugestie recenzentów;

3. Małgorzata Strzelecka, Benita Wiatrak, Paulina Jawień, Żaneta Czyżnikowska, Piotr Świątek, 2023, New Schiff bases derived from dimethylpyridine-1,2,4-triazole hybrid as cytotoxic agents targeting gastrointestinal cancers: Design, synthesis, biological evaluation and molecular docking studies. Bioorganic Chemistry, 139, art. 106758.

(autorzy, rok wydania, tytuł, czasopismo lub wydawca, tom, strony)

mój udział polegał na: mój udział polegał na: współopracowaniu koncepcji i planu wykonywanych badań, zsyntetyzowaniu tytułowych związków oraz potwierdzeniu ich tożsamości metodami spektralnymi, interpretacji oraz opisaniu wyników przeprowadzonych badań, współtworzeniu początkowej wersji manuskryptu, korespondencji z redakcją oraz opracowaniu wersji finalnej, uwzględniającej sugestie recenzentów.

Jednocześnie oświadczam, że wymienione powyżej publikacje, za zgodą wszystkich Współautorów, wchodzą w skład monotematycznego cyklu stanowiącego podstawę mojej rozprawy doktorskiej.

Uniwersytet Medyczny we Wrocławiu
KATEDRA I ZAKŁAD CHEMII LEKÓW
asystent

mgr Małgorzata Strzelecka

podpis autora

Uniwersytet Medyczny we Wrocławiu
KATEDRA I ZAKŁAD CHEMII LEKÓW
kierownik

dr hab. Piotr Świątek, prof. uczelni

podpis promotora

Wrocław, 08.02.2024

Dr hab. Piotr Świątek, prof. uczelni
Katedra i Zakład Chemii Leków
Wydział Farmaceutyczny
Uniwersytet Medyczny im. Piastów Śląskich we Wrocławiu
ul. Borowska 211a, 50-556 Wrocław

OŚWIADCZENIE WSPÓŁAUTORA

Oświadczam, że w pracach:

1. Piotr Świątek, Teresa Głomb, Agnieszka Dobosz, Tomasz Gębarowski, Kamil Wojtkowiak, Aneta Jezierska, Jarosław J. Panek, Małgorzata Świątek, Małgorzata Strzelecka, 2022, Biological Evaluation and Molecular Docking Studies of Novel 1,3,4-Oxadiazole Derivatives of 4,6-Dimethyl-2-sulfanylpyridine-3-carboxamide. International Journal of Molecular Sciences, 23, art. 549.

2. Małgorzata Strzelecka, Teresa Głomb, Małgorzata Drąg-Zalesińska, Julita Kulbacka, Anna Szewczyk, Jolanta Saczko, Paulina Kasperkiewicz-Wasilewska, Nina Rembiałkowska, Kamil Wojtkowiak, Aneta Jezierska, Piotr Świątek, 2022, Synthesis, Anticancer Activity and Molecular Docking Studies of Novel N-Mannich Bases of 1,3,4-Oxadiazole Based on 4,6-Dimethylpyridine Scaffold. International Journal of Molecular Sciences, 23, art. 11173.

3. Małgorzata Strzelecka, Benita Wiatrak, Paulina Jawień, Żaneta Czyżnikowska, Piotr Świątek, 2023, New Schiff bases derived from dimethylpyridine-1,2,4-triazole hybrid as cytotoxic agents targeting gastrointestinal cancers: Design, synthesis, biological evaluation and molecular docking studies. Bioorganic Chemistry, 139, art. 106758.

mój udział polegał na współtworzeniu koncepcji prac, opracowaniu planu badań, nadzorze merytorycznym nad przeprowadzonymi badaniami z zakresu syntezy związków, analizie otrzymanych wyników, przygotowaniu końcowych wersji manuskryptu i ich edycji po uwagach recenzentów.

Jednocześnie wyrażam zgodę, aby wymienione powyżej artykuły zostały włączone do cyklu publikacyjnego będącego podstawą rozprawy doktorskiej mgr Małgorzaty Strzeleckiej.

Uniwersytet Medyczny we Wrocławiu
KATEDRA I ZAKŁAD CHEMII LEKÓW
dr hab. Piotr Świątek, prof. uczelni

podpis promotora

podpis współautora

Wrocław, 06.02.2024 r.
(miejscowość, data)

Mgr Teresa Glomb
(tytuł, imię i nazwisko)

Katedra i Zakład Chemii Leków
Wydział Farmaceutyczny
Uniwersytet Medyczny im. Piastów Śląskich we Wrocławiu
ul. Borowska 211a, 50-556 Wrocław
(miejsce zatrudnienia)

OŚWIADCZENIE WSPÓŁAUTORA

Oświadczam, że w pracach:

1. Piotr Świątek, Teresa Glomb, Agnieszka Dobosz, Tomasz Gębarowski, Kamil Wojtkowiak, Aneta Jezierska, Jarosław J. Panek, Małgorzata Świątek, Małgorzata Strzelecka, 2022, Biological Evaluation and Molecular Docking Studies of Novel 1,3,4-Oxadiazole Derivatives of 4,6-Dimethyl-2-sulfanylpyridine-3-carboxamide. International Journal of Molecular Sciences, 23, art. 549.

(autorzy, rok wydania, tytuł, czasopismo lub wydawca, tom, strony)

mój udział polegał na: pomocy w pisaniu, edytowaniu i analizie formalnej manuskryptu, tworzeniu części graficznej, pomocy w sporządzaniu bibliografii

2. Małgorzata Strzelecka, Teresa Glomb, Małgorzata Drąg-Zalesińska, Julita Kulbacka, Anna Szewczyk, Jolanta Saczko, Paulina Kasperkiewicz-Wasilewska, Nina Rembiałkowska, Kamil Wojtkowiak, Aneta Jezierska, Piotr Świątek, 2022, Synthesis, Anticancer Activity and Molecular Docking Studies of Novel N-Mannich Bases of 1,3,4-Oxadiazole Based on 4,6-Dimethylpyridine Scaffold. International Journal of Molecular Sciences, 23, art. 11173.

(autorzy, rok wydania, tytuł, czasopismo lub wydawca, tom, strony)

mój udział polegał na: pomocy w pisaniu i analizie formalnej manuskryptu, pomocy w sporządzaniu bibliografii

Jednocześnie wyrażam zgodę, aby wymienione powyżej artykuły zostały włączone do cyklu publikacyjnego będącego podstawą rozprawy doktorskiej mgr Małgorzaty Strzeleckiej.

Teresa Glomb

podpis współautora

Uniwersytet Medyczny we Wrocławiu
KIEROWNIK ZAKŁADU CHEMII LEKÓW
dr hab. Piotr Świątek, prof. uczel.

podpis promotora

Wrocław, 2024-01-30
(miejscowość, data)

Dr Agnieszka Dobosz
(tytuł, imię i nazwisko)

Katedra Podstaw Nauk Medycznych i Immunologii
Zakład Podstaw Nauk Medycznych
Wydział Farmaceutyczny
Uniwersytet Medyczny im. Piastów Śląskich we Wrocławiu
ul. Borowska 211, 50-556 Wrocław
(miejsce zatrudnienia)

OŚWIADCZENIE WSPÓŁAUTORA

Oświadczam, że w pracy:

Piotr Świątek, Teresa Glomb, Agnieszka Dobosz, Tomasz Gębarowski, Kamil Wojtkowiak, Aneta Jezierska, Jarosław J. Panek, Małgorzata Świątek, Małgorzata Strzelecka, 2022, Biological Evaluation and Molecular Docking Studies of Novel 1,3,4-Oxadiazole Derivatives of 4,6-Dimethyl-2-sulfanylpyridine-3-carboxamide. International Journal of Molecular Sciences, 23, art. 549.

(autorzy, rok wydania, tytuł, czasopismo lub wydawca, tom, strony)

mój udział polegał na:

Napisaniu metodyki, wyników i dyskusji do części pracy dotyczącej badania cytotoksyczności, działania antyoksydacyjnego oraz hamującego w stosunku do cyklooksygenaz COX-1 i COX-2 badanych pochodnych oksadiazolowych.

Jednocześnie wyrażam zgodę, aby wymieniony powyżej artykuł został włączony do cyklu publikacyjnego będącego podstawą rozprawy doktorskiej mgr Małgorzaty Strzeleckiej.

A. Dobosz

podpis współautora

Uniwersytet Medyczny we Wrocławiu
KATEDRA I ZAKŁAD PODSTAW NAUK LEKÓW
Kierownik
dr hab. Piotr Świątek, prof. uczelni

podpis promotora

Wrocław 01.02.2024

(miejscowość, data)

Dr Tomasz Gębarowski
(tytuł, imię i nazwisko)

Katedra Biostruktury i Fizjologii Zwierząt
Uniwersytet Przyrodniczy we Wrocławiu
Kożuchowska 1/3, 51-631 Wrocław
(miejsce zatrudnienia)

OŚWIADCZENIE WSPÓŁAUTORA

Oświadczam, że w pracy:

Piotr Świątek, Teresa Glomb, Agnieszka Dobosz, Tomasz Gębarowski, Kamil Wojtkowiak, Aneta Jezierska, Jarosław J. Panek, Małgorzata Świątek, Małgorzata Strzelecka, 2022, Biological Evaluation and Molecular Docking Studies of Novel 1,3,4-Oxadiazole Derivatives of 4,6-Dimethyl-2-sulfanylpyridine-3-carboxamide. International Journal of Molecular Sciences, 23, art. 549.

(autorzy, rok wydania, tytuł, czasopismo lub wydawca, tom, strony)

mój udział polegał na:

zaplanowaniu i pomocy w wykonaniu badań biologicznych z wykorzystaniem modelu hodowli komórkowych

Jednocześnie wyrażam zgodę, aby wymieniony powyżej artykuł został włączony do cyklu publikacyjnego będącego podstawą rozprawy doktorskiej mgr Małgorzaty Strzeleckiej.

Tomasz Gębarowski

podpis współautora

Uniwersytet Medyczny we Wrocławiu
KATEDRA I ZAKŁAD Chemii [illegible]
[illegible]
dr hab. Piotr Świątek, prof. [illegible]

podpis promotora

Wrocław, 31.01.2024
(miejscowość, data)

mgr Kamil Wojtkowiak
(tytuł, imię i nazwisko)

Zespół Struktury i Dynamiki Makroukładów
Wydział Chemii
Uniwersytet Wrocławski
ul. F. Joliot–Curie 14, 50–383 Wrocław
(miejsce zatrudnienia)

OŚWIADCZENIE WSPÓŁAUTORA

Oświadczam, że w pracach:

1. Piotr Świątek, Teresa Glomb, Agnieszka Dobosz, Tomasz Gębarowski, Kamil Wojtkowiak, Aneta Jezierska, Jarosław J. Panek, Małgorzata Świątek, Małgorzata Strzelecka, 2022, Biological Evaluation and Molecular Docking Studies of Novel 1,3,4-Oxadiazole Derivatives of 4,6-Dimethyl-2-sulfanylpyridine-3-carboxamide. International Journal of Molecular Sciences, 23, art. 549.

(autorzy, rok wydania, tytuł, czasopismo lub wydawca, tom, strony)

mój udział polegał na:
współudziale w wyborze metodologii badań, wyborze oprogramowania i zapewnieniu do niego dostępu oraz walidacji; współudziale w formalnej analizie oraz w procesie badawczym; współudziale w redagowaniu początkowej wersji manuskryptu; współudziale w wizualizacji wyników.

2. Małgorzata Strzelecka, Teresa Glomb, Małgorzata Drąg-Zalesińska, Julita Kulbacka, Anna Szewczyk, Jolanta Saczko, Paulina Kasperkiewicz-Wasilewska, Nina Rembiałkowska, Kamil Wojtkowiak, Aneta Jezierska, Piotr Świątek, 2022, Synthesis, Anticancer Activity and Molecular Docking Studies of Novel N-Mannich Bases of 1,3,4-Oxadiazole Based on 4,6-Dimethylpyridine Scaffold. International Journal of Molecular Sciences, 23, art. 11173.

(autorzy, rok wydania, tytuł, czasopismo lub wydawca, tom, strony)

mój udział polegał na:
współudziale w wyborze oprogramowania i zapewnieniu do niego dostępu, a także walidacji; współudziale w formalnej analizie oraz w procesie badawczym; współudziale w redagowaniu początkowej wersji manuskryptu; współudziale w wizualizacji wyników.

Jednocześnie wyrażam zgodę, aby wymienione powyżej artykuły zostały włączone do cyklu publikacyjnego będącego podstawą rozprawy doktorskiej mgr Małgorzaty Strzeleckiej.

Wojtkowiak

podpis współautora

Uniwersytet Medyczny we Wrocławiu
KATEDRA I ZAKŁAD CHEMII LEKÓW
Kierownik
dr hab. Piotr Świątek, prof. uczelni

podpis promotora

Wrocław 31.01.2024
(miejscowość, data)

dr hab. Aneta Jezierska, prof. UWr
(tytuł, imię i nazwisko)

Zespół Struktury i Dynamiki Makroukładów
Wydział Chemii
Uniwersytet Wrocławski
ul. F. Joliot–Curie 14, 50–383 Wrocław
(miejsce zatrudnienia)

OŚWIADCZENIE WSPÓŁAUTORA

Oświadczam, że w pracach:

1. Piotr Świątek, Teresa Glomb, Agnieszka Dobosz, Tomasz Gębarowski, Kamil Wojtkowiak, Aneta Jezierska, Jarosław J. Panek, Małgorzata Świątek, Małgorzata Strzelecka, 2022, Biological Evaluation and Molecular Docking Studies of Novel 1,3,4-Oxadiazole Derivatives of 4,6-Dimethyl-2-sulfanylpyridine-3-carboxamide. International Journal of Molecular Sciences, 23, art. 549.

(autorzy, rok wydania, tytuł, czasopismo lub wydawca, tom, strony)

mój udział polegał na:
współudziale w wyborze oprogramowania i zapewnieniu do niego dostępu oraz walidacji; współudziale w formalnej analizie; współudziale w redagowaniu finalnej wersji manuskryptu uwzględniającej sugestie recenzentów; współudziale w nadzorowaniu prac badawczych.

2. Małgorzata Strzelecka, Teresa Glomb, Małgorzata Drąg-Zalesińska, Julita Kulbacka, Anna Szewczyk, Jolanta Saczko, Paulina Kasperkiewicz-Wasilewska, Nina Rembiałkowska, Kamil Wojtkowiak, Aneta Jezierska, Piotr Świątek, 2022, Synthesis, Anticancer Activity and Molecular Docking Studies of Novel N-Mannich Bases of 1,3,4-Oxadiazole Based on 4,6-Dimethylpyridine Scaffold. International Journal of Molecular Sciences, 23, art. 11173.

(autorzy, rok wydania, tytuł, czasopismo lub wydawca, tom, strony)

mój udział polegał na:
współudziale w wyborze metodologii oraz wyborze oprogramowania i zapewnieniu do niego dostępu, a także walidacji; współudziale w formalnej analizie oraz w procesie badawczym; współudziale w redagowaniu zarówno początkowej, jak i finalnej wersji manuskryptu uwzględniającej sugestie recenzentów; współudziale w nadzorowaniu prac badawczych.

Jednocześnie wyrażam zgodę, aby wymienione powyżej artykuły zostały włączone do cyklu publikacyjnego będącego podstawą rozprawy doktorskiej mgr Małgorzaty Strzeleckiej.

Aneta Męsiorska

podpis współautora

Uniwersytet Medyczny we Wrocławiu
KATEDRA I ZAKŁAD CHEMII LEKÓW
Kierownik
dr hab. Piotr Świątek, prof. uczel.

podpis promotora

Wrocław, 31.01.2024 r.
(miejscowość, data)

dr hab. Jarosław J. Panek, prof. UWr
(tytuł, imię i nazwisko)

Zespół Struktury i Dynamiki Makroukładów
Wydział Chemii
Uniwersytet Wrocławski
ul. F. Joliot–Curie 14, 50–383 Wrocław
(miejsce zatrudnienia)

OŚWIADCZENIE WSPÓŁAUTORA

Oświadczam, że w pracy:

1. Piotr Świątek, Teresa Glomb, Agnieszka Dobosz, Tomasz Gębarowski, Kamil Wojtkowiak, Aneta Jezierska, Jarosław J. Panek, Małgorzata Świątek, Małgorzata Strzelecka, 2022, Biological Evaluation and Molecular Docking Studies of Novel 1,3,4-Oxadiazole Derivatives of 4,6-Dimethyl-2-sulfanylpyridine-3-carboxamide. International Journal of Molecular Sciences, 23, art. 549.

(autorzy, rok wydania, tytuł, czasopismo lub wydawca, tom, strony)

mój udział polegał na:
współudziale w wyborze oprogramowania i zapewnieniu do niego dostępu oraz walidacji; współudziale w formalnej analizie; współudziale w redagowaniu finalnej wersji manuskryptu uwzględniającej sugestie recenzentów; współudziale w nadzorowaniu prac badawczych.

Jednocześnie wyrażam zgodę, aby wymieniony powyżej artykuł został włączony do cyklu publikacyjnego będącego podstawą rozprawy doktorskiej mgr Małgorzaty Strzeleckiej.

Jarosław Panek
podpis współautora

Uniwersytet Medyczny we Wrocławiu
KATEDRA I ZAKŁAD CHEMII LEKÓW

dr hab. Piotr Świątek, prof. uczelni
podpis promotora

Wrocław 08.02.2024

Mgr Małgorzata Świątek
Uniwersytecki Szpital Kliniczny we Wrocławiu
ul. Borowska 213, 50-556 Wrocław

OŚWIADCZENIE WSPÓŁAUTORA

Oświadczam, że w pracy:

Piotr Świątek, Teresa Głomb, Agnieszka Dobosz, Tomasz Gębarowski, Kamil Wojtkowiak, Aneta Jezierska, Jarosław J. Panek, Małgorzata Świątek, Małgorzata Strzelecka, 2022, Biological Evaluation and Molecular Docking Studies of Novel 1,3,4-Oxadiazole Derivatives of 4,6-Dimethyl-2-sulfanylpyridine-3-carboxamide. International Journal of Molecular Sciences, 23, art. 549.

mój udział polegał na przeszukiwaniu baz literaturowych, analizie uzyskanych wyników, opracowaniu części manuskryptu.

Jednocześnie wyrażam zgodę, aby wymieniony powyżej artykuł został włączony do cyklu publikacyjnego będącego podstawą rozprawy doktorskiej mgr Małgorzaty Strzeleckiej.

Małgorzata Świątek

podpis współautora

Uniwersytet Medyczny we Wrocławiu
KATEDRA I ZAKŁAD CHEMII LEKÓW

dr hab. Piotr Świątek, prof. uczelni

podpis promotora

Wrocław, 30.01.2024 r.

miejscowość, data

Dr hab. Małgorzata Drąg-Zalesińska
(tytuł, imię i nazwisko)

Zakład Histologii i Embriologii
Wydział Lekarski
Uniwersytet Medyczny im. Piastów Śląskich we Wrocławiu
ul. Chałubińskiego 6a, 50-368 Wrocław
(miejsce zatrudnienia)

OŚWIADCZENIE WSPÓŁAUTORA

Oświadczam, że w pracy:

Małgorzata Strzelecka, Teresa Głomb, Małgorzata Drąg-Zalesińska, Julita Kulbacka, Anna Szewczyk, Jolanta Saczko, Paulina Kasperkiewicz-Wasilewska, Nina Rembiałkowska, Kamil Wojtkowiak, Aneta Jezierska, Piotr Świątek, 2022, Synthesis, Anticancer Activity and Molecular Docking Studies of Novel *N*-Mannich Bases of 1,3,4-Oxadiazole Based on 4,6-Dimethylpyridine Scaffold. International Journal of Molecular Sciences, 23, art. 11173.

(autorzy, rok wydania, tytuł, czasopismo lub wydawca, tom, strony)

mój udział polegał na:

wykonaniu testu kometowego metodą neutralną oraz analiza uszkodzeń DNA.

Jednocześnie wyrażam zgodę, aby wymieniony powyżej artykuł został włączony do cyklu publikacyjnego będącego podstawą rozprawy doktorskiej mgr Małgorzaty Strzeleckiej.

Małgorzata Drąg-Zalesińska

podpis współautora

Uniwersytet Medyczny we Wrocławiu
KIEROWNIK ZAKŁADU HISTOLOGII I EMBRIOLOGII
dr hab. Piotr Świątek, prof. uczelni

podpis promotora

Wrocław 08.02.2024
miejscowość, data

Dr hab. inż. Julita Kulbacka, prof. UMW
(tytuł, imię i nazwisko)

Katedra i Zakład Biologii Molekularnej i Komórkowej
Wydział Farmaceutyczny
Uniwersytet Medyczny im. Piastów Śląskich we Wrocławiu
ul. Borowska 211a, 50-556 Wrocław
(miejsce zatrudnienia)

OŚWIADCZENIE WSPÓŁAUTORA

Oświadczam, że w pracy:

Małgorzata Strzelecka, Teresa Glomb, Małgorzata Drąg-Zalesińska, Julita Kulbacka, Anna Szewczyk, Jolanta Saczko, Paulina Kasperkiewicz-Wasilewska, Nina Rembiałkowska, Kamil Wojtkowiak, Aneta Jezierska, Piotr Świątek, 2022, *Synthesis, Anticancer Activity and Molecular Docking Studies of Novel N-Mannich Bases of 1,3,4-Oxadiazole Based on 4,6-Dimethylpyridine Scaffold.* International Journal of Molecular Sciences, 23, art. 11173.

(autorzy, rok wydania, tytuł, czasopismo lub wydawca, tom, strony)

mój udział polegał na:

Dobraniu metodologii do badań in vitro, weryfikacji wyników biologicznych oraz finalnej rewizji przygotowanego przez autorkę manuskryptu.

Jednocześnie wyrażam zgodę, aby wymieniony powyżej artykuł został włączony do cyklu publikacyjnego będącego podstawą rozprawy doktorskiej mgr Małgorzaty Strzeleckiej.

Uniwersytet Medyczny we Wrocławiu
KATEDRA I ZAKŁAD BIOLOGII
MOLEKULARNEJ I KOMÓRKOWEJ
kierownik
dr hab. inż. Julita Kulbacka, prof. uczelni

podpis współautora

Uniwersytet Medyczny we Wrocławiu
KATEDRA I ZAKŁAD BIOLOGII
kierownik
dr hab. Piotr Świątek, prof. uczelni

podpis promotora

Wrocław, 06.02.2024r.
miejscowość, data

Dr Anna Szewczyk
(tytuł, imię i nazwisko)

Katedra i Zakład Biologii Molekularnej i Komórkowej
Wydział Farmaceutyczny
Uniwersytet Medyczny im. Piastów Śląskich we Wrocławiu
ul. Borowska 211a, 50-556 Wrocław
(miejsce zatrudnienia)

OŚWIADCZENIE WSPÓŁAUTORA

Oświadczam, że w pracy:

Małgorzata Strzelecka, Teresa Glomb, Małgorzata Drąg-Zalesińska, Julita Kulbacka, Anna Szewczyk, Jolanta Saczko, Paulina Kasperkiewicz-Wasilewska, Nina Rembiałkowska, Kamil Wojtkowiak, Aneta Jezierska, Piotr Świątek, 2022, Synthesis, Anticancer Activity and Molecular Docking Studies of Novel *N*-Mannich Bases of 1,3,4-Oxadiazole Based on 4,6-Dimethylpyridine Scaffold. International Journal of Molecular Sciences, 23, art. 11173.

(autorzy, rok wydania, tytuł, czasopismo lub wydawca, tom, strony)

mój udział polegał na:

wykonaniu analiz mikroskopowych

Jednocześnie wyrażam zgodę, aby wymieniony powyżej artykuł został włączony do cyklu publikacyjnego będącego podstawą rozprawy doktorskiej mgr Małgorzaty Strzeleckiej.

podpis współautora

Uniwersytet Medyczny we Wrocławiu
KATEDRA I ZAKŁAD BIOLOGII MOLEKULARNEJ I KOMÓRKOWEJ

dr hab. Piotr Świątek, prof. uczelni

podpis promotora

Wrocław, 30/01/2023
miejscowość, data

Dr hab. inż. Paulina Kasperkiewicz-Wasilewska, prof. uczelnie
(tytuł, imię i nazwisko)

Katedra Chemii Biologicznej i Bioobrazowania
Wydział Chemiczny
Politechnika Wrocławska
Wyb. Wyspiańskiego 27
50-370 Wrocław
(miejsce zatrudnienia)

OŚWIADCZENIE WSPÓŁAUTORA

Oświadczam, że w pracy:

Małgorzata Strzelecka, Teresa Głomb, Małgorzata Drąg-Zalesińska, Julita Kulbacka, Anna Szewczyk, Jolanta Saczko, Paulina Kasperkiewicz-Wasilewska, Nina Rembiałkowska, Kamil Wojtkowiak, Aneta Jezierska, Piotr Świątek, 2022, Synthesis, Anticancer Activity and Molecular Docking Studies of Novel *N*-Mannich Bases of 1,3,4-Oxadiazole Based on 4,6-Dimethylpyridine Scaffold. International Journal of Molecular Sciences, 23, art. 11173.

(autorzy, rok wydania, tytuł, czasopismo lub wydawca, tom, strony)

mój niewielki udział polegał na: pomocy przy obrazowaniu przy użyciu mikroskopu konfokalnego

Jednocześnie wyrażam zgodę, aby wymieniony powyżej artykuł został włączony do cyklu publikacyjnego będącego podstawą rozprawy doktorskiej mgr Małgorzaty Strzeleckiej.

---
podpis współautora

Uniwersytet Medyczny im. Włodzimierza
KATEDRA I ZAKŁAD BIOCHEMII LEKARSKIEJ
Kierownik
dr hab. Piotr Świątek, prof. uczelni

---
podpis promotora

7.02.2024r.

miejscowość, data

Dr inż. Nina Rembiałkowska
(tytuł, imię i nazwisko)

Katedra i Zakład Biologii Molekularnej i Komórkowej
Wydział Farmaceutyczny
Uniwersytet Medyczny im. Piastów Śląskich we Wrocławiu
ul. Borowska 211a, 50-556 Wrocław
(miejsce zatrudnienia)

OŚWIADCZENIE WSPÓŁAUTORA

Oświadczam, że w pracy:

Małgorzata Strzelecka, Teresa Glomb, Małgorzata Drąg-Zalesińska, Julita Kulbacka, Anna Szewczyk, Jolanta Saczko, Paulina Kasperkiewicz-Wasilewska, Nina Rembiałkowska, Kamil Wojtkowiak, Aneta Jezierska, Piotr Świątek, 2022, Synthesis, Anticancer Activity and Molecular Docking Studies of Novel *N*-Mannich Bases of 1,3,4-Oxadiazole Based on 4,6-Dimethylpyridine Scaffold. International Journal of Molecular Sciences, 23, art. 11173.

(autorzy, rok wydania, tytuł, czasopismo lub wydawca, tom, strony)

mój udział polegał na:

zaplanowaniu i przeprowadzeniu badań biologicznych z udziałem komórek prawidłowych i nowotworowych dotyczących cytotoksyczności związków (test MTT, test klonogenny) oraz testu podwojenia populacji.

Jednocześnie wyrażam zgodę, aby wymieniony powyżej artykuł został włączony do cyklu publikacyjnego będącego podstawą rozprawy doktorskiej mgr Małgorzaty Strzeleckiej.

Uniwersytet Medyczny we Wrocławiu
KATEDRA I ZAKŁAD BIOLOGII
MOLEKULARNEJ I KOMÓRKOWEJ
adiunkt
dr inż. Nina Rembiałkowska

podpis współautora

Uniwersytet Medyczny we Wrocławiu
KATEDRA I ZAKŁAD [illegible]
dr hab. Piotr Świątek, prof. uczelni

podpis promotora

Wrocław 1.02.2024
miejscowość, data

Dr hab. Benita Wiatrak
(tytuł, imię i nazwisko)

Katedra i Zakład Farmakologii
Wydział Lekarski
Uniwersytet Medyczny im. Piastów Śląskich we Wrocławiu
ul. J. Mikulicza-Radeckiego 2, 50-345 Wrocław
(miejsce zatrudnienia)

OŚWIADCZENIE WSPÓŁAUTORA

Oświadczam, że w pracy:

Małgorzata Strzelecka, Benita Wiatrak, Paulina Jawień, Żaneta Czyżnikowska, Piotr Świątek, 2023, New Schiff bases derived from dimethylpyridine-1,2,4-triazole hybrid as cytotoxic agents targeting gastrointestinal cancers: Design, synthesis, biological evaluation and molecular docking studies. Bioorganic Chemistry, 139, art. 106758.

(autorzy, rok wydania, tytuł, czasopismo lub wydawca, tom, strony)

mój udział polegał na: wykonaniu badań in vitro

Jednocześnie wyrażam zgodę, aby wymieniony powyżej artykuł został włączony do cyklu publikacyjnego będącego podstawą rozprawy doktorskiej mgr Małgorzaty Strzeleckiej.

Benita Wiatrak
podpis współautora

Uniwersytet Medyczny we Wrocławiu
KATEDRA I ZAKŁAD FARMAKOLOGII
Kierownik
dr hab. Piotr Świątek, prof. uczelni
podpis promotora

Wrocław, 29.01.2024
miejscowość, data

Dr hab. Żaneta Czyżnikowska
(tytuł, imię i nazwisko)

Katedra i Zakład Podstaw Nauk Chemicznych
Wydział Farmaceutyczny
Uniwersytet Medyczny im. Piastów Śląskich we Wrocławiu
ul. Borowska 211a, 50-556 Wrocław
(miejsce zatrudnienia)

OŚWIADCZENIE WSPÓŁAUTORA

Oświadczam, że w pracy:

- Małgorzata Strzelecka, Benita Wiatrak, Paulina Jawień, Żaneta Czyżnikowska, Piotr Świątek, 2023, New Schiff bases derived from dimethylpyridine-1,2,4-triazole hybrid as cytotoxic agents targeting gastrointestinal cancers: Design, synthesis, biological evaluation and molecular docking studies. Bioorganic Chemistry, 139, art. 106758.

(autorzy, rok wydania, tytuł, czasopismo lub wydawca, tom, strony)

mój udział polegał na wykonaniu dokowania molekularnego i opisania otrzymanych w ten sposób wyników.

Jednocześnie wyrażam zgodę, aby wymienione powyżej artykuły zostały włączone do cyklu publikacyjnego będącego podstawą rozprawy doktorskiej mgr Małgorzaty Strzeleckiej.

Uniwersytet Medyczny we Wrocławiu
KATEDRA I ZAKŁAD
PODSTAW NAUK CHEMICZNYCH
kierownik
dr hab. Żaneta Czyżnikowska

podpis współautora

Uniwersytet Medyczny we Wrocławiu
KATEDRA I ZAKŁAD CHEMII LEKÓW
kierownik
dr hab. Piotr Świątek, prof. uczelni

podpis promotora

Wrocław 01.02.24

miejscowość, data

Mgr inż. Paulina Nowotarska (z d. Jawień)
(tytuł, imię i nazwisko)

Katedra Biostruktury i Fizjologii Zwierząt
Uniwersytet Przyrodniczy we Wrocławiu
ul. Norwida 25/27, 50-375 Wrocław
(miejsce zatrudnienia)

OŚWIADCZENIE WSPÓŁAUTORA

Oświadczam, że w pracy:

Małgorzata Strzelecka, Benita Wiatrak, Paulina Jawień, Żaneta Czyżnikowska, Piotr Świątek, 2023, New Schiff bases derived from dimethylpyridine-1,2,4-triazole hybrid as cytotoxic agents targeting gastrointestinal cancers: Design, synthesis, biological evaluation and molecular docking studies. Bioorganic Chemistry, 139, art. 106758.

(autorzy, rok wydania, tytuł, czasopismo lub wydawca, tom, strony)

mój udział polegał na: Pomocy w wykonaniu badań biologicznych modelu hodowli komórkowych

Jednocześnie wyrażam zgodę, aby wymieniony powyżej artykuł został włączony do cyklu publikacyjnego będącego podstawą rozprawy doktorskiej mgr Małgorzaty Strzeleckiej.

Paulina Nowotarska (z d. Jawień)

podpis współautora

Uniwersytet Medyczny we Wrocławiu
KATEDRA I ZAKŁAD CHEMII LEKÓW
kierownik
dr hab. Piotr Świątek prof. uczelni

podpis promotora